
Editorial Office of *Earth's Cryosphere (Kriosfera Zemli)*
Institute of Geography, Russian Academy of Sciences
37, Vavilova, office 22, Moscow, 117312, Russia
Editor N.V. Arutyunyan
Phone: (499) 124-54-22, e-mail: kriozem@gmail.com

Journal promoted by
Russian Academy of Sciences, Siberian Branch, Novosibirsk
Institute of Earth's Cryosphere, Tyumen

Editorial Manager *M.A. Trashkeeva*
Designed by *O.M. Varaksina*
Typeset by *N.M. Raizvikh*
English text by *T.I. Perepelova*

Front cover: Exposed ground ice, Yamal Peninsula, western coast, photograph by *E.A. Slagoda*

Published by Academic Publishing House "Geo",
3/1, Musy Dzhalilya, Novosibirsk, 630055, Russia
Phone: (383) 335-64-30, e-mail: crio@izdatgeo.ru
http://www.izdatgeo.ru
Printed by "Talleres" Ltd., 33/1, Lazareva str., Novosibirsk, 630084, Russia, phone: (383) 271-01-30

SIBERIAN BRANCH
RUSSIAN ACADEMY OF SCIENCES
INSTITUTE OF EARTH'S CRYOSPHERE

SCIENTIFIC JOURNAL
EARTH'S CRYOSPHERE

Founded in January 1997	Quaterly	Vol. XV, No. 4	October–December 2011

CONTENTS

SCIENTIFIC JOURNAL
EARTH'S CRYOSPHERE

Kriosfera Zemli, 2011, vol. XV, No. 4, pp. 3–7 http://www.izdatgeo.ru

PHYLOSOPHICAL ISSUES OF CRYOLOGY

CRYOSOPHY: AN OUTLOOK OF THE COLD WORLD

V.P. Melnikov, V.B. Gennadinik

Institute of Earth's Cryosphere,
Siberian Branch of the Russian Academy of Sciences, PO box 1230, Tyumen, 625000, Russia; melnikov@ikz.ru

The outlook of the cryosphere in the present scientific community has been changing rapidly. Rather than being a danger, the sphere of ice and cold is taken as an active element of the universe, a wealth, and a source of wellbeing and new potentialities for the mankind. This is the reason for increasing recent interest to the cold world among different scientists and, on the other hand, for broadening the scope of the classical permafrost science. It is time to create a new school of thought, that of cryosophy. Cryosophy should focus on the role of cold matter in the ever changing world and on the basic properties of the cryosphere. The presented snapshot of highlights of the cryosphere from the early Universe to the life origin, which remain little discussed in the permafrost community, illustrates the urgent need in new ontological approaches.

The turn of the century has been marked in permafrost science by dramatic changes in the views of its very object. At the dawn of cryology, permafrost was treated as ill in terms of practice (see, for instance, P.I. Koloskov's preface to the book of *Sumgin* [*1927*]). That long remained the leading attitude while continuous struggle against cryogenic hazard narrowed the scope of studies and promoted the search for technological solutions rather than scientific research. It is not until the recent decade that the cryosphere has been understood to be a universal phenomenon, a matter-energy element of the Universe, a wealth, and a source of life, human wellbeing, and civilization progress. This change of values brought about new methodological approaches and, furthermore, different views of the research subject and goals.

The subject of cryology is changing as the scope of research has been expanding with diverse issues from the life origin to agriculture enhancement, from extraterrestrial missions to records of historic events. Proper understanding among scientists who work in these different fields requires updating the system of concepts by enlarging their meaning and modifying concepts, even the old ones which have withstood the test of time.

It is urgent at the moment to depart from the conventional boundaries between disciplines and to develop a new panoramic outlook of the object (cryosphere) and methods of research, taking into account the current advances in other sciences, in order to finally create a basis for cryosophy as a new ontological line in philosophy [*Melnikov, 2010*].

Cryosophy aims at understanding the role of cold matter in the evolving matter-energy interplay, as well as in the origin and maintenance of life. The new science should focus on the most general properties of the cryosphere and its basic links with other components of the Universe. The research should stem from both classical (applicable to simple physical and chemical systems) and synergetic (for complex systems, including biological ones) approaches using both the methods that yield knowledge of things and the information logistic methods which provide knowledge of knowledge [*Melnikov et al., 2005*].

Ice and its phase change – the focus of cryology – has been the subject of diverse sciences and research fields. The chart of Fig. 1 shows different aspects of ice and the roles it plays in the world.

Boxes on the two sides of the "space" axis represent the hierarchy of objects and media in which ice is the major control. This pattern corresponds to the classical approaches viewing ice as something people meet in the everyday life, the cryosphere being the best instrumentally explored sphere of the Earth. However, it is time to revise the views of ice as a superplanetary object.

The history of the Universe, since the big bang when matter just sprang out of elementary particles (protons, neutrons, and electrons), has been linked with hydrogen which, along with helium, was the first to form on cooling. The Cryosphere is super-systematic, as follows from the fact that ice had existed prior to the origin of the Solar System with its planets and ever before water and life appeared on the Earth. Moreover, it will remain in the Universe even after the Sun expands and heats up, and after our Earth transforms into something like a lifeless hot planet.

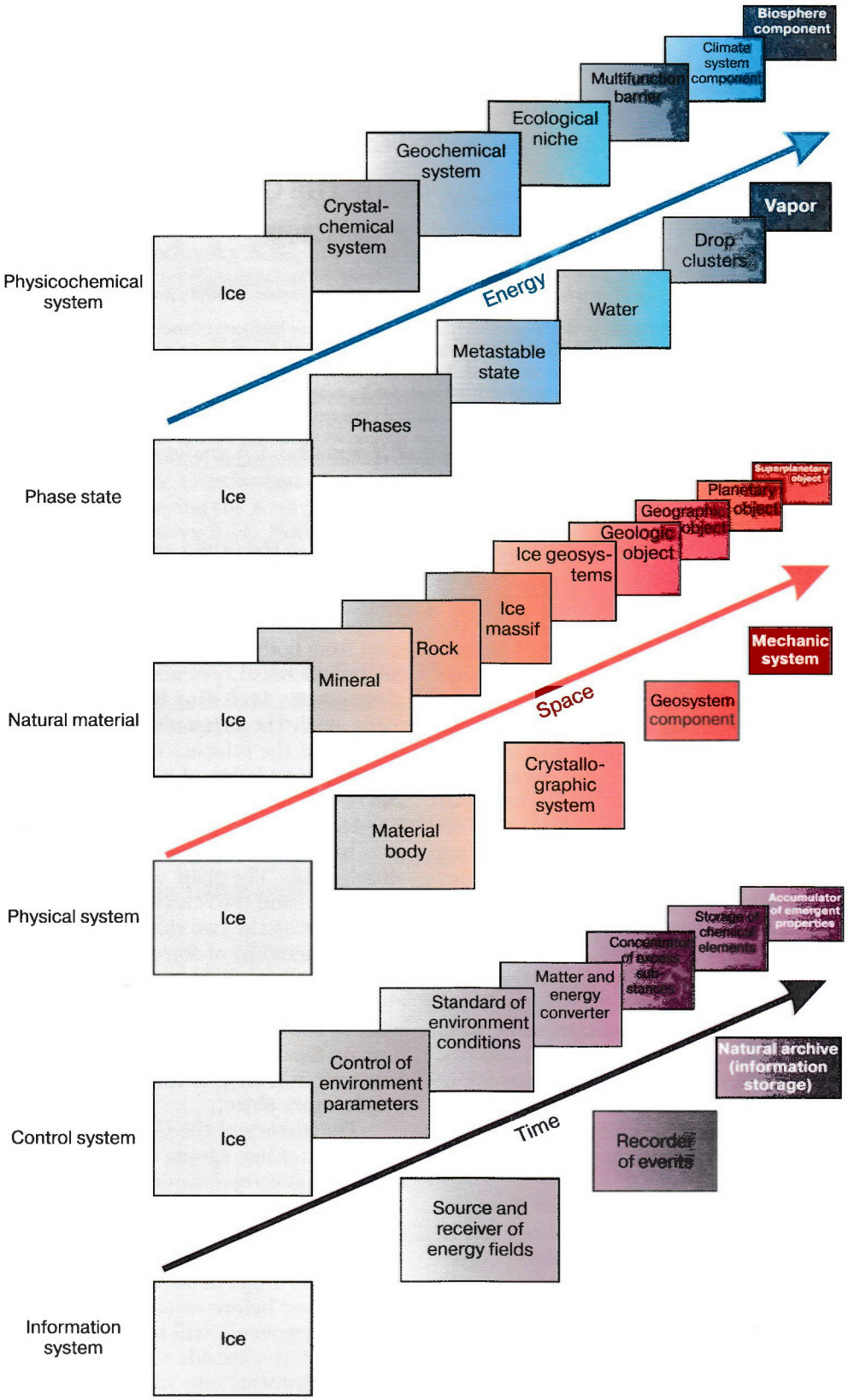

Fig. 1. Ice as a multifunction system.

The diversity of conditions on the planets and other large objects in the Solar System (distances from the Sun, orbits, year and day durations, presence or absence of atmosphere, etc.) prompts that the terrestrial cryosphere is not unique but is, instead, a common phenomenon being special though in its bioprotective ability.

The recent advances in space exploration furnish impressive evidence of cryogenic processes on the primary planets and their satellites. People are waiting for ever more wonderful things to learn against which the Earth's permafrost would not look so fascinating, but it will certainly remain of vital importance to humans and to all living beings on our home planet.

Let us turn back to our chart (Fig. 1). The "energy" axis illustrates the phase states of ice and its functions. Compared to single-state water, ice has far greater phase diversity, with its seventeen states out of which eleven are explicit. This diversity shows up in various physicochemical and biological processes, including such a common thing as precipitation: rainfall of one type, snowfall of eight types, and two mixed types of ice-water precipitation.

Ice is sometimes interpreted as a mere by-product of water transformations. What people commonly speak of are three aggregate states of water but not of ice. This is a purely subjective human attitude, as intuitively (and biologically) water seems closer to people than ice. This attitude is standard but not normal, and this is not fortuitous: the standard conditions people stand the best are those of 1 bar (1 kPa) pressure and 25 °C temperature while the normal natural conditions are, respectively, 1.01 bar and 0 °C.

There are different properties brought together in ice which is at the same time elastic and plastic, crystalline and amorphous, semiconducting and dielectric, light and hard (lighter than water but harder than steel). Ice follows a certain trend toward an ideal structure: its order increases while entropy decreases with time at a constant low temperature [*Maeno, 1988*].

Ice crystals are built uniquely of hydrogen bonds, i.e., ice can be a standard to estimate hydrogen bonds. At the same time, hydrogen bonds are indispensable in proteins, nucleic acids, or biopolymers. They have been crucial to the very life origin as all biochemical processes in living beings are associated with breaking and resuming hydrogen bonds.

The complexity of the ice structure and its off-equilibrium phase change are sufficient for self-organizing synergetic behavior and formation of stable macroscopic objects. One such object, a drop cluster, is shown in the energy scale (Fig. 1) between water and vapor. Drop clusters are stable dissipative structures in the form of ordered tiny condensate balls of the same size which appear in the gradient zone over a locally heated liquid phase [*Fedorets, 2004*]. Phenomena of this kind may be a missing link between the organic and inorganic matter.

The "time" axis (Fig. 1) presents cryogenic systems in terms of information, resources, and cybernetics. The cryosphere changes the characteristic times and rates of processes and stores records of the other terrestrial spheres, which has an intimate relation with synergetic processes and with the life origin and evolution.

A topical objective of cryology is contributing to the knowledge of geological history through studying the effect of glaciations on the evolution of the biotic and abiotic components in the crust. Till the present, permafrost scientists have dealt mainly with the Quaternary but the most interesting things apparently occurred 2–2.5 billion years earlier. It is since 2.5 Ga that the Earth has experienced repeated glacial cycles of different durations and intensities. A correlation has been discovered between the beginning and end of glacial cycles and the composition of atmosphere, especially CO_2 and sulfur [*Dobretsov, 2004*]. However, the history before 2.5 Ga likewise calls for new approaches and hypotheses. The scientific community has been split into partisans and opponents of the "hot" and "cold" models of the early Earth. The "snowball" scenario when the planet was fully covered with ice [*Kirschvink et al., 1997*] may have repeated many times, and the task of cryology is to discover traces of those periods.

It is necessary to determine the functions and physicochemical and other manifestations of ice in the early geological history to gain insights into how traces of events happening in cold times may in principle look. This may be "cryo-traceology", a special new field to concern with interaction of ice with biogenic and abiogenic components of the medium.

The cryosphere is subject to various natural cycles, this cyclicity being obviously more diverse than it is commonly thought. In cold seasons (autumn, winter, and spring in the Northern Hemisphere), circadian (diurnal) cycles become essential in cryogenic systems. The ice-water phase change that stabilizes the temperature regime for the living world occurs during a day. The yearly cyclicity is more prominent: snow and ice can keep stable for a long time creating cryogenic conditions. Note that the diurnal cycles naturally disappear in polar regions (the polar day and night are six months long), and living beings likewise adapt to these patterns (e.g., reindeer lack biological clock). Other longer-period cycles are associated with the solar activity (11- and 270-year cycles).

A more complex cyclicity shows up in glaciers. Evaporated ice molecules crystallize in clouds at the atmospheric temperature filter and precipitate as snowfall. If snow fails to melt during the warm season, the accumulated viscoplastic mixture of ice and

granular snow makes up a glacier. The glacier gradually slides down by gravity into the zone of ablation where it degrades mechanically, melts, and evaporates. Thus, each glacier has its own characteristic life time controlled by climate (temperature and moisture) and geography (terrain and rock structure). The glacier cycles may have different periodicities, from several years in highlands and subpolar regions to tens of thousand years in Greenland or Antarctic. It is interesting to investigate the interaction of different cycles in systems of this kind.

The cyclic processes in the cryosphere likewise demonstrate the parentage of the cold and the life: both undergo entropy cycles at intense heat and mass exchange. The birth of a living being, as well as the formation of ice out of water and vapor, reduces entropy and produces self-organized complex systems.

It is evidently the atmosphere, with its thermal shield aggregating water molecules into ice particles, that holds back water on the Earth. This is a factor crucial to the origin of life. Any change in the Earth's cryosphere anyhow influences the evolution of the life-sustaining environment. Atmospheric ozone had formed about 400 Ma ago and let the life move from the ocean to the land [*Dobretsov, 2004*]. Judging by the vertical pattern of air-borne ozone similar to the air stratification, it is the weakness of hydrogen bonds that allows creatures to leave water for existing freely on the land (or, in the same way, to leave land for the troposphere).

Hydrogen has been critical to the energy budget of oldest biological systems [*Fedonkin, 2000*] being the primary source of electrons and protons, the basic substrate of microbial life, and the energy base of metabolism [*Wackett et al., 1994*]. It controls the strength and plasticity of macromolecules; molecular hydrogen (H_2) maintains trophic (energy) relations between microorganisms that live on different substrates; this is actually the primary builder of an ecosystem prototype. In the world of prokaryotes, hydrogen, as an energy-related element, guided competition among many groups. Furthermore, the reducing ability of molecular hydrogen and its capability of forming proton gradients as a way to save energy, as well as many other properties, evidence that hydrogen has been the most important element and a key agent in the life origin.

The science of cryology focuses on transformations and interactions of the primary elements of hydrogen and oxygen. Cryosophy may occupy its niche in the cryosphere research through working out life evolution theories viewing the evolution beyond the limits of a specific planet. Ice, the precursor of water, dates back to the very beginning of the Universe when there appeared hydrogen and then oxygen whose aggregation and hydrogen bonding laid the basis of the animate and inanimate nature.

The origin of terrestrial life was possibly preceded by a prebiological evolution stage [*Galimov, 2001*]. According to a hypothesis by *Diakonov* [*1994*], the self-similarity of biospheric and civilization crises (acceleration of historic time) recognized in the four billion-years history of the Earth indicates that the beginning of the prebiological evolution coincided with the formation of the galactic disc about 10 Ga ago. That was exactly the time when ice appeared as a special phase offering an example of molecular interaction to all living beings.

The fact that the mean annual air temperature on the Earth long remained about the ice-water transition point appears quite natural. Ice, like water, possesses exceptional thermostatic properties which, along with its wide spread over the ground surface, allows the cryosphere to stabilize the temperature regime. Note that the heat capacity of water (4.183 kJ/kg·K) is five times the mean heat capacity of soil, and its bulk heat capacity is 3300 times that of air. The high heat capacities of water and ice (2.06 kJ/kg·K) make them the Earth's principle storage of the solar energy. The very phase change point has additional (likewise abnormal) thermal stability: specific heat of ice melting is five times as high as in gold (332 against 66.2 kJ/kg) and is higher than, say, in mercury by a factor of 28 (12 kJ/kg).

The temperature stability defines the conditions favorable for the living nature while ice acts as a bioprotector that stabilizes the parameters of the environment.

The cryology-biology union began since the earliest years of the permafrost science in the USSR. Just remember the exciting finds of mammoths or reviving insects recovered from frozen ground in the first half of the 20th century.

The today's works in cryobiology are as fascinating to read as science fiction, with all those caterpillars and butterflies that return to life after staying long frozen to –269 °C, or invertebrates (rotifers and nematodes) that withstood freezing to –271 °C in the dry state. After all that, life in natural permafrost would appear a "resort" for microorganisms.

As the Vostok ice cores from Antarctica showed, nature has been much more prudent than man in maintaining the temperature regime for hundreds of thousand years having provided smooth cooling and warming, exactly what is needed to let organisms adapt to new conditions. The knowledge gained from paleobiota is just a good beginning, and the main discoveries are to come.

One practical objective of cryology is to get the same life support from permafrost as the extremophilic microbes do. In this respect ice can be considered a habitat or, more precisely, a stable nonequilibrium coevolving system in which microorganisms are intrinsic components of ice or frozen rocks.

Another challenge for joint efforts of biology and cryology is understanding the function of ice in the punctuated equilibrium of Eldredge and Gould in the context of sustaining life. Ice has too many advantages over other media being a shield against killing radiation, a thermostat with the minimum temperature gradients, protection against chemical or biological mutagenic agents, and, finally, a constantly renewing medium.

A recent example of the kinship between the cold and the living comes from a discovery that bacteria (specifically, *Pseudomonas syringae*) may be responsible for most of rain and snow being ice nucleators [*Christner et al., 2008*]. Bacteria were found out to be able of traveling long distances together with clouds and cause snowfall all over the world at quite high temperature. There is nothing surprising about it, as the relatively light bacteria can act as crystallization nuclei and seeds for the new phase at the heights where rain and snow originate and where the heavier objects can never rise.

Vernadsky [*2001*] wrote that the living matter had a strong control over the formation and regulation of geochemistry and physics of the biosphere, atmosphere, and the hydrosphere. The cryosphere, in turn, may be a link between the Earth and the life: first it cherished the life and then offered an example of maintaining suitable life conditions.

There are diverse processes in which ice or water near the phase change point are crucial. They show up in obvious or paradoxical ways. The various facts make up a mosaic, a sort of a puzzle the clue being the kinship between ice and life and their ability to form composite objects and stable systems with new emergent properties.

Cryology has been assimilating ever more terminology uncommon to a classical applied science, such as diversity, stability, complexity, or emergent behavior; systems are brought together into meta-systems, and simple models give way to hierarchies of models. Thereby it becomes a multidisciplinary and actual science, with a focus at urgent practical needs. As the subject of study has been increasingly expanding, the methods available in cryology can no longer lead to the wanted ends.

Today, when knowledge is growing rapidly and various sciences are interfingering while the education principles and position of a scientist in the world are changing, cryosophy should become the cryology of the future, should broaden the scope of the latter, develop a high-performance methodology, and provide guidelines for the prospects and expected results of research.

Cryosophy should maintain the interest to cryogenic processes and phenomena, to the "short circuit" between the life and the cold, in classical permafrost scientists, as well as in those engaged in biophysics, biology, meteorology, planetary research, all those who deal with problems new to the scientific community. As soon as results from other sciences have received new interpretations in terms of cryology and have been projected onto the sphere of cold, cryologists themselves will no longer rediscover, with enthusiasm of neophytes, the things known for ages.

References

Christner B.C., Morris C.E., Foreman C.M., et al., 2008. Ubiquity of biological ice nucleators in snowfall. Science, 319 (5867), 1214, DOI: 10.1126/science.1149757

Dobretsov N.L., 2004. Known and unknown in evolution. Science First Hand, 0 (1), 1–17.

D'yakonov I.M., 1994. The Paths of History. From the Primitive Man to Nowadays [in Russian]. Vostochnaya Literatura, Moscow, 384 pp.

Fedonkin M.A., 2000. The cold dawn of animal life. Priroda, No. 9, 3–11.

Fedorets A.A., 2004. Drop clusters. Letters to ZhETF, 79 (8), 457–459.

Galimov E.M., 2001. The phenomenon of life: between equilibrium and nonlinearity, in: The Origin and Principles of the Evolution [in Russian]. Editorial URSS, Moscow, 256 pp.

Kirschvink J.L., Ripperdan R.L., Evans D.A., 1997. Evidence for a large-scale reorganization of early Cambrian continental masses by inertial interchange: true polar wander. Science, 277 (5325), 541–545.

Maeno N., 1988. The Science of Ice [Russian Translation from Japanese]. Mir, Moscow, 231 pp.

Melnikov V.P., 2010. Cold and wisdom: an academician's fortune and life meaning, in: The Epoch in Persons [in Russian]. Epokha, Moscow, pp. 154–165.

Melnikov V.P., Gennadinik V.B., Gennadinik B.I., 2005. Let the cold science have a philosophic background, in: Philosophy and the Future of Civilization [in Russian]. Book 1, Sovremennye Tetradi, Moscow, p. 374.

Sumgin M.I., 1927. Permafrost in the USSR Territory [in Russian]. Far East Geophysical Observatory, Vladivostok, 134 pp.

Vernadsky V.I., 2001. The Biosphere [in Russian]. Noosfera, Moscow, 244 pp.

Wackett L.P., Sadowsky M.J., Newman L.M., et al., 1994. Metabolism of polyhalogenated compounds by a genetically engineered bacterium. Nature, 368, 627–629.

Received
2 February 2011

SCIENTIFIC JOURNAL
EARTH'S CRYOSPHERE

Kriosfera Zemli, 2011, vol. XV, No. 4, pp. 8–13 http://www.izdatgeo.ru

EARTH'S CRYOLOGY: ENVIRONMENTAL AND REGIONAL PROBLEMS

GEOCRYOLOGICAL CHRONICLES OF RUSSIA

S.M. Fotiev

Institute of Earth's Cryosphere, Siberian Branch of the Russian Academy of Sciences, PO box 1230, Tyumen, 625000, Russia; kriozem@gmail.com

The author was the first to compile two geocryological Chronicles: simplified for the Late Cenozoic) (the last 3.5 Ma) and more detailed for the Neopleistocene (Brunhes epoch) (the last 800 kur). These Chronicles comprise the geocryological interpretation of Baikal climatic chronicle, compiled by a large team of scientists, and based on the identified relation of diatom valves and biogenic silica percentage in bottom sediments of the Baikal lake on the severity of natural setting.

LATE CENOZOIC GEOCRYOLOGICAL CHRONICLE (3.1–0.0 Ma)

The Late Cenozoic chronicle is a geocryological interpretation of the Baikal diatomic record[1] [*Karabanov et al., 2000*]. The Late Cenozoic chronicle (Fig. 1) clearly presents time spans within the late Pliocene–Holocene cryogenic period comprized by three cold epochs separated by longterm warm climatic epochs [*Fotiev, 2005*]. The beginning of the Pliocene–Holocene cryogenic period in Siberia coincided with the onset of a stable climate cooling in the Pacific [*Shackleton et al., 1990; Fotiev, 2005*].

First Pliocene cryogenic epoch (3.10–3.08 Ma) was the shortest (only 20 kyr) and the least cold. Judging by the diatom percentage (less than 20 %)[2] it was during that time that the climatic setting provided perennial freezing and formation of permafrost[3]. The mean annual air temperature (T_a) was 3–5 °C lower than that at present. High-temperature (0 to −3 °C), thin (0–100 m), and discontinuous or sporadic permafrost was formed in southern Siberia. At the same time, in northern Siberia, both climate and geocryologic setting were probably severer and permafrost continuous[4].

Between 3.08 and 2.82 Ma BP, when the diatom percentage increased to 48–60 % (with a peak at 2.9 Ma), the climate was relatively warm (Fig. 1). During the 250 kyr time span, permafrost degraded fully or partly in southern Siberia, while no thawing from the surface occurred in the colder northern areas of Siberia. The mean annual ground temperature (T_g) varied considerably though within negative interval.

Second Pliocene cryogenic epoch (2.82–2.47 Ma) was marked by the coldest climate and severest geothermal settingof the entire cryogenic period (Fig. 1) [*Fotiev, 2009*]. There are reasons to hypothesize that the climate became colder as the orogenesis in Eurasia (the Sayan, Altai, Himalaya, Pamir, and Tien Shan mountain systems) impeded the transport of warm and wet air from the Indian ocean. Many scientists agree that the Late Pliocene cooling correlates with the oldest glaciations in the mountains of Transbaikalia, Altai, and Sayan and with the earliest glacial clay deposition marked by iceberg rafting signature in the Baikal lake sediments. Yet, no traces of these old glaciations have been discovered [*Karabanov et al., 2001; Kuz'min et al., 2001a; Williams et al., 2001*].

The second cryogenic epoch, in turn, consisted of nine chrons: five cryochrons and four thermochrons (Fig. 1). The climate of cryochrons was cold or very cold, according to diatom data (0–2 %), with a peak at 2.60–2.63 Ma, and was even colder than during the Sartan time. The mean annual air temperature was 10–15 °C colder than it is now. Permafrost was low-temperature, thick, and continuous, even in southern Siberia, in northern Siberia, continuous permafrost was as cold as −30 °C and thick (>300 m).

[1] The Baikal continuous climate chronicle of the past 5 Myr has been obtained in the course of exhaustive studies of the lake sediments by a large team involved in the Baikal Drilling Project (BDP) [*Bezrukova et al., 1999; Karabanov et al., 2000, 2001; Williams et al., 2001; Kuz'min et al., 2001a, b; Khursevich et al., 2001; Prokopenko et al., 2001*].

[2] For more details of geocryological interpretation of the Baikal climate chronicle see [*Fotiev, 2005, 2009*].

[3] Permafrost is the rock strata with temperature below 0 °C, and comprises frozen, cryotic and dry frozen deposits.

[4] The latitude zoning of climate parameters held all over the cryogenic period.

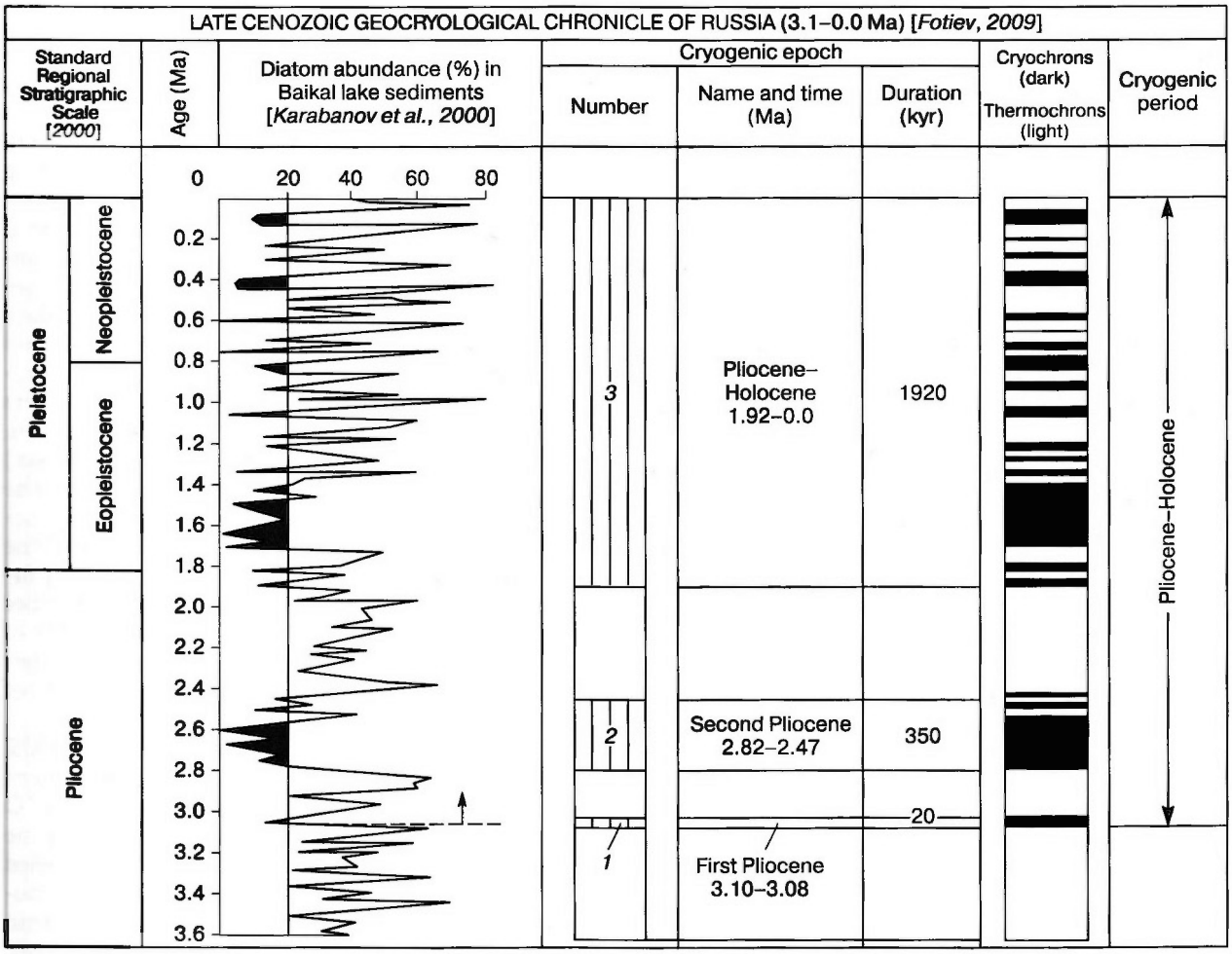

Fig. 1. Late Cenozoic geocryological chronicle of Russia (3.1–0.0 Ma).

Diatom abundances averaged over five data points [*Karabanov et al., 2000*].

The thickness of permafrost exceeded the thickness of **freshwater zone** in artesian basins and hydrogeological **massifs (aquifers)**. Two layers of frozen and cryotic **rocks** with cryopegs formed in artesian basins, **and layers** of frozen rocks and dry permafrost were **formed in hydrogeological** massifs [*Fotiev, 1978*]. This **permafrost** structure in the subsurface of the Siberian **Platform** has persisted till present. Relatively low **diatom** percentage (19–25 %) indicate quite a cold **climate** during thermochrons. The permafrost formed **during** cryochrons never degraded even in southern **Siberia** where it persisted continuously over 350 kyr **(Fig. 1)**.

In the northern part of permafrost zone[5] T_g **though** increased significantly during thermochrons **yet remained** negative, and the permafrost never **thawed from the** surface. Permafrost degradation **from below** was negligibly small because of low heat flux and abundant cryopegs within the layer of cryotic rocks. Permafrost in West Siberia apparently degraded from below more rapidly as the heat flux was higher [*Kurchikov, Stavitsky, 1987; Balobaev, 1991*].

The interval of 2.47–1.92 Ma (the end of Late Pliocene) in southern Siberia was an over 500 kyr spell of moderately warm to warm climate, as indicated by a relatively high (25–65 %) production of diatoms (Fig. 1). The permafrost that formed during the second Pliocene cryogenic epoch fully or almost fully degraded. However, the rather strong and long climate warming did not cause degradation of permafrost from above in the northern areas, though the negative T_g increased markedly.

Third Pliocene–Holocene cryogenic epoch (1.92–0.0 Ma) started 1.92 Ma ago when the diatom percentage in the Baikal lake sediments decreased to 10–12 %, and is ongoing (Fig. 1) [*Fotiev, 2005, 2009*].

[5] Permafrost zone – area extent of the rock strata with temperature below 0 °C.

In the beginning of this cryogenic epoch, there were two short and relatively warm cryochrons during which permafrost formed in southern Siberia.

The interval between 1.75 and 1.40 Ma BP (the first half of Eopleistocene, according to the Russian stratigraphic code) was an epoch of a very cold climate as follows from the Baikal diatomic chronology (Fig. 1)[6]. The epoch is subdivided into seven chrons: four cryochrons and three thermochrons (Fig. 1). During the cryochrons, T_a was 10–15 °C lower than the present one. Low-temperature (up to −10 °C) thick continuous permafrost formed even in the southernmost regions of Siberia. During the extremely cold cryochrons southern limit of permafrost area extended as far as Mongolia and China. Therefore, no zones of discontinuous or sporadic permafrost existed in the southern part of the Siberian Platform. In northern Siberia, T_g decreased to −30 °C or lower, and permafrost thickness likely exceeded 500–700 m. Permafrost degradation during the thermochrons was incomplete even in southernmost Siberia as the climate remained relatively cold (diatoms percentage as low as 12 to 25 %). Therefore, during the first half of Eopleistocene permafrost persisted continuously for at least 350 kyr even in southern Siberia.

The second half of the Eopleistocene and in Neopleistocene was a period of rather variable climate in southern Siberia judging by dramatic and essential variations in diatom percentages between 0 to 80 % (Fig. 1). The climatic and geocryological setting during cryochrons were almost as cold as those in the first half of Eopleistocene, while climate of thermochrons wes much warmer. During extremely warm thermochrons when the diatom production increased to 80 % (peak at 1.01 Ma BP), T_a was 3–4 °C warmer than now, and permafrost in southern areas degraded rapidly from both above and below (Fig. 1). In the northern Siberia with its severe climate T_g remained very low during both cryochrons and thermochrons varying within the negative interval and aggrading from below.

NEOPLEISTOCENE (BRUNHES EPOCH) GEOCRYOLOGICAL CHRONICLE (0.8–0.0 Ma)

The geocryological chronicle is based on the interpretation of the Baikal biogenic silica ($SiO_{2\ biog}$) record (Fig. 2) [*Prokopenko et al., 2001; Fotiev, 2005, 2009*]. The Neopleistocene geocryological chronicle thirty nine well pronounced chrons are subdivided: 20 cryochrons and 19 thermochrons (Fig. 2). The cryochrons (with negligibly low $SiO_{2\ biog}$) look like U-shaped troughs in the $SiO_{2\ biog}$ chronicle, with flat or inclined floors, while the thermochrons (more than 80 % $SiO_{2\ biog}$) appear as prominent sharp peaks [*Karabanov et al., 2001; Prokopenko et al., 2001*]. This pattern is a clear evidence of a steadiness of severe climate in cryochrons and abrupt dramatic warming during thermochrons.

Compiling the geocryological chronicle required the use of three chronologies. The 39 chrons distinguished by the author in the Neopleistocene of Siberia (20 cryochrons and 19 thermochrons) correlate with 19 marine isotope stages (MIS) with 10 cold and 9 warm stages of the oxygen isotope ($\delta^{18}O$) stratigraphy (Fig. 2) [*Shackleton et al., 1990*]. The time limits of some chrons perfectly match the MIS boundaries, but some isotope stages comprise several (up to six) distinct cryochrons and thermochrons[7], which the $\delta^{18}O$ stratigraphy actually misses. The generally accepted Standard Regional Stratigraphic Scale of the Quaternary of the West Siberian Plain [*2000*] includes 14 horizons (epochs), i.e. less than the number of MIS. In order to cancel this disparity, some MIS of different ages were in some models brought together [*Fotiev, 2009*], which distorted the age bounds of some intervals.

The model suggested by the author [*Fotiev, 2005, 2009*], is based on the correlation of the northern West Siberian glacials and interglacials with the $\delta^{18}O$ scale after [*Karabanov et al., 2001*]; the gaps in the latter chronology (MIS 9, 10, 12, 13, 19) are labeled with conventional names. Cryochrons and thermochrons are distinguished [*Fotiev, 2005, 2009*] within the age limits of each MIS [*Shackleton et al., 1990*], and correlated with the respective intervals of the regional stratigraphy (Fig. 2).

The time between 800 and 426 kyr BP (Early Neopleistocene) in Siberia included 17 chrons (9 cryochrons and 8 thermochrons) corresponding to eight (four cold and four warm) marine isotope stages. The Middle Neopleistocene interval 426–127 kyr BP comprise 18 chrons (9 cryochrons and 9 thermochrons) correlated with six (3 cold and 3 warm) stages of the marine $\delta^{18}O$ stratigraphy. The Late Neopleistocene from 127 to 11 kyr BP is divided into four chrons (2 cryochrons and 2 thermochrons) that correspond to four (two cold and two warm) MIS. The West Siberian Karginian warm cycle (MIS-3) does not show up in the Baikal biogenic silica record[8] (Fig. 2), and that was the reason why MIS-4, MIS-3, and MIS-2 were joined into a single Zyryanka–Sartan cryochron.

Low $SiO_{2\ biog}$ contents in the Baikal lake sediments indicate several coldest and longest cryochons

[6] Extremely low diatom percentages of 0–3 % (the lowest at 1.63 Ma) indicate a climate and geothermal setting colder than during the Sartan time.

[7] These climate oscillations are most often attributed to orbital forcing [*Kuz'min et al., 2001b*].

[8] According to some models [*Baulin et al., 1981*], the zone of permafrost degradation from the surface extended in southern West Siberia as far as 65–66° N during the optimum of the Karginian warm stage.

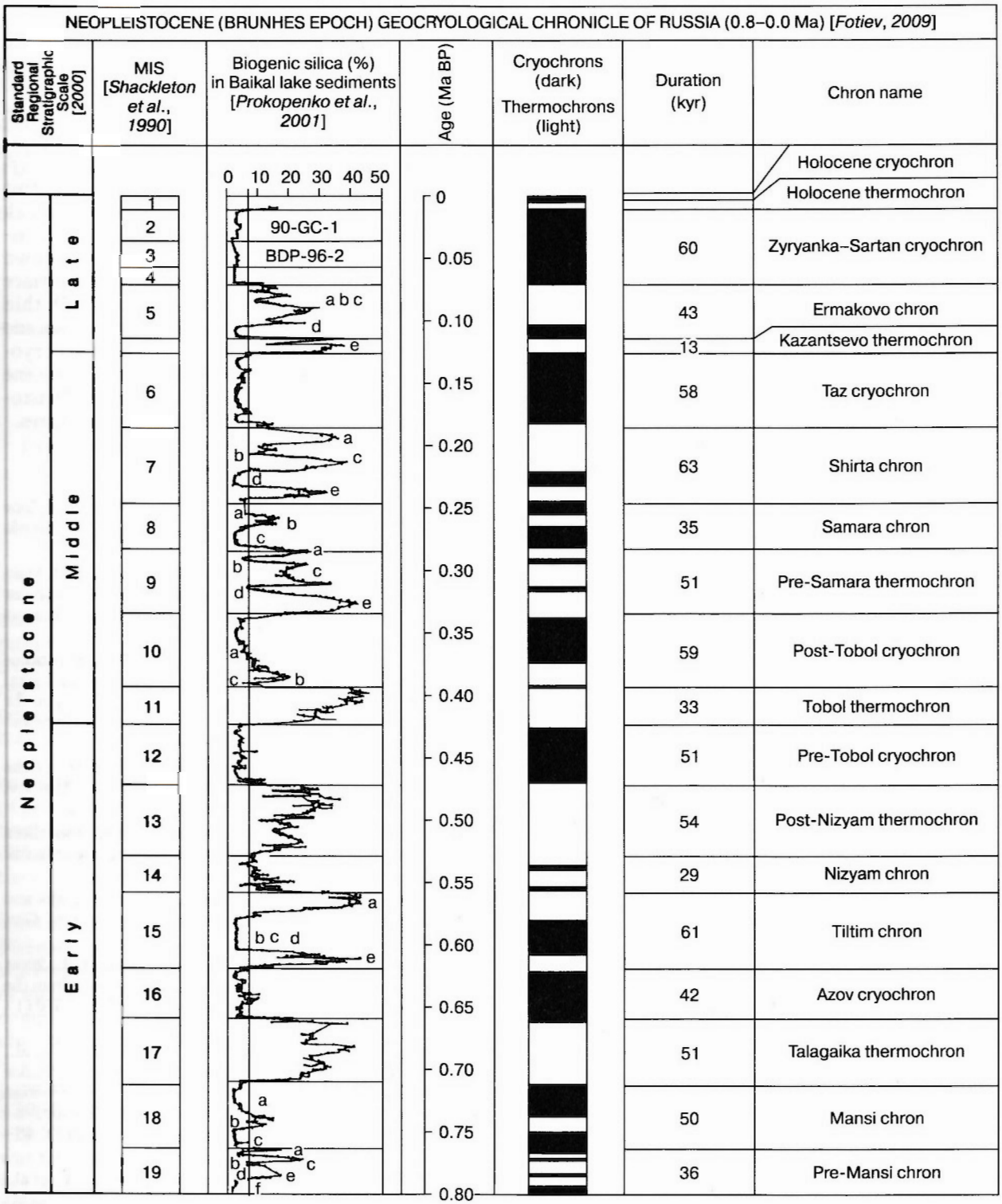

Fig. 2. Neopleistocene (Brunhes epoch) geocryological chronicle of Russia (0.8–0.0 Ma).

in Neopleistocene, namely (Fig. 2), Asov (MIS-16) and pre-Tobol (MIS-12) in the early Neopleistocene, post-Tobol (MIS-10a), Samara (MIS-8c), and Taz (MIS-6) in the Middle Neopleistocene, and the Zyryanka-Sartan (MIS-4, MIS-3, MIS-2) in the Late Neopleistocene. The climatic and geocryological setting during the extremely cold Neopleistocene cryochrons were as follows [*Fotiev, 2009*]: (1) T_a throughout the permafrost area was 8–15 °C lower than that at present; (2) long-lasting, low-temperature (–3 to –25... –30 °C), thick (from 300 to 700–1500 m) and continuous permafrost formed over the entire permafrost area; (3) zones of high-temperature (0 to –3 °C), thin (0 to 150 m) and discontinuous (including sporadic) permafrost were outside the region in West Siberia and were absent from East Siberia as the southern permafrost extent reached the territory of Mongolia and China; (4) the subaerial permafrost area was of the largest extent due to perennial frozen ground in the emerged shelf and southern margins of permafrost area. It extended from 47 to 78° N (over 3300 km) along the 70° E meridian, and from 52 to 79.5° N or over 3000 km along 105° E (excluding the southern mountains and the northern islands).

According to relatively high contents of $SiO_{2\,biog}$ in the sediments of Lake Baikal, the warmest and longest were (Fig. 2) the Talagaika (MIS-17) and post-Nizyam (MIS-13) thermochrons in the Early Neopleistocene, the Tobol (MIS-11) and Shirta (MIS-7) thermochrons in the Middle Neopleistocene, and the Kazan (MIS-5e) in the Late Neopleistocene (127–114 kyr BP). The extremely warm thermochrons of Neopleistocene were characterized by the following climate and permafrost-related features [*Fotiev, 2009*]: (1) T_a was 2–4 °C higher than now and dramatically (10–15 °C) higher than during the previous cryochrons; (2) permafrost degraded completely in the southern and partly in the central part of permafrost area; (3) permafrost did not degrade from the surface in the northern permafrost area where the climate was still cold, though T_g increased considerably remaining however below zero; (4) permafrost degraded partly from the surface only in submerged limnic environments; (5) the N–S extent of permafrost decreased as a result of marine transgression and complete permafrost degradation in the southern regions.

The Holocene comprises two chrons (Fig. 2) subdivided according to the specific features of cryogenic metamorphism. T_a during the thermochron from 11.0 kyr BP to the end of t he thermal optimum[9] rose 10–15 °C higher than in the minimum of the Sartan thermal minimum almost all over the permafrost area. Nevertheless, active permafrost degradation (full or partial), both from above and from below, was limited to the plains of southern Siberia. In the northern part of permafrost area, T_g was rising essentially but remained negative, partial degradation of permafrost was restricted to areas underneath numerous thermokarst lakes. During the cryochron from the end of the thermal maximum to present, T_g became 3–5 °C lower than in the thermal optimum on all over the permafrost area; high-temperature, thin, and discontinuous or sporadic permafrost formed in central and southern regions of Siberia.

The boundary between the Northern and Southern geocryological zones is quite prominent at present and coincides with the link up of permafrost layers of Holocene and Pleistocene ages. The permafrost is low-temperature (–2 to –13 °C or lower), thick (300 to 1500 m), continuous, predominantly of Pleistocene age north of this boundary, sinking down southward of this boundary, replaced in the surface layer by mainly high-temperature (0 to –2 °C), thin (0 to 150 m), discontinuous, permafrost of Holocene age. In the northern part of the Southern geocryological zone, within the artesian basins the Holocene permafrost is separated from the deep-seated Pleistocene permafrost by a layer of positive temperatures.

References

Balobaev V.T., 1991. The Thermal Field of the Permafrost Zone in the North Asian Lithosphere [in Russian]. Nauka, Novosibirsk, 193 pp.

Baulin V.V., Chekhovsky A.L., Sukhodolsky S.E., 1981. Main evolution stages of permafrost in Russian European Northeast and in West Siberia, in: The History of Permafrost in Eurasia [in Russian], Nauka, Moscow, pp. 41–60.

Bezrukova E.V., Kulagina N.V., Letunova P.P., Shestakova O.N., 1999. Climate and vegetation changes in the Baikal region for the last 5 Ma, according to palynological data on the Baikal sediments. Geologiya i Geofizika (Russian Geology and Geophysics), 40 (5), 739–749 (722–731).

Fotiev S.M., 1978. The Hydrogeothermal features of the permafrost area of the USSR [in Russian]. Nauka, Moscow, 236 pp.

Fotiev S.M., 2005. Cryochrons and thermochrons of southern Siberia for the past 5 Ma: Paleogeographic implications of Baikal lake sediment data. Kriosfera Zemli, IX (1), 13–27.

Fotiev S.M., 2009. Cryogenic Metamorphism of Rocks and Groundwater: Conditions and Consequences [in Russian]. Geo, Novosibirsk, 279 pp.

Karabanov E.B., Kuz'min M.I., Williams D.F., et al., 2000. Late Cenozoic global cooling in Central Asia: evidence from the sedimentary chronicle of Lake Baikal. Dokl. Earth Sci., 370 (1), 61–66.

Karabanov E.B., Prokopenko A.A., Williams D.F., et al., 2001. Glacial and interglacial periods of Siberia: the Lake Baikal paleoclimatic chronicle and correlation with West Siberian stratigraphic scheme (the Brunhes Chron). Geologiya i Geofizika (Russian Geology and Geophysics), 42 (1), 48–63(41–54).

Khursevich G.K., Karabanov E.B., Prokopenko A.A., et al., 2001. Detailed diatom biostratigraphy of Baikal sediments during the Brunhes chron and climatic factors of species formation. Geologiya i Geofizika (Russian Geology and Geophysics), 42 (1), 108–129 (97–116).

[9] The ages and durations of the Holocene climate optimum varied over the permafrost area.

Kurchikov A.R., Stavitsky B.P., 1987. Heat Flow in Petroleum Provinces of West Siberia [in Russian]. Nedra, Moscow, 134 pp.

Kuz'min M.I., Karabanov E.B., Kawai T., et al., 2001a. Deep drilling on Lake Baikal: main results. Geologiya i Geofizika (Russian Geology and Geophysics), 42 (1), 8–34 (3–28).

Kuz'min M.I., Karabanov E.B., Prokopenko A.A., et al., 2001b. Late Cenozoic rhythms and climate change in Asia, from Baikal Deep Drilling data, in: Global Change [in Russian]. Izd. SO RAN, Filial "Geo", Novosibirsk, pp. 146–159.

Prokopenko A.A., Karabanov E.V., Williams D.F., et al., 2001. Biogenic silica chronicle of the Lake Baikal response to the climatic forcing during the Brunhes. Quatern. Res., 55, 123–132.

Shackleton N.J., Berger A., Peltier W.R., 1990. An alternative astronomical calibration of the Lower Pleistocene time scale based on ODP site 677. Trans. Roy. Soc., Edinburgh, Earth Sciences, 81, 251–261.

The Standard Regional Stratigraphic Scale of the Quaternary of the West Siberian Plain [in Russian]. SNIIGGiMS, Novosibirsk, 2000, 64 pp.

Williams D.F., Karabanov E.B., Prokopenko A.A., et al., 2001. The Late Pliocene–Pleistocene sedimentary chronicle of Lake Baikal: benchmarks for paleoclimatic and biostratigraphic reconstructions. Geologiya i Geofizika (Russian Geology and Geophysics), 42 (1), 35–47 (29–40).

Received
5 March 2011

Kriosfera Zemli, 2011, vol. XV, No. 4, pp. 13–16 http://www.izdatgeo.ru

PERMAFROST RESPONSE TO CLIMATE WARMING

V.N. Konishchev

Lomonosov Moscow State University, Department of Geography, 1, Leninskie Gory, Moscow, 119991, Russia; vkonish@mail.ru

The response of permafrost to global Late Pleistocene–Holocene warming has been investigated in the ice complex of Yakutia. Thermokarst erosion of the complex was found out to depend on the properties of landscape and its components that change as a consequence of warming. In addition to the degradation tendency, aggradational stabilization in ice complex remnants may occur in certain conditions as formation of a protective layer.

Any external effect on permafrost, including climate, is never direct, unlike on a glacier surface, but is rather mediated by the overlying vegetation, soil, active layer, i.e., by various landscape components. The resulting positive and negative feedbacks control the permafrost responses which differ in intensity and may show unexpected trends.

Changes in surface conditions attendant with warming or cooling may change the evolution trend of permafrost and cause its aggradation or degradation. They may act either together with or against the climate trend and, correspondingly, amplify or damp the climate effect [*Koreisha et al., 1997*].

An illustrative example in this respect may come from dynamics of the ice complex over the latest Pleistocene–Holocene interval. An ice complex (IC) is a complex of syngenetically frozen sediments, tens of meters thick, which are thermally unstable. Such complexes were deposited in harsh Late Pleistocene climates between 50–40 and 12–11 kyr BP.

At that time, the mean annual temperature of permafrost was as low as −25...−28 °C or locally −30 °C in northern Yakutia and no warmer than −10 °C in central Yakutia, while the air temperature was naturally still lower [*Konischev, 1997*]. The map in Fig. 1 shows the extent of the Yakutian ice complex except shelf where it was destroyed by the Holocene transgression of the Arctic seas.

The dramatic climate change at the Last Glacial–Holocene boundary caused permafrost warming and gave rise to thermokarst erosion of the ice complex, which has been the main evolution process in its terrain-forming deposits through the past 13–12 kyr.

The basic landforms in the present North and Central Yakutian coastal lowland include, besides river valleys, the so-called *yedomas* (IC remnants) and *alas* depressions (result of subsidence of thawed permafrost) that reach surface areas of tens of square kilometers. Alases occupy up to 75 % of the northern Yakutian coastal plains [*Lomachenkov et al., 1965; Bosikov, 1978*] and up to 50 % in central Yakutia [*Ivanov, 1981*].

Although being approximate, these estimates indicate that the ground surface composed of IC deposits is more strongly affected by thermokarst processes in northern Yakutia than in its central part. The reason is that alases in both northern and central areas of Yakutia result from water ingression (showing up as the number and sizes of lakes) rather than from climate warming per se or from other temperature agents.

The glacial deposition completed in the end of the last cryochron (Last Glacial), and the top surfaces of its remnants (yedomas) generally have experienced no denudation since then. This inference follows from many radiocarbon dates showing latest Pleistocene ages of the youngest IC deposits [*Ivanov, 1981; Kaplina, 1981*]. Therefore, through the Holocene the IC deposits have been subject to different alteration trends [*Shur, 1988*].

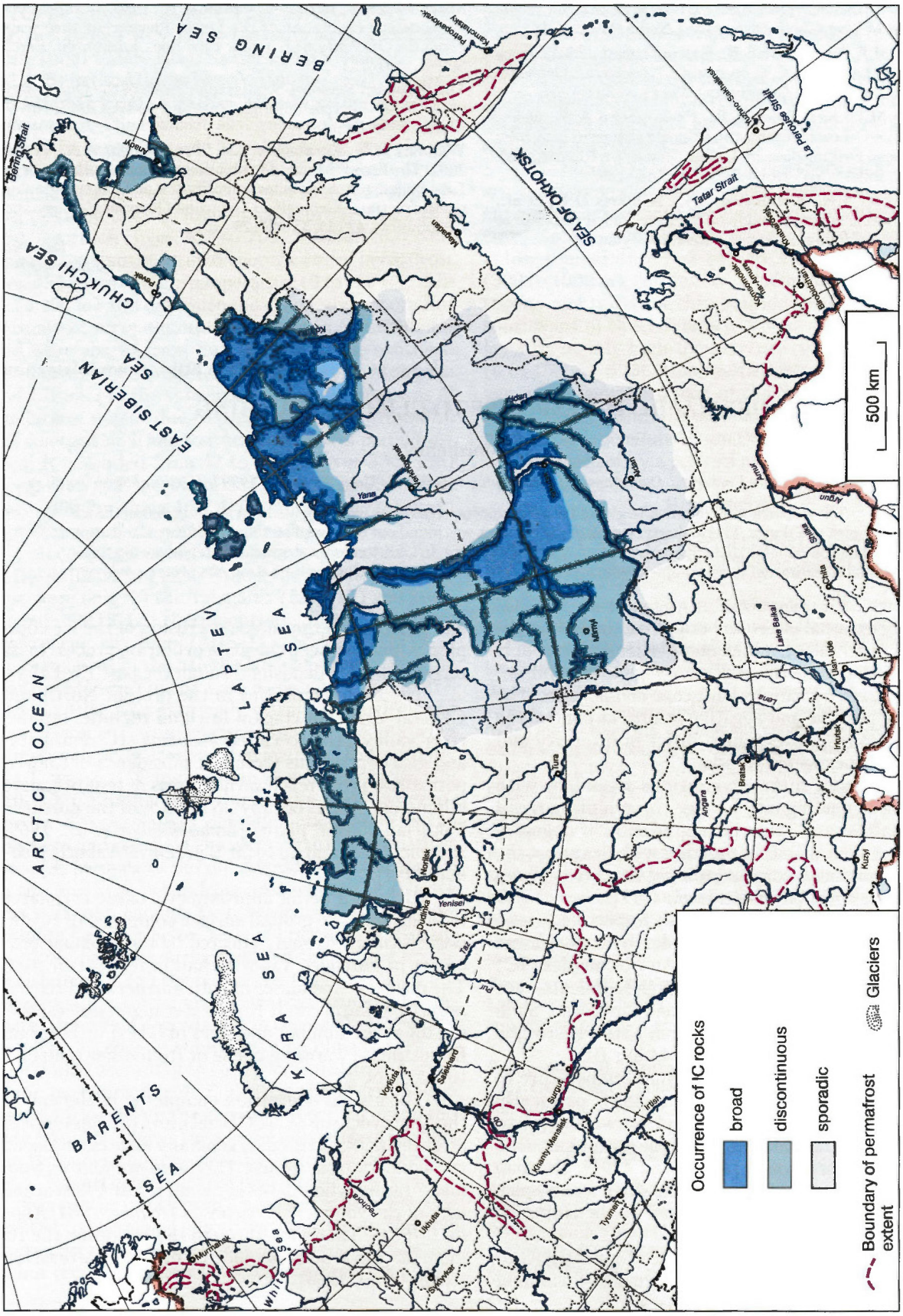

Fig. 1. Map of ice complex.
Compiled by V.N. Konishchev and N.A. Koroleva after [*Romanovsky, 1993; Konishchev, 1997; Kunitsky, 2007; Streletskaya et al., 2007*].

Some factors acted in latest Pleistocene–Holocene time that preserved the IC remnant top surfaces and made them more stable.

Since the 1940s, it has been understood that there exists a protective layer underneath the active layer [*Efimov and Grave, 1940*], namely, a 1.5–2.0 m thick frozen layer was found under thick forest between alases in Central Yakutia. However, deforestation increased the thaw depth by 30–40 % (originally 1.3–1.4 m) and the protective layer started thawing.

The protective layer is widespread on IC remnant surfaces in northern coastal plains as well but has been referred to in different ways: either a "cover" [*Kaplina, 1981*] or a "transition" layer [*Shur, 1984*].

This layer is remarkable by a very high ice content (up to 60–70 %) and by massive-agglmerate or reticulate cryostructures. It is most often silty and has a thickness of 1.5–1.7 m.

The origin of the protective layer is controversial. It was interpreted as a remnant from the Holocene climate optimum [*Kaplina, 1981; Konchenko, 1999*], but there are views [*Gravis, 1969; Torgovkin, 1988; Shur, 1988*] that the thaw depth in the Holocene decreased rather than increasing because of greater soil moisture contents and profuse growth of hydrophilic vegetation (moss and subshrubs).

The effect of landscape changes was to decrease the thaw depth in unthawed areas through the Holocene history of the ice complex, after its deposition had been completed. As a result, the permafrost surface became shallower and there formed an ice-rich transition layer [*Shur, 1988*].

Another essential agent is moisture migration from the active layer into the upper permafrost, which has been well studied both in field and in laboratory [*Parmuzina, 1978; Ershov, 1979; Konstantinov, 1991*].

The ice-rich transition cover is widespread on IC surfaces and is an important screen that protects permafrost from various effects of climate warming, including temperature variations. That is why *protective* (the original term from [*Efimov and Grave, 1940*]) appears to be a better name than *cover* or *intermediate* for the layer of high ice content in the upper permafrost.

The destructive effect of the Holocene warming and the thermokarst erosion of IC deposits is only one component of the permafrost response to climate change. Another component is stabilization as a consequence of physiographic changes such as increasing soil moisture, growth of hydrophilic moss, or accumulation of soil organic matter.

It is owing to the protective layer, that a great part of the ice complex has survived through more than 10 kyr and remains an important environment control of permafrost-related landscapes and ecology over a vast territory of East Siberia.

In northern Yakutian coastal, the protective layer formed when the temperature rise from −22...−28 to −8...−10 °C allowed moisture migration from the active layer into the underlying frozen ground. In Arctic areas, it is as thin as 0.4–0.5 m and cannot prevent the ground below it from thawing associated with active layer dynamics. As a result, the upper ice complex becomes prone to destruction, such as, for instance, the Yedoma section of the Oiyagos Yar which misses Sartan strata (an effect called *frontal thermal planation* in [*Tomirdiaro and Chernenkii,1987*]). On the contrary, the ice complex degrades very little from the surface in areas further to the south, as far as southern Yakutia, where the protective layer thickens up to 1.5–2.0 m.

In addition to the reported physiographic features of alas formation, the protective layer is subject to spatial inversion.

References

Bosikov N.P., 1978. Alas distribution in central Yakutia, in: Periglacial Conditions in Highland and Plainland Asia [in Russian]. Institute of Permafrost, Yakutsk, pp. 113–118.

Efimov G.F., Grave N.A., 1940. Buried ice in the area of lake Abalakh. Sots. Stroitelstvo, Nos. 10–11, 67–78.

Ershov E.D., 1979. Moisture Transport and Cryostructures of Fine-Grained Rocks [in Russian]. Moscow University Press, Moscow, 214 pp.

Gravis G.F., 1969. Slope Wash Deposits of Yakutia [in Russian]. Nauka, Moscow, 128 pp.

Ivanov M.S., 1981. The Cryostructure of Quaternary Deposits in the Lena-Aldan Basin [in Russian]. Nauka, Novosibirsk, 125 pp.

Kaplina T.N., 1981. The Late Cenozoic history of permafrost in northern Yakutia, in: The History of Permafrost in Eurasia [in Russian], Nauka, Moscow, pp. 153–181.

Konchenko L.A., 1999. Peculiarities of spatial changes of the thickness of active layer under climate warming (from cryolithological data). Kriosfera Zemli, III (4), 32–38.

Konishchev V.N., 1997. The cryolithogenic method for estimating paleotemperature conditions during formation of ice complex and subaerial periglacial sediments. Kriosfera Zemli, I (2), 23–28.

Konstantinov S.A., 1991. Formation of the structure of upper permafrost in the southern Gyda Peninsula. Vestnik Moscow Univ., Ser. 5. Geogr., No. 4, 48–53.

Koreisha M.M., Vtyurin B.I., Vtyurina E.A., 1997. Underground ice and icing, in: World Snow and Ice Resources. An Atlas [in Russian]. IG RAN, Moscow, Volume 2, Book 2, pp. 9–32.

Kunitsky V.V., 2007. Nival Lithogenesis and the Ice Complex of Yakutia [in Russian]. Author's Abstract, Doctor Thesis, Yakutsk, 46 pp.

Lomachenkov V.S., 1965. Neotectonic structures in the present topography of the Yana-Indigirka coastal plain and the adjacent shelf, in: The Anthropogene in Arctic and Subarctic Areas [in Russian]. Nedra, Moscow, pp. 115–121.

Parmuzina O.Yu., 1978. The cryogenic structure and some features of ice separation in the active layer. Problems of Cryolithology, Transactions, Moscow University, Moscow, Issue 7, 141–164.

Romanovsky N.N., 1993. Fundamentals of Cryogenesis in the Lithosphere [in Russian]. Moscow University, Moscow, 335 pp.

Shur Yu.L., 1984. The intermediate layer, in: Periglacial Physical-Geological Processes: Fundamentals of Modeling [in Russian]. Nauka, Moscow, pp. 40–54.

Shur Yu.L., 1988. Upper Permafrost and Thermokarst [in Russian]. Nauka, Novosibirsk, 212 pp.

Streletskaya I.D., Gusev E.A., Vasiliev A.A., et al., 2007. New results of Quaternary sediment studies of Western Taimyr: New data. Kriosfera Zemli, XI (3), 14–28.

Tomirdiaro S.V., Chernenkii B.I., 1987. Cryogenic-aeolian deposits in Eastern Arctic and Subarctic Areas [in Russian]. Nauka, Moscow, 197 pp.

Torgovkin Ya.I., 1988. Some features of the cryogenic structure of the ice complex in the Kolyma Plain, in: Studies of Permafrost and Periglacial Phenomena [in Russian]. Institute of Permafrost, Yakutsk, pp. 97–100.

Received
4 February 2011

Kriosfera Zemli, 2011, vol. XV, No. 4, pp. 16–21 **http://www.izdatgeo.ru**

BURIED SNOW IN THE LENA-AMGA PLAIN

V.B. Spektor, V.V. Spektor, N.T. Bakulina*

Melnikov Permafrost Institute, Siberian Branch of the Russian Academy of Sciences, 36, Merzlotnaya str., Yakutsk, 677010, Russia; vspektor@mail.ru
** State Committee of the Sakha Republic (Yakutia) on Geology and Mineral Resources, State Unitary Enterprise "Centrgeoanalitika", 13, Kirova str., Yakutsk, 677000, Russia*

Some new forms of buried stratified ice have been discovered in the Late Pleistocene section of the Lena-Amga Plain (Central Yakutia, Russia) in the course of core drilling at several watershed sites elevated to 220–250 m asl. The buried ice, which belongs to the traditionally distinguished ice complex, makes three separate layers of firn (snow recrystallized to difference degrees), at the depths 12.0 to 17.0, 23.3 to 24.5, and 33.6 to 39.0 m below the ground surface lying under wedge ice found in the uppermost section between 2.5 and 5.0 m. The firn layers are separated by syngenetically frozen sandy silt and silt.

INTRODUCTION

Buried ice is widespread in plainland Central Yakutia, especially in the Lena–Amga–Aldan interfluve (Lena-Amga Plain) where it belongs to the ice complex [*Soloviev, 1959; Katasonov, 1975, 1979; Ivanov, 1984*]. The ice complex of the area consists of up to 70–80 m thick fine-grained sediments that bear frozen water in the form of ice wedges and structure-forming ice. The total permafrost thickness reaches hundreds of meters, the upper layer of at least 100 m being syngenetically frozen ground.

More evidence of the composition, age, and geomorphic setting of the ice complex has been obtained recently through core drilling in the Lena-Amga Plain, at altitudes 220–250 m asl (Fig. 1), run by the Institute of Permafrost (Yakutsk) [*Spektor and Spektor, 2002*].

Boreholes drilled at several sites of the plain near watersheds stripped previously unknown forms of buried stratified ice which turned out to be snow recrystallized to difference degrees (firn). The discovery of firn ice in drill sections, a very important outcome of the drilling project, provides clues to the Late Pleistocene climate in the area and has additional implications for the origin of the ice complex.

FIELD DATA

The most complete section with different forms of buried ice was found in the borehole drilled in 2004 at 62°08′ N, 131°18′ E, 82 km east of Yakutsk city. The experiment of 2004 consisted in core drilling with successive bit diameters of 147, 127, 108, 89, and 76 mm, and core recovery using an air-flushing system. Thus obtained undisturbed core material selected for further studies was then transported, in the frozen state, to an underground laboratory of the Institute of Permafrost (Yakutsk).

The core section included three ice layers of different thicknesses: wedge ice in the uppermost part at 2.5–5.0 m below the ground surface and two firn layers at 12.0–17.0 m and 33.6–39.0 m separated by syngenetically frozen sandy silt and silt [*Spektor et al., 2008*].

Another hole drilled in 2011 three meters off the former one provided more details of the section as it tapped layered ice at two depth intervals of 13.5–14.2 m and 23.31–24.50 m below the ground surface. Additionally, the upper and lower snow cover was sampled above the hole (5–10 and 30–40 cm below the snow surface, respectively, the total snow thickness at the time of 19.03.2011 being 43 cm).

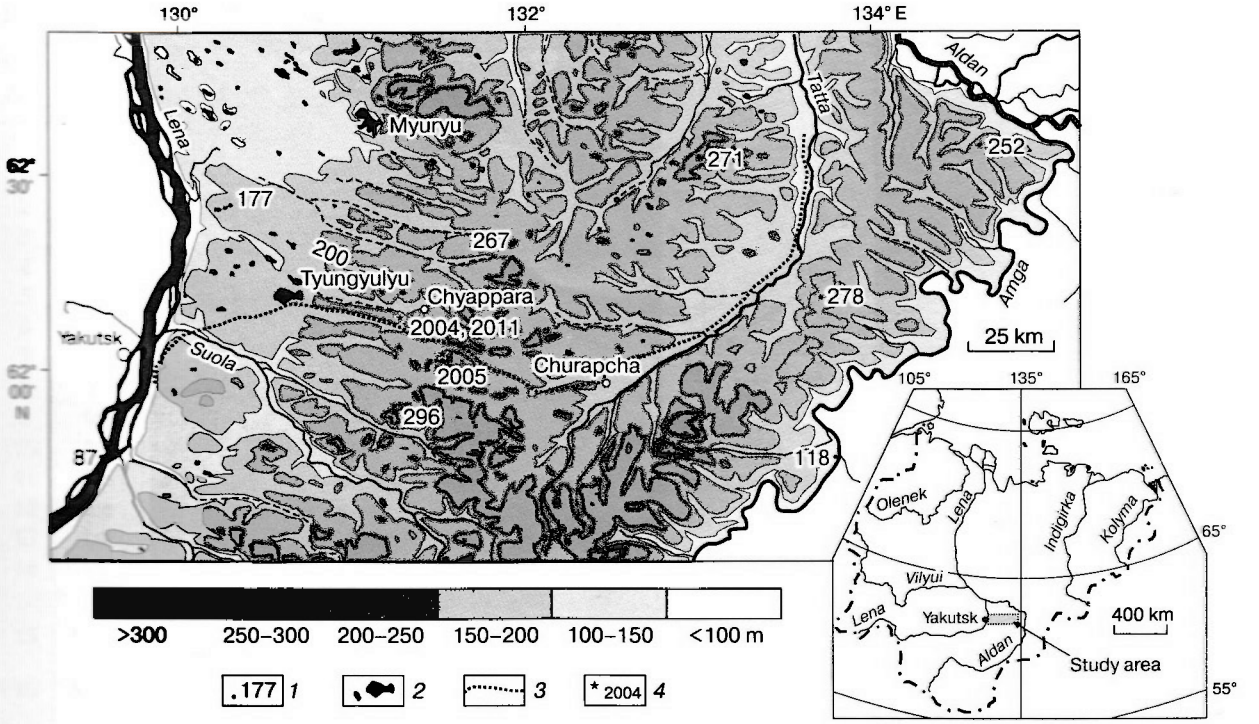

Fig. 1. Location map of boreholes in the Lena-Amga Plain (Central Yakutia).

1 – elevations, meters above sea level; *2* – lakes; *3* – roadway; *4* – boreholes.

One more borehole, which was drilled in 2005 at 94 km east of Yakutsk (62°04′ N, 131°33′ E), stripped firn buried at 2.8–8.2 m below the surface. This firn layer correlates with the 33.6–39.0 m interval of the 2004 borehole in its stratigraphic position, structure, and texture.

The ice layers in the drill section of 2004 were as follows.

Uppermost layer (2.5–5.0 m): wedge ice. The stripped ice wedge is at least 30 cm wide and about 2.5 m thick. Ice is transluscent and yellowish, has a vertical banded texture (1–2 cm wide bands), and encloses various mineral and organic lenses and elongate gas bubbles.

Upper firn layer (12.0–17.0 m): thinly stratified ice with very fine, fine, or less often coarse particles (Fig. 2, *a*). In our view, this ice type may result from recrystallization of buried snow. Buried snow within this depth interval is poorly compressed and weakly recrystallized, and shows intricate stratification. The whole firn layer consists of several smaller banded layers of (i) 3–5 cm thick pure banded firn, (ii) 1–2 cm thick banded firn with soil, and (iii) 1–4 cm thick brecciated and coarse-crystalline firn (Fig. 2, *b*).

The compacted snow layer includes tentatively distinguished annual cycles consisting of pure white snow (formed in wet and warm seasons) and grayish snow with mineral particles (dry and cold season). Each cycle is 2–3 mm thick, with about 20 such cycles in a banded layer, i.e., there were at least 20 year-long spells of harsh climate.

The 1–3 cm thick layers of coarse-crystalline firn consist of up to 5 mm round or rectangular ice crystals with molten edges. There are pieces of columnar upright ice crystals, which is typical of firn glaciers.

Lower firn layer (33.6–39.0 m): stratified ice, slightly denser and more strongly recrystallized than that in the upper layer. In the lower portion of the interval, ice layers alternate with frozen silt which, in turn, grades into lens-type or reticulate ice-rich soil.

The section of the 2011 borehole drilled near that of 2004 included two layers of stratified ice we sampled: one between 13.5 and 14.2 m and the other between 23.31 and 24.50 m below the surface. It was coarse-crystalline ice with its structure similar to that of the lower firn layer at 33.6–39.0 m (see above).

The uppermost section contained wedge ice 2.5 m below the surface lying under massive light brown silt and a thin soil layer at the top. Between the ice (firn) layers, the drill hole tapped syngenetically frozen silt and sandy silt with reticulate or massive cryostructures in the depth intervals 5.0–12.0 and 17.0–33.6 m. Massive silt is cut in many places by branching thin (a few mm to 3 cm) nearly upright cracks filled with ice.

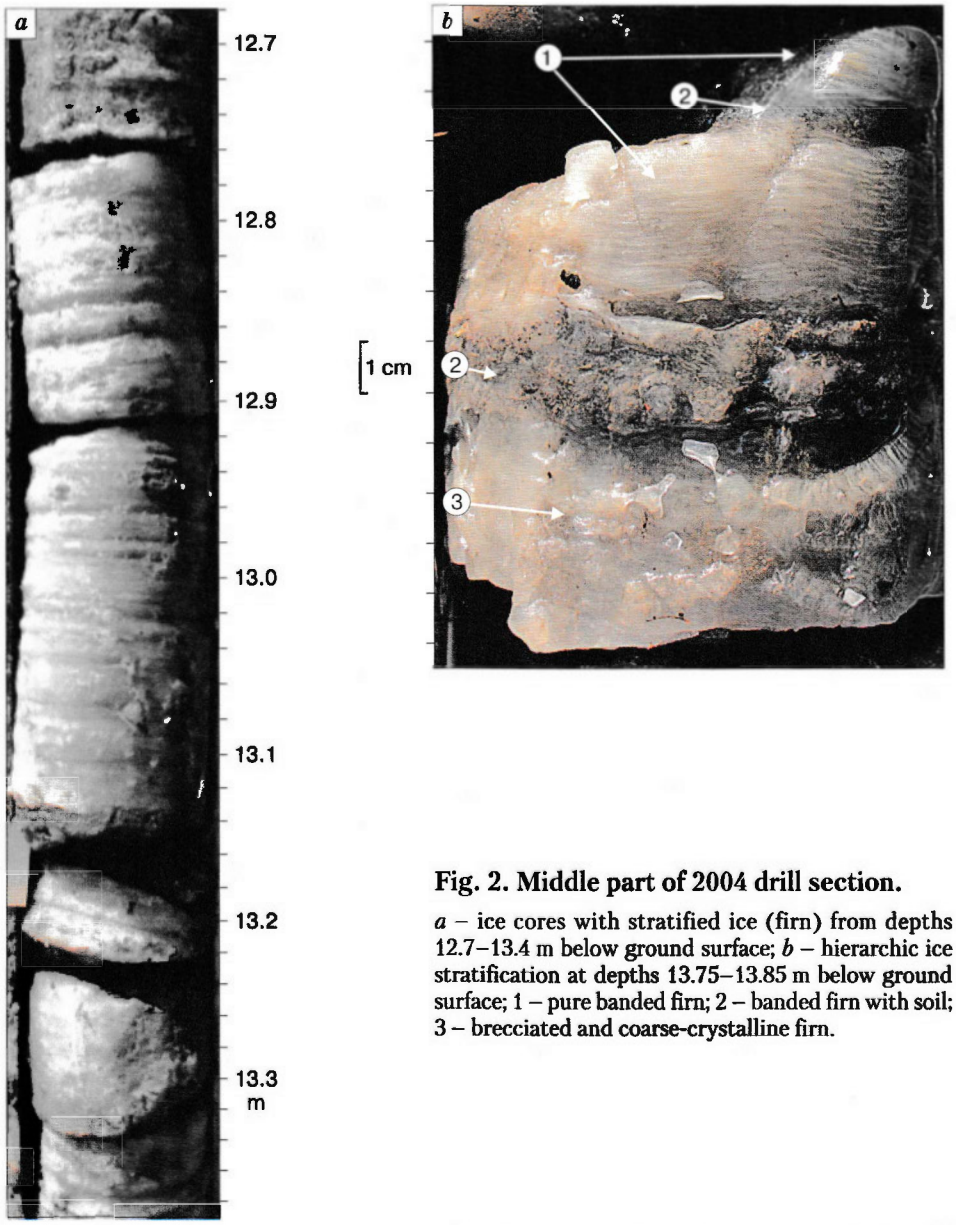

Fig. 2. Middle part of 2004 drill section.

a – ice cores with stratified ice (firn) from depths 12.7–13.4 m below ground surface; *b* – hierarchic ice stratification at depths 13.75–13.85 m below ground surface; 1 – pure banded firn; 2 – banded firn with soil; 3 – brecciated and coarse-crystalline firn.

LABORATORY MEASUREMENTS

Isotope composition of ice and snow. The oxygen and hydrogen isotope compositions of buried firn ice from the borehole of 2004 was studied at the Laboratory of Isotope and Nuclear-Physics Methods (Science & Technology Center, All-Russian Research Institute of Hydrogeology and Engineering Geology, VSEGINGEO, Moscow, reports by V.A. Polyakov and A.F. Bobkov). The samples of ice from the 2011 borehole and fresh snow cover of the same year were analyzed at the Laboratory of Isotope Geochemistry and Geochronology (Institute of Geology of Mineral Deposits, Petrography, Mineralogy, and Geochemistry, IGEM, Moscow, reports by E.O. Dubinina). The results are synthesized in Table 1 and in Fig. 3.

The oxygen isotope composition ($\delta^{18}O$) of firn ice sampled from the intervals 13.5–14.1 and 23.4–24.41 m varies in a narrow range relative to the SMOW standard, according to data of the IGEM Laboratory. In the upper interval, $\delta^{18}O$ is from –32.25 to –29.20 ‰, and deuterium (δD) ranges from –213.5 to –236.9 ‰. The respective ranges in the lower interval are between –31.70 ‰ and –30.32 ‰ $\delta^{18}O$ and –234.7 to –219.9 ‰ δD. Firn from the 12.0–17.0 and 33.6–39.0 m intervals was analyzed at the VSEGINGEO Laboratory, one sample from each interval. The results (Table 1) were similar to the $\delta^{18}O$ and δD data for the 13.5–14.1 and 23.4–24.41 m intervals.

Table 1. $\delta^{18}O$ and δD contents in buried firn of the Lena-Amga Plain and surface snow cover

No.	Deposit	Sampling interval, m below ground surface	$\delta^{18}O$, ‰	δD, ‰
		Borehole 2011		
1	Ice	13.50–13.58	–29.73	–213.5
2	Ice	13.62–13.70	–29.20	–214.3
3	Ice	13.72–13.80	–29.77	–223.8
4	Ice	13.82–13.90	–30.44	–232.0
5	Ice	13.92–14.00	–31.20	–236.9
6	Ice	14.05–14.10	–32.25	–232.1
7	Ice	23.41–23.44	–30.54	–219.9
8	Ice	23.51–23.56	–30.32	–223.8
9	Ice	23.62–23.68	–30.73	–226.7
10	Ice	23.71–23.78	–30.95	–230.0
11	Ice	23.88–23.94	–31.55	–234.7
12	Ice	24.00–24.07	–31.70	–232.5
13	Ice	24.25–24.30	–31.63	–229.1
14	Ice	24.37–24.43	–31.23	–225.3
		Surface snow cover above borehole 2011		
15	Snow	Upper layer, 5–10 cm below ground surface	–38.63	–288.8
16	Snow	Lower layer, 30–40 cm below ground surface	–31.60	–229.3
		Borehole 2004		
17	Ice	12.0–16.0	–30.60	–275.0
18	Ice	33.50–33.65	–26.60	–226.0

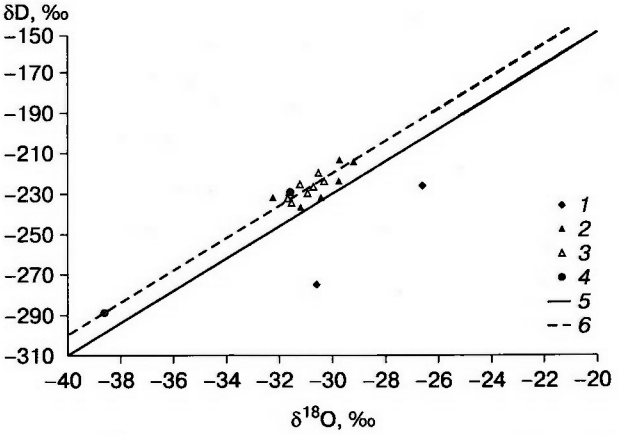

Fig. 3. $\delta^{18}O$ vs. δD relationship in buried firn of Lena-Amga Plain and in present surface snow cover.

1 – samples from 2004 borehole; *2* – samples from 2011 borehole, interval 13.5–14.2 m below ground surface; *3* – samples from 2011 borehole, interval 23.31–24.5 m; *4* – snow cover above borehole of 2011; *5* – global meteoric water line; *6* – local meteoric water line.

The isotope composition of the analyzed ice samples is almost identical to that of meteoric water in Central Yakutia [*Popp, 2006*]. The values of $\delta^{18}O$ and δD in snow are related as $y = 7.66x - 2.90$, with the lower and upper bounds of –42 to –19 ‰ $\delta^{18}O$ and –330 to –180 ‰ δD. The local meteoric water line for Central Yakutia differs from the global line [*Ferronsky and Polyakov, 2009; Craig, 1961*] in lower $\delta^{18}O$, while δD is the same.

The snow isotope composition reported in [*Popp, 2006*] was obtained in samples collected in November through April of 1997/98 near Yakutsk. The snow we sampled near the borehole of 2011 gave –38.63 ‰ $\delta^{18}O$ in the upper layer (5–10 cm below the surface) and –31.6 ‰ $\delta^{18}O$ in the layer 30–40 cm below the surface, which is almost the same as in the buried firn.

Spore-and-pollen composition. Spore-pollen assemblages in the core samples differ qualitatively and quantitatively from the present ones. The present spore-pollen spectra of the topsoil (0–0.1 m) are dominated by tree and shrub pollen (68.4–75.0 %), with 28.7 and 17.0 % grasses and subshrub species, respectively, the spores being 2.9 and 8.0 %.

Subaerial loam lying under present loam and wedge ice, as well as the upper wedge-ice layer (0.75–4.0 m) contains mostly grasses and subshrub pollen (62.7–67.0 %), with highest percentages of *Cyperaceae* (27.2–16.8 %) and *Poaceae* (12.4–36.1 %). The spores (27.8–20.8 %) belong mainly to *Polypodiaceae* (20.1–7.2 %). Tree and shrub pollen, of relatively low percentages (9.5–12.2 %), consist of *Betula middendorfii, Betula exilis* (7.7–9.0 %) and *Alnaster* (0.3–1.5 %).

These spore-pollen spectra of the upper section correspond to a tundra environment.

Spore-pollen assemblages in lacustrine loam lying between wedge ice and buried snow (interval 10.11–12.15 m) and in bluish-gray silt with plant detritus (interval 7.50–10.11 m) are poor, with 100–296 grains found in no more than four specimens. The spectra are dominated by grasses (35.0–90.3 %), especially xerophytes: *Chenopodiacae* (0.5–47.5 %), *Poaceae* (7.6–40.0 %), *Artemisia* (7.0–27.8 %), *Cichoriaceae* (1.0–26.7 %), and *Caryophyllaceae* (0.5–5.8 %). The tree-shrub pollen (7.7–37.2 %, most often 22.0 %) is almost uniformly distributed over the section and consists of *Betula nana* (1.7–20.0 %, the percentages growing upwards), *Alnaster* (0.5–4.0 %), *Salix* (0.5–4.0 %), and *Pinus pumila* (0.5–9.9 %, the percentages likewise growing upwards). The tree pollen includes higher percentages of *Larix* (1.8–10.0 %) and lower percentages of *Betula* sect. *Albae* (0.5–7.0 %), *Pinus sylvestris* (0–1.8 %), and sporadic *Picea.*

Spores are from 3.2 to 39.0 %, most of them being *Bryales* (1.2–24.4 %) and *Polypodiaceae* (0.5–29.0 %) species. The samples contain *Pediastrum* green alga and other microfossils. Note that the interval is rich in redeposited material from Mesozoic and Cenozoic sediments.

The taxonomic composition and relative percentages of the spore-pollen spectra at these depths correspond to tundra and steppe landscapes dominated by xerophytes and sparsely growing larch-birch or larch-pine forests (forest-tundra). Large percentages of green moss spores and *Cyperaceae* pollen, as well as some pollen of beach and water plants, indicate hypnum bog and sedge fen environments.

The spore-pollen spectra in samples of buried firn and underlying silt between 12.15 and 17.35 m differ from those in the interval above in having rather high percentages of tree-shrub pollen (13.7–44.0 %), which are however lower than grasses and subshrubs (47.1–70.3 %).

Trees and shrubs are small-leave angiosperms (12.4–36.0 %), mostly *Betula nana* (5.5–24.0 %). *Betula* sect. *Albae* is from 3.0 to 12.0 %, *Alnaster* and *Salix* are from a few grains to 5.0 % and 3.0 %, respectively.

The spectra of conifers (2.1–15.1 %) comprise greater percentages of *Larix* (1.0–10.0 %), lower percentages of *Pinus sylvestris* (0.3–5.3 %), and sporadic grains of *Picea sibirica* and *Pinus pumila*.

The components in grass and subshrub pollen from this depth interval again change in relative amounts: the percentages of *Artemisia* (9.6–16.0 %), *Poaceae* (6.0–24.0 %), and *Chenopodiacae* (4.0–14.8 %), and especially *Ericales* (5.0–13.0 %) are higher than in the overlying section while *Cichoriaceae* are lower (1.8–13.0 %).

The composition of spores (5.5–13.7 %) in this interval misses *Selaginella sibirica* and includes lower percentages of *Bryales* (1.1–5.6 %) and *Hepaticae* (few grains to 3.5 %) mosses but higher percentages of *Sphagnum* (0.3–3.0 %).

The low abundances of spore and pollen (100–223 grains in two or three specimens) and low percentages of tree pollen in the spectra prompt that deposition was in open landscapes with sparse forests but extensive steppes and saline-land heaths which were dominated by wormwood-goosefoot and grass communities, with heath and shrub patches. The sparse forests consisted of *Larix* or locally *Pinus sylvestris*, *Betula platyphylla*, and, possibly some *Picea*.

Slightly higher percentages of shrub birch, quite abundant *Ericales*, and greater spread of mesophytic grasses and *Sphagnum*, as well as lower percentages of xerophytes (*Chenopodiacae* and *Selaginella sibirica*) may be, to a certain extent, evidence of a slightly warmer and wetter climate compared to that of the previous interval, though a severe environment likely persisted.

Periglacial alluvium (20–31 m) and lower part of buried firn (31–43 m) bear the lowest amounts of spore and pollen (13 to 128 grains in one to five specimens). Seven out of sixteen specimens were almost barren (containing a few grains). The spore-pollen assemblages consist mainly of grasses (47.0–83.0 %), especially *Chenopodiacae* (to 56.0 %) whose percentages hold nearly the same in all samples. *Poaceae* and *Artemisia* are likewise quite high: up to 20.4 % and 10.0 %, respectively. All spectra contain notable amounts of *Caryophyllaceae* (0.3–11.2 %), *Cichoriaceae* (1.1–6.9 %), and *Asteraceae* (0.3–3.0 %). Grasses (*Ericales*, *Rosaceae*, *Onagraceae*, *Polygonaceae*) are rare or sporadic.

Tree and shrub pollen is 4.0–23.9 %, or occasionally as high as 34.0 %, being mainly *Larix* (0.3–19.0 %). Less abundant is *Pinus sylvestris* (0–4.0 %), *Betula platyphylla* (0–5.0 %) and *Betula nana* (*B. Middendorffii*, *B. exilis*), *Alnaster*, and *Pinus pumila*.

The compositions of spores, diverse microfossils, and redeposited pollen and spores from older sediments are similar to their counterparts from the overlying layers.

The spore-pollen spectra represent vegetation of periglacial steppe tundra with sporadic forests and swampy lowlands in a very cold climate.

DISCUSSION

Judging by the isotope compositions, the discovered layers of buried stratified ice are congenetic and similar to the present snow. The latter fact, along with fine grain sizes, banding, presence of columnar ice crystals, and horizontal stratification, allows us to identify the buried ice as firn.

The presence of firn is evidence of alternating positive and negative temperatures and dramatic changes in moisture contents of near-surface air.

The discovery of snow patches in the southern plainland part of the Lena River catchment indicates that the summer air temperatures were only slightly above zero during some spells of the Late Pleistocene. By analogy with present Arctic areas, one may infer that the mean annual air temperature in Central Yakutia did not rise above –20 °C during those cold spells, which is about 10 °C lower than the today temperature.

Mean annual air temperatures are known to correlate with mean annual $\delta^{18}O$ in precipitation [*Dansgaard, 1964*]. The $\delta^{18}O$ content in water of a basin approximately correspond to that at the snow-rain boundary in the respective area or to the highest content in snow [*Popp, 2006*]. In our case, with the obtained –29.2 ‰ $\delta^{18}O$, the mean annual air temperature may have been as low as –20 °C, the winter and summer means being, respectively, –45... –50 °C and slightly above +5 °C. The relatively cold summer temperatures are corroborated by the vegetation composition corresponding to steppe-tundra, or occasionally, forest-tundra environments in the time when the ice-bearing sediments were deposited. Snow patches may have been preserved in small depressions on hillslopes which were shaded though being elevated, and thus were favorable for snow accumulation.

CONCLUSIONS

Thus, the investigated three layers of stratified ice were formed on the ground surface and are most likely buried snow patches (firn). The buried ice has its isotope composition similar to that of snow in the study area. The sediments that host the buried ice lenses bear spore-pollen assemblages corresponding to cold climates of Late Pleistocene glacials.

The presence of buried firn, ice, and ice soil in the upper sedimentary section of the Lena-Amga Plain means that the upper syngenetic permafrost of the area underwent a more complex evolution than it was thought before. Until recently, syngenetic frozen ground in Central Yakutia was attributed to a cold and dry climate with sharp seasonal temperature variations which produced wedge ice and maintained a large extent of a thick ice complex. However, the reduced thickness of the ice complex and the existence of several layers of buried snow recrystallized to different degrees indicates that syngenetic permafrost was formed in a relatively wet climate at quite low summer air temperatures, as it commonly occurs in areas subject to glaciation. On the other hand, the very fact of firn preservation and burial is evidence of rather rapid sedimentation which may occur only under tectonic (or rather glacial-tectonic) subsidence.

According to climate and permafrost reconstructions, the greatest portion of syngenetic permafrost in Central Yakutia originated under the influence of a large ice sheet, most likely the Verkhoyansk one.

References

Craig H., 1961. Isotopic variations in meteoric waters. Science, 133, 133–149.

Dansgaard W., 1964. Stable isotopes in precipitation. Tellus, 19, 435–463.

Ferronsky V.I., Polyakov V.A., 2009. The Isotope Composition of the Earth's Hydrosphere [in Russian]. Nauchnyi Mir, Moscow, 632 pp.

Ivanov M.S., 1984. Cryogenic structure of Quaternary sediments in the Lena-Aldan Basin [in Russian]. Nauka, Novosibirsk, 126 pp.

Katasonov E.M. (Ed.), 1979. Structure and Isotope Ages of Alas Deposits in Central Yakutia [in Russian]. Nauka, Novosibirsk, 96 pp.

Katasonov E.M., 1975. Cryological-facies analysis of Pleistocene deposits and paleogeography of Central Yakutia, in: Pleistocene Paleogeography and Periglacial Environments [in Russian]. Nauka, Novosibirsk, pp. 16–22.

Popp S., 2006. Late Quaternary Environment of Central Yakutia (NE Siberia): Signals in Frozen Ground and Terrestrial Sediments. Mathematisch-Naturwissenschaftlichen Fakultät der Universität Potsdam, Potsdam, 85 pp.

Soloviev P.A., 1959. Permafrost in the Northern Lena-Amga Plain [in Russian]. Izd. AN SSSR, Moscow, 144 pp.

Spektor V.B., Spektor V.V., 2002. The origin of the Lena-Amga high periglacial plain. Kriosfera Zemli, VI (4), 3–12.

Spektor V.B., Spektor V.V., Bakulina N.T., 2008. New data on the Ice Complex of the Lena-Amga rivers plain (Central Yakutia), in: Proc. Ninth Intern. Conf. on Permafrost, Univ. of Alaska Fairbanks, Fairbanks, Book 2, pp. 1681–1684.

Received
22 February 2011

Kriosfera Zemli, 2011, vol. XV, No. 4, pp. 21–25 http://www.izdatgeo.ru

LANDSCAPE GEOCHEMICAL TRACERS OF CONTAMINATION IN DELTAS OF RIVERS DISCHARGING INTO THE ARCTIC BASIN

E.M. Korobova[1], N.G. Ukraintseva[2], V.V. Surkov[3], E.A. Dombrovskaya[2]

[1] *Vernadsky Institute of Geochemistry and Analytical Chemistry, Russian Academy of Sciences, 19, Kosygin str., Moscow, 119991, Russia; korobova@geokhi.ru*
[2] *Institute of Earth's Cryosphere, Siberian Branch of the Russian Academy of Sciences, PO box 1230, Tyumen, 625000, Russia; ukraintseva@mail.ru*
[3] *Lomonosov Moscow State University, Department of Geography, 1, Leninskie Gory, Moscow, 119991, Russia; vsurkov@yandex.ru*

Terrestrial ecosystems located in the Yenisei and Pechora delta and estuary zones have been studied for radionuclide and heavy metal contamination from remote global and regional sources. Radionuclides and heavy metals in soil, water, and plants were determined at different distances from the sea on landscape-geochemical transects across riverbanks and delta islands. In the Yenisei delta and estuary zone, local ^{137}Cs accumulation was found being associated with operation of the Krasnoyarsk Chemical Combine. The highest ^{137}Cs were measured at test sites located on islands within the Yenisei delta front, which thus appears to be a natural barrier for river-borne contaminant fluxes into the Arctic basin. Heavy metals (Cu and Ni) in mosses and willow (leaves) species collected on terraces and watersheds in the lower Yenisey showed a slowly increasing trend toward the Norilsk Combine. The measured ^{137}Cs contamination of the Pechora test sites was within the global background. Relatively high Cu and Zn were revealed in Pechora water sampled 3 km downstream of Naryan-Mar city. These patterns may be used for purposive contamination tracing.

INTRODUCTION

The deltas of the Yenisei and the Pechora, two large rivers in northern Russia, are of interest for their terrigenous input into the Arctic basin. The reported study focuses on radionuclide and heavy metal contamination of terrestrial ecosystems in the lower reaches of the Yenisei and Pechora rivers at different distances from global- and regional-scale polluters, and on redistribution of this contamination in the conjugated landscapes.

Pollution in the region comes mostly from the Norilsk Nickel Combine (NNC) with its influence zone exceeding 150 km [*Ermakov and Ukraintseva, 2005*] and from the Krasnoyarsk Chemical Combine (KCC) which has contaminated the Yenisei floodplain downstream of the Combine [*Vakulovsky et al., 1995; Kuznetsov et al., 2000; Sukhorukov et al., 2004*]. The Pechora catchment belongs to few areas with almost undisturbed ecosystems and thus may serve for a reference standard against which to study natural processes in deltas and estuaries of large northern rivers [*Resolution..., 2000*]. Nevertheless, its territory has suffered from atmospheric radionuclide fallout during nuclear tests and from the consequences of the Chernobyl accident. According to *Nifontova* [*2000*] and the *Radioactive Contamination Atlas* [*1998*], ^{137}Cs contamination has duplicated after the Chernobyl accident (as measured in 1995).

METHODS

Landscape geochemical transects across different floodplain levels, ancient terraces of the Yenisei and Pechora, and the watershed periphery were located at different distances from the sea. The sampling sites were chosen at places of geochemical contrasts with presumably maximum accumulation of river- and airborne radioactive elements. The soil profiles were sampled in increments of 2, 5 and 10 cm down to the table of permafrost or groundwater (30 to 120 cm). The sampled plants were dominant species of high food and tracer importance (mosses, lichens, grasses, sedges, horsetail, willow and alder). The concentration of radionuclides was measured in air-dried samples (as air-dry weight) using a *Canberra* gamma-ray spectrometer (USA), analysts Borisov A.P. (Vernadsky Institute of Geochemistry, Moscow) and Kirov S.S. (*Radon* R&D Company), to an accuracy no worse than 5–10 % (^{137}Cs in soil) and 3 to 35 % (^{137}Cs in plants). The content of heavy metals in soil and plant samples was measured by XFA with the help of *ORTEC-TEFA* and *SPARK-1* mass spectrometers, analysts Sorokin S.E. (Dokuchaev Institute of Soil, Moscow) and Sizov E.M. (Vernadsky Institute of Geochemistry, Moscow). Samples of water and aqueous extracts were analyzed at the Dokuchaev Institute of Soil, Moscow (analyst Grishina R.V.) and at the Esenin Ryazan' State University, by Atomic Adsorption Spectroscopy, AAS (analyst Tobratov S.A.). Micrometer- and nanometer-size particles from groundwater were extracted on membrane filters following the procedure developed at the Vernadsky Institute of Geochemistry (Moscow) [*Shkinev, 2009*]. Trace elements in these size fractions were determined by V.K. Karandashev.

CONCENTRATIONS AND DISTRIBUTION OF ^{137}Cs

The average concentration of ^{137}Cs in soils and plants is on the average within the global background. However, it may vary markedly (Table 1) depending on the polluting source, the geomorphology of the test sites, the type of soil and fluvial deposits, and the plant species.

In the lower reaches of the Yenisei, the ^{137}Cs density is the highest (up to 88 kBq/m^2) in the delta front near settlement Ust'-Port within the low floodplain of the Pashkov Island. The contamination is regional-scale and comes from the Krasnoyarsk Chemical

Table 1. **^{137}Cs in landscape components, air-dry weight (at time of measurements)**

Location of landscape transects	Number of test sites	^{137}Cs, Bq/kg			
		Soil	Plants		
			Mosses	*Willow* leaves	*Horsetail*
Yenisei delta, settlement Ust'-Port					
High terraces	6	1.3–282	10–137	26–108	12–53
Right-bank floodplain	5	0.2–117	30; 49	21–81	9–15
Island floodplain	7	0.8–325	10	17–61	19–44
Pechora Gulf, Bolvansky Cape	3	16–156	62; 118	67; 142	54–119
High terraces					
Pechora delta (settlements Yushino, Bol. Sopka, Iskateli)	5	30–215	31–125	n/d	–
High terraces					
Riverbank floodplain	1	10	–	56	–
Island floodplain	5	2.5–20	–	24–51	7–109

Note. Dash is not sampled, n/d is not determined.

Combine. The ^{137}Cs concentrations are notably lower in the Yenisei intradelta (floodplain of the Tysyara Island) (20 and 25 kBq/m^2) but are likewise above the global background (2.0–2.9 kBq/m^2). According to our estimates, the Tysyara site receives up to 30 % of total river discharge. The high floodplains and terraces are contaminated to a lesser degree, about the global fallout (0.4–2.8 kBq/m^2). Relatively enhanced contamination (twice the background) observed in transaccumulative (interhill) depressions may be produced by ^{137}Cs transport with surface run-off.

In the lower reaches of the Pechora, the ^{137}Cs activity and density (Table 1) are the highest (150 to 215 Bq/kg) in tundra soils on watersheds and on terraces of different heights (from 7.6 to 30 m above the low-water river level). The southern terraces are less contaminated (settlement Bol. Sopka) than the northern ones (Bolvansky Cape, settlement Yushino). The greater contamination in the latter may be due to their proximity to nuclear test sites. Unlike the Yenisei lower reaches, the activity of radiocesium in floodplain soils (2.5–25 Bq/kg) is an order of magnitude lower than on terraces. This is consistent with the absence of considerable regional radioactive polluters in the Pechora drainage area. Yet, the total contamination in floodplain soils (especially on islands: 2–6 kBq/m^2) is commensurate with or locally higher than that on terraces (1.0–2.4 kBq/m^2), i.e., contaminants accumulate in floodplain areas.

The ^{137}Cs patterns in soil profiles are of three main types: (1) maximum element concentration near the soil surface; (2) contaminated top organic soil layer buried as a result of solifluction or slumping; (3) contaminated horizons repeatedly buried during seasonal cycles of flooding and alluvial deposition. The three patterns are characteristic of soils from, respectively, watershed and terrace (1), hillslope (2), and floodplain (3) landscapes. Peat-gley and especially peat soils in terraces show relatively enhanced ^{137}Cs concentrations at the active layer base where soil solutions accumulate at the boundary with permafrost and are subject to periodic freezing.

The general trend of ^{137}Cs biosorption by dominant plant species is an increase in the series grasses < alder, willow (leaves) < lichens < horsetail < mosses (green part) < mosses (lower brown part). The tundra plants show the highest soil-plant transfer factors (TF), as high as transfer from hydromorphic soil in the zone of Chernobyl pollution. The species that are more active potassium accumulators commonly have lower TF for ^{137}Cs [*Korobova, 2009*].

CONCENTRATIONS AND DISTRIBUTION OF HEAVY METALS (Cu, Ni, Zn)

Test sites in the lower reaches of the Yenisei show insignificant contamination with heavy metals. Their concentrations and distribution depend on the distance from the regional source. For instance, Ni concentrations increase toward the Norilsk Combine in mosses (3–5 times) and willow leaves (2–3 times) that grow on terraces and in watersheds (Fig. 1). The distribution of copper has the same patterns. The reason is obviously the air transport and the subsequent fallout of metals, as well as their secondary redistribution with river and surface runoff. The redistribution is evident in relatively higher concentrations of elements in fine alluvium and, as well as in the presence of buried contaminated floodplain soils. Enhanced Cu, Ni, and Zn in top and supra-permafrost soil horizons of high terraces in the Yenisei delta front (Fig. 2) result either from local surface contamination or from natural biological and cryogenic accumulation. Heavy metals, especially Ni and Zn, have relatively high concentrations in fine suspended sediment load in floodplain soil groundwater. The highest

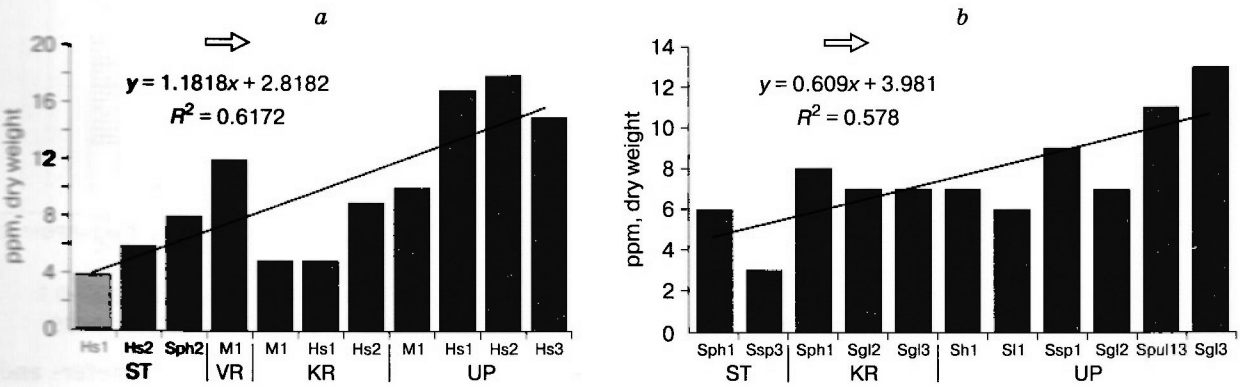

Fig. 1. Ni in mosses (*a*) and willow leaves (*b*) samples from terrace ecosystems in the Yenisei delta.

Arrow points to the Norilsk Nickel Combine. Capitalized abbreviations stand for names of test sites: ST – Cape Shaitansky; VR – settlement Vorontsovo; KR – settlement Karaul; UP – settlement Ust'-Port. 1, 2, 3 are elementary landscape systems: 1 – alluvial (high terraces), 2 – transitory (slopes), and accumulative (depressions) (3). Other abbreviations are plant species: Hs – *Hylocomium splendens*; Sph – *Sphagnum* sp.; M – mean *Sphagnum* sp. sample; Sgl – *Salix glauca* L.; Sh – *Salix hastata* L.; Sl – *Salix lanata* L.; Spul – *Salix pulchra* Cham.; Sph – *Salix phylicifolia* L.; Ssp – *Salix* sp.

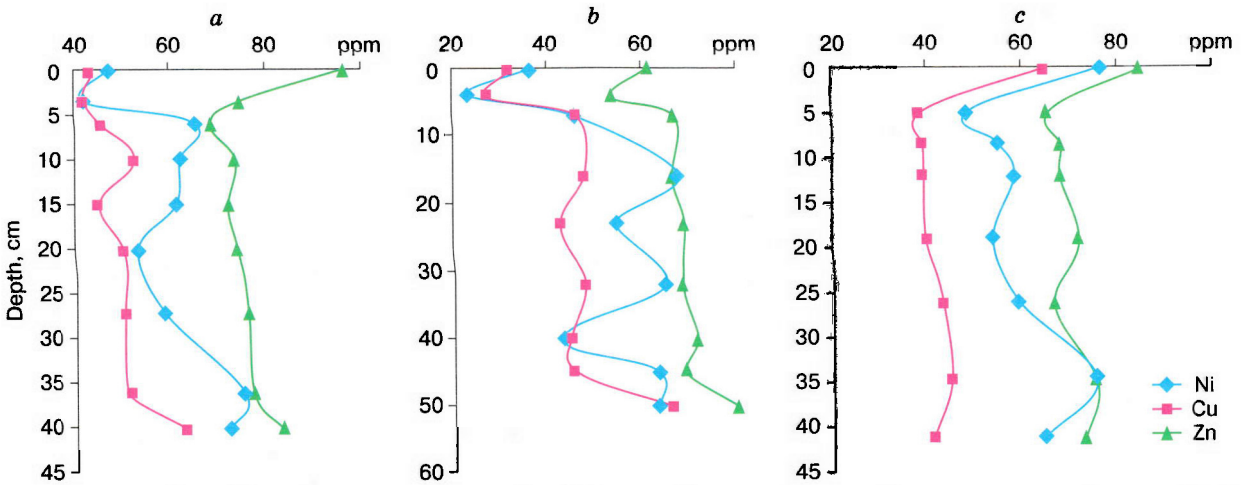

Fig. 2. Vertical profiles of Cu, Ni, Zn in soils of chemically conjugate tundra systems (settlement Ust'-Port):

a – eluvial system, *b* – transitory system, *c* – eluvial-accumulative system.

Ni percentages (30–80 %) occur in suspended particles larger than 0.45 μm (Fig. 3)[1].

Floodplain soil groundwater bears higher Ni concentrations in islands within the delta front (Pashkov Island). Therefore, the delta front landscape systems serve as barriers to riverine transport of contaminants.

According to the heavy metal measurements of 2010 in the Pechora water, contamination is low (0.5 μg/l^3 Cu and 2.8 μg/l^3 Zn on average) in the large river arms but increases three- to five-fold in small tortuous channels and near delta islands where water is slow (up to 1.5–2.0 μg/l^3 Cu and 7–15 μg/l^3 Zn). Significant pollution in the river is due to the

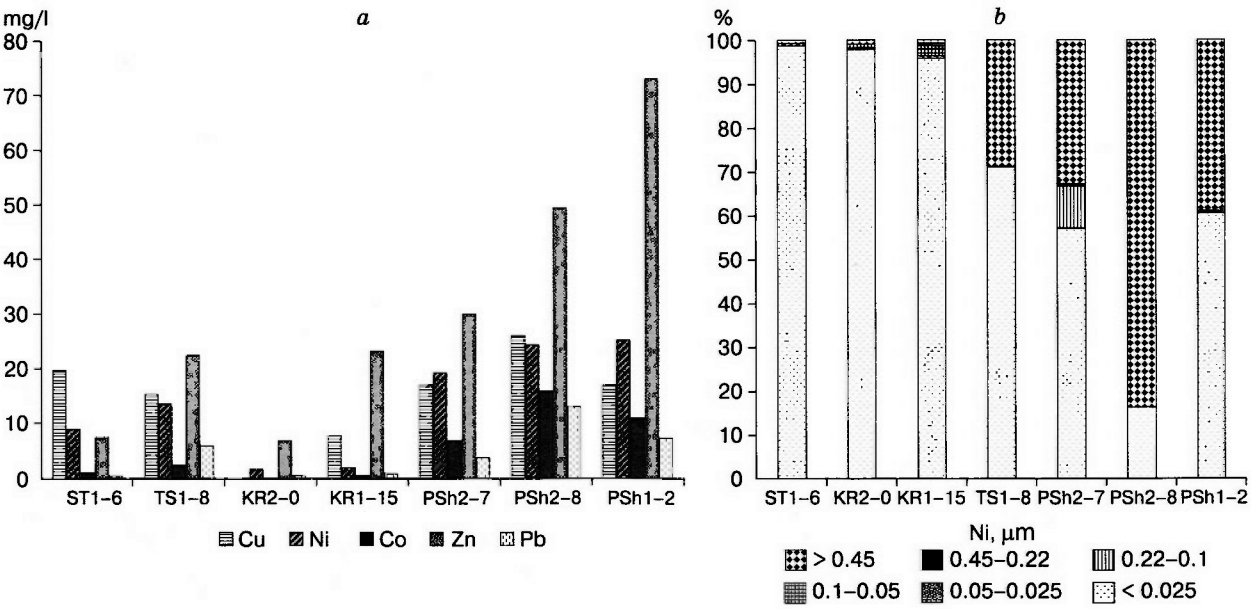

Fig. 3. Heavy metals in soil groundwater (*a*) and Ni partitioning among fractions of micrometer- and nanometer-size particles (μm) extracted by membrane filtration from soil groundwater samples (*b*).

Capitalized abbreviations stand for names of test sites: ST – Cape Shaitansky; KR – settlement Karaul; TS – Tysyara Island; PSh – Pashkov Island. 1–6, 2–7, etc. are indices of transects (left) and sampling sites (right).

[1] The fraction <0.45 μm is commonly classified as a natural soil solution. Actually, these are solutions of dispersed soil particles, which is confirmed by membrane filtration.

Naryan-Mar city: Zn is as high as 28 μg/l[3] in the river water 3 km downstream of Iskateli neighborhood (northern outskirts of the city), which is almost three times the maximum permissible concentration (MPC) for fisheries waters (10 μg/l[3]).

CONCLUSIONS

Landscape-geochemical studies in the lower reaches of the Yenisei and Pechora rivers discharging into the Arctic basin have confirmed the possibility of tracing radionuclide and heavy metal contamination of landscape systems due to global- and regional-scale sources. Delta front island systems can act as barriers to riverine transport of contaminants. The observed accumulation patterns of elements in different components of chemically conjugated landscape systems can be used for reference in pollution tracing and monitoring.

The cooperation of the crew of R/V *Akademik Petrov* and the researchers from SevPINRO in the organization of cruises is greatly appreciated. The work was carried out as part of the INCO-COPERNICUS Project *Establish* and was supported by the Earth Science Department of the Russian Academy of Sciences, as well as by grants 08-05-00872 and 10-05-10027k from the Russian Foundation for Basic Research.

References

Ermakov S.Yu., Ukraintseva N.G., 2005. An experience of biological remediation of the territory of the Pelyatka oil-condensate field, in: Biospheric Functions of Soils. Workshop, Book of Abstracts, Pushchino, pp. 33–34.

Korobova E.M., Ukraintseva N.G., Brown J., Standring W., 2009. Radionuclide distribution in the lower Yenisey and Pechora reaches: Landscape geochemical signatures and patterns of global and regional contamination, in: M.N. Gallo, M.H. Ferrari (Eds.), River Pollution Research Progress, NOVA Publ., N.Y., pp. 91–156.

Kuznetsov Yu.V., Legin V.K., Strukov V.N., et al., 2000. Uranium-series elements in deposits of the Yenisei floodplain. Radiochimiya, 42 (5), 470–477.

Nifontova M.G., 2000. Concentrations of long-lived synthetic radionuclides in the moss-lichen cover of highland plant communities. Ekologiya, No. 3, 202–205.

Radionuclide Contamination of European Russia, Bielorussia, and the Ukraine. An Atlas [in Russian]. Federal Geodetic and Mapping Surveys of Russia, Institute of Global Climate and Environment, Rosgidromet and RAN, Moscow, 1998, pp. 12–13.

Resolution of the International Pechora Symposium "Ecosystems of Eurasian Large River Deltas" (Syktyvkar, Komi Republic, Russia, 11–15 September, 2000. http://ib.komisc.ru/add/old/t/ru/ir/vt/00-38/08.html

Shkinev V.M., 2009. Membrane methods in geochemical studies. Proc. V International School of Earth Sciences ISES-2009, 30 p. http://www.ises.su/2009

Sukhorukov F.V., Degermendzhi A.G., Belolipetsky V.M., et al., 2004. Distribution and Migration of Radionuclides in the Yenisei Valley [in Russian]. Izd. SO RAN, Novosibirsk, 287 pp.

Vakulovsky S.M., Kryshev I.I., Nikitin A.I., et al., 1995. Radioactive contamination of the Yenisei river. J. Environ. Radioactivity, 29 (3), 225–236.

Received
14 February 2011

Kriosfera Zemli, 2011, vol. XV, No. 4, pp. 25–28 http://www.izdatgeo.ru

BIOGEOCHEMISTRY OF PERMAFROST LANDSCAPES IN WEST SIBERIA: IMPLICATIONS FOR ECOLOGY AND SUSTAINABILITY

D.V. Moskovchenko

Institute of Northern Development, Siberian Branch of the Russian Academy of Sciences, PO box 2774, Tyumen, 625003, Russia; land@ipdn.ru

The study concerns with biogeochemistry of landscapes in the Yamal Peninsula, including the trace-element composition of different soils and abundances of plant nutrients. The sustainability of plant-soil systems in permafrost terrains has been recognized to have two major controls: the biosorption activity of plants and contents of biogenic elements in soils. The former factor stabilizes the material composition of landscapes and shows up especially in zonal systems. The other factor controls the rate of revegetation in industrially disturbed areas, the azonal soils being best provided with mineral nutrients.

The vegetation cover has been universally accepted to be the principal control in processes responsible for the sustainability of permafrost landscapes [*Tyurtikov, 1974; Meltser, 1994; Tsibulsky, 1995; Moskalenko, 1996; Ermokhina, 2009*]. Vegetation, and peat derived from it, stabilize the thermal regime of soils and thus prevent permafrost from degradation. On the other hand, vegetation is the most changeable

landscape component prone to surficial and subsurface impacts. Thus, investigation into the structure and functions of plant biota is a basic approach in estimating the ecology and sustainability of tundra landscapes.

The patterns of vegetation depend directly on soil chemistry. Lichens prevail in sandy tundra soils with low peat contents [*Dobrinsky, 1995*], willow shrub communities grow mostly on marine sediments with highly saline soil waters [*Ermokhina, 2009*]. Vegetation on soils depleted in major and trace elements is poor, and such landscapes are weakly sustainable. Thus, the sustainability of plant-soil systems is, to a large extent, a function of their chemical structure meant as the spatial and composition patterns of leaching and enrichment zones [*Glazovskaya, 1988*]. The structure of landscape-geochemical systems results from a long evolution with its general trend following Vernadsky's law of increasing biogeochemical energy in living matter [*Vernadsky, 1980*].

The biogeochemistry of permafrost plant-soil systems has been studied in soil and plant samples collected through environmental profiling in the Arctic and Subarctic tundra of the Yamal Peninsula (Bovanenko and Tambei oil fields). Sampling was along landscape profiles (sequences or catenas) that traverse different geomorphic levels and, correspondingly, record different ecological conditions. Another objective was to explore soil composition changes at development sites (petroleum wells and clusters).

According to data on the biotic component of the landscape sequences, the endmembers commonly have a simple structure of cenoses and low biodiversity. For instance, the driest and wettest Subarctic tundra biotopes miss shrubbage. Plant communities growing on depleted and relatively dry sandy soils show less diverse taxonomic compositions than those on wetter and richer loamy soils of sedge-shrub-sphagnum tundra [*Moskalenko, 2006*]. The Yamal tussock and sphagnum bogs have reduced spectra of life forms [*Telyatnikov, 2003*], their simplified biotic structure being evidence of nutrients and energy shortage and poor self-regulation.

Therefore, we explored the compositions of plants and soils in different ecological sequences. Plants are known to be more active element absorbers in zonal watershed tundra ecosystems than in very wet or very dry areas. The biosorption activity for trace elements is the highest in shrubs (*Betula nana, Salix glauca, S. lanata*), the edificators of Subarctic tundras, but is low in grasses, sedges, and sphagnum that dominate the intra-zonal systems [*Dobrinsky, 1995*]. The same trends appear in the topsoil peat compositions. Biosorption is the most active in zonal tundra soils in flat watersheds. The highest contents of Mn and Zn, which are the most rapidly accumulated elements, are in peat from yernik (dwarf birch)-lichen-green moss tundra. Hydromorphic subacid soils show weaker biosorption and higher lateral migration of substances and lower contents of biogenic elements in peat (Table 1). The total coefficient of biological accumulation (ratio of average measured element concentrations to their average in soil) is the highest in zonal tundra systems of flat watersheds.

Thus, vegetation in the latter systems, which reflect the most faithfully the environment features ("invariant" systems according to V. Sochava), has the highest geochemical activity developed in the course of long evolution. This fact shows up in the biogeochemical structure of soils, namely in high compositional diversity of organic topsoils and poor element enrichment in the mineral horizons. This is biological accumulation preventing elements from transport in water that stabilizes the composition of a

Table 1. **Trace-element compositions of peat topsoil (Bovanenko oil field)**

Soils, geography, vegetation	Element									Rk
	Mn	Cr	Ba	Sr	Ni	Co	Cu	Zn	Pb	
Peat-gley soils of watersheds in tussock shrub-lichen-green moss tundra, $n = 32$	3.0 / 3650	0.7 / 124	2.1 / 1834	0.8 / 169	0.6 / 61	1.1 / 25	0.8 / 46	2.3 / 202	**1.1 / 24**	2.0
Peat-gley soils of watershed slopes in grassy willow tundra, $n = 6$	2.6 / 3167	0.6 / 120	1.7 / 1467	1.3 / 262	0.7 / 68	1.3 / 28	0.8 / 44	1.3 / 112	**0.9 / 19**	1.8
Bog soils of swales in shrub-sedge-moss tundra, $n = 8$	1.2 / 1483	0.6 / 113	1.7 / 1500	1.1 / 225	0.7 / 73	1.0 / 23	0.8 / 47	1.0 / 82	**1.1 / 25**	1.6
Transitional bog soils in carex-eriophorum-sphagnum tundra, $n = 4$	1.7 / 2050	0.6 / 120	1.9 / 2000	0.8 / 150	0.7 / 70	1.4 / 30	1.0 / 55	0.9 / 80	**1.1 / 25**	1.8
Alluvial soils of near-terrace floodplain, $n = 6$	1.3 / 1500	0.6 / 120	1.7 / 1500	1.0 / 200	0.6 / 60	0.5 / 10	0.5 / 30	0.5 / 40	**0.7 / 15**	1.1

Note. n is the number of samples; Rk is the total biological accumulation (ratio of average measured concentrations of elements to their average soil abundance). Element composition of soils: numerator is the ratio of element concentration in soil to that in soil parent material; denominator is the average measured element concentration, ppm.

Table 2. **Chemical composition of soils in Arctic tundra (Yamal Peninsula)**

Soil	pH_{KCl}	pH_{H_2O}	Organic matter	N_{total}	P_2O_5	K_2O	CEC	TAB
			%		ppm		mmol/100 g	
Peat-gley tundra	4.8	5.9	45.2	0.23	63	240	1.5	4.7
Supra-permafrost gley	5.0	6.6	0.55	0.03	114	225	1.5	0.5
Podzol	4.9	6.5	1.2	0.04	98	231	1.6	1.2
Bog-tundra	4.0	5.5	14.5	0.38	80	190	2.8	8.9
Fen	4.4	5.5	23.2	0.44	33	232	1.2	8.6
Alluvial	5.2	6.5	3.1	0.17	178	286	2.1	6.9

Note. CEC is the cation exchange capacity; TAB is the total absorbed bases.

landscape, the biotic component thus being the crucial intrinsic factor of its self-regulation and stabilization.

Comparison of peat compositions in different climate zones shows that the tundra soils are depleted in many trace elements. Average contents of Zn, Ni, Pb, Cu, and Co in forest peatland are, respectively, 940, 180, 120, 89, and 45 mg per kg of ash [*Dobrodeev, 1990*], which is much higher than in the Yamal peat. The trace-element depletion in the tundra peat is due to prolonged biological cycles and intense leaching. The low intensity of biological cycles in tundra landscapes and the related low self-regulation are responsible for their vulnerability to industrial disturbance [*Perelman and Kasimov, 1999*].

Soils in northern West Siberia are deficient in many plant nutrients necessary for rapid and efficient revegetation in disturbed areas [*Vasilievskaya et al., 1986*]. Technogenic loads at development sites change dramatically the geochemical framework of landscapes. Specifically, soils at drilling sites are contaminated with petrochemical products, Ba, Sr, and Pb [*Moskovchenko, 1998*]. Disturbance to peat topsoil reduces the store of organic matter, potassium, and nitrogen. Mechanic damage and pollution cause degradation or extermination of plant communities, while the remediation efficiency depends on the availability of mineral nutrients.

According to agrochemistry data for the Yamal soils, zonal tundra peat-gley soil systems are depleted in P and have low cation exchange capacity (CEC) and total absorbed bases (TAB). Depleted compositions are observed in podzol soils of flat watersheds and gley soils in areas of sporadic permafrost. On the contrary, soils of intra-zonal systems have high concentrations of mineral plant nutrients. Alluvial soils have highest P and K enrichment, while peat in bog-tundra and fen soils is the richest in nitrogen (Table 2). This is vegetation in the overwetted areas that shows the highest recovery potential. Revegetation is the most rapid in thin peatbogs [*Liverovsky et al., 1980*] or in fens and water-filled swales [*Moskalenko and Shur, 1975*].

Thus, the sustainability of zonal and azonal plant-soil systems has different controls that depend on the chemical composition of soils. The sustainability of zonal systems, meant as capability of preserving their structure, depends on how efficient the vegetation is in the use of material and energy resources. This efficiency is expressed quantitatively in high biological accumulation of elements in peat. The sustainability as an ability of rapid recovery after being industrially disturbed ("elasticity") is the maximum in azonal systems and depends on the contents of plant nutrients in soils.

References

Dobrinsky L.N. (Ed.), 1995. The Nature of the Yamal Peninsula [in Russian]. Nauka, Ekaterinburg, 435 pp.

Dobrodeev O.P., 1990. Heavy-metal biogeochemistry of peatland, in: Transactions, Biogeochemical Laboratory, Moscow, Vol. XXI, pp. 53–61.

Ermokhina K.A., 2009. Phytoindication of Exogenic Processes in Tundras of Central Yamal [in Russian]. Author's Abstract, Candidate Thesis, Moscow, 24 pp.

Glazovskaya M.A., 1988. Geochemistry of Natural and Industrial Landscapes of the USSR [in Russian]. Vysshaya Shkola, Moscow, 328 pp.

Liverovsky Yu.A., Popov A.I., Smirnov V.V., 1980. Remediation of industrially disturbed natural landscapes in the extreme North, in: Environment Conservation while Permafrost Development [in Russian]. Collection of Papers. Nauka, Moscow, pp. 111–115.

Meltser L.I., 1994. Aspects of plant ecology in sustainability of landscapes in the Yamal, in: West Siberia: Problems of Development [in Russian]. Institute of Northern Development, Tyumen, pp. 128–141.

Moskalenko N.G, Shur Yu.L., 1975. Typical disturbance to ecosystems of northern West Siberia from laying works, and the possibilities for remediation, in: Environment Conservation while Development of Permafrost Areas. Proc. All-Union Workshop [in Russian]. Institute of Permafrost, Yakutsk, pp. 96–108.

Moskalenko N.G., 1996. Dynamics of tundra landscapes in northern West Siberia and anthropogenic effects. Izvestia RGO, Issue 5, pp. 67–74.

Moskalenko N.G., 2006. Plant communities of Yamal coasts as a subject for biodiversity study and compiling of electronic databases. Kriosfera Zemli, X (2), pp. 90–95.

Moskovchenko D.V., 1998. Petroleum Production and Environment: Ecological and Geochemical Analysis of the Tyumen Region [in Russian]. Nauka, Novosibirsk, 112 pp.

Perelman A.I., Kasimov N.S., 1999. Geochemistry of Landscapes [in Russian]. Astreya-2000, Moscow, 763 pp.

Telyatnikov M.Yu., 2003. Vegetation of Typical Tundras in the Yamal Peninsula [in Russian]. Nauka, Novosibirsk, 121 pp.

Tsibulsky V.R., (Ed.), 1995. The Environment of the Yamal Peninsula [in Russian]. Institute of Northern Development, Tyumen, Book II, 104 pp.

Tyrtikov A.P., 1974. Vegetation Dynamics and Permafrost Evolution in West Siberia [in Russian]. Moscow University Press, Moscow, 153 pp.

Vasilievskaya V.D., Ivanov V.V., Bogatyrev L.G., 1986. Soils of Northern West Siberia [in Russian]. Moscow University Press, Moscow, 286 pp.

Vernadsky V.I., 1980. Problems of Biogeochemistry [in Russian]. Transactions, Biogeochemical Laboratory, Moscow, Vol. XVI, 320 pp.

Received
17 February 2011

SCIENTIFIC JOURNAL
EARTH'S CRYOSPHERE

Kriosfera Zemli, 2011, vol. XV, No. 4, pp. 29–32 http://www.izdatgeo.ru

PERMAFROST MONITORING AND PREDICTION

ASSESMENT OF PERMAFROST STABILITY UNDER CONTEMPORARY CLIMATIC CHANGES

G.V. Malkova, A.V. Pavlov, Yu.B. Skachkov*

Institute of Earth's Cryosphere, Siberian Branch of the Russian Academy of Sciences, 86, Malygina str., Tyumen, 625000, Russia; galina_malk@mail.ru
** Melnikov Institute of Permafrost, Siberian Branch of the Russian Academy of Sciences, 36, Merzlotnaya str., Yakutsk, 677010, Russia; skachkov@mpi.ysn.ru*

The contemporary climate trends within the permafrost extent in Russia have been evaluated and mapped on the basis of synthesized meteorological data during the period from 1965 to 2010. The reasons of lagging of permafrost temperature trends from the trends of mean annual air temperature have been examined. The small-scaled maps of permafrost thermal stability under the contemporary climate warming have been worked out.

The global warming tendency has been evident for the past 100–110 years. The climate patterns since 1995 have become notably more variable, with frequent anomalies. On this background, mean annual air temperatures show increasing trends in Arctic regions and their immediate surroundings while the warming rates in some Subarctic areas are slowing down or even locally experience a reversal (Turukhansk, Aldan, Olekminsk) [*Melnikov et al., 2007; Pavlov, 2008a; Pavlov and Malkova, 2010*].

The frequency of modern climate anomalies is commonly estimated by comparing meteorological data over the past decade with the norm, using three air warming grades (Δt_{air}): weak ($\Delta t_{air} < 0.7$ °C), temperate (0.7 °C $\leq \Delta t_{air} \leq 1.0$ °C), and strong ($\Delta t_{air} >$ >1 °C) [*Pavlov and Malkova, 2005*].

Inasmuch as mean annual air temperatures for the past decade (2000–2010) have been anomalously strong in many areas, there are only two warming grades (temperate and strong) used in the map of Fig. 1. The climate norm (imaging by dint of isolines, Fig. 1) varies within the permafrost extent from –2 to –16 °C. Warming is strong over most of the territory (temperature rise more than 1 °C) while temperate climate warming are restricted to local areas in the European north, in West and Central Siberia, and in the Russian Far East (Primorie).

In order to highlight regional features of warming patterns, one has to calculate mean annual air temperature trends for different time limits. The basic map of these trends was presented earlier for 1965–2000 [*Pavlov and Ananieva, 2004; Pavlov and Malkova, 2005*]. Having continued the observations till 2010, we picked the modern trends and compared them with those for the period from 1965 to 2000. The 1965–2000 mean annual air temperature trends (Fig. 2) divided into seven grades (see the color code in Fig. 2) make up prominent N–S (western Arctic and Subarctic areas) and W–E (eastern sector) zones. The warming rates are the highest (to 0.08 °C/yr) in southern Siberia and the lowest (less than 0.03 °C/yr) in the European North and in West and Central Siberia.

Unlike these, the air temperature trends for 1965–2010 (isolines at 0.01 °C/yr in Fig. 2) have markedly different patterns, namely (1) the orientations of contour lines have changed in a way that no W–E or N–S features show up any longer; (2) the variations of trend values are generally much lower; (3) the minimum trends (0.03...0.04 °C/yr) are concentrated in the Lena-Olenek interfluve, in the middle reaches of the Yenisei, and in the northern Yamal Peninsula; (4) the maximum trends (0.06 °C/yr or more) are recorded in southern Siberia, central Yakutia, and in the Chukchi Peninsula.

Taking into account the great climate variability through the past decade, each following year may be expected to bring about more correction to the mean linear air temperature trends and thus change the mapped patterns.

Permafrost monitoring at the steady-state-stations since the late 1960s shows an increasing trend of frozen ground temperatures to follow the climate warming [*Skachkov et al., 2005, 2007; Malkova, 2010*]. The contemporary mean annual ground temperature trends are highly variable over the permafrost extent but the warming rates are most often within two thirds of the air values. The air temperature trends range from 0.02 to 0.07 °C/yr while the range for frozen ground is from 0.004 to 0.050 °C/yr. Air warming causes the strongest effect on the permafrost temperature patterns in the case of stable long-term unidirectional trends in both air temperature and snow

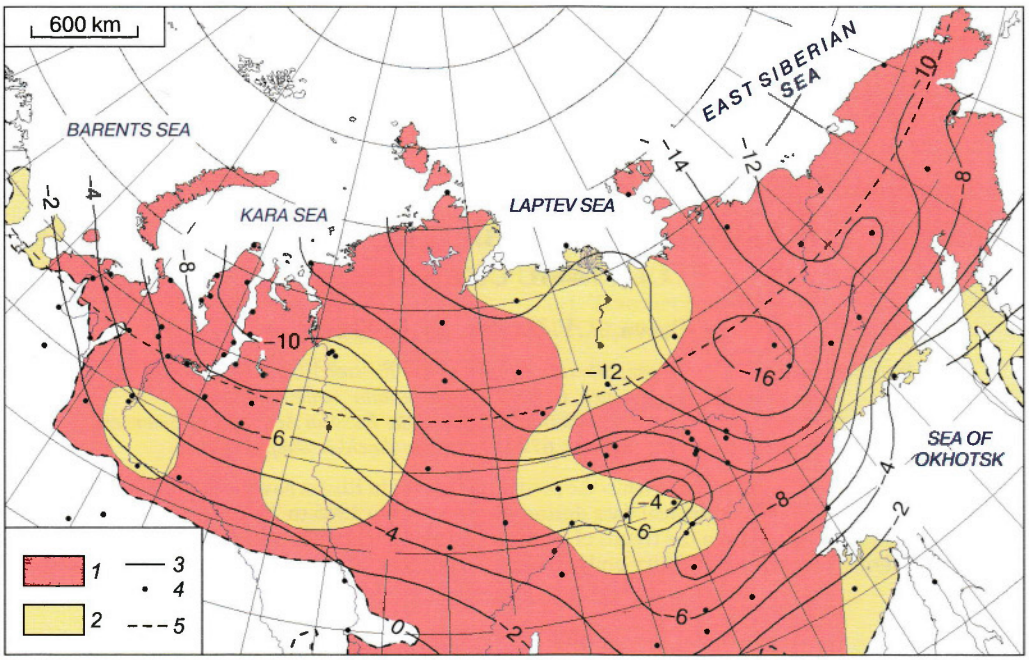

Fig. 1. Variations of mean annual air temperature in northern Russia over the past decade.

1, 2 – temperature rise relative to climate norm: *1* – strong ($\Delta t_{air} > 1$ °C), *2* – temperate (0.7 °C ≤ $\Delta t_{air} \leq 1.0$ °C); *3* – mean annual air temperature isolines (climate norm); *4* – weather stations; *5* – southern limits of cryolithozone.

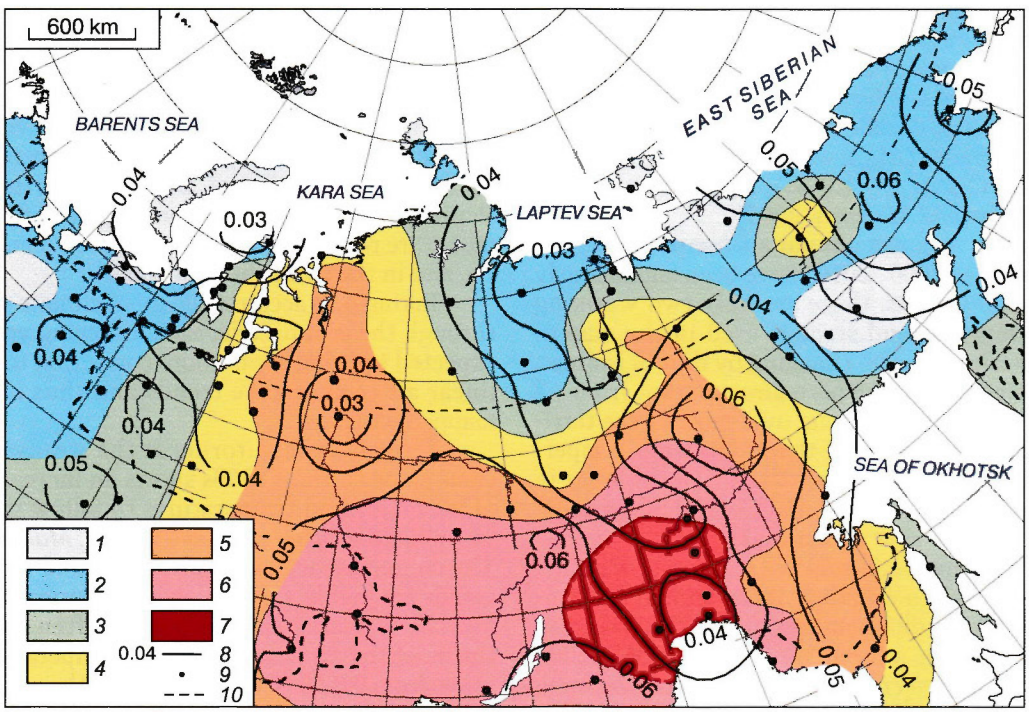

Fig. 2. Mean annual air temperature trends in northern Russia.

1–7 – trend (warming rate), in °C/yr, for 1965–2000: *1* – less than 0.02; *2* – 0.02–0.03; *3* – 0.03–0.04; *4* – 0.04–0.05; *5* – 0.05 – 0.06; *6* – 0.06–0.07; *7* – more than 0.07; *8* – trend (warming rate), in °C/yr, for 1965–2010; *9* – reference weather stations; *10* – southern limits of cryolithozone.

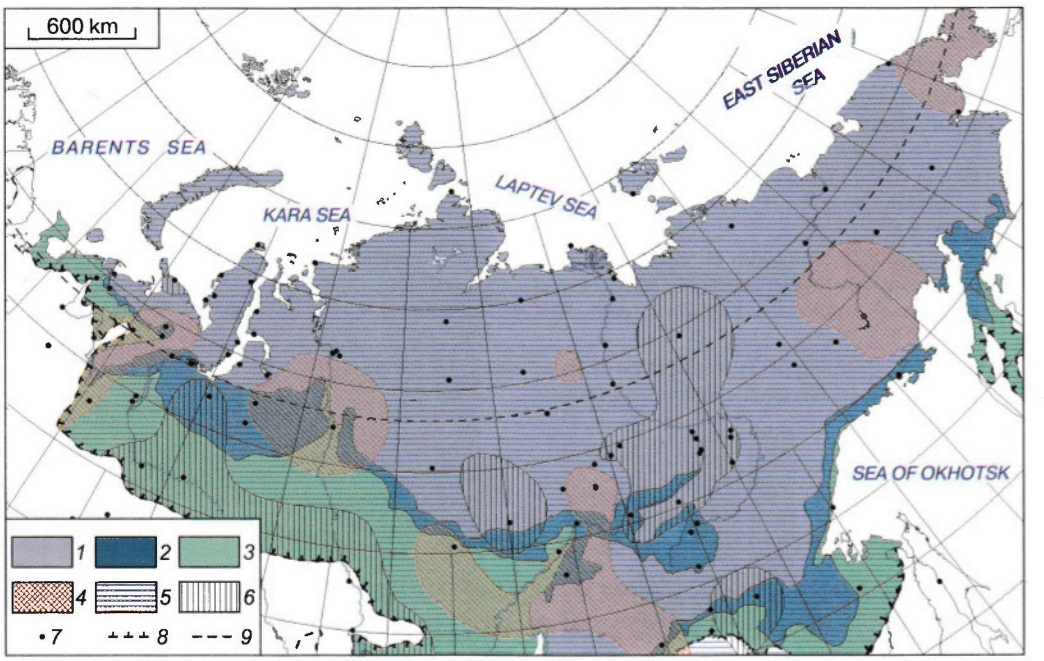

Fig. 3. Map of thermal stability of frozen ground in cryolithozone of Russia.

1–3 – extent of permafrost: *1* – continuous, *2* – discontinuous, *3* – sporadic and patched; *4–6* – thermal stability: *4* – low ($K_\alpha > 0.75$), *5* – medium ($0.50 < K_\alpha \leq 0.75$), *6* – high ($K_\alpha \leq 0.50$); *7* – weather stations and observation sites; *8* – southern limits of cryolithozone; *9* – Arctic circle.

thickness [*Pavlov, 2008b; Pavlov and Malkova, 2010; Pavlov et al., 2010*].

It is convenient to estimate the stability of frozen ground and its sensitivity to climate change using the dimensionless coefficient $K_\alpha = \alpha_{tg} / \alpha_{ta}$, which is the ratio of mean annual temperature trends of ground (α_{tg}) to that of air (α_{ta}) [*Pavlov and Malkova, 2009*].

The coefficient $K_\alpha \leq 0.50$ corresponds to a high stability of frozen ground (long-term temperature changes below 50 %: the ground temperature trends are more than twice slower than the air temperature ones); the range $0.50 < K_\alpha \leq 0.75$ corresponds to medium stability (the ground temperature trends are slower than the air temperature ones for a factor of 1.5 or 2); at $K_\alpha > 0.75$ the permafrost stability is low.

These grades were used to map the thermal stability of upper permafrost (Fig. 3). The greatest part of the permafrost zone pertains into the range $0.50 < K_\alpha \leq 0.75$ corresponding to medium warming stability, while the areas of high and low stability are local.

In spite of rapid recent warming, permafrost in southern Yakutia remains highly stable, as a result of variability in snow thickness and a strong control from winter freezing patterns and peculiarity of snow accumulation [*Skachkov, 2008*]. Note that frozen ground temperatures in the south of West Siberia and in the Russian Far East do not show increasing trends synchronous with the air warming. The reason may be that the permafrost is high-temperature (close to 0 °C) and much heat coming from the Sun is spent on phase change in the ground [*Pavlov and Malkova, 2009*]. However, if stable warming continues, frozen ground can thaw all over those areas. Especially vulnerable is permafrost in the Komi Republic, in the middle reaches of the Yenisei, and in the Baikal region where it is discontinuous or sporadic and shows rapid warming rates.

Thus, monitoring and small-scale GIS mapping of permafrost are efficient tools to study the geocryological consequences of climate warming. The reported studies allowed compiling a set of small-scale maps, with thermal stability division, and estimating the responses of permafrost to the contemporary climate change.

References

Malkova G.V., 2010. Mean-annual ground temperature monitoring on the steady-state-station Bolvansky. Kriosfera Zemli, XIV (3), 3–14.

Melnikov V.P., Pavlov A.V., Malkova G.V., 2007. Consequences of contemporary global change in permafrost. Geografiya i Prirodnye Resursy, No. 3, 19–27.

Pavlov A.V., 2008a. Permafrost Monitoring [in Russian]. Geo, Novosibirsk, 229 pp.

Pavlov A.V., 2008b. Contemporary ground temperature trends in northern Russia. Kriosfera Zemli, XII (3), 22–27.

Pavlov A.V., Ananieva G.V., 2004. Assessment of the contemporary air temperature change over permafrost territory of Russia. Kriosfera Zemli, VIII (2), 3–9.

Pavlov A.V., Malkova G.V., 2005. Contemporary changes of climate in northern Russia. Album of small-scale maps [in Russian]. Geo, Novosibirsk, 54 pp.

Pavlov A.V., Malkova G.V., 2009. Smal-scale mapping of trends of contemporary ground temperature changes in the Russian North. Kriosfera Zemli, XIII (4), 32–39.

Pavlov A.V., Malkova G.V., 2010. Permafrost dynamics in the changing climate through the 20th–21st centuries. Izv. RAN. Ser. Geogr., No. 5, 44–51.

Pavlov A.V., Perlshtein G.Z., Tipenko G.S., 2010. Actual aspects of modeling and prediction of the permafrost thermal state under climate change conditions. Kriosfera Zemli, XIV (1), 3–12.

Skachkov Yu.B., 2008. Contemporary variability of snow cover parameters in Yakutia, in: Cryogenic Resources of Arctic and Highland Terrains. State and Prospects of Engineering Permafrost Studies. Proc. Intern. Conf., Express, Tyumen, pp. 271–274.

Skachkov Yu.B., Skryabin P.N., Varlamov S.P., 2007. Results of 25-year long summer permafrost monitoring at the Chabyda site (Central Yakutia), in: Cryogenic Resources of Arctic Regions. Proc. Intern. Conf. TyumNGU, Salekhard, Book 1, pp. 167–170.

Skachkov Yu.B., Skryabin S.P., Varlamov S.P., 2005. Effects of contemporary climate change on permafrost in Central Yakutia, in: Proc. 3rd Russian Cryological Conference [in Russian]. Moscow University Press, Moscow, Book 2, pp. 146–152.

Received
3 February 2011

Kriosfera Zemli, 2011, vol. XV, No. 4, pp. 32–35 **http://www.izdatgeo.ru**

LANDSCAPE INDICATION OF LOCAL PERMAFROST VARIABILITY (URENGOY TERRITORY, WEST SIBERIA)

N.G. Ukraintseva, D.S. Drozdov, K.A. Popov, A.G. Gravis, G.V. Matyshak*

Institute of Earth's Cryosphere, Siberian Branch of the Russian Academy of Sciences, PO box 1230, Tyumen, 625000, Russia; ukraintseva@mail.ru
**Lomonosov Moscow State University, Department of Soil Science, 1-12, Leninskie Gory, Moscow, 119992, Russia*

The highly variable properties of frozen ground make engineering-geological mapping in the permafrost zone impossible without cryological monitoring. Integrate monitoring of natural and technogenic landscapes has been run at test sites in southern forest-tundra and southern tundra (area of Urengoy oil-gas-condensate field) by remote sensing along with surface route and instrumental (automated) surveys and GIS mapping. As a result, a set of map models have been obtained that demonstrate obvious relationship between the landscape features and the thicknesses of peat and active layer. The studies have revealed a new indicator of the permafrost thermal state.

INTRODUCTION

Several test sites were set up in northern West Siberia in 1974–1976 to monitor space-time variations in properties of frozen ground. Two sites were on the left bank of the Pur River, within the Urengoy oil-gas-condensate field, one in southern forest-tundra (UKPG-5) and the other in southern tundra (UKPG-15) [*Drozdov et al., 2010a*]. In 2008, the observations at the two sites became complemented with thaw depth monitoring on a 100 × 100 m grid, with a spacing of 10 m, as part of the CALM International Project (Circumpolar Active Layer Monitoring). Exhaustive landscape studies at the CALM sites have yielded a set of map models that demonstrate obvious relationship between the local landscape features and the thicknesses of peat and active layer.

METHODS

The test sites within the Urengoy oil-gas-condensate field were created as early as in 1975–1976. Permafrost temperature monitoring was performed as yearly measurements in 10–12 m deep boreholes; since 2008, the monitoring has been continuous due to permanent loggers that provide year-round records. Local undisturbed and disturbed ecosystems associated with different landscapes within the CALM sites have been classified (at the level of landscape facies), investigated in terms of above-surface phytomass, and mapped to scale 1:5000 (Fig. 1, *A*). Maps of this kind, based on the landscape-indication approach, can be used as a basis for estimating local variations in the active layer thickness and for map modeling [*Moskalenko, 1999; Bozhilina and Ukraintseva, 2010*].

LANDSCAPE SYSTEMS: STRUCTURE AND CRYOTIC PROPERTIES

The CALM site in southern forest-tundra (UKPG -5) is located within fluviolacustrine plain IV in the Nadym-Pur subprovince of coastal (marine)

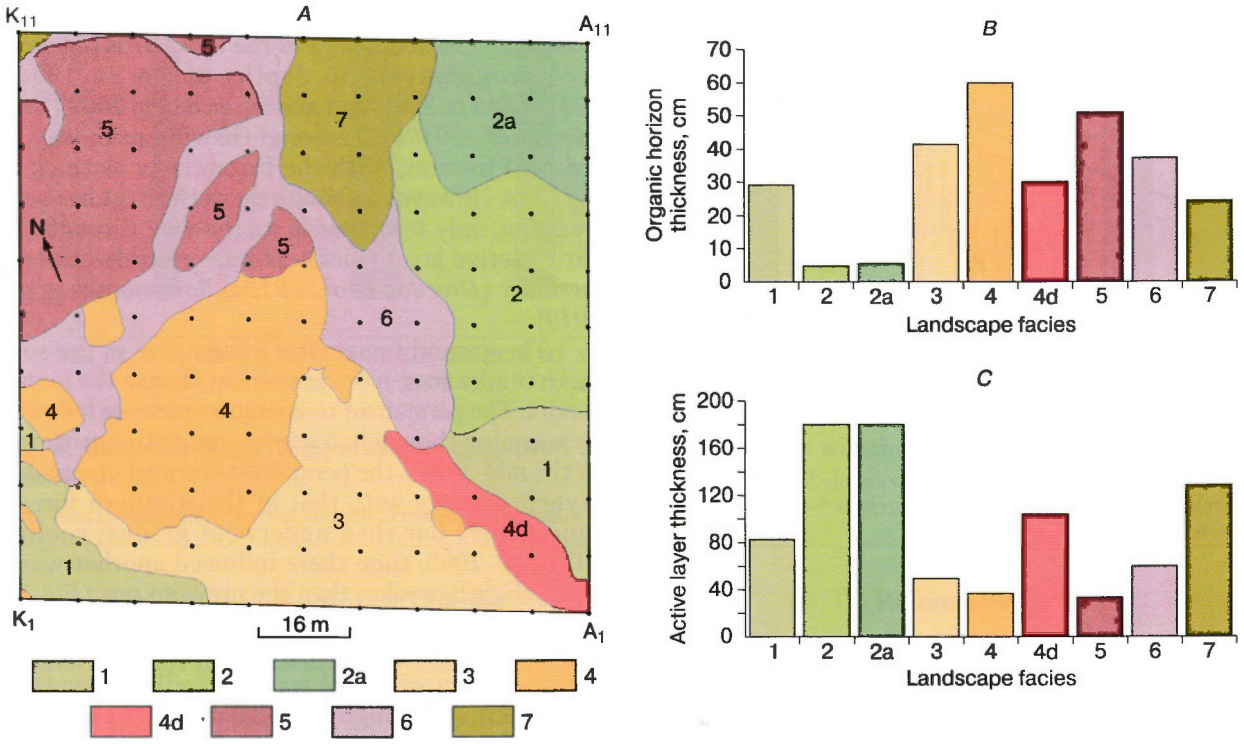

Fig. 1. CALM site in southern forest-tundra (UKPG-5).

A – landscape map; *B* – thickness of organic soil horizon; *C* – active layer thickness (seasonally thawed or seasonally frozen). Landscape facies: 1 – hilly open shrub-moss areas; 2 – sparse larch-lichen forests; 2a – same, with sag-and-swell microtopography; 3 – flat-hill cloudberry-sphagnum peatbogs; 4 – polygonal ledum-sphagnum-lichen peatbogs; 4d – same, but disturbed areas with old ruts; 5 – polygonal dwarf-birch (yernik)-ledum-lichen peatbogs; 6 – hummocky grass-shrub-moss ravines; 7 – ravines with shrub-grass-moss birch thickets (yernik) (to 1.0–1.5 m high). A_1, A_{11}, K_1, K_{11} are indices of points at CALM sites.

and fluviolacustrine plains. The plain is composed of loam-sand deposits, often overlain with peat. Permafrost, mostly with high ice contents, is continuous or discontinuous and occupies over 80 % of the surface area. The landscapes are largely affected by frost cracks and thermokarst and are swampy.

The dominant landscape facies at the site is watershed peatbog which and larch-lichen open forest both shrubby ravines along a creek valley (Fig. 1, *A*). The above-surface phytomass[1] measured as air-dry weight per area is 1–3 kg/m^2 in the peatbog and exceeds 5 kg/m^2 in the larch open forest [*Ukraintseva et al., 2010*]. The active layer thickness (seasonally thawed layer) is inversely proportional to the total thickness of organic soil horizons (Fig. 1, *B*, *C*). Underneath the larch open forest, the permafrost table is as deep as 4–8 m, and the ground is seasonally frozen.

The CALM site of southern tundra (UKPG-15) is located within coastal plain III composed mainly of loam. The permafrost is ice-rich (total water contents 60 % in loam and 21–28 % in sand) and continuous from the surface. The site has a uniform facies structure dominated by grass-shrub-moss-lichen tundra with a thin organic soil layer; limited dwarf willow and birch thickets and sporadic grass-sphagnum bogs are restricted to ravines. In the bottoms of large erosional landforms, there are low perennial frost heaves. The phytomass is 1.7–2.3 kg/m^2, or 0.8–1.2 kg/m^2 without litter. The active layer thickness is from 80–90 to 100–115 cm [*Ukraintseva et al., 2010*].

PERMAFROST MONITORING RESULTS

The permafrost temperature over the 1974–2008 period showed a positive trend all over the study area [*Drozdov et al., 2010a*]. Borehole temperature logging at the southern forest-tundra site, along with geophysical data, indicate permafrost table deepening on the background of steady ground temperature increase associated with global warming through the recent decades (Fig. 2) [*Shur and Jorgenson, 2007; Pavlov, 2008; Melnikov et al., 2009; Romanovsky et al., 2010*]. For instance, the permafrost table underneath

[1] Phytomass is measured in air-dry weight units per surface area unit (square meter, hectare, etc.).

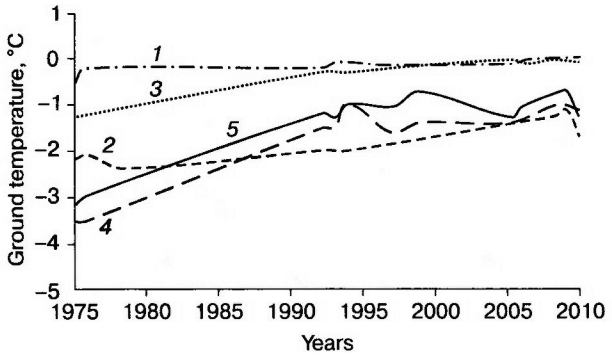

Fig. 2. Time-dependent ground temperature variations at depth of zero annual amplitude (southern forest-tundra).

1 – borehole 5-01, larch forest; *2* – borehole 5-02, peatbog; *3* – borehole 5-05, ravine shrub; *4* – borehole 5-06, slope tundra; *5* – borehole 5-09, bog edge, peat.

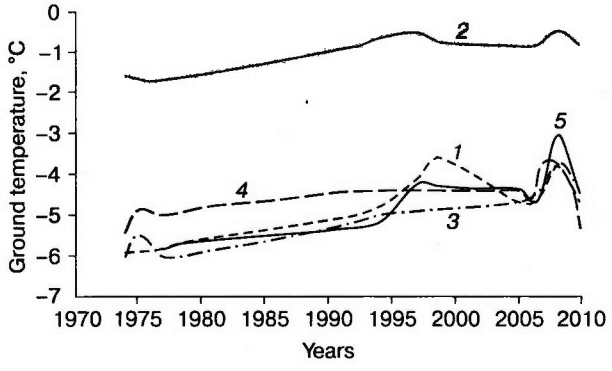

Fig. 3. Time-dependent ground temperature variations at depth of zero annual amplitude (southern tundra).

1 – borehole 15-03, tundra with peat; *2* – borehole 15-06, slope alder wood; *3* – borehole 15-08, moss-lichen tundra; *4* – borehole 15-20, moss-lichen tundra; *5* – borehole 15-21, disturbed moss-lichen tundra.

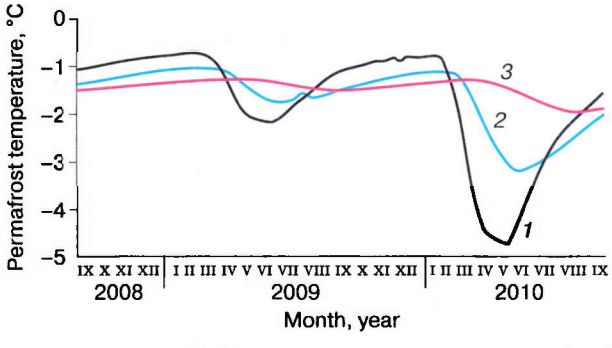

Fig. 4. Permafrost temperature in watershed peatbog (southern forest-tundra).

Depths: *1* – 3 m; *2* – 5 m; *3* – 10 m.

the sparse larch forest was at the surface (1.5–2.0 m seasonally thawed layer) in the late 1970s but lowered progressively to depths of 3 m in 1994–1997, 4.5 m in 2005, and as deep as 8 m in 2009 [*Drozdov et al., 2010b*]. Seasonal thawing gave way to seasonal freezing, with the frozen layer as thick as over 2 m. However, although the permafrost has been warming, only few cases of its thawing through the entire active layer thickness were recorded instrumentally [*Drozdov et al., 2010a; Romanovsky et al., 2010*].

The ground temperature anomalies in the southern tundra were more prominent than in the forest-tundra. The permafrost temperature increase followed air warming though had uneven oscillating patterns. In the mid-1990s, the permafrost warmed up notably (synchronously with that at the southern forest-tundra site) but then underwent gradual cooling till 2004–2005; then there followed another warm wave, slightly weaker than the previous one (Fig. 3). The permafrost temperature was originally higher (−1.7 °C in 1974) than in the surrounding area, but the warming trend was markedly lower (less than 1 °C) under high (1.5–3.0 m) alder shrubs on southern slopes protected from cold, due to the shrub buffer [*Drozdov et al., 2010a, b; Ukraintseva et al., 2010*].

The general climate trends within the Urengoy oil-gas field began to change in the fall of 2009. Abrupt cooling in fall time followed by an anomalously cold and low-snow winter (2009/10) led to an up 0.5 °C decrease in permafrost temperature at the active layer base in most landscape facies (Figs. 2, 3). The temperature drop was still greater in the upper section: e.g., 3 and 1.5 °C cooling at subsurface depths 3 and 5 m, respectively, in a watershed peatbog within the southern forest-tundra (Fig. 4). Note that no permafrost cooling was observed in the 3 to 8 m thick near-surface ground under open forest and shrubs because of the damping effects of phase transitions (Fig. 2).

A NEW INDICATOR OF THE PERMAFROST THERMAL STATE

A new parameter of large diagnostic importance for the state of permafrost and thawing rate has been revealed in data inventory from weather stations in the vicinity of the test sites within the subzones of southern forest-tundra (Novyi Urengoy) and southern tundra (Yamburg). This is the duration of time in spring and fall when diurnal air temperatures fluctuate between positive and negative, which we called briefly an "across 0 °C" season. This season may be as long as 1.5 months or more in the Urengoy field, while the monthly and ten-day means may remain positive or negative, the passage across 0 °C being reduced to

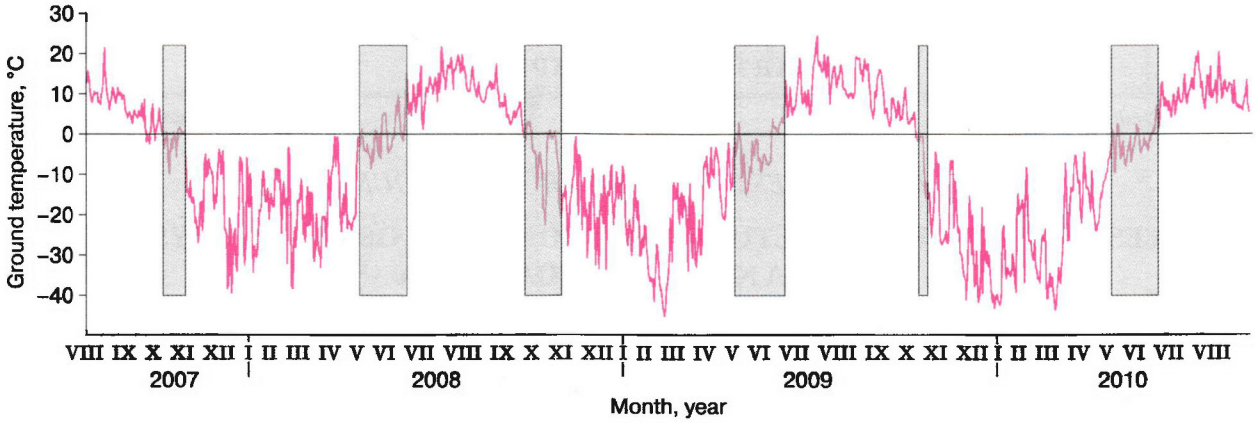

Fig. 5. Mean daily air temperatures measured at Novyi Urengoy weather station (southern forest-tundra).

Gray bars correspond to spring and fall across 0 °C seasons.

single points (ends of months or ten-day spans). Meanwhile, the duration of the across 0 °C time calculated from air temperature daily means may be a meaningful indicator of the thermal state of permafrost. For instance, prominent shortening of this time in the fall of 2009 (Fig. 5) was accompanied by notable permafrost cooling in the following year of 2010 (Figs. 2–4).

CONCLUSIONS

The rate and depth of permafrost thawing in forest-tundra are largely controlled by diverse vegetation with considerable amounts of above-surface phytomass. As a result, there arises a pattern of alternating zones of deep and shallow permafrost table, the active layer being additionally buffered by organic soil horizons.

The soil and vegetation control of the permafrost temperature and active layer thickness at the southern tundra site is much smaller than in the southern forest-tundra.

The duration of the season when mean daily air temperatures fluctuate between positive and negative may be of significant diagnostic value as an indicator of the thermal permafrost state. The latter inference requires further support with more observations.

The study was carried out as part of TSP (Thermal State of Permafrost) and CALM (Circumpolar Active Layer Monitoring) International Projects and of research programs of the Russian Academy of Sciences (RAS) and the RAS Siberian Branch. It was additionally supported by grants 08-05-00872 and 09-05-10030k from the Russian Foundation for Basic Research.

References

Bozhilina E.A., Ukraintseva N.G., 2010. Specialized field surveys for nature mapping. Geodeziya i Kartografiya, No. 6, 36–41.

Drozdov D.S., Ukraintseva N.G., Tsarev A.M., et al., 2010a. Changes of permafrost temperature field and geosystem state on Urengoy oi-gas-field territory during the last 35 years (1974–2008). Kriosfera Zemli, XIV (1), 22–31.

Drozdov D.S., Ukraintseva N.G., Tsarev A.M., 2010b. Active layer and permafrost table lowering in the Tundra/Forest-tundra transition zone at Urengoi oil-gas field (West Siberia), in: Thermal State of Frozen Ground in a Changing Climate during the IPY: Abstracts, III European Conference on Permafrost (EUCOP III), Svalbard, Norway, p. 102.

Melnikov V.P., Drozdov D.S., Pavlov A.V., et al., 2009. Climate change and response of northern ecosystems, in: Global Change and Adaptation Mechanisms. Proc. Workshop, Moscow, pp. 36–37.

Moskalenko N.G., 1999. Anthropogenic Dynamics of Vegetation in Plainland Permafrost Areas of Russia [in Russian]. Nauka, Novosibirsk, 280 pp.

Pavlov A.V., 2008. Monitoring of Permafrost [in Russian]. Geo, Novosibirsk, 229 pp.

Romanovsky V.E., Drozdov D.S., Oberman N.G., et al., 2010. Thermal state of permafrost in Russia. Permafrost and Periglacial Processes, 21 (2), 136–155. (Special Issue: The International Polar Year http://onlinelibrary.wiley.com/doi/10.1002/ppp.683/abstract).

Shur Y.L., Jorgenson M.T., 2007. Patterns of permafrost formation and degradation in relation to climate and ecosystems. Permafrost and Periglacial Processes, 18, 7–19.

Ukraintseva N.G., Drozdov D.S., Popov K.A., et al., 2010. Active layer response to biomass and soil-vegetative cover changes at CALM-site in the Tundra/Forest-tundra transition zone (West Siberia, Urengoi oil-gas field), in: Thermal State of Frozen Ground in a Changing Climate during the IPY: Abstracts, III European Conference on Permafrost (EUCOP III), Svalbard, Norway, p. 107.

Received
18 February 2011

SCIENTIFIC JOURNAL
EARTH'S CRYOSPHERE

Kriosfera Zemli, 2011, vol. XV, No. 4, pp. 36–37 http://www.izdatgeo.ru

PROPERTIES OF ICE AND FROZEN GROUND

INVESTIGATING THE STRUCTURE AND PROPERTIES OF ICE-LIKE SYSTEMS: A NOVEL APPROACH

M.V. Kirov

Institute of Earth's Cryosphere, Siberian Branch of the Russian Academy of Sciences, PO box 1230, Tyumen, 625000, Russia; kirov@ikz.ru

A novel combinatorial topological approach is suggested to investigate the structure and properties of ice and other ice-like systems. The approach is based on discrete models of molecular interaction, as well as on combinatorial optimization algorithms, and provides a general idea of the energetics and other properties of numerous proton configurations with different arrangements of hydrogen atoms (protons) in hydrogen bonds. The new approach was applied to develop a special crystallographic database of proton configurations for unit cells of widespread gas hydrate frameworks. A new type of hidden molecular asymmetry of ice-like systems was discovered which is caused by non-invariance of hydrogen-bound frameworks with respect to direction changes in all H-bonds. The optimal proton configurations of polyhedral water clusters has been calculated using a specially developed max-plus-algebraic method for combinatorial optimization of quasi-one-dimensional systems.

The ordinary ice is remarkable for having disordered positions of hydrogen atoms (protons). The proton positions in hydrogen bonds (H-bonds) make up a great number of configurations, and this number grows exponentially with the size of the system [*Eizenberg and Kautsman, 1975*]. Yet, the energy and other characteristics depend on the specific arrangement of protons in H-bonds. Energy difference within the set of all possible proton configurations may exceed the ice melting heat. It is extremely difficult to investigate in detail ice properties with regard to the proton positions in H-bonds. Note that the complexity of an object is defined by the minimum of information required for its detailed description [*Kolmogorov, 1965*].

A novel combinatorial topological approach suggested by *Kirov* [*2010*] to investigate the structure and properties of ice and other ice-like systems with a tetrahedral coordination of H-bonds is based on discrete models of molecular interaction. These approximate models are designed to provide a generalized idea of properties that characterize the set of all proton configurations. The discrete models of molecular interaction have a clear physical background, and this makes the new combinatorial topological approach advantageous over the more frequently used statistical approach which aims at finding formal correlation relationships between the energy (or other parameters) and the set of structural invariants.

The discrete models of molecular interaction estimate the energy of a system from the number of preferred structure fragments. The high predictive capacity and utility of the models have been validated through our collaboration with experts in quantum-chemical modeling (S.S. Xantheas, Pacific Northwest National Laboratory, USA). Figure 1 shows for polyhedral water clusters in the form of gas hydrate cavities and distributions of discrete optimized proton configurations [*Kirov et al., 2008*]. The energy detachment of these proton configurations (black fields in Fig. 1) is especially prominent in the plane "energy U – total dipole moment D". Additional geometrical optimization of proton configurations calculated from the discrete models of molecular interaction was performed using rigid intermolecular potentials. For cavity D, we used also one of the most advanced potentials (TTM2-F) that takes into account the inner degrees of freedom of molecules (Fig. 1, panel *b*). Gray points in the left in this case correspond to the configurations that lost their original polyhedral geometry on optimization.

The properties of large macroscopic samples of ice and other ice-like systems commonly do not manifest explicitly their dependence on the structure of the proton subsystem because of averaging over all possible configurations. However, in simulation with a small model cell, the result obviously depends on the position of protons in H-bonds, i.e., on the original orientation of molecules. It should be emphasized that this dependence records the real nanostructural heterogeneity of ice-like systems. A good solution for this difficulty, feasible with advanced computing facilities, may come from special proton configuration databases which include all possible positions of hydrogen atoms

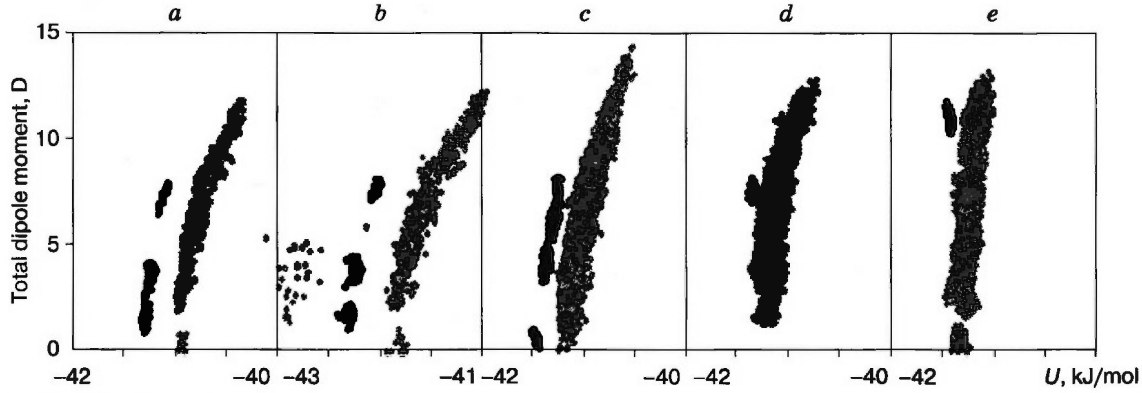

Fig. 1. Distribution of proton configurations at ground (black) and following (gray) energy levels, for polyhedral water clusters in the form of gas hydrate cavities.

Gas hydrate cavities and number of pentagonal and hexagonal faces in polyhedra: *a* – D(5^{12}), *b* – D, TTM2-F, *c* – T($5^{12}6^2$), *d* – H($5^{12}6^4$), *e* – E($5^{12}6^8$).

(protons), along with the position of oxygens in the unit cell. At present, exhaustive databases have been developed for most widespread gas hydrate frameworks: TS-IV, HS-III, CS-I, which allows upgrading the methods of studying gas hydrates due to regard for the structure of the proton subsystem.

The simplified combinatorial topological approach allowed discovering a new type of hidden molecular symmetry in ice-like systems, or more precisely an *antisymmetry*. Changing the directions of all H-bonds may be tried as an additional antisymmetry operation. The discovered symmetry was found out to be approximate (not exact) because the hydrogen-bonded ice-like systems were not invariant with respect to the removal of all H-bonds. The antisymmetry of proton configurations, as well as its relation with stability, were investigated for a great number of ice-like systems (cyclic and polyhedral water clusters and various gas hydrate frameworks). The study has led to a hypothesis that the supramolecular asymmetry of ice-like systems associated with the approximate antisymmetry can define a particular type of ordering in these systems and be the primary cause of the origin and stability of mirror asymmetry in living systems at the molecular level (homochirality of biopolymers).

The combinatorial topological approach was applied in developing a special max-plus algebraic method for global combinatorial optimization of quasi-one-dimensional discrete systems. Max-plus algebra is a field in modern mathematics which uses the simpler operations of maximization and summation instead of the common arithmetic summation and multiplication. With the new optimization method, the classes of energy-lowest proton configurations were exactly calculated for polyhedral water clusters from a cube to a fullerene, including those in the form of cavities of commonest gas hydrates. The new max-plus-algebraic method of combinatorial structural optimization is easily programmable and can be extended to systems of any chemical nature.

The high efficiency of the approximate combinatorial topological approach to modeling ice-like systems is due to their complex multilevel molecular organization. Different modeling levels correspond to specific organization levels. For instance, the model of H-bonded networks takes into account the topology and geometry of the bond framework. The discrete models of molecular interaction take an approximate account of the energy preferability of the proton positions in H-bonds. The approximate antisymmetry of hydrogen bonding reflects a new virtually unexplored organization level in complex ice-water systems. Complex multilevel systems of this kind are increasingly becoming the focus of modern natural sciences.

References

Eizenberg D., Kautsman V., 1975. The Structure and Properties of Water. Oxford University Press, London, 242 pp.

Kirov M.V., 2010. A Combinatorial Topological Approach in Investigating the Structure and Properties of Ice-Like Systems [in Russian]. Doctor of Science Thesis, Moscow, 303 pp.

Kirov M.V., Fanourgakis G.S., Xantheas S.S., 2008. Identifying the most stable networks in polyhedral water clusters. Chem. Phys. Lett., 461 (4–6), 180–188.

Kolmogorov A.N., 1965. Three approaches to the quantitative definition of information. Problems of Information and Transmission, 1 (1), 1–7.

Received
16 February 2011

Kriosfera Zemli, 2011, vol. XV, No. 4, pp. 38–40 http://www.izdatgeo.ru

CONTRIBUTION OF ICE MOVEMENT TO HEAT AND MASS TRANSFER PROPERTIES OF POROUS SOLIDS

V.S. Kolunin, A.V. Kolunin, A.D. Pisarev

Institute of Earth's Cryosphere, Siberian Branch of the Russian Academy of Sciences, PO box 1230, Tyumen, 625000, Russia; askold@ikz.ru

The results of experiments are presented for heat and mass transfer through water-saturated ceramics with an ice inclusion. Temperature gradient dependences of heat and mass fluxes are obtained at different average temperatures. Possible reasons are suggested to explain the difference of the experimental data from theoretical prediction.

As water-saturated fine-grained soil freezes up, water is normally driven toward the freezing front and soil moisture increases. Structural changes in freezing soil are especially intense in the frozen part, where the temperature approaches the freezing point, and are accompanied by heat and mass transfer. Ice can move relative to soil particles as a consequence of regelation thus contributing to heat and mass transfer. This motion can be induced by different thermodynamic forces, such as gradients of pressure, temperature, and concentration.

The behavior of cryosols in a gradient temperature field reveals properties that seem to be unexpected. Water in a closed system of a uniform fully saturated frozen soil migrates towards lower temperatures under a temperature gradient about the natural one [*Ershov, 1979*]. In an open system, on the contrary, the mass flux through a soil sample is in the direction of the temperature gradient [*Perfect and Williams, 1980*]. The reason is that the deformability of soil skeleton is crucial in the former case of a closed system (water content changes being impossible otherwise) but is insignificant in the case of an open system while the motion of ice relative to the soil skeleton becomes of major importance.

Both factors should be taken into account in modeling heat and mass transfer in frozen soil. Furthermore, one has to bear in mind that deformation of a soil skeleton is always attendant with motion of ice relative to soil particles.

The problem is in finding the general laws of the relative motion of solid phases in frozen and freezing soils. The sequence of steps in the solution implies that the soil skeleton deformation were excluded from consideration, e.g., by means of using porous materials with a stiff matrix.

In this study we report the results of experiments on heat and mass transfer through ceramics with an ice inclusion under a temperature gradient and compare them with theoretical prediction.

Figure 1, *a* shows the main unit of the experimental device. The sample is a water-saturated ceramic cylinder with a cavity (Fig. 1, *b*).

Before the experiment, the system was vacuumed and filled with distilled water. The experiment was run in conditions of an open system at negative temperatures and a zero pressure difference at the sample boundaries. The cavity in the sample center was filled with ice. The ceramics at the side of the cavity consisted of three rings separated by thin sealant (13). That is why water transport through the middle of the sample was assumed to be by regelation.

The temperature gradient induces water flux in the system. The volumetric water flow rate was measured from motion of meniscus in capillary tubes (7) connected to the cell input and output (Fig. 1). For heat flux measurements, standard cylinders (3) were set tightly against the external bases of brass fins (2); heat transfer was through the cylinders to massive heat-exchangers maintained at a constant temperature (5). Axial heat flux in the cell was estimated, according to the Fourier law, from temperatures measured at the bases of cylinders (3).

A single run took from 18 to 36 hours, the time during which constant temperature was maintained at the heat exchangers. Water flux through the sample was measured likewise for the same period.

Ceramics is a phase barrier that prevents ice from penetrating into vessels (14) for the temperature range 0...–0.05 °C.

In most runs, root mean square deviation from the mean temperature did not exceed 0.0005 °C in the heat exchangers and 0.005 °C in brass fins.

The experimental data were compared with the theory using specially designed software [*Kolunin, 2005*] applied also to solve the associated problems of heat in the interior of the main unit and filtration in ceramics. The input parameters were the temperature of heat exchangers and the pressure in the tubes. The software was used to estimate the velocity of ice mov-

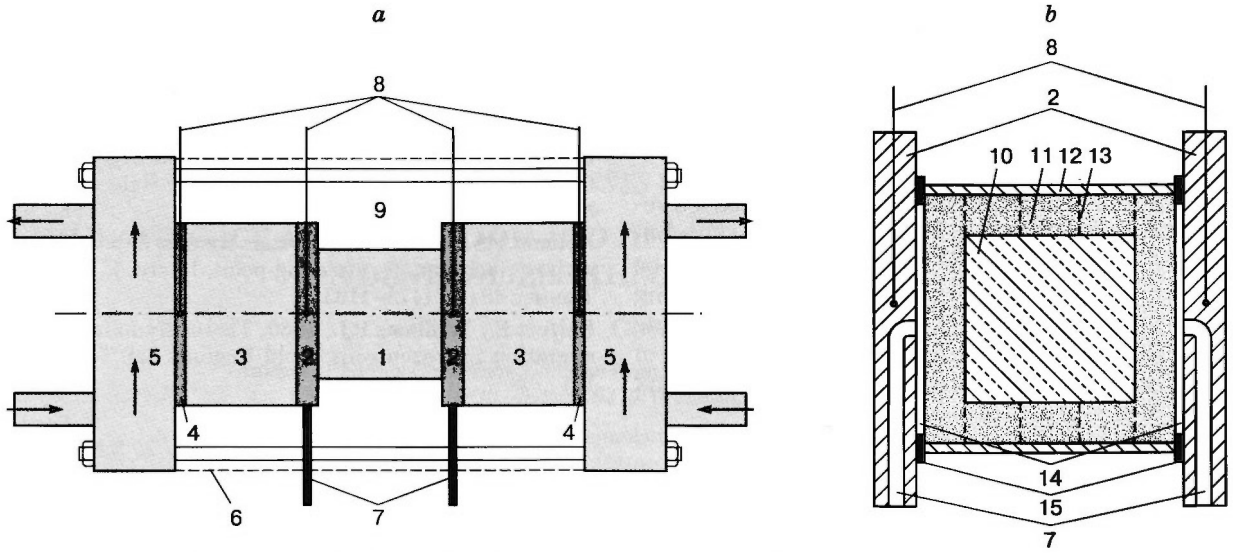

Fig. 1. Layout of the system for investigating heat and mass transfer in porous solids.

a – general layout: 1 – sample, 2 – brass fins, 3 – plexiglass cylinders, 4 – copper plates, 5 – brass heat exchangers which thermostatic liquid is pumped through, 6 – copper foil screen, 7 – water channels, 8 – measuring ends of difference thermocouples, 9 – foam plastic; *b* – measured sample: 10 – cavity (ice), 11 – porous ceramics, 12 – plastic cartridge, 13 – joint of porous ceramic rings, 14 – water-filled clearance vessels, 15 – rubber sealants.

ing in the cavity plane, the temperature of the brass fins, and the fluxes of heat and moisture through the sample bases.

The flux of material through the sample was assumed to be in the direction of the temperature gradient. The heat and water fluxes depended almost linearly on the temperature difference (Fig. 2). As the mean temperature decreased, other things being equal, the fluxes decreased proportionally. Compared with theoretical prediction, the experimental points are below the calculated ones (Fig. 2, *a*, *b*).

The regleation movement of ice in the cell cavity can produce spatially separated heat sources and sinks thus contributing to heat transfer through the cells. The effective thermal conductivity of a cell (λ) depending on ice velocity was predicted to be 1.53 W/(m·K) and decreased nearly by a factor of 1.5 when ice was fixed relative to the ceramics. The average experimental thermal conductivity coefficient was 1.26 W/(m·K) (Fig. 2, *a*), which corresponds to an observed ice velocity about 1.7 times lower than the predicted one. The theoretical ice velocity may be

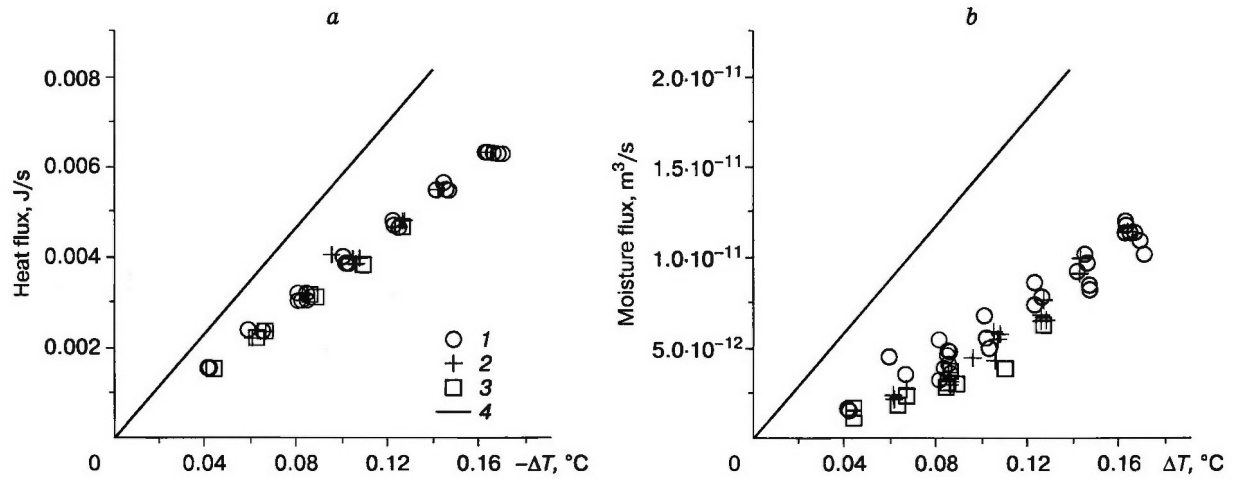

Fig. 2. Heat (*a*) and water (*b*) fluxes through sample as a function of temperature difference ΔT at its base surfaces.

1–3 – experimental data at average temperatures –0.02 °C, –0.03 °C, –0.04 °C, respectively; line is theoretical prediction.

higher because it neglects the resistance of unfrozen water films between the ice and the ceramics in the phase change domain.

The thermal osmotic coefficient calculated from experiment data (Fig. 2, *b*) turned out to be 2–3 times as low as the predicted value.

The difference between real and predicted ice velocities alone cannot account for the disparity between the experiment and the theory. There must be some channels between the domains of ice melting and water freezing that never freeze up and provide liquid phase (water) exchange between the bases of ice cylinders thus decreasing the moisture flux through the sample and, as a consequence, decreasing the thermal osmotic coefficient as well.

References

Ershov E.D., 1979. Moisture Transport and Cryotextures in Fine-Grained Rocks [in Russian]. Moscow University Press, Moscow, 216 pp.

Kolunin V.S., 2005. Heat and mass transfer in porous media with ice inclusion near freezing-point. Intern. J. Heat Mass Transfer, 48 (6), 1175–1185.

Perfect E., Williams P.J., 1980. Thermally induced water migration in frozen soils. Cold Regions Sci. Technol., 3, 101–109.

Received
20 February 2011

SCIENTIFIC JOURNAL
EARTH'S CRYOSPHERE

Kriosfera Zemli, 2011, vol. XV, No. 4, pp. 41–45 http://www.izdatgeo.ru

PHYSICO-CHEMICAL PROCESSES IN ICE AND FROZEN GROUND

SIMULATING ICE ACCUMULATION AND DEFORMATIONS ON GROUND FREEZING: A GENERALIZED THEORETICAL MODEL

J.B. Gorelik

Institute of Earth's Cryosphere, Siberian Branch of the Russian Academy of Sciences, PO box 1230, Tyumen, 625000, Russia; gorelik@ikz.ru

A single system of equations is suggested to simulate moisture transport responsible for segregated and injected ice accumulation and to calculate jointly the respective parameters and deformation in freezing ground. The system includes balance equations for heat and mass (water and soil skeleton) at the freezing front. Water fluxes for each mechanism are found with additional equations. The model allows predicting deformation patterns in surface foundations in the case of segregated ice accumulation and the percentage of mineral component in forming frozen structures for the case of injection. For the injection mechanism, there exists a critical water flux above which pure ice forms. The predicted parameters of injected ice accumulation agree with the field observations of the structure and composition of natural ice deposits, as well as with the results of specially designed laboratory experiments.

INTRODUCTION

Soil freezing is commonly attendant with redistribution of moisture below the freezing front, its accumulation in the frozen zone (in the form of various ice bodies which may reach quite big sizes), nonuniform deformation of freezing soil and loading on engineering structures with buried or surface foundations. Moisture flow in unfrozen soil which can cause stress and heaving may differ in origin, but those responsible for segregated and injected ice accumulation are considered to be most important [*Kudryavtsev, 1978*]. The segregation mechanism is explained in terms of surface and capillary forces near the boundary between the frozen and unfrozen portions of freezing soil [*Beskow, 1947; Miller 1978; Grechischev et al., 1980; Gorelik and Kolunin, 2002*]. These forces act like a pump which drives water upward to the freezing front. This mechanism (and segregated ice accumulation) most often works in very fine-grained soils, such as silt-size loamy sand and loam or clay, that freeze in open systems bordering open water. Ice accumulation by this mechanism produces stratified (or other) structures where pure ice lenses alternate with soil [*Ershov, 1979*]. Water fluxes, as well as the whole segregated ice accumulation process, depend largely on temperatures along the fringe of freezing soil, its mass transfer and thermophysical properties, and on external loading transferred to the base of the growing ice lens.

An exhaustive theoretical frost heave model was suggested by *O'Neill and Miller* [*1985*], and its simpler quasi-stationary analog was discussed in detail in [*Gorelik and Kolunin, 2002*]. The model can account for the basic elements of the migration process (water fluxes, ice accumulation parameters, deformation, and depth-dependent changes in heaving stress) at the level of a laboratory sample. Yet, attempts of applying this knowledge to predict the effect on real engineering structures in freezing soil meet serious difficulties. For instance, the heaving stress on piles [*Orlov, 1962*] and surface foundations [*Sazhin et al., 1984*] increases with freezing depth according to field evidence but decreases in the case of laboratory samples [*Gorelik and Kolunin, 2002*]. This paradox is due to difference in ice lens loading: all load on a laboratory sample is transferred to the base of the growing ice lens while in real engineering structures it is redistributed following the deformation parameters of the freezing soil and the unfrozen ground beneath it.

The origin of injection flux is best understandable in the case of a closed volume freezing from above: a closed system without moisture input from outside. The freezing soil is fringed by impermeable walls and bottom (e.g., frozen soil or unfrozen dense clay) and consists of water-saturated coarse material (sand or debris). Rigid bonding between the freezing soil and the water-tight fringe reduces, possibly down to zero, vertical deformation along the walls. Because of the water-ice density difference, this produces high pressure (freezing pressure) in the water near the walls and a water flux from the freezing front inward the unfrozen soil. This flux (injection) is concentrated along the freezing front at the sites which are the

farthest from the confining walls and thus can heave under the freezing pressure. Zones of this heaving are at the same time the zones of excess ice accumulation if they are fed through the injection mechanism. The freezing soil adjacent to its rigid fringe can be called a zone of liquid moisture feeding (recharge) of the heaving zone.

Thus, appropriate simulation of the injection mechanism requires bearing in mind the deformability of freezing soil. Injected ice accumulation basically has no limitation from the soil grain size. According to data from large deposits of ground ice, most of them are of injection origin [*Baulin et al., 1967*]. Yet, until recently there were no theoretical models (nor reports of experimental studies) available in the literature for injected ice accumulation.

SYSTEM OF EQUATIONS IN THE MODEL AND ITS ANALYSIS

In [*Gorelik, 2008, 2010*] a single approach was suggested to solve the ice accumulation problem and to model the attendant mechanic effects for both mechanisms. The approach is based on balance equations at the freezing front, with an additional relationship between the velocities of the freezing soil boundaries:

$$j_h(H) = \kappa\rho_i n_f \dot{H}, \tag{1}$$

$$(n_f - n_u)\dot{z}_f = -(1-n_f)\dot{z}_s, \tag{2}$$

$$\rho_w j_u(H) = \rho_i n_f \dot{z}_s + (\rho_w n_u - \rho_i n_f)\dot{z}_f, \tag{3}$$

$$\dot{z}_s - \dot{z}_f = \dot{H}. \tag{4}$$

Equations (1), (2), and (3) represent the heat balance and the mass balances of soil skeleton and water, respectively. The function $j_h(H)$ is the heat flux difference between the frozen and unfrozen portions of the ground, which depends on the frozen soil thickness H. When the temperature gradient $G(H)$ from the unfrozen zone is specified, the function $j_h(H)$ becomes

$$j_h(H) = \lambda_f \frac{t_f - t_s}{H} - \lambda_u G(H). \tag{5}$$

In (1)–(5) λ_f, λ_u, ρ_w, ρ_i, and κ are, respectively, the thermal conductivities of frozen and unfrozen soil, water and ice densities, and the heat liberated or consumed in the ice-water phase transition; t_s and t_f are the temperatures of freezing (on the ground surface) and phase transition (at the freezing front), respectively; n_u, n_f are the porosities of, respectively, unfrozen and frozen soil at the freezing front; z_s, z_f are the positions of the ground surface and the freezing front at a given time; $j_u(H)$ is the water flux from the unfrozen zone toward the freezing front (a function of H). The dotted variables (here and below) are the time derivatives. In the applied coordinates, the Oz axis is perpendicular to the freezing front and directed upward, and the unfrozen zone is fixed. The velocities of the boundaries $\dot{z}_s, \dot{z}_f$ are positive if they move upward and negative if they move downward.

Unlike the model by *O'Neill and Miller* [*1985*], the problem formulation in the suggested approach includes a single front: a freezing zone is absent and water accumulates at the freezing front. Furthermore, we use, for the first time, the mass balance equation for the soil skeleton (2) which allows describing ice accumulation in the freezing soil in terms of porosity (n_f). The latter is a continuous function of the freezing depth, unlike the discrete presentation of the structure parameters as in [*O'Neill and Miller, 1985*] which is quite cumbersome. The principal advantage of the new approach is the possibility, hard to effectuate otherwise, of formulating and solving problems for ice accumulation by both processes jointly with nonuniform deformation in freezing soil (with regard to external loading).

The main problem consists in specifying the water flux function $j_u(H)$ in (3) as a function of freezing depth with regard to the applied load, the freezing temperature, and the properties of specific soil. As the function has been specified, one arrives at a closed system of equations for four time-dependent unknowns H, z_f, z_s, n_f. The porosity of frozen soil n_f (depending parametrically on H) characterizes ice accumulation in the freezing soil and can be used to predict the deformation of the latter and other parameters of the process.

The function $j_u(H)$ can be either empirical or derived theoretically from water flux models. Before demonstrating the application of the suggested approach to specific problems, it is pertinent to dwell upon some general properties of system (1)–(4).

Successive removal of $\dot{z}_s, \dot{z}_f, \dot{H}$ from these equations gives an equation for the frozen soil porosity $n_f(H)$ as related to heat and water fluxes ($j_h(H)$ and $j_u(H)$, respectively). The function $n_f(H)$ expressed via the dependence of the fluxes on the freezing depth is

$$n_f(H) = \frac{n_u \rho_w j_h(H)}{\rho_w n_u + \rho_i (1-n_u) j_h(H) - \kappa\rho_w \rho_i (1-n_u) j_u(H)}. \tag{6}$$

In the absence of water flux ($j_u(H) = 0$), the porosity n_f is depthward constant and coincides with that of soil frozen in a closed system [*Gorelik, 2007*]:

$$n_f(H) = \frac{\rho_w n_u}{\rho_w n_u + \rho_i (1-n_u)} = \text{const}. \tag{7}$$

For the case of segregated ice, the model of *O'Neill and Miller* [*1985*] implies that the water flux $j_u(H)$ at any fixed H cannot exceed the maximum, unlike that in the stationary process, and satisfies the condition [*Gorelik et al., 1998*]

$$j_h(H) = \kappa\rho_w j_u(H). \tag{8}$$

Then, following (6) one obtains $n_f = 1$, i.e., pure ice forms, which is prerequisite to the ice lens growth in [*O'Neill and Miller, 1985*]. Furthermore, $\dot{z}_f = 0$ in this case, according to (2), i.e., the freezing front remains fixed relative to the underlying unfrozen soil while ice accumulation inside the freezing soil becomes fully transformed into upward motion (heaving) of the surface z_s. The value $n_f = 1$ being the limit porosity at the maximum water flux, the denominator in (6) is always positive and never zeroes at any intermediate flux value.

During injected ice accumulation, the deformation (and velocity) of the freezing soil surface is zero along its rigid fringe ($\dot{z}_s = 0$). The same happens in the ice segregation process at rather high stress on the freezing soil. In this case, (2) gives $n_f = n_u$, i.e., all excess water formed during segregation is forced away from the freezing front. The flow off the freezing front is found from (3) with regard to (4):

$$j_u = -n_u \dot{H} \Delta\rho_{wi} / \rho_w, \qquad (9)$$

where $\Delta\rho_{wi} = \rho_w - \rho_i$. The flux is negative (inward the unfrozen soil) since $\dot{H} > 0$. Thus, the porosity of the forming frozen soil in the case of segregated ice accumulation is in the range $n_u \le n_f \le 1$, the lower and upper bounds corresponding, respectively, to the minimum (9) and maximum (8) fluxes.

In the case of injected ice accumulation, there is no upper constraint for water flux while the lower bound corresponds to the value defined by (9). The flux of (8) is critical for the injection mechanism. As the flux changes from minimum to critical, the porosity n_f changes monotonically from n_u to 1 (according to (6)), and the respective velocity of the freezing front $\dot{z}_f$ remains negative but decreases monotonically in magnitude from the maximum (at $n_f = n_u$) to zero (at $n_f = 1$). Thereby ice soil forms with different relative percentages of ice and soil. When the flux exceeds its critical value, the velocity $\dot{z}_f$ becomes positive, i.e., the freezing front moves off the fixed unfrozen zone, while the gap between this front and the unfrozen soil skeleton becomes filled with water; the porosities thereon become $n_f = n_u = 1$ and provide the second limit solution to (2). Physically it means that in the case of injected ice accumulation, at a supercritical water flux, the ice lens inside the freezing layer can grow in the presence of a continuously thickening water lens below it (until the water fluxes freeze up completely). Thus, the magnitude of water flux relative to its critical value should largely control the composition and structure of ice formed by the injection mechanism.

EXAMPLES OF MODEL APPLICATION

As it was shown in [*Gorelik, 2008*], the injected water flux during freezing of a closed soil volume depends on the surface area ratio between the zones of recharge and heaving. Heaving in the freezing soil and the attendant pressure are estimated using an additional mechanic strain equation and the conservation law for a confined water mass. According to the calculated freezing front velocity $\dot{z}_f$ and horizontal porosity (n_f) change, the predicted structure of injection-induced frost heaves corresponds to that observed in the field [*Mackay, 1978*]: an ice core encircled (in the map view) by ice-rich soil, with high ice contents decreasing away from the core; the ice core (nothing but the core) lies over a lens of clear water which gives an artesian flow when stripped (a subpingo water lens).

Laboratory physical modeling of injected ice accumulation [*Gorelik, 2009*] confirms the principal theoretical inferences: (1) ice soil with high soil percentages forms at below-critical injection water flux; 2) pure ice grows as water flux exceeds the critical magnitude. Furthermore, injected ice accumulation in the conditions of oscillating temperature patterns on the freezing soil surface produces rhythmically layered ice bodies or ice with sporadic lenses of coarse mineral material (Fig. 1).

The calculation procedure for the heaving and parameters of segregated ice accumulation was reported in [*Gorelik, 2010*]. For a surface foundation in the form of a flexible round disk with the radius R loaded uniformly with the stress σ, one estimates first deformation in the freezing soil and the response the latter receives from unfrozen foundation soil at any fixed H (Fig. 2). The freezing soil is treated as an elastic plate and the underlying unfrozen ground as an elastic halfspace. Note that modeling in [*Gorelik, 2008*] showed the principle possibility to include the rheology of frozen soil if the elastic solution is known. The deformation and the response are the functions of H, σ and the distance from the plate center r. Deformation in frozen soil occurs as settlement. The response is concentrated along the unfrozen-frozen soil boundary and, when taken with the opposite sign, defines the stress σ_R applied to growing ice lenses located in frozen soil in the immediate vicinity of the freezing front. It is noteworthy that for a laboratory sample, the stress σ_R is uniform and coincides with σ (the effect from the weight of its frozen portion is vanishing). In the model, however, this stress depends largely on the mechanic behavior of the frozen soil: if the latter is very stiff, σ_R will be independent of σ but depend uniquely on its gravitational pressure (which is often much less than σ). As a result, the predicted parameters of the laboratory sample and the natural structure behave in different ways.

After the stress σ_R has been estimated, one can find the water flux function $j_u(H)$ which likewise depends parametrically on σ and r. This function can be defined using a special software suggested in

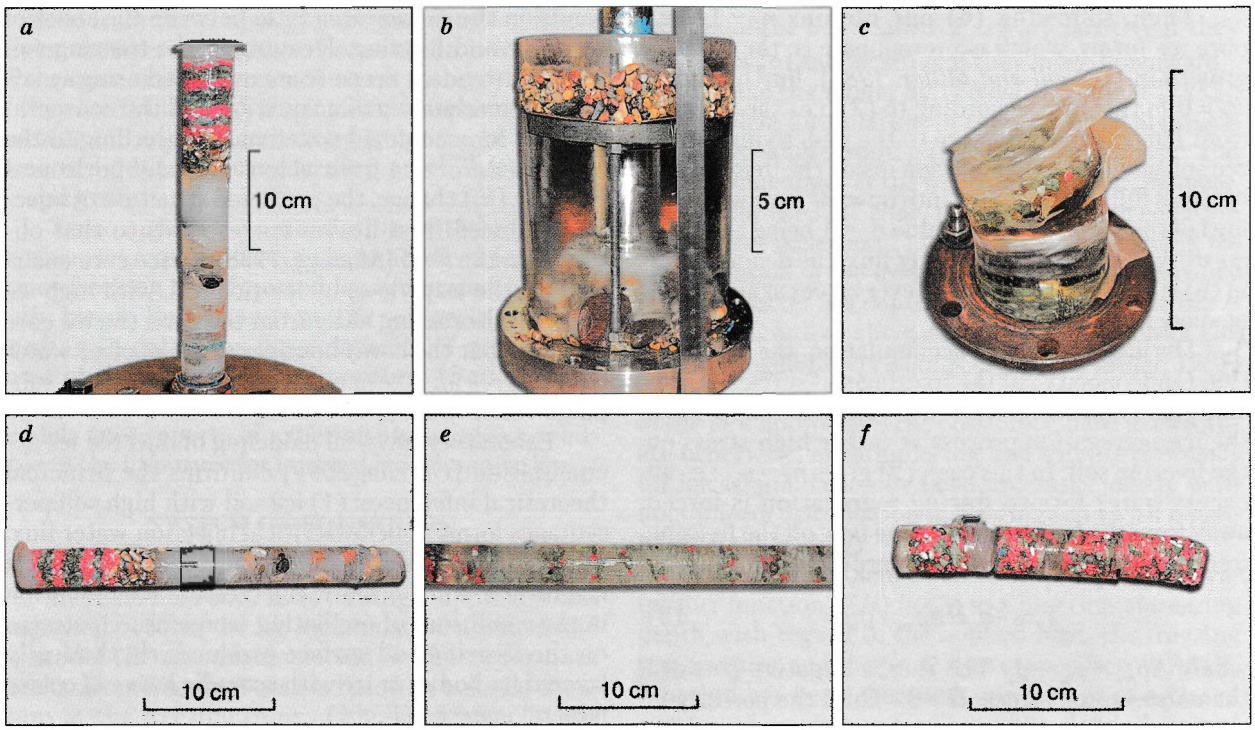

Fig. 1. Photograph of experiment results:

a – injection-fed frozen soil (deformation zone inside recharge zone); *b* – frozen soil in a feeding vessel; *c* – injection-fed frozen soil (deformation zone outside recharge zone); *d* – injection-fed frozen soil at above-critical water flux; *e* – rhythmically layered frozen soil at above-critical water flux; *f* – frozen soil (ice soil) at below-critical water flux.

[*Gorelik, 2010*], which is based on the scheme of *O'Neill and Miller* [*1985*]. The further procedure consists in obtaining the ice accumulation corresponding to the porosity n_f, heaving and total (heaving and settlement) deformation in a foundation using (1)–(4) as functions of the initial parameters. Thus, all model parameters depend on the freezing depth, the plate radius, the applied stress, and the soil properties. These dependences agree well, qualitatively and in the order of magnitude, with data of field experiments on deformation of surface foundations reported in [*Sazhin et al., 1984; Sazhin and Borshchev, 1987*].

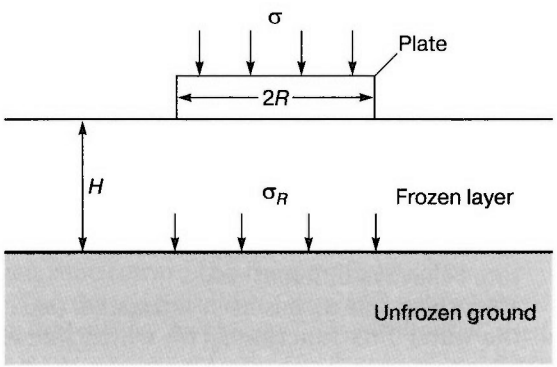

Fig. 2. Surface foundation.

The model was applied to explain the behavior of pipelines in permafrost terrains. It was once suggested to reduce the thermal effect from gas pipelines on frozen soil and to increase the soil stability by means of gas cooling. This solution was partly put into practice but the result turned out to be ambiguous. There was reliable evidence of pipe segments emerging along the line even at pipe's negative buoyancy. This effect may be due to heaving stress from freezing soil on a buried structure. The main elements of the procedure of estimating deformation in freezing soil were applied to a buried pipeline with gas cooled to below 0 °C (Fig. 3). In the cases of Fig. 3, *a*, *b*, deformation is decaying and the position of the pipeline stabilizes inside the ground. However, the pipeline can be forced out to the ground surface after several seasonal freezing-thawing cycles when a frozen soil connection forms in cold seasons between the cold pipeline and the frozen soil (Fig. 3, *c*, *d*).

CONCLUSIONS

The reported examples show that the suggested method for modeling ice accumulation jointly with related deformation in freezing soil allows explaining

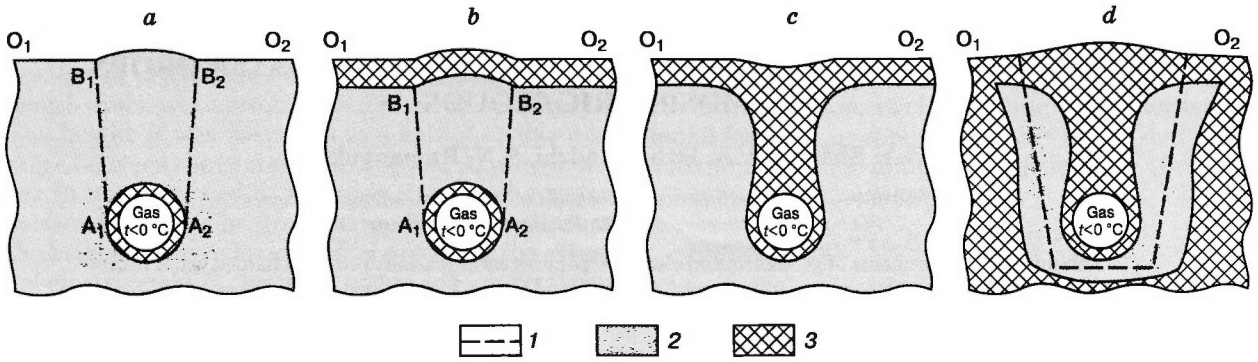

Fig. 3. Relative position of a cold pipeline and active layer (O_1O_2 is ground surface):

a – an unfrozen site in sporadic permafrost, warm season (A_1B_1, A_2B_2 – surfaces of unfrozen soil displacement); *b* – same in cold season, with disconnected frozen elements; *c* – same, with an ice-soil connection between pipe and frozen soil; *d* – a site of continuous permafrost, cold season, with an ice-soil connection: *1* – original trench profile; *2* – unfrozen soil; *3* – frozen soil.

important features of the processes at different mechanisms of moisture transport toward the freezing front. For the case of segregated ice accumulation, the problem to be formulated and solved is estimating heaving-induced deformation in elements of engineering structures. For the injection mechanism, the model can predict the amount of mineral component in ice-rich soil along the lateral extent of the freezing soil. In the latter case, there exists a critical water flux, with pure ice forming (in local zones of the freezing soil) above this critical value and ice-rich soil with high soil percentages forming below it.

This can provide explanation for the composition and structure of natural ice bodies and for specially designed laboratory experiments.

The new approach has a number of advantages over the existing methods based on discrete ice accumulation models. Further development of the method can be useful for geotechnical applications and analysis of geological processes.

The study was carried out as part of Basic Research Program 13 of the Earth's Science Department of the Russian Academy of Sciences.

References

Baulin V.V., Belopukhova E.B., Dubikov G.I., et al., 1967. Geocryological Conditions of the West Siberian Plain [in Russian]. Nauka, Moscow, 214 pp.

Beskow G., 1947. Soil freezing and frost heaving with special application to roads and railroads. Technol. Inst., Evanston, Illinois, USA, 145 pp.

Ershov E.D., 1979. Water Transport and Cryostructures in Fine-Grained Rocks [in Russian]. Moscow University Press, Moscow, 214 pp.

Gorelik J.B., 2008. The mechanism of ice formation in connection with deformation of freezing layer, in: Proc. 9th Intern. Conf. on Permafrost. Fairbanks, Alaska, USA, pp. 535–540.

Gorelik J.B., Kolunin V.S., Reshetnikov A.K., 1998. Rigid-ice model and stationary growth of ice, in: Proc. 7th Intern. Conf. on Permafrost. Yellowknife, Canada, pp. 327–333.

Gorelik J.B., 2007. Ice formation regimes at ground freezing. Kriosfera Zemli, XI (4), 42–49.

Gorelik J.B., 2009. Modeling ice accumulation in freezing ground at injection water input. Kriosfera Zemli, XIII (3), 45–53.

Gorelik J.B., 2010. Methods for calculating deformation in engineering structures caused by heaving of a freezing layer. Kriosfera Zemli, XIV (1), 50–62.

Gorelik J.B., Kolunin V.S., 2002. Physics and Modeling Periglacial Processes in the Lithosphere [in Russian]. Geo, Novosibirsk, 318 pp.

Grechischev S.E., Chistotinov L.V., Shur Yu.L., 1980. Periglacial Physical-Geological Processes and their Prediction [in Russian]. Nedra, Moscow, 384 pp.

Kudryavtsev V.A. (Ed.), 1978. General Geocryology [in Russian]. Moscow University Press, Moscow, 464 pp.

Mackay J.R., 1978. Sub-pingo water lenses, Tuktoyaktuk Peninsula. Can. J. Earth Sci., 15 (8), 1219–1297.

Miller R.D., 1978. Frost heaving in non-colloidal soils, in: Proc. 3rd Intern. Conf. on Permafrost. Ottawa, Nat. Res. Coun. Canada, pp. 708–713.

O'Neill K., Miller R.D., 1985. Exploration of a rigid ice model of frost heave. Water Resource Res., 21 (3), 281–296.

Orlov V.O., 1962. Frost Heaving in Very Fine-Grained Soils [in Russian]. Izd. AN SSSR, Moscow, 188 pp.

Sazhin V.S., Borshchev V.V., 1987. Interaction of short bored foundations with heaving soils, in: Foundations, Foundation Soils, and Soil Mechanics [in Russian]. Gosstroi SSSR, Moscow, pp. 5–7.

Sazhin V.S., Borshchev V.V., Sazhin A.V., 1984. Interaction of short bored foundations with weakly heaving foundation soils, in: Foundations, Foundation Soils, and Soil Mechanics [in Russian]. Gosstroi SSSR, Moscow, pp. 21–23.

Received
12 February 2011

Kriosfera Zemli, 2011, vol. XV, No. 4, pp. 46–48 http://www.izdatgeo.ru

FORMATION OF SPATIALLY ORDERED STRUCTURES BY WATER DROPS IN ATMOSPHERIC CLOUDS

A.V. Shavlov, V.A. Dzhumandzhi, S.N. Romanyuk

Institute of Earth's Cryosphere, Siberian Branch of the Russian Academy of Sciences, PO box 1230, Tyumen, 625000, Russia; shavlov@ikz.ru

Laboratory measurements of geometric and electrical parameters of spatially ordered charged water drops prompt that such structures may form in atmospheric clouds and in fog. The ordered structures of water drops influence the surface tension and shear viscosity of clouds.

The extraterrestrial space and terrestrial atmosphere contain a great number of dust particles which constitute the so-called dusty plasma. At certain conditions, dust particles – like atoms and molecules – can form ordered structures as in crystals or liquids [*Fortov et al., 2004*]. With formation of these structures, dusty plasma behaves as a non-Newtonian liquid: first, it does not flow at some shear stress below the critical value and, second, its shear viscosity decreases as shear stress increases. According to laboratory measurements [*Vorona et al., 2007*], the contribution of the ordered component into shear viscosity of dusty plasma can reach tens of percent or more.

We [*Shavlov and Dzhumandzhi, 2010*] hypothesized that structure formation by charged water drops and ice crystals may be possible also in clouds and in fog, the structures being able to change the physical and mechanic properties of the atmosphere. Ordered structures of water drops were obtained at laboratory conditions over a heated water surface [*Fedorets, 2004*]. In those experiments, water drops, several tens of micrometer in diameter, were localized in a single layer and were hexagonally ordered relative to one another, with a spacing of two to five drop diameters; the height of the layer above the water surface was commensurate with the drop diameter.

In this respect, given that water drops are capable of structure formation, the objectives of our study were to measure their charges inside a drop structure, to calculate surface tension in this structure, and to estimate the effect the drop structures may cause on the properties of atmospheric clouds and fog.

Drop clusters were obtained experimentally following a procedure similar to one reported in [*Fedorets, 2004*]. See Fig. 1 for a typical ordered drop structure, with its round shape being evidence of surface tension. The geometric and electrical parameters of the drop clusters were investigated as a function of temperature T (Fig. 2), namely the spacing L, the diameter D, the height above the water surface H, and

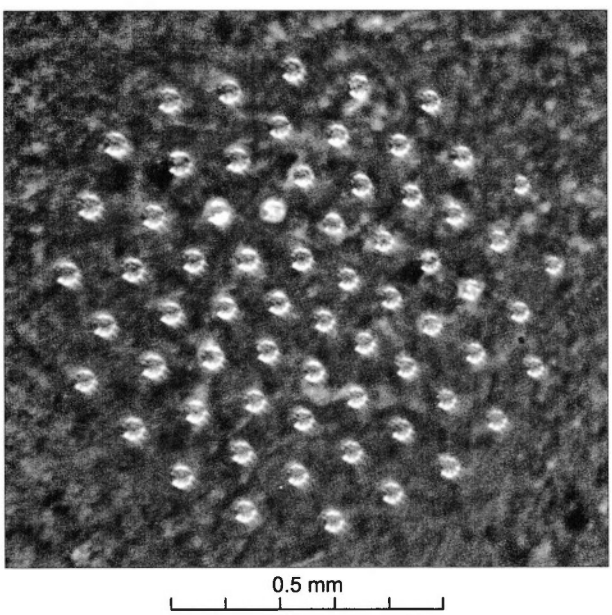

Fig. 1. A plane spatially ordered structure of water drops.

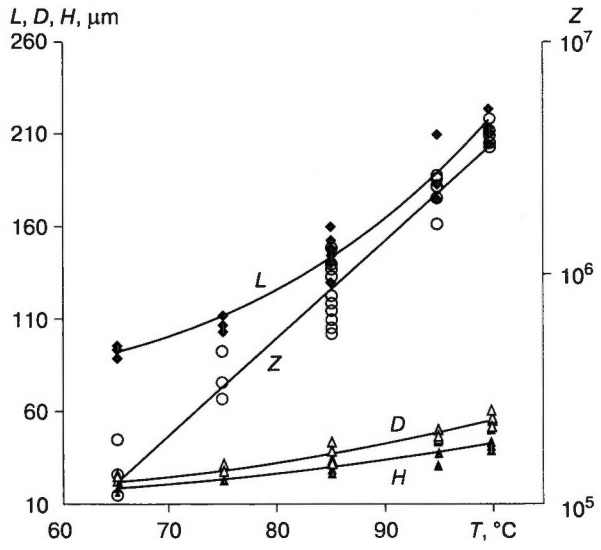

Fig. 2. Temperature dependences of the spacing L, diameter D, height above the water surface H, and charge Z of water drops.

the charge Z (in elementary charge units). The geometric parameters were estimated according to the number of pixels in a video image recalculated into length units, to an error of ±0.5 pixel or ±2 microns. The height H was measured as a half of visible distance between the centers of a drop and its mirror image in water viewed at an angle close to the water surface tangent. The drop charge Z was found from the height relative change $\Delta H/H$ caused by the external electric field E_{ex} between water and an electrode above the drop structure, as

$$Z = \frac{Mg}{eE_{ex}} \frac{\Delta H}{H}.$$

The equation for the drop charge was obtained assuming electric-gravity equilibrium between the charged drop and the charged water surface of the same polarity:

$$Mg = Ze(E + E_{ex}),$$

where E is the field produced by the charged water surface (inversely proportional to the height $E \sim 1/H$); M is the mass of a drop; g is the gravitation acceleration; e is the unit charge. In this way, the charge of water drops was estimated to an error of ±15 %, while the error in water surface temperature was (+1/ – 10) °C.

The parameters showed decreasing trends as the temperature decreased (Fig. 2) and, within the 60–100 °C range we investigated, were related as

$$D \approx 1.26H, L \approx 4.8H, Z \sim D^4.$$

Both water drops and water surface below them were positively charged, the charge polarity apparently being defined by the fact that more hydroxide than hydrogen ions pass from water to vapor during evaporation. The charge Z of a drop changed as a function of its diameter D more rapidly than D^2, i.e., additionally to the drop's surface area, which is proportional to D^2, it must depend on the rate of the water-to-vapor phase transition.

The drop spacing L was hypothesized to be twice the Debye length (L_D) in vapor:

$$L = 2L_D.$$

In order to check the hypothesis, we calculated, using the Debye equation, the concentration of charge carriers for the case of a plane charged water surface, and found the Debye length. For the latter we obtained the theoretical relationship $L = 2.7H$, in which the factor 2.7 is in an order-of-magnitude agreement with the factor 4.8 in the empirical relationship $L \approx 4.8H$. This appears to be satisfactory support for our hypothesis. The $2L_D$ spacing of particles in dusty plasma was validated experimentally [*Fortov et al., 2004*] and theoretically [*Shavlov and Dzhumandzhi, 2010*].

The L and L_D relationships were used to predict whether water drops may form spatially ordered structures (clusters) in atmospheric clouds and in fog. The calculated theoretical concentration of ordered drops can be compared with the empirical concentration of drops in clouds using the Debye length found from the air conductivity $a = 10^{-13}$ Ohm^{-1}·m^{-1} and the average ion diffusion coefficient $B = 10^{-8}$ m^2/s [*Grigoriev and Meilikhov, 1991*]:

$$L_D = (\varepsilon_0 B/a)^{0.5} = 10^{-3} \text{ m},$$

where ε_0 is the electric constant.

The concentration of drops calculated as $N = (2L_D)^{-3} = 1.5 \cdot 10^8$ m^{-3} turned out to be of the same order of magnitude as the statistically average concentration of water drops in clouds and fogs, which is $N = 3 \cdot 10^8$ m^{-3} [*Mazin and Khrgian, 1989*]. Thus, indeed, water drops can form ordered structures in clouds and fogs.

The surface tension of a drop structure is given by [*Shavlov and Dzhumandzhi, 2010*]

$$\sigma = \frac{e^2}{24\varepsilon_0} Z^2 N.$$

The drop charge Z in clouds reaches 10^3–10^6 [*Grigoriev and Meilikhov, 1991*]. At $Z = 10^4$, for instance, $\sigma = 10^{-11}$ J/m^2. Knowing the surface tension σ, one can estimate the stability of the drop structure surface to shear flow using the Kelvin–Helmholtz stability criterion

$$\frac{\rho v^2}{2} \le \frac{2\pi}{x}\sigma,$$

where $\rho = 1$ kg/m^3 is the air density; $v = \frac{\partial v}{\partial l} l$ – is the interfacial velocity difference; $\frac{\partial v}{\partial l} = 3 \cdot 10^{-3}$ s^{-1} is the average gradient of the medium horizontal velocity along the normal to the ground surface; $l = 10^{-3}$ m is the thickness of the surface layer of the drop structure equal to the Debye length; x is the characteristic length of the instability zone.

Therefrom $5 \cdot 10^{-12} \le 10^{-10}/x$, which fulfills at $x < x_0 = 20$ m.

Thus, the surface of a cloud drop structure can be stable to shear flow when the cloud size is within a few tens of meters. In larger clouds, the surface acquires a roughness with the characteristic size x_0. It follows from the above that structure formation in water drops can be an important agent in the stability of the cloud geometry.

The shear viscosity η of a drop cluster can be estimated and compared with that of air using a formula similar to the Frenkel equation [*Fabelinsky, 1997*]:

$$\eta = C \exp\left(\frac{U}{kT}\right),$$

where $C \sim hN$; h is the Plank constant; N is the concentration of particles; U is the viscosity activation energy; k is the Boltzmann constant; T is the temperature.

Shear viscosity was investigated with reference to the dislocation mechanism of shear flow typical of crystals. The activation energy of dislocations in metal and ion crystals U is known to be 10^3–10^4 times as low as the atomic bond energy U_b. Describing numerically the viscosity of a dust crystal with the above formula requires that U were 1500 times lower than $U_b = Z^2kT/6$ [*Shavlov and Dzhumandzhi, 2010*]. The viscosity of a drop structure estimated with the activation energy $U = U_b/1500$ was $\eta = 10^{-23}$ Pa·s at $Z = 10^4$, which is much lower than the air viscosity 10^{-5} Pa·s. However, already at $Z = 10^5$ this viscosity can reach or even exceed the air viscosity.

The viscosity increase may lead to a decrease in convective thermal conductivity. For instance, in some convection problems, the Rayleigh number $R = g\beta Ad^3/(\chi\mu)$ can characterize the stability of gas in the gravity field in the presence of a downward temperature gradient A, where β is the thermal expansion coefficient; χ is the gas thermal diffusivity; μ is the kinematic viscosity; d is the characteristic linear size of the structure. Viscosity changes control the presence (absence) of free convection and the heat transfer rate.

Thus, structure formation by water drops in an atmospheric cloud can change notably its hydrodynamics and heat transfer patterns. This effect may be more prominent in the clouds that contain ice crystals with their charges tens of times those of water drops.

The existence of spatially ordered structures of water drops and ice crystals in atmospheric clouds and fogs, as well as their effect on mechanic and thermophysical properties of clouds appears to be quite realistic. This phenomenon is worth being studied in detail in terms of atmospheric physics, as well as in terms of Earth's cryology which is a science that deals with objects containing water near or below the freezing (crystallization) point.

References

Fabelinsky I.L., 1997. Macroscopic and molecular shear viscosity. Uspekhi Fizicheskikh Nauk, 167 (7), 721–733.

Fedorets A.A., 2004. Drop clusters. Letters to ZhETF, 79 (8), 457–459.

Fortov V.E., Khrapak A.G., Khrapak S.A., et al., 2004. Dusty plasma. Uspekhi Fizicheskikh Nauk, 174 (5), 495–544.

Grigoriev I.S., Meilikhov E.Z. (Eds.), 1991. Physical Parameters. A Handbook [in Russian]. Energoizdat, Moscow, 1232 pp.

Mazin I.P., Khrgian A.Kh. (Eds.), 1989. Clouds and Cloudy Atmosphere [in Russian]. Gidrometeoizdat, Leningrad, 647 pp.

Shavlov A.V., Dzhumandzhi V.A., 2010. Spatially ordered structures in storm clouds and fogs. Phys. Lett. A., 374, 2561–2565.

Vorona N.A., Gavrikov A.V., Ivanov A.S., et al., 2007. Viscosity of plasma-dust liquid. ZhETF, 132 (4), 941–948.

Received
15 February 2011

Kriosfera Zemli, 2011, vol. XV, No.4, pp. 48–50 **http://www.izdatgeo.ru**

INTENSIFICATION OF ELECTROCHEMICAL PROCESSES AT THE METAL-ICE INTERFACE

A.V. Shavlov, A.D. Pisarev, A.A. Ryabtseva

Institute of Earth's Cryosphere, Siberian Branch of the Russian Academy of Sciences, PO box 1230, Tyumen, 625000, Russia; shavlov@ikz.ru

Electrochemical corrosion at the metal-ice interface has been explored in laboratory by measuring copper corrosion rates at the front of water crystallization, as well as the electrode potentials of some metals in water and in ice. The experimental data were used to test a numerically grounded model of corrosion acceleration at the crystallization front.

Design of foundations with regard to processes in frozen ground is an important engineering issue in permafrost areas. Significant damages are incurred yearly from corrosion of engineering structures associated with electrochemical reactions in which metals loose atoms – and, hence, their mechanic strength – at contacts with ice and ice-rich soils. According to expert appraisal, corrosion of pipelines laid in permafrost is commensurate to or greater than that in the forest steppe zone [*Velikotsky, 2010*], though the mean annual ground temperature in the former is tens of degrees lower than in the latter. The high corrosion activity of frozen ground is due to the presence of ice and to specific physicochemical processes on its surface.

The electrochemical corrosion of metals results from half-reactions of metal oxidation at the metal-liquid interface $Me \rightarrow Me^{z+} + ze^-$ or, most often, from the oxygen reduction half-reactions $(\frac{1}{4}O_2 + H^+ + e^- \rightarrow \frac{1}{2}H_2O)$ where Me is the metal, z is its oxidation degree, and e^- is the electron. In the absence of oxygen, a few metals with negative electrode potential may reduce hydrogen ions instead of oxygen reduction, namely $H^+ + e^- \rightarrow \frac{1}{2}H_2$. Corrosion may also occur by a chemical rather than electrochemical mechanism: $Me + Ox \rightarrow Me^{z+} + Red$, where Ox, Red are the oxidized and reduced forms of the reactants, respectively.

We have explored corrosion at the metal-ice interface (where ice acts as liquid) in laboratory by measuring copper corrosion rates at the front of water crystallization and ice melting and the electrode potentials of Al, Cu, Fe, and Pb in ice. Then, on this basis, we tested a tentative model of the corrosion process.

The experimental procedure consisted in recording electrical conductivity variations in a thin metal film [*Shavlov et al., 2006*], with the basic assumption that metal atoms involved in the redox reaction quit the electron transport process thus decreasing the conductivity. The method allowed recording corrosion while it is going on. We used thin copper films deposited on quartz or woven-glass reinforced wafers in a VUP-5 thermal vacuum evaporator. The films had a surface area of 0.5 × 2.0 cm, at an electrode spacing of 2 cm, a resistance about 10 Ω, and a temperature coefficient of resistance about that in copper. The average thickness of the films was 20 monoatomic layers (estimated from the amount of evaporated metal and the distance to the wafer). The films were exposed to air for more than 12 hours, whereby an oxide layer formed on their surface and the resistance stabilized. The films that were exposed to air for a long time were noted to be more vulnerable to corrosion in the following tests. According to its position in the reactivity series, copper can corrode only by reduction of oxygens, the reduction of hydrogens being thermodynamically forbidden.

A prepared copper film, with a 3–4 mm drop of distilled water poured on its surface, was vacuumed in an enclosed volume. The drop partially evaporated and froze up quickly by heat loss with vapor. As the drop froze up, the film resistance increased irreversibly for ~2 %, as measured with a V7-34A ohmmeter to an error less than 0.1 %. In some tests, water was frozen with a nitrogen cryostat but the resistance change was then less prominent, possibly, because cooling was slower. See Fig. 1 (curve *1*) for an empirical surface density time series $I(t)$ of the reactant copper atoms since the onset of crystallization (surface densities were calculated from the resistances of the films). The film thickness change was ~$5 \cdot 10^{-10}$ m, or about one monoatomic layer. Repeated tests with water freezing at the same film surface site gave more or less the same film thickness decrease. Thus, corrosion apparently developed with sufficient amounts of the initial reactants, and neither the latter nor the reaction products were involved in diffusion transport to and from the reaction front. Corrosion may be constrained by the reaction potential barrier it has to overcome. No corrosion acceleration was observed on ice melting.

Note that the irreversible conductivity decrease of the copper film on water crystallization was not due to a non-chemical process, such as mechanical disturbance of the film surface by friction on ice. Tests with noble metals (e.g., silver which is similar to copper in its mechanic properties) did not show any resistance change on water crystallization.

The measured metal electrode potentials in ice have implications for the thermodynamic efficiency of a reaction. Direct potential measurements are dif-

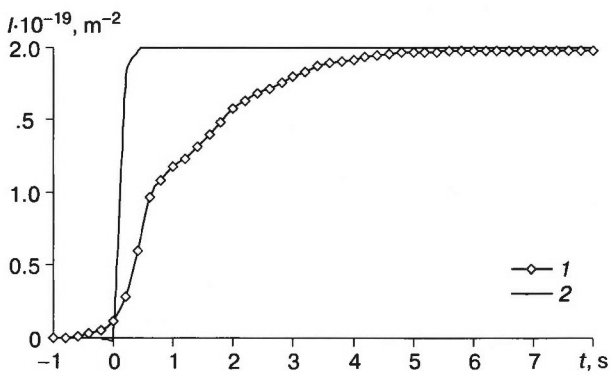

Fig. 1. Measured (*1*) and predicted (*2*) time dependences of the surface density (I) of copper atoms involved in the reaction.

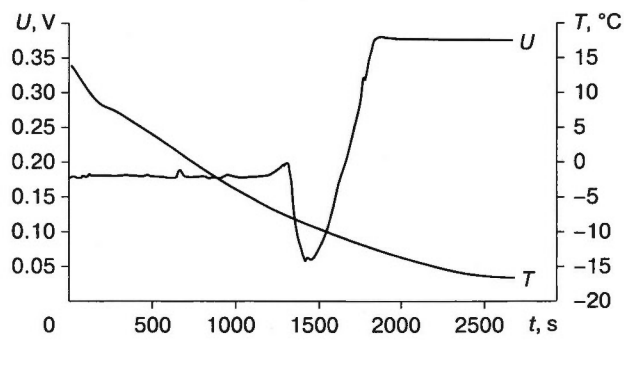

Fig. 2. Time dependences of the potential (U) of copper-lead galvanic couple and the temperature (T) of cooler during water freezing.

ficult because of hardly removable polarization of electrodes associated with their passivation and overpotential on circuit closing. Therefore, the main focus was on the behavior of voltage in galvanic couples formed by electrodes of different metals and a liquid (distilled water) as the latter froze up. Water was cooled down with a cooler connected to a flow thermostat. The potential was measured to an error of ±10 mV; the temperature absolute error was ±1 °C.

Figure 2 shows typical voltage and temperature time series. The galvanic couple consisted of a copper (positive) and a lead (negative) electrodes. The potential difference between the electrodes in water was 0.17 V. As the electrodes were polarized, the potential of the couple was less than that for the standard electrode potentials of 0.47 V. Cooling caused almost no voltage change. After the liquid in the space between the electrodes froze up as the cooler temperature reached −8 °C, voltage increased to 0.38 V. Voltage in the galvanic couples Cu–Al, Cu–Fe, and Fe–Pb behaved in the same way: increased by a factor of 1.5–2 as the liquid froze up. When ice melted, the potentials returned to the previous values for water.

The observed freezing-related behavior of voltage in galvanic couples indicates that the standard electrode potentials increase at the water → ice transition. As a result, the redox reactions in ice, including corrosion, are more thermodynamically efficient than those in liquid, though the very process in ice may be slow.

The experimental data on corrosion of metals at the crystallization front was explained by nonequilibrium accumulation of ice charge carriers (ion and orientation defects) repulsed by the ice [*Shavlov and Ryabtseva, 2007*]. These carriers may diffuse toward the ice-metal interface where they recombine with energy release. The released energy can be further transferred to the reactants by means of collisions and used to overcome the reaction barrier, which pushes up the corrosion.

The concentration N of nonequilibrium charge carriers required to account for the experimental surface densities of the reactant copper atoms ($I = 2 \cdot 10^{19}$ m^{-2}, Fig. 1) was calculated as $N = I/L$, where L is the diffusion length. The obtained values were $N = 10^{25}$ m^{-3} (at $L = 3 \cdot 10^{-6}$ m) for ion defects (hydrogen and hydroxide ions) and $N = 10^{28}$ m^{-3} (at $L = 2 \cdot 10^{-9}$ m) for orientation defects. The latter concentration is realistic being about the equilibrium concentration of orientation defects in water while the former value can never be achieved in practice as it is orders of magnitude in excess of the equilibrium concentration of protons in water (10^{20} m^{-3}). Thus, the orientation defects are the most probable corrosion agents on water crystallization.

We calculated the concentration of orientation defects at the crystallization front and the intensity of their recombination in ice and in water. At a low crystallization rate, almost all nonequilibrium defects (99.5 %) were found to be repulsed by the crystallization front and to recombine in water, and only 0.5 % recombined in ice. At fast crystallization, instead, the nonequilibrium defects recombined mostly in ice for the lack of time for repulsion. Note that the recombination energy in ice is much higher than in water (0.68 against ~0.03 eV, respectively) and is sufficient to overcome the corrosion barrier, which is 0.52 eV for copper. Therefore, one can expect corrosion to be the most intense at a high crystallization rate. It can exceed the isothermal corrosion already after this rate becomes faster than 10^{-7} m/s.

By the potential barrier of electrochemical corrosion we mean the energy-consuming formation of hydrogen ions, i.e., the active particles required for the reaction. We hypothesize that hydrogen ions may form during dissociation of water molecules at the account of the recombination energy of orientation defects. In the case of chemical corrosion, the reaction barrier corresponds to the energy required for overcoming short-distance repulsion in the reactants.

The discussed mechanism of corrosion acceleration is rather universal. It may account for intensification of any reactions in frozen liquid which are controlled by the capacity of overcoming the potential barrier. In addition to the corrosion issues, other applications are improving the technology of nondestructive low-temperature storage of biological preparations and medicines, or food.

References

Velikotsky M.A., 2010. Corrosion activity of soils in various climate zones. Vestnik Moscow Univ., Ser. 5. Geografiya, No. 1, 21–27.

Shavlov A.V., Ryabtseva A.A., 2007. The mechanism of metal corrosion acceleration in ice associated with structural changes and crystallization of water. Zhurn. Fiz. Khimii, 81 (7), 1186–1191.

Shavlov A.V., Pisarev A.D., Ryabtsev A.A., 2006. Electroconductivity dynamics of metal films in ice under its structural transformation. The mechanism of corrosion acceleration. Kriosfera Zemli, X (3), 42–48.

Received
19 February 2011

Kriosfera Zemli, 2011, vol. XV, No. 4, pp. 51–52 http://www.izdatgeo.ru

A NEW CLASS OF WATER DISPERSIONS RESISTANT TO FREEZING-THAWING

L.S. Podenko, N.S. Molokitina, V.V. Shalamov

Institute of Earth's Cryosphere, Siberian Branch of the Russian Academy of Sciences, PO box 1230, Tyumen, 625000, Russia; lpodenko@yandex.ru

A new class of water dispersions has been obtained through encapsulation by silica nanoparticles with polyvinyl alcohol. This form is more stable than the previous ones against freeze-thaw cycles. The new systems are advantageous over dry water in stability and contents of liquid water, being similar to the latter in the degree of liquid phase dispersion.

Hydrophobic silica nanoparticles can stabilize disperse systems consisting of fine water drops (so-called powdered or dry water) [*Schutte and Schmitz, 1968*]. Dry water behaves as powder, is free-flowing, and contains up to 98 wt.% liquid phase. As it has been shown recently, gas hydrate formation with dry water is faster than with bulk water or crushed ice [*Wang et al., 2008; Carter et al., 2010*]. The acceleration of gas hydrate formation with the use of dry water stabilized by hydrophobic nanoparticles is relevant to the technologies of natural gas transportation and storage in the hydrate form [*Gudmundson et al., 2000; Kanda et al., 2005; Watanabe et al., 2008*].

Dispersion of water and aqueous solutions in the presence of hydrophobic silica nanoparticles may lead to water encapsulation [*Forny et al., 2009*]. Such systems of encapsulated water are of broad use in petroleum chemistry, medicine, and biotechnologies [*Solodovnik, 1980*]. The low-temperature applications require systems stable against freezing-thawing cycles.

Earlier we showed [*Podenko et al., 2010*] that dry water subjected to freezing and thawing becomes layered as water drops coalesce with one another. *Carter et al.* [*2010*] obtained a "dry gel" modification of dry water, which is stable against water phase change, by adding gellan gum (an aqueous solution of polysaccharide) instead of water. Note that this technique requires large amounts of the polymer (20 wt.%) and much energy for powdering the highly viscous gel.

We have investigated the feasibility of using polyvinyl alcohol (PVA) for increasing the stability of disperse systems encapsulated by silica nanoparticles. The PVA polymer was chosen for the capability of its aqueous solutions to form heterogeneous gels as a result of freezing-thawing cycles (cryogels) [*Lozinsky, 1998*]. The structure of the obtained disperse systems was analyzed by means of optical microscopy and proton magnetic resonance spectroscopy on a Niumag *MicroMR* NMR pulsed relaxometer, operated at the resonance frequency 20 MHz, following the procedure reported in [*Podenko et al., 2010*].

The study included experiments on dispersing the PVA solution in the presence of hydrophobic silica nanoparticles (aerosil R 202). For this purpose, a mixture of 95 wt.% PVA aqueous solution (State Standard 10779-78) and 5 wt.% nanometer powder aerosil R 202 was stirred for 60 s at a blender speed of 18,750 revolutions per minute; the concentration of the polymer was 5 wt.%. Gel formation was catalyzed with 1 wt.% boric acid. The viscosity of the starting water gels did not exceed 40 mm^2/s.

The resulting water dispersion of PVA (PVA dispersion) had a consistency of paste (unlike the powdery dry water we obtained at the same dispersion conditions). The PVA dispersion had its density almost 1.5 times higher than the apparent density of dry water (0.86 against 0.53 kg/l) approaching the density of 5 % PVA (0.98 g/l). Therefore, the dispersion contained ~84 vol.% PVA solution. According to optical microscopy (Fig. 1), the disperse phase of the obtained system consisted of micron-size drops and their aggregates.

The greater density of the PVA dispersion is evidence of a more compact arrangement of drops in it relative to dry water. The reason of the difference

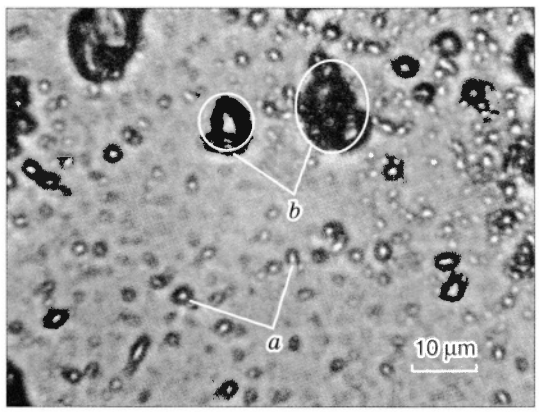

Fig. 1. Polyvinyl alcohol (PVA) dispersion.
a – individual particles, *b* – aggregates of particles.

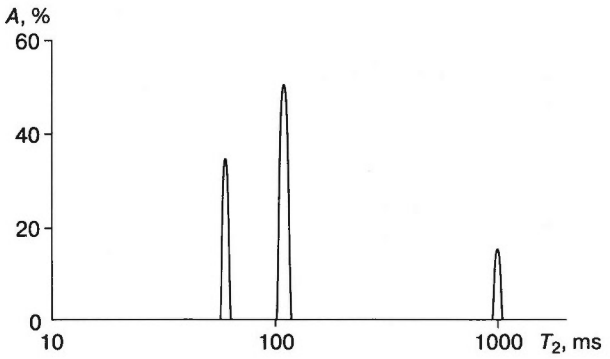

Fig. 2. Distribution (A) of spin-spin relaxation (T_2) of PVA dispersion at 32 °C.

may be as follows. The disperse drops in dry water are stabilized by self-assembling hydrophobic silica (aerosil) nanoparticles which provide its flowability, i.e., low apparent density [*Forny et al., 2007*]. Polyvinyl alcohol is a high-molecular surfactant [*Lozinsky, 1998*] and becomes adsorbed on the surfaces of aerosol particles thus preventing them from assembling and formation of a large spatial network. As a result, the polymer drops become stabilized by particles of much smaller sizes, which provides very high concentrations of drops in the disperse system.

The obtained PVA dispersions were investigated in terms of their structure and stability against freezing-thawing cycles in the respective experiments in a liquid cryostat. The temperature schedule was as follows: first the liquid was cooled at 0.5 °C/min from T_{wf} = 25 °C to T_{wf} = −15 °C (T_{wf} is working fluid temperature), and then heated at the same rate back to T_{wf} = 25 °C. The samples were placed in test tubes 10 mm in diameter; the sample temperature (T_{sm}) was monitored with a thermocouple placed in the same tubes.

The data were plotted in a T_{wf} vs. T_{sm} thermogram. The samples showed a crystallization peak at T_{wf} ~ −12 °C while cooling and a melting peak at T_{wf} > −0.5 °C while heating. Unlike dry water [*Podenko et al., 2010*], the freezing-thawing cycles caused no stratification in PVA dispersion, i.e., the solution remained disperse after freezing and thawing.

The structure of PVA dispersions was analyzed from their patterns of spin-spin relaxation times (T_2) (Fig. 2). The T_2 pattern, like in the case of dry water, consisted of three relaxation components (Fig. 2), which indicates polydisperse size distribution of drops. We estimated the drop sizes from the parameters of T_2 distribution according to the technique reported in [*Podenko et al., 2010*]. We found out that ~10 μm drops and/or their agglomerates constituted 15 % of the PVA solution, and the other drops were ~2 μm. Note that the percentage of ~10 μm drops and/or their agglomerates decreased about five-fold after a freezing-thawing cycle, while the other drops grew to only ~3 μm, i.e., no relatively large water drops have formed.

Therefore, the presence of PVA in a disperse system increases its freezing-thawing stability. The mechanism of this stabilization may consist in increasing mechanic stability of individual drops as they develop a polymer cryogel structure.

Thus, a new class of water dispersions has been obtained through encapsulation by hydrophobic silica nanoparticles with polyvinyl alcohol. The new systems are advantageous over dry water being easy to obtain, high in liquid water phase (84 vol.%), and stable against freezing and thawing. The latter property allows using PVA dispersions at subzero temperatures.

This work was supported by grant 07-05-00102 from the Russian Foundation for Basic Research and was carried out as part of basic research program 13.7.4 of the RAS Presidium and as a part of interdisciplinary project 62 of the RAS Siberian Branch.

References

Carter B.O., Wang W.X., Bray C.L., et al., 2010. Gas storage in "Dry Water" and "Dry Gel" clathrates. Langmuir, 26 (5), 3186–3193.

Forny L., Pezron I., Saleh K., et al., 2007. Storing water in powder form by self-assembling hydrophobic silica nanoparticles. Powder Technol., 171 (1), 15–24.

Forny L., Saleh K., Pezron I., et al., 2009. Influence of mixing characteristics for water encapsulation by self-assembling hydrophobic silica nanoparticles. Langmuir, 189 (2), 263–269.

Gudmundson J.S., Andersson V., Levik O.I., et al., 2000. Hydrate technology for capturing stranded gas. Ann. New York Acad. Sci., 912, 403–410.

Kanda H., Uchida K., Nakamura K., 2005. Economics and energy requirements on natural gas ocean transport in form of natural gas hydrate pellets, in: Proc. 5th Intern. Conf. on Gas Hydrates, Trondheim, Norway, Vol. 4, pp. 1276–1283.

Lozinsky V.I., 1998. Cryotropic gel formation from polyvinyl alcohol solutions. Uspekhi Khimii, 67 (7), 641–655.

Podenko L.S., Komissarova N.S., Shalamov V.V., et al., 2010. Water freezing in hydrophobic silica nanoparticles, from proton nuclear magnetic resonance spectroscopy. Vestnik TyumGU, No. 6, 4–11.

Schutte D., Schmitz F.T., Brunner H., 1968. Predominantly aqueous composition in fluffy powdery form approximating powdery solids behavior and process for forming same. Patent USA, 3393155 (Degussa).

Solodovnik V.D., 1980. Micro-encapsulation [in Russian]. Khimiya, Moscow, 216 pp.

Wang W.X., Bray C.L., Adams D.J., et al., 2008. Methane storage in dry water gas hydrates. J. Amer. Chem. Soc., 130 (35), 11608–11609.

Watanabe S., Takahashi S., Mizubayashi H., et al., 2008. Demonstration project of NGH land transportation system, in: Proc. 6th Intern. Conf. on Gas Hydrates, Vancouver, Canada, pp. 211–241.

Received
26 February 2011

SCIENTIFIC JOURNAL
EARTH'S CRYOSPHERE

Kriosfera Zemli, 2011, vol. XV, No. 4, pp. 53–55 http://www.izdatgeo.ru

THERMOPHYSICAL PROCESSES IN PERMAFROST

THE RADIATION HEAT BUDGET OF THE ANTARCTIC AND MARS POLAR REGIONS: COMPARATIVE ANALYSIS

O.N. Abramenko, I.A. Komarov, V.S. Isaev

Lomonosov Moscow State University, Department of Geology, 1, Leninskie Gory, Moscow, 119991, Russia; oleg_abramenko@inbox.ru, ilya_komarov@mail.ru, tpomed@rambler.ru

The time and space radiation heat patterns have been investigated at five polar Antarctic sites (Novolazarevskaya, Molodezhnaya, Bellinshausen, Mirny, and Vostok). Similar variability appears in data from Mars polar ice caps. The reported comparative analysis allows evaluating the contributions from different thermophysical components of the radiation heat budget in the Antarctic and Mars high-latitude regions.

The study has focused on comparing quantitative and qualitative parameters that represent the radiation heat budget in Antarctica and in polar Mars. Mars is a planet with a thin atmosphere, a thick cryosphere, and permanent ice caps at both poles. On the Earth, it is the Antarctic that is similar to the Mars high-latitude regions, especially to the northern cap consisting mostly of water ice; similar are the surface areas and the ice sheet thicknesses (Table 1). The Antarctic climate is the most severe (the coldest natural temperature ever recorded on Earth was –89.2 °C at the Vostok station) and the least affected by anthropogenic loads.

We analyzed records from five Antarctic stations (Novolazarevskaya, Molodezhnaya, Bellinshausen, Mirny, and Vostok) collected by the Arctic and Antarctic Research Institute from the start of observations (1958–1971) through 2008–2009 (till 1992 at Molodezhnaya). The stations are located on or near the shore, or in the continent interior (on ice or within Antarctic oases). The inventory consisted of the following data:

(1) long-term average solar flux during selected observation periods (at clear sky, with cloud amounts less than 2, and at up to 10);

(2) statistically processed data on monthly and yearly totals of the radiation budget components;

(3) statistically processed data on monthly and yearly totals of direct beam solar radiation at normal incidence and atmospheric clearness index.

As part of the 53rd Russian Antarctic Expedition, one of us [*Abramenko, 2009*] set up a test station at the Novolazarevskaya site, in the Schirmacher oasis located 80 km far from the northern Antarctic coast in the central Queen Maud Land. The objective was to test the method for measuring the surface heat budget, to monitor the temperature, the thermal conductivity, and the thaw depth. The annual temperature cycles were monitored with loggers which were courtesy of the Fairbanks University (Alaska, USA). The test station was operated within the limits of the CALM program (Circumpolar Active Layer Monitoring) [*Brown et al., 2000*].

At the stations Bellinshausen, Novolazarevskaya, Molodezhnaya, Mirnyi, and Vostok, the normal beam solar radiation was from 33 to 56 % and dominated over other radiation components that varied in the following ranges: 6 to 26 % reflected, 3 to 23 % absorbed, 6 to 32 % scattered, and 9 to 17 % radiation on a horizontal surface (Table 2). The estimated total annual heat balance of the ice surface was negative, from –20 to –40 W/m^2.

Inside the domain there are zones with a positive balance, such as oases, ice-free ridges, and stationary water clearings. In oases, the annual heat budget is 110 W/m^2. The annual totals of the radiation components range as follows: normal beam radiation from 102 to 830 W/m^2, horizontal radiation from 48 to 199 W/m^2, scattered radiation from 67 to 179 W/m^2, total radiation from 19 to 329 W/m^2, and back radia-

Table 1. **Ice parameters of Antarctic and Martian ice caps, compared**

Area	Surface area, km^2	Maximum ice thickness, km	Ice	
			volume, km^3	composition
Antarctic	$1.4 \cdot 10^7$	4.8	$26.7 \cdot 10^6$	H_2O
Mars South Pole cap	$3.9 \cdot 10^5$	3.7	$1.6 \cdot 10^6$	H_2O and mostly CO_2
Mars North Pole cap	$6.8 \cdot 10^5$	2.0	$1.4 \cdot 10^6$	CO_2 and mostly H_2O

Table 2. **Radiation heat budget components at different Antarctic sites, compared, W/m²**

Site	Radiation budget	Beam radiation		Solar radiation	
		normal	horizontal	total	backscattered
Vostok	–6.7	344.7	105.0	147.8	111.8
Novolazarevskaya	37.2	181.2	67.3	125.0	26.7
Molodezhnaya	38.6	144.5	62.8	134.0	50.5
Mirnyi	–8.5	148.2	62.4	135.3	108.1
Bellinshausen	20.2	42.2	20.7	7.8	45.2

tion from 65 to 263 W/m². The monthly means of climate parameters at the selected stations were: albedo 0.2–0.9, air moisture 48–90 %, wind speed 2.9–13.4 m/s.

The time and space patterns of the surface radiation heat budget components in the Mars polar regions were investigated using the Global Mars Climate Database produced jointly by Laboratoire de Météorologie Dynamique du CNRS (LMD, Paris) and Atmospheric, Oceanic and Planetary Physics, Department of Physic (AOPP, Oxford University, Oxford, England UK) [*The global Mars Climate Database*].

The ranges of annual reflected radiation generally for the Mars high latitudes are 414–750 W/m² for the northern ice cap and 532–840 W/m² for the southern ice cap. The absorbed radiation ranges are, respectively, 658 to 2016 W/m² and 702 to 1539 W/m². The radiation data for the northern and southern polar regions were processed on a space grid for the coordinates 90°, 86.2°, 82.5°, 78.8°, 75° N and S; 135°, 90°, 45°, 0° W and 45°, 90°, 135°, 180° E to analyze annual cycles of the surface and atmospheric infrared radiation, absorbed and reflected radiation, and mean monthly surface temperatures. Other parameters were mean diurnal and monthly temperatures of the surface and lower atmosphere (5 m above the surface) estimated for midnight and noon times and winter and summer mean diurnal variations of wind speed.

The radiation heat budget components were calculated with an equation used to process the Earth's ground surface data [*Budyko, 1956*]. Turbulent heat transfer was found as the surface-air temperature difference (according to GMCD) multiplied by the heat transfer coefficient. The latter was assumed to be 2–5 W/(m²·K) proceeding from empirical data obtained in laboratory at pressures and temperatures typical of the Mars high latitudes [*Lebedev and Perelman, 1973*]. The heat spent for sublimation (ablimation) of CO_2 or H_2O ice was evaluated from mean annual values of the process intensity obtained using GMCD. The CO_2 and H_2O ice sublimation heat was estimated with regard to its temperature dependence [*Komarov, 2003*]. The heat flux from the surface to the ice was calculated as a solution to the thermal conductivity differential equation at the respective boundary conditions. The models included a two-layer section for the northern ice cap and a three-layer section for the southern cap [*Komarov and Isaev, 2010*].

The components of the radiation heat budget in the Earth's Antarctic and Mars's high latitudes demonstrate qualitatively similar patterns, but there is some difference in their magnitudes. Namely, backscattered and absorbed radiation is slightly lower on Mars than at the Antractic Novolazarevskaya site (Table 3). Unlike the Earth, the Mars surface temperature is due mostly to beam solar heat rather than atmospheric heat transport. As a result, the temperature may be locally 272 K while the mean of the north ice cap periphery in the early summer is 235 K (Ls = 90°, where Ls is solar latitude). Generally, the mean diurnal air temperature at 5 m above the Mars surface varies through a year from 143.1 to 249.9 K on the southern ice cap and from 147.8 to 230.4 K on the northern cap.

Table 3. **Annual means of heat-radiation budget components at sites of Martian poles and Antarctic Novolazarevskaya site**

Site	Location	Radiation budget components, W/m²					Heat budget components, W/m²		
		Short-wave solar radiation			Albedo	Effective long-wave radiation	Heat loss for evaporation (sublimation)	Heat flux to rocks	Turbulent heat transfer
		total	reflected	adsorbed					
Novolazarevskaya	11° E 70° S	125.0	26.7	98.3	0.2	61.1	$1 \cdot 10^{-3}$	1.1	34.9
Mars South Pole cap	0° E 82.5° S	60.4	14.5	45.9	0.2	26.9	20.5	0.1	0.7
Mars North Pole cap	0° E 82.5° N	57.3	17.2	40.1	0.3	24.1	18.0	0.1	0.5

According to our estimates of the permafrost thickness and the Mars cryosphere as a whole, the permafrost is from 1000 m thick at the equator to 3600–3750 m at the polar caps [*Komarov and Isaev, 2010*]. The mean thickness of frozen ground is 2300 m, which is greater than the terrestrial mean. The total ice volume in a 2300 km thick spherical layer (the Mars outer radius being 3394 km) is $(0.4–2.0)\cdot10^8$ km^3, as estimated by different authors, which is about two orders of magnitude more than the total volume of the polar ice caps.

We greatly appreciate overall support by V. V. Lukin, the head of Antarctic expeditions at AARI (Arctic and Antarctic Research Institute), as well as the aid of S.R. Verkulich, the head of the 53rd Russian Antarctic campaign, and the whole team of Novolazarevskaya Station.

The study of Mars data was supported by grants 04-05-65110 and 09-05-07045 from the Russian Foundation for Basic Research.

References

Abramenko O.N., 2009. Methods for investigating the surface radiation heat budget components and thaw depths in Schirmacher oasis (Antarctica). Vestnik Moscow Univ., Ser. 4. Geol., No. 4, 67–69.

Brown J., Hinkel K.M., Nelson E.F., 2000. The Circumpolar Active Layer Monitoring (CALM) program: research designs and initial results. Polar Geogr., 24 (3), 165–258.

Budyko M.I., 1956. Heat Budget of the Earth's Surface [in Russian]. Gidrometeoizdat, Leningrad, 256 pp.

Komarov I.A., 2003. Termodynamics and Heat-and-Mass Transfer in Permafrost [in Russian]. Nauchnyi Mir, Moscow, 603 pp.

Komarov I.A., Isaev V.S., 2010. The Cryology of Mars and other Planets of the Solar System [in Russian]. Nauchnyi Mir, Moscow, 232 pp.

Lebedev D.P., Perelman T.L., 1973. Heat and Mass Transfer in Vacuum Sublimation [in Russian]. Energiya, Moscow, 336 pp.

The global Mars Climate Database. (http://www-mars.lmd.jussieu.fr/).

Received
9 February 2011

SCIENTIFIC JOURNAL
EARTH'S CRYOSPHERE

Kriosfera Zemli, 2011, vol. XV, No. 4, pp. 56–59 http://www.izdatgeo.ru

PERIGLACIAL EFFECTS AS A RECORD OF HISTORIC AND CLIMATE EVENTS

PERIGLACIAL PHENOMENA IN THE ALTAI MOUNDS, MONGOLIA

E.A. Slagoda, V.P. Melnikov, Yu.N. Garkusha*, O.L. Opokina

Institute of Earth's Cryosphere, Siberian Branch of the Russian Academy of Sciences, PO box 1230, Tyumen, 625000, Russia; eslagoda@ikz.ru
** Institute of Archaeology and Ethnography, Siberian Branch of the Russian Academy of Sciences, 17, Akad. Lavrentieva, Novosibirsk, 630090, Russia*

Mound permafrost is common to the mountains of Altai, Kazakhstan, Mongolia, and China. Natural mounds in terrains affected by seasonal and perennial cryogenesis are often hard to tell from manmade burial sites. Mounds in northwestern Mongolia have been found out to lie over ice-rich sediments that differ in color and structure and over standing blocks, a setting typical of ancient tombs. The culturally undisturbed rocks beneath the mounds have lost their natural colors and structures as a consequence of frost heaving and weathering. The high ice contents of cryogenically eroded bedrocks, as well as intense frost shattering and sorting of debris result from local flooding of the active layer under the mound. The periglacial processes appear to have acted for 3000 years after the burial mound had been put up.

Archaeological sites in cold regions of the Earth (Arctic, West and East Siberia, highland Mongolia and China) often lie within past or present permafrost. The international multidisciplinary archaeological expedition of 2006, with permafrost scientists in the team, opened a new page in joint studies of the Earth's history [*Molodin and Parzinger, 2006*]. For archaeologists, who search for cultural objects and traces of human activity, the natural environment is a substrate to act upon while permafrost is a mean of conservation and, besides, something that poses problems to excavation. For cryologists, however, permafrost is an ages-long record of natural and man-caused events that took place during and after the burial. The Mongolia-2006 joint team faced the challenge of identifying whether cryogenic structures in the vicinity of mounds were of natural or cultural origin.

The northern highlands of Mongolia, including the southern slope of the Sailyugem Range, belong to an area of dry continental climate and to a zone of permafrost [*Melnikov, 1974*] subject to related seasonal thawing and frost shattering, heaving, and sorting of rock debris. Polygonal patterns with soil wedges, flat pentagonal mounds, dome-shaped heaves, rings and bands of debris, and standing stones resemble manmade structures by their geometry. The Sailyugem Range is known to be a place where several Bronze and Iron Age burial sites with flat or underground graves (4–0.1 kyr BC) were found [*Polosmak, 2001*].

Geophysical surveys [*Epov et al., 2006*] detected an ice lens and geometrical objects similar to burial chambers at depth to 2.5 m underneath Ulan-Daba-1 mound (Fig. 1). The objectives of the project included looking into the ice formation mechanism and checking the hypotheses of natural or manmade origin of geological heterogeneity, bearing in mind that there were cases of stepped multiple tombs.

The mound of the Ulan-Daba Pass is located in the right-hand side of the Shetk-Oigor-Gol valley at the elevation 2577 m and rests upon an alluvial fan overlying the exarated surface of jointed schists. The fan (subaerial delta of a side tributary) apparently formed after glacier retreat in the second half of the Holocene, possibly, in a cold and dry climate [*Dorofenyuk, 2008*]. Undisturbed rocks near Ulan-Daba-1 mound comprise (Fig. 2, trench 1) (i) black modern and brown fossil stony soils, with relic holes of lemmings and mice; (ii) stratified talus and alluvial reddish-brown debris with sand and clay matrix and carbonate or iron-hydroxide coats. The sediments have low water contents (7.2–9.7 %). They were deposited in a subaerial environment, the deposition being accompanied by shattering, debris sorting, soil formation, and repeated freezing of the active layer. The present active layer in the mound vicinity (southern side of a narrow valley) is 1.8–2.0 m thick and lies over permafrost with the water content 9.2 % (Fig. 2).

Prior to the excavations, Ulan-Daba-1 mound was a flat hill 15 m in diameter, rising 0.5 m above the ground surface, buried under modern soil with tilted schist blocks exposed at the center. The mound structure consisted of (i) a cover of clean small (under 0.2 m) plate-like schist pebbles and angular stones; (ii) a fence and an armor of clay-cemented round

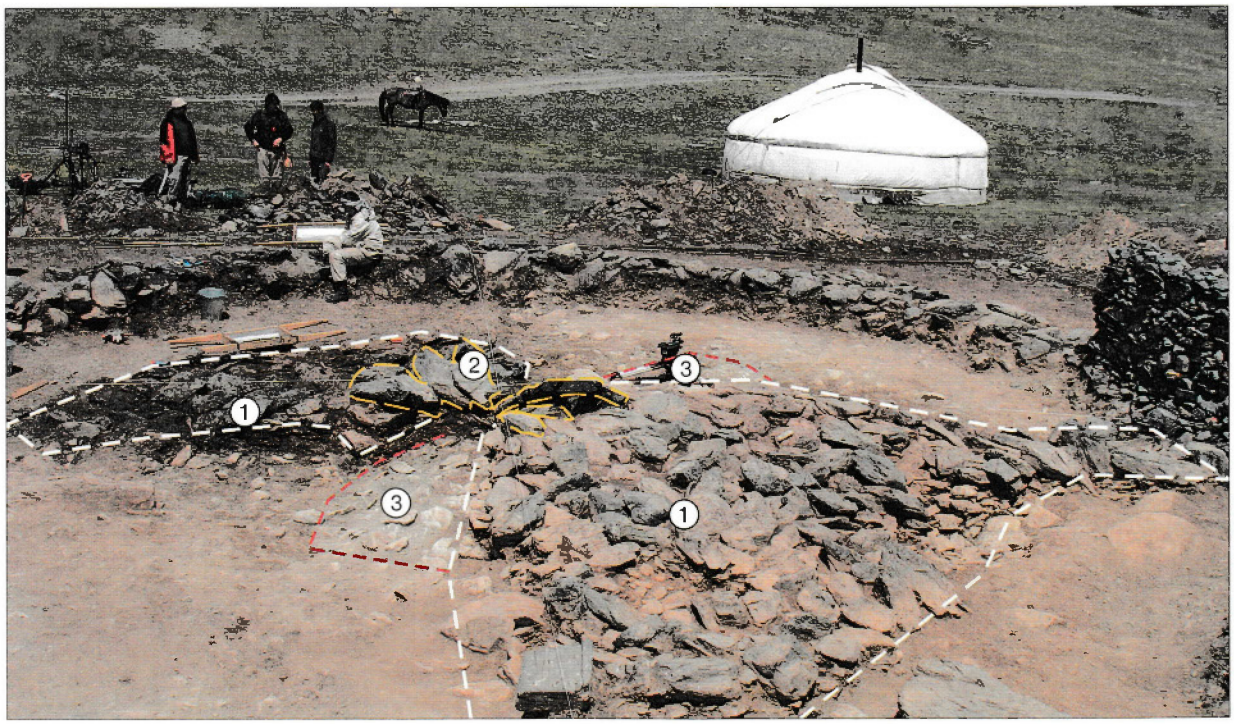

Fig. 1. Excavation at Ulan-Daba-1 mound:

① – fragments of dismounted stone armor (white dash line); ② – schist blocks, tomb remnants (yellow dash line); ③ – quadrangular contour of the false grave under the mound filled with whitish rocks (red dash line).

boulders; (iii) a bank and large (0.5–1.1 m) elongate blocks which are fragments of a stone burial chamber at the center. The burial chamber collapsed and the depression became filled with schist pebbles. The exposed tops of the blocks looked eroded by wind and thaw water while the lower parts were fixed with brown debris-bearing loamy sand, debris, and modern soil. Underneath there were pieces of human bones with a ^{14}C age of (2982 + 23) yr BP (KIA31153)[1]. The bank in the form of a flat hummock was composed of loose debris with thin schist plates. Judging by abraded carbonate crusts on the debris, the bank was built with the use of reddish soil and rocks picked inside the fence. The bank material showed higher water contents (16.5–29.0 %) than the rocks around the mound (Fig. 2).

Below the armor and the bank, there was a rectangular outcrop of unconsolidated light gray rocks including *in situ* debris and colorless schist plates. The rocks had no analogs among the local reddish-brown deposits and were encircled with large standing schist blocks, which made them looking like a filled grave. The excavation section displayed a rectangular 1.5–1.7 m wide pit that crosscut stratified reddish-brown sediments and holes of soil-dwelling animals to a depth of 1.7 m (Fig. 2). That was the active layer with a depthward increase in water content from 5.5 to 15.5 %, containing more sand and less coarse deposits relative to the surrounding ground (Fig. 2). The pit floor was bounded from below by frozen coarse rocks. The pit was called a "false grave" as no burial was found on the floor.

Further down the section (to the depth 2 m) there followed coarse frozen ground composed of flat schist blocks positioned tile-like one upon another and cemented with reddish sand and debris-bearing loamy sand with thin lens-type and reticulate cryostructures (water content 16.8 %). Note that tile patterns are also typical of cultural structures.

At the depth 2.0–2.5 m there appeared the geometric objects predicted by geophysical surveys: standing flat schist blocks with their juxtaposed narrow sides making up two adjacent angular-oval chambers (1.0 × 1.5 m) within the excavated area. The space inside and between the blocks was filled with ice-bearing debris loam and sand upon a fractured basal layer, with water content 30–61 % (Fig. 2). Glassy ice formed up to 10 cm thick crusts around the blocks

[1] Dated at Leibniz Laboratory for Radiometric Dating and Stable Isotope Research, Christian Albrecht University, Kiel, Germany.

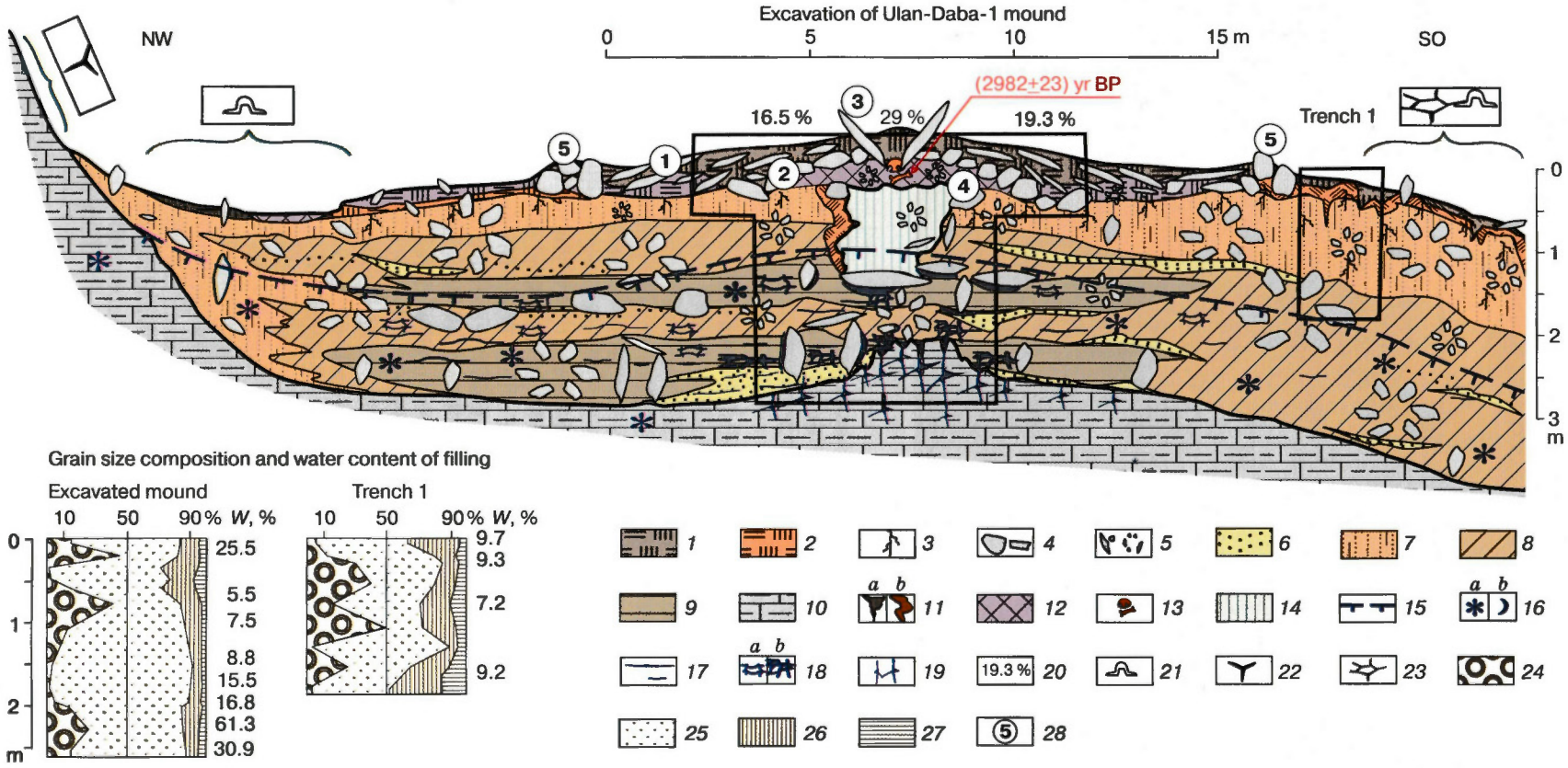

Fig. 2. Cross section of Ulan-Daba-1 mound and alluvium in Shetk-Oigor-Gol valley, Sailyugem Range.

Natural environment: *1* – modern black soil; *2* – fossil brown soil; *3* – plant roots buried *in situ*; *4* – boulders, blocks, plates; *5* – rock debris and annular structures; *6* – sand, gravel; *7* – sandy loamy sand; *8* – loamy sand; *9* – sandy loam; *10* – bedrock (schist, siltstone, sandstone); *11* – soil wedges (*a*), burrow holes (*b*); *12* – made ground; *13* – human bones. Cryogenic features: *14* – false grave, zone of frost weathering; *15* – permafrost boundary; *16–20* – cryostructure: *16* – massive (*a*), crust-like (*b*), *17* – lens-type, *18* – reticulate (*a*), basal (*b*), *19* – blocky, *20* – water content (wt. %); *21* – surface signature of frost heaving; *22* – surface signature of frost shattering; *23* – surface remnant polygon; *24–27* – grain size composition: *24* – 20.0–2.0 mm, *25* – 2.0–0.05 mm, *26* – 0.05–0.005 mm, *27* – less than 0.005 mm. Numerals in circles mark manmade structures (mound elements): ① – stone cover; ② – stone armor; ③ – depression made by collapsed tomb stones; ④ – bank; ⑤ – fence.

and enclosed thin layers of the host loam. The ice was found out to have nitrate-calcium-sodic major-element chemistry with high contents of sulfates (21 mg/l) and magnesium (14.5 mg/l), and a trace-element composition with V, Ti, Mo, W, B, Se, and Sr higher than in snow and ice fields, etc.[2]

The coarse deposits were underlain by a shattered surface of schists with eluvium (ice-filled vertical cracks more than 0.5 m high and up to 0.05 m wide).

The reported data indicate that the pit and the structure underneath the mound were not manmade, and the talus and fan deposits did not undergo later cultural perturbation. The schist blocks collapsed after the tomb had been looted and have survived till today making a depression which can retain snow. The light-gray rocks of the false grave were deposited in a subaerial delta and experienced post-depositional frost weathering and heaving in the active layer after the burial mound had been put up.

The water content pattern, high ice percentage, and the anomalous chemistry of ice and eluvium imply percolation of water enriched in organic and bronze particles, as well as local flooding of the active layer beneath the mound. The geometric structure of standing blocks was produced by sorting and emergence during deposition and seasonal and syngenetic ground freezing. Snow retention upon the mound provided additional moisture supply to the permafrost surface and the formation of an ice-rich zone in alluvial fan deposits and in cryogenic eluvium.

The structure of the culturally undisturbed and naturally altered rocks beneath Ulan-Daba-1 mound records the following sequence of events for the past 12 kyr after the retreat of the Pleistocene ice sheet in that part of the Sailyugem Range:

1. Frost weathering and formation of eluvium in the uppermost gray schist;

2. Burial of eluvium on the side of the Shetk-Oigor-Gol valley under subaerial alluvium of a tributary delta, about 8–4 kyr BP, at a high stand of moraine damlakes. The alluvium deposition was attendant with seasonal and syngenetic freezing and formation of circular systems of standing stones similar to burial structures in their shapes and sizes;

3. A stone armor, a bank, and a surface burial chamber were built about 3 kyr BP; the collapse of the burial chamber caused snow retention in the depression and ensuing local wetting of the active layer under Ulan-Daba-1 mound. That event was responsible for the formation, in the upper permafrost, of segregated ice with its chemistry and high content unusual for the arid climate of the area;

4. A discolored local rectangular zone formed for the past 3 kyr after the burial as a result of erosion and intense frost shattering of original dark deposits. Abundant sand particles and a relatively low content of silt at the site indicates incomplete frost weathering [*Konishchev et al., 2005*].

Therefore, new evidence has been obtained that rocks within geometric zones beneath burial mounds can loose their natural properties as a result of local frost weathering. Thus, till nowadays, the works of ancient people influence natural periglacial processes and upper permafrost.

The study was carried out as part of Basic Research Programs of the Presidium of the Russian Academy of Sciences (20.7) and the RAS Earth Science Department (11.4).

References

Dorofenyuk N.I., 2008. Paleogeographic Reconstructions for Last Glacial and Holocene Inner Asia [in Russian]. Author's Abstract, Doctor Thesis, Moscow, 49 pp.

Epov M.I., Manshtein A.K., Manshtein Yu.A., et al., 2006. Resistivity surveys for frozen Pazyryk tombs in Altai, in: Problems of Archaeology, Ethnography, and Anthropology of Siberia and Adjacent Areas [in Russian]. IAET SO RAN, Novosibirsk, XII (1), 510–515.

Konishchev V.N., Lebedeva-Verba M.P., Rogov V.V., et al., 2005. Cryogenesis of Holocene and Late Pleistocene Deposits in the Altai and Periglacial Regions of Europe [in Russian]. GEOS, Moscow, 133 pp.

Melnikov P.I. (Ed.), 1974. Geocryology of Mongolia [in Russian]. Nauka, Moscow, 200 pp.

Molodin V.I., Parzinger H., 2007. An international team of scientists investigates a tomb of an Altai nomad. National Geographic Russia, 6.

Polosmak N.V., 2001. Ukok Riders [in Russian]. INFOLIO-press, Novosibirsk, 336 pp.

Received
7 February 2011

[2] Analyzed at Limnological Institute, Irkutsk, by Prof. T.V. Khodzher and Dr. L.P. Golobokova.

SCIENTIFIC JOURNAL
EARTH'S CRYOSPHERE

Kriosfera Zemli, 2011, vol. XV, No. 4, pp. 60–62 http://www.izdatgeo.ru

PERIGLACIAL PROCESSES ON ARCTIC SHELF AND COAST

OFFSHORE PERMAFROST IN THE KARA SEA

P.V. Rekant, A.A. Vasiliev*

All Russian Institute of Ocean Geology, 1, Angliysky pr., St. Petersburg, 190121, Russia; rekant@mail.ru
** Institute of Earth's Cryosphere, Siberian Branch of the Russian Academy of Sciences, 86, Malygina str., Tyumen, 625026, Russia*

Problems of identifying submarine permafrost in the Kara Sea shelf from seismic-acoustic data are considered. Seismic-acoustic markers indicate the presence of permafrost in the southeastern Kara Sea and in the Yamal shelf to depths of 120 m. Additionally, acoustic permafrost (APF) markers are inferred near the Severnaya Zemlya within local seafloor highs surrounded with 100–120-m isobaths. The existence of permafrost at greater sea depths is most likely an exception and may be due to neotectonic subsidence. The permafrost extent in the Kara Sea has been mapped with GIS tools and the respective database on its setting has been developed. The submarine permafrost table lies at 5–60 m below the sea floor. According to statistical processing of the collected seismic-acoustic data, the subbottom depth to permafrost is most often (47 %) in the range 10–20 m. Gas seeps showing up as noise in seismic-acoustic wavefields are hypothesized to have a genetic relationship with submarine permafrost.

INTRODUCTION

Submarine permafrost is remnant terrestrial permafrost that formed during times of sealevel lowstand of the Last Glacial (20–18 kyr BP) and was flooded during the last transgression (16–5 kyr BP). The flooded permafrost has thawed from above and from below, and partly saline rocks became cooled. Thus submarine permafrost has acquired its present state.

The extent and structure of submarine permafrost at the Kara shelf remain underexplored. The main ideas are based on near-shore engineering-geological drilling data [*Rokos et al., 2001; Rokos and Tarasov, 2007*].

Although there have been several publications on the subject, the limits and depths of submarine permafrost have not been reliably constrained for the lack of explicit geological evidence [*Melnikov and Spesivtsev, 1995*]. For this reason, the permafrost extent has been most often mapped proceeding from expert appraisal while the latter is applicable to small-scale maps only [*Rokos et al., 2001; Rokos, Tarasov, 2007*].

METHODS

High-resolution seismic-acoustic methods are commonly used for crosswell correlation when explicit geological evidence is insufficient. The today's advanced data acquisition and processing techniques allow using seismic records as an independent source of geological information. With the seismic facies analysis, the seismic wavefield can image the ground structure to depths 60–70 m, including permafrost [*Shlezinger, 1998; Rokos et al., 2001; Rokos and Tarasov, 2007*]. A seismic-acoustic section is in the first approximation equivalent to a geologic cross section, the resolvable seismic sequences and subsequences being correlated with geologic (stratigraphic) units, such as strata, suites, horizons, etc. Undisturbed patterns of stratified sediments in a seismic section indicate the absence of submarine permafrost (Fig. 1, *A*).

Among factors that can disturb the seismic image in a given region there are cryogenic and post-cryogenic effects in sediments, as well as structures associated with free gas. Jointly they can produce intricate patterns difficult for interpretation (Fig. 1, *B*).

As it was shown for the shelves of the Pechora and Laptev Seas [*Rekant et al., 2009*], submarine permafrost in a seismic section is detectable from high-amplitude reflections which are seismic-acoustic markers of distinct post-depositional characteristics (Fig. 1, *B*). The permafrost table commonly corresponds to a prominent reflector of normal polarity caused by abrupt acoustic velocity rise in frozen ground.

The presence in the sediments of just little free gas produces seismic interference evident as bright spots or vertical blanking zones (Fig. 1, *B*). These gas structures are called gas seeps (GS) and are hypothesized to have a paragenetic relationship with submarine permafrost [*Rokos et al., 2001; Rokos and Tarasov,*

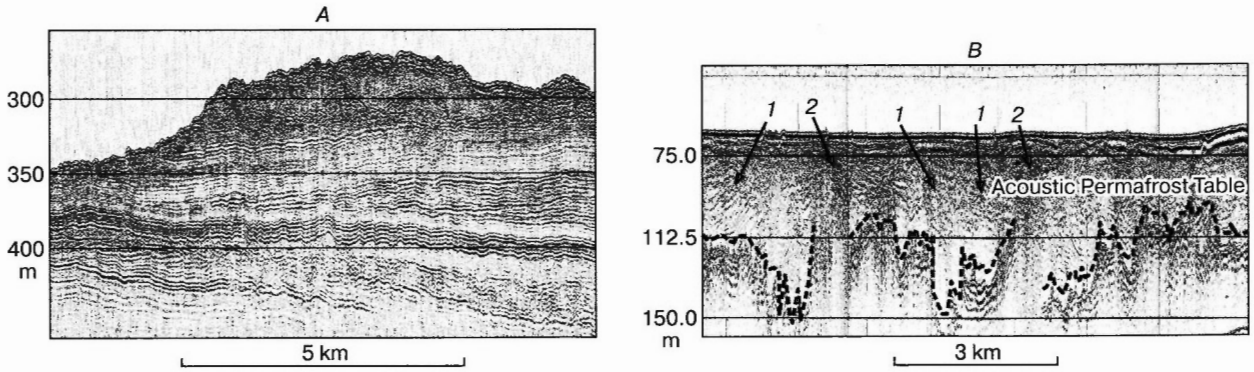

Fig. 1. Fragments of seismic-acoustic profiles in the Kara Sea:

A – a typical seismic image of a section free from submarine permafrost; *B* – a typical seismic image of areas with submarine permafrost. *1* – sites of cryogenic sediment deformation above permafrost; *2* – gas seeps that show up as vertical dead zones.

2007], specifically, to be controlled by taliks [*Rokos et al., 2001; Rekant et al., 2009*].

The seismic-acoustic results agree well with regional drilling data. Most of shoreface and inner shelf logs from the western Yamal (e.g., near Cape Kharasavey) show faster dip of the permafrost table (40 m or more) in a strand between the shoreline and the ~5–7-m sea depth. A similar pattern appears from seismic-acoustic data (Fig. 2).

RESULTS

Processing of more than 100,000 km of seismic-acoustic profiles in total has revealed several zones of prominent markers of acoustically defined permafrost (APF), as well as zones where such markers are poorly pronounced but are inferred (Fig. 3). The APF markers are most reliably detectable within a broad strand in the southern Kara Sea and in the western

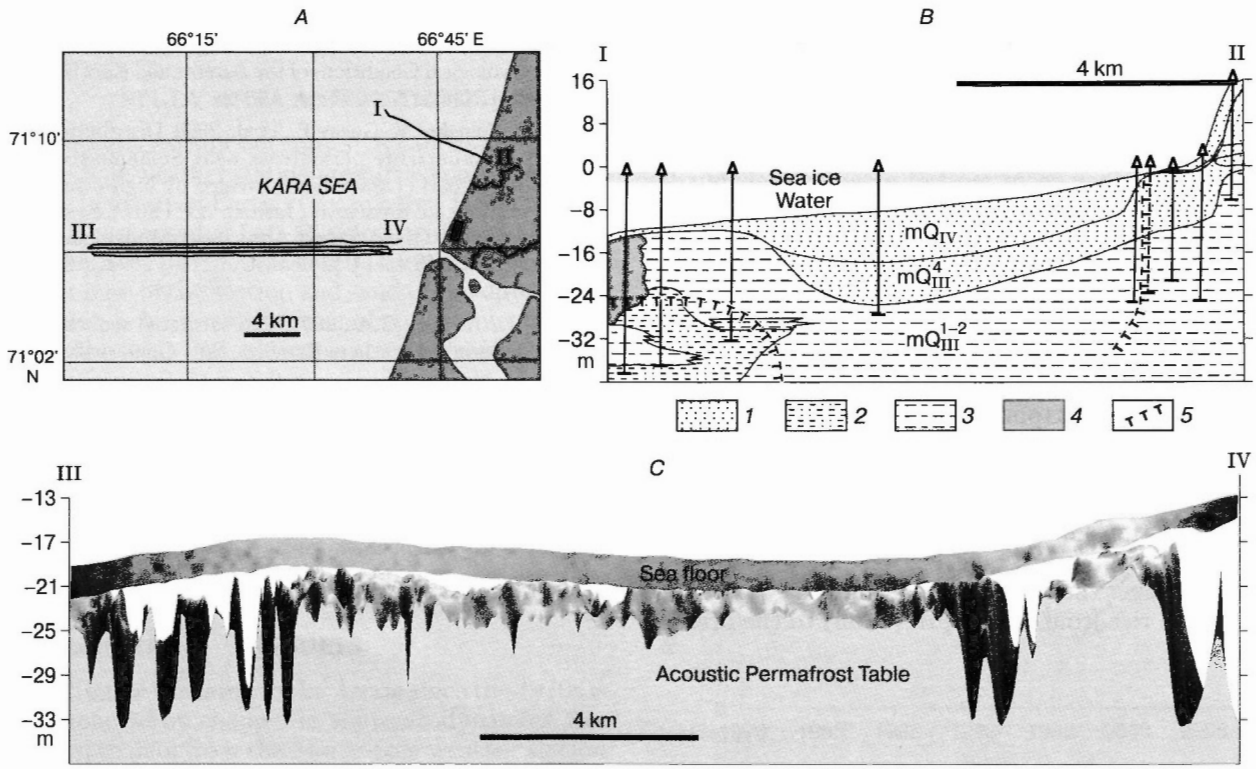

Fig. 2. Processed seismic-acoustic data and drilling results from Cape Kharasavei, compared.

A – location map of seismic-acoustic and drilling profiles; *B* – drilling profile I–II [*Melnikov and Spesivtsev, 1995*]; *1* – sand; *2* – silt; *3* – pelitic silt; *4* – clay; *5* – permafrost table; *C* – position of the submarine permafrost table along profile III–IV: a fragment of a 3D model derived from seismic-acoustic data.

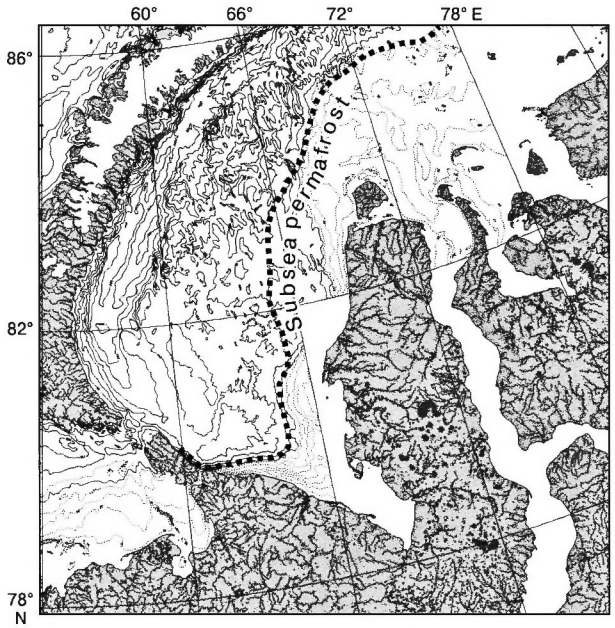

Fig. 3. Map of submarine permafrost in the Kara Sea based on seismic-acoustic data.

Yamal shelf. The extent of submarine permafrost is controlled mainly by the present sea depth. The greatest number of permafrost markers falls within the depth range 100–120 m.

Permafrost is almost absent from sea depths below 120 m, except for a few areas of steady neotectonic subsidence.

Of special interest are zones of gas seeps. As our data show, they occur most often within reliably detected or inferred permafrost zones. This is implicit evidence of their genetic linkage. Gas seeps may originate from zones of a deeply buried permafrost table at the account of gas released during permafrost degradation.

The permafrost table is from 5 to 60 m below the sea floor. According to statistical processing of the data, the subbottom depths to permafrost show a nearly lognormal distribution, at least in the southwestern part of the Kara Sea and in the Yamal shelf, being most often (47 %) in the range 10–20 m. Statistical relationships between the permafrost table and sea depths show direct correlation only when the water is deeper than 40 m. The reason may be in rapid sealevel rise from that depth (40 m) to the present level.

CONCLUSIONS

Acoustic markers of submarine permafrost are reliably detectable in the southeastern Kara Sea and in the Yamal shelf to water depth of 120 m. There are also inferred APF markers near Severnaya Zemlya within local seafloor highs nested in areas of 100–120-m isobaths. The existence of permafrost at greater sea depths is most likely an exception and may be due to neotectonic subsidence.

The permafrost table is from 5 to 60 m below the sea floor. The subbottom depths to permafrost show a lognormal distribution and are most often within 10–20 m.

Statistical relationships between the permafrost table and sea depths show direct correlation only when the water is no shallower than 40 m. The reason may be in rapid sealevel rise from the depth of 40 m to the present level.

The permafrost extent in the Kara Sea has been mapped with GIS tools and the respective database on its conditions has been developed.

There is apparently a paragenetic relationship between gas seeps and submarine permafrost, and the markers of gas seeps may additionally indicate deeply buried submarine permafrost.

References

Melnikov V.P., Spesivtsev V.I., 1995. Engineering-Geological and Geocryological Conditions of the Barents and Kara Shelves [in Russian]. Nauka, Novosibirsk, 198 pp.

Rekant P., Tumskoi V., Gusev E., et al., 2009. Distribution and features of submarine permafrost near Semenoskoe and Vasilievskoe shoals (Laptev Sea) revealed by high-resolution seismic profiling, in: Kassens H., Lisitzin A.P. (Eds.), System of the Laptev Sea and the Adjacent Arctic Seas: Modern and Past Environments [in Russian]. Moscow University Press, Moscow, pp. 332–348.

Rokos S.I., Tarasov G.A., 2007. Gas-saturated sediments of bays and gulfs in the southern Kara Sea. Bull. Quaternary Commission, 67, 66–75.

Rokos S.I., Kostin D.A., Dlugach A.G., 2001. Free gas and permafrost in shallow sediments of the Pechora and Kara inner shelves, in: Sedimentological Processes and the Evolution of Marine Systems in Oceanic Periglacial Conditions [in Russian]. KNC RAN, Apatity, Book 1, pp. 40–51.

Shlezinger A.E., 1998. Regional Seismic Stratigraphy [in Russian]. Nauchnyi Mir, Moscow, 379 pp.

Received
10 February 2011

Kriosfera Zemli, 2011, vol. XV, No. 4, pp. 63–65 http://www.izdatgeo.ru

COASTAL DYNAMICS OF THE WESTERN YAMAL

A.A. Vasiliev, R.S. Shirokov, G.E. Oblogov, I.D. Streletskaya*

Institute of Earth's Cryosphere, Siberian Branch of the Russian Academy of Sciences, 86, Malygina str., Tyumen, 625026, Russia; al.a.vasiliev@gmail.com
**Lomonosov Moscow State University, Department of Geography, 1, Leninskie Gory, Moscow, 119992, Russia*

Long-term monitoring of coastal dynamics in the Western Yamal, at the Marre-Sale key site has shown a mean coastal retreat at 1.7 m/yr, with the maximum 3.3 m/yr and the minimum 0.5 m/yr. The time-dependent variations in the retreat rate show cyclic patterns. The change in beach and shoreface elevation in thermal erosion coasts reaches 0.7 m and can be either positive or negative. First quantitative estimates give 0.3 m maximum elevation change of accumulative surfaces.

INTRODUCTION

The coastal dynamics in the western Russian Arctic has been insufficiently explored. The problem is especially topical for the western Yamal coast with the initiated development of Kruzenshtern and Kharasavey gas-condensate fields and prospected construction of related structures for condensed gas processing and transport. The coastal erosion of the West Yamal was monitored in different field campaigns at capes Burunnyi, Kharasavey, and Marre-Sale, as well as within the Baidaratskaya Guba pipeline traverse [*Voskresensky and Sovershaev, 1998; Vasiliev et al., 2001*]. Note that the monitoring was mostly restricted to measuring the retreat rates of the coastal cliff edges.

STUDY AREA AND METHODS

Integrate studies of coastal dynamics around the Marre-Sale weather station are carried out since 1978 by the Institute of Earth's Cryosphere (Tyumen). The coast is composed of Late Pleistocene deposits of 15–30 m high sea terraces (II and III), with saline marine clay at base of the section and sand in the upper part. The area belongs to the zone of continuous permafrost. The mean annual temperature of frozen ground ranges from –2.5 to –6.0 °C.

The monitoring parameters at the site included meteorology and marine hydrology, dynamics of permafrost conditions, coastal retreat rate (measured yearly against fixed benchmarks and by repeated laser transit survey of cliff edge and cliff base locations), and shoreface elevation (leveled yearly along a fixed coast-orthogonal profile).

RESULTS

Climate warming in the Arctic since the 1970s is accompanied by changes in sea hydrodynamics. According to data from the Marre-Sale weather station over this period, the spring break-up of the seaice cover begins at approximately same dates, except for natural variations, while freeze-up has moved to later dates. Correspondingly, the ice-free period when the coast is exposed to hydrodynamic forcing has become longer (20 days longer on average for 1970 through 2010). Note that this increase is attributed to the fall season when the coast is strongly eroded by frequent storms.

The monitored sea-wave parameters (height, period, wavelength, and duration) show no regular increase associated with climate warming. Therefore, one may expect no steady acceleration of coastal erosion, even if warming continues and the period of active coastal dynamics becomes ever longer. See Fig. 1 for average annual coastal retreat rates measured over 4.5 km of the coast.

The coastal retreat rate at Marre-Sale changes periodically rather than increasing since the late 1970s (Fig. 1). Erosion was most rapid in 1998–1999 and 2006–2010 but slowest in 1978–1979 and 1999–2000, the average being 1.7 m/yr. The retreat rate does not experience direct climate forcing [*Vasiliev et al., 2006*]. The effect of climate is rather implicit, via local changes in synoptic conditions, in atmospheric pressure and wind (and related fetch). A close relationship between coastal erosion in the Kara Sea and the total wind-wave energy was discovered earlier

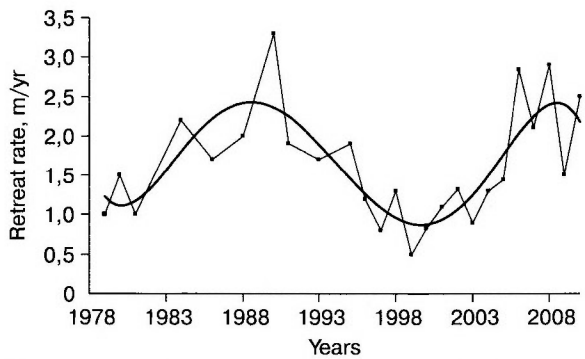

Fig. 1. Coastal retreat rate at Marre-Sale site.
Heavy line is approximation.

Table 1. **Long-term average coastal erosion rate at West Yamal**

Area	Cliff height, m	Lithology	Coastal erosion rate, m/yr			Reference
			max.	min.	av.	
Between Skuratov and Burunnyi Capes	8	Clay with sand interbeds	–	–	0.8	[*Voskresensky and Sovershaev, 1998*]
Burunnyi Cape	14	Clay	2.5	0.6	1.2	[*Vasiliev et al., 2006*]
Kharasavey Cape	10–25	Clay with sand interbeds, sand	4.5	0.4	–	[*Solomatin, 1992*]
			–	–	2,0	[*Kamalov et al., 2002*]
			3.0	0.5	1.4	[*Vasiliev et al., 2006*]
			2.3	0.51	1.3	[*Yuriev, 2009*]
Beluzhii Cape	to 40	Sand	1.0	0.5	–	[*Voskresensky and Sovershaev, 1998*]
Marre-Sale Cape	10–30	Sand over loam	–	–	1.8	[*Troitsky and Kulakov, 1976*]
			1.8	1.0	1.6	[*Shur et al., 1984*]
			3.3	0.5	1.7	[*Vasiliev et al., 2001*]
Southwestern coast of Baidaratskaya Guba Gulf	10–25	Sand over loam	0.9	0.05	0.4–0.5	[*Dubikov, 1997*]
	6–10	Sand, peat	0.7	0.3	–	

[*Vasiliev et al., 2006*] and confirmed through recent observations. Coastal retreat data from the West Yamal obtained by different authors are synthesized in Table 1.

There has been very little research of beach and shoreface elevation changes. Yearly elevation monitoring has been carried out at Marre-Sale since 2006 to a sea depth of 1.5 m by repeated leveling in early September, the heights (depths) being tied to a fixed elevation reference (Fig. 2). The datum is the waterline position at the time of measurements in 2006. The maximum beach elevation change (0.5 m) was observed in 2006–2007. In the shoreface, especially near the shore, the respective maximum was 0.6 m. Note that elevation change in the shoreface (at least close to the beach) can be either positive or negative. The sea-floor was eroded and subsided in 2006–2009, but it uplifted by aggradation in 2009–2010 after long storms.

The maximum beach elevation change as a consequence of brief post-storm events at Marre-Sale was estimated proceeding from geological conditions. Drilling stripped a 0.05–0.1 m thick pebble marker bed lying under 0.6 m thick sand and over an inclined surface of dense heavy clay with signature of erosion. Pebble layers normally form during maximum storm wave cutting and pebble deposition. Thus, the magnitude of wave-induced elevation change is measured as the total sand and pebble thickness, i.e., 0.7 m. This estimate roughly corresponds to that obtained during studies along the pipeline traverse of the Baidaratskaya Guba Gulf (0.5–0.7 m).

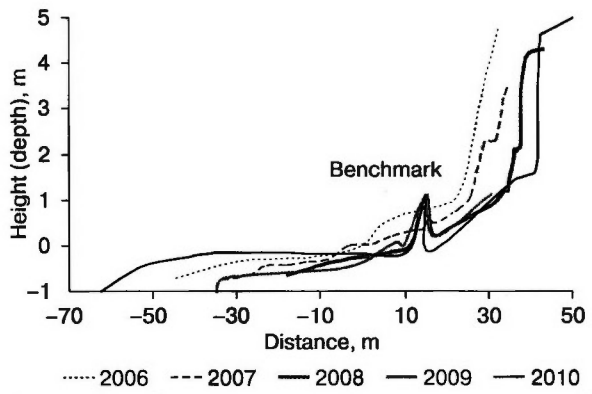

Fig. 2. Shoreface elevation change at Marre-Sale site.

The maximum sea-floor change on offshore beach was about 2 m [*Dubikov, 1997*]. These are approximate reference estimates for the whole West Yamal area.

An elevation change in low accumulative surfaces was observed at the Marre-Sale Koshki site where about 0.3 m of sand was deposited by long storms in 2010. The sand deposits have fully covered the earlier landforms and made a large sand field in place of the laida. Thus, the aggradation rate was 0.3 m/yr. This appears to be the only quantitative estimate of elevation change in marine aggradation surfaces.

CONCLUSIONS

- Long-term average coastal retreat rate has been monitored and estimated to reach 1.7 m/yr at the Marre-Sale site. The slowest rate of 0.5 m/yr was measured at the site of the Baidaratskaya Guba gas pipeline traverse.
- The maximum beach elevation change is 0.7 m; that of shoreface can be either positive or negative and is generally 0.6 m in magnitude, but can reach 2.0 m along offshore beach.
- The maximum elevation change observed in accumulative surfaces is 0.3 m.

The study was carried out as part of Program 20 ("World Ocean") of the RAS Presidium, Project "Permafrost of Arctic Seas and Continental Margin in Western Eurasia: Present State, Dynamics, Geocryological History, Transformation of Frozen and Cooled Grounds, and Hydrocarbon Emanation."

References

Dubikov G.I. (Ed.), 1997. Environmental Conditions of the Baidaratskya Guba Gulf [in Russian]. GEOS, Moscow, 432 pp.

Kamalov A.M., Ogorodov S.A., Arkhipov V.V., 2002. Coastal dynamics of the Western Yamal, in: Extreme Cryogenic Phenomena: Basic and Applied Aspects, Proc. Intern. Conf., Pushchino, pp. 63–64.

Shur Yu.L., Vasiliev A.A., Veisman L.I., et al., 1984. Methods for studying thermal erosion rates, in: Coastal Dynamics in the Permafrost Zone [in Russian]. Nauka, Novosibirsk, pp. 5–12.

Solomatin V.I. (Ed.), 1992. Environmental Geology of the North (Fundamentals of Geocryology) [in Russian]. Moscow University Press, Moscow, 270 pp.

Troitsky S.L., Kulakov A.P., 1976. Sealevel change and coastal topography, in: Problems of Exogenic Relief Formation [in Russian]. Nauka, Moscow, Book 1, pp. 351–426.

Vasiliev A.A., Pokrovsky S.I., Shur Yu.L., 2001. Dynamics of the thermal erosion coast of West Yamal. Kriosfera Zemli, V (1), 44–52.

Vasiliev A.A., Streletskaya I.D., Cherkashev G.A., et al., 2006. Coastal dynamics of the Kara Sea. Kriosfera Zemli, X (2), 56–67.

Voskresensky K.S., Sovershaev V.A., 1998. Surficial processes in the Arctic coastal dynamics, in: Coastal Dynamics in the Russian Arctic [in Russian]. Moscow University Press, Moscow, pp. 35–48.

Yuriev I.V., 2009. Problems of gas field exploitation in coastal zone of Western Yamal. Kriosfera Zemli, XIII (1), 46–54.

Received
11 February 2011

Kriosfera Zemli, 2011, vol. XV, No. 4, pp. 65–68 **http://www.izdatgeo.ru**

COASTAL EROSION AS A DESTABILIZING FACTOR OF CARBONATE BALANCE IN THE EAST SIBERIAN ARCTIC SEAS

S.O. Razumov, M.N. Grigoriev

Melnikov Permafrost Institute, Siberian Branch of the Russian Academy of Sciences, 36, Merzlotnaya str., Yakutsk, 677010, Russia; razum55@mail.ru

The carbonate balance in the Arctic seas of East Siberia is in reciprocal relationship with climate change and destructive coastal dynamics. Thermal and wave erosion of permafrost coast associated with global warming destabilizes the marine CO_2 – carbonate system by increasing dramatically the partial pressure of CO_2 in coastal waters to 800–900 ppm and facilitating its release into air. The ongoing warming and growing activity of coastal processes can reduce the ability of the eastern Arctic seas for CO_2 uptake.

INTRODUCTION

Arctic seas are important regulators of atmospheric carbon dioxide in the Northern Hemisphere. In the summer season they may be expected to act as sinks of excess CO_2, but there is evidence [*Razumov, 2003; Pipko et al., 2005*] that the surface waters are oversaturated with CO_2 which evades into the atmosphere in some areas of Arctic seas. The potential of seawater for CO_2 uptake from the atmosphere depends on the relative percentages of components in the CO_2 – carbonate system, or the carbonate balance. This balance in coastal-shelf waters is subject to the influence of climate-controlled erosion processes in the permafrost coast.

EFFECT OF COASTAL EROSION ON THE CARBONATE BALANCE OF COASTAL-SHELF WATERS IN ARCTIC SEAS

The uptake of atmospheric CO_2 by the eastern Arctic seas and increasing fluxes of organic carbon and carbonates (dissolved or solid) affect the seawater carbonate balance. In the East Siberian seas, the rapidly retreating coast with high contents of ground ice is the main source of terrigenous input to the shelf. Coastal erosion (mainly by thermal processes and waves) supplies about $4 \cdot 10^6$ tons of organic carbon into the Laptev and East Siberian seas, which is more than in all other Arctic seas [*Grigoriev et al., 2006*]. A part of carbon dioxide that is absorbed from the air and released in organic carbon oxidation is spent on dissolving calcium carbonate, whereby seawater becomes more alkalic. The water alkalinity in the East Siberian Sea did not change much from the 1920s to the early 1950s but it grew by the early 1990s (by 0.21 mg·equivalent/liter on average and by 0.25–0.40 mg·equivalent/liter in the southern sea part).

Carbon dioxide can either evade from seawater or invade into it at specific weather conditions in the ice-free season with moderate winds and calm spells. For instance, $CaCO_3$ saturation west of the Kolyma Delta is within 0.77 while the CO_2 partial pressure is from 89 to 164 ppm [*Razumov, 2003*]. This pressure being almost 2–4 times as low as the atmospheric

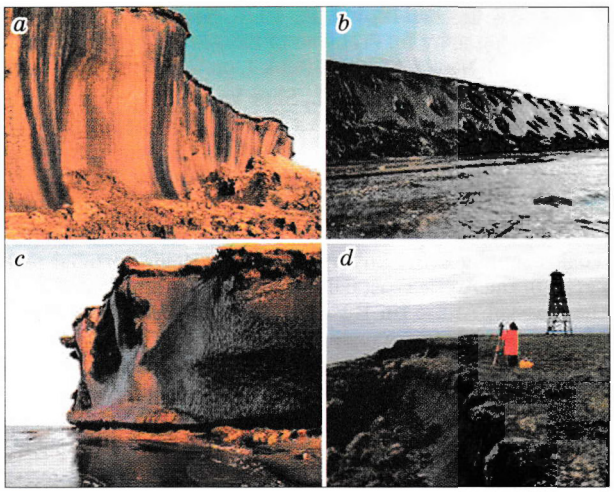

Fig. 1. Ice-rich coastal cliffs of Arctic seas:

a – Bolshoi Lyakhovsky Island, *b* – Anabar-Olenek coast, *c* – Muostakh Island, *d* – Bykovsky Peninsula.

mean of high latitudes, one can expect invasion of carbon dioxide. In the Kolyma Delta, however, more CO_2 is rather released than absorbed as its partial pressure in seawater reaches 300 to 600 ppm, possibly, due to intense oxidation of organic carbon carried by the river.

Thermal and wave erosion of permafrost coast is responsible for significant variations of physicochemical parameters and, as a consequence, interferes with the CO_2 – carbonate balance in the coastal zone. The rate of coastal erosion in the eastern Arctic seas changes in space and time depending on summer air temperatures and ice conditions, as well as on recurrence and duration of storms. Erosion slowed down during relative cooling between the 1950s and early 1970s in the Russian eastern Arctic, and the coast of the Laptev and East Siberian seas retreated at a mean rate of 2–6 m/yr [*Are, 1985*]. The coast of the two seas consists mainly of silt-size loamy sand and sandy loam with thick ice wedges up to 7–8 m wide, the total ice content of soil reaching 30 to 90 vol. % (Fig. 1).

Relative climate warming through the past forty years increased the duration of ice-free seasons in the eastern Arctic, the surface area of open water, and the frequency of storms. The mean summer air temperature rose 1.3–1.5 °C above the climate norm, the storm recurrence increased by 3–4 %, and the total duration of active wave dynamics on the permafrost coast grew, on average, from 58 to 100 hr/yr. The coastal retreat in zones of rapid erosion in the Laptev and East Siberian seas accelerated to 4–8 m/yr on average reaching locally as high as 12 m/yr (Fig. 2), with the maximum erosion rate 17–25 m/yr [*Razumov, 2000; Grigoriev and Zhang, 2008*]. As the ice-rich coast is being rapidly eroded, oxidation of organic carbon rises dramatically the partial pressure of carbon dioxide in seawater (to 800–900 ppm) and facilitates its release into air (Fig. 3) [*Razumov, 2003; Pipko et al., 2005*].

Thus, carbon dioxide is released from the coastal zone of the East Siberian Sea between the New Siberian islands and the Chaun Bay, in common meteorological conditions, and is absorbed by water in the eastern sea part. The release grows with increasing thermal erosion and occurs even offshore as far as the De Long Strait. Active thermal erosion of mainland and islands in the southeastern Laptev Sea results in prevalent release of CO_2.

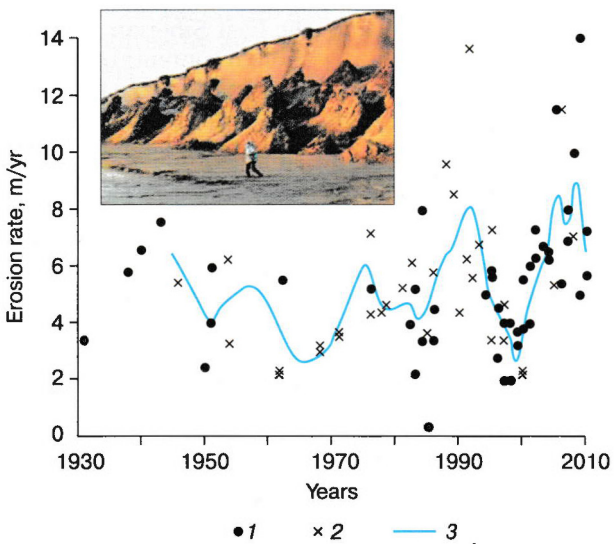

Fig. 2. Variations in mean rate of coastal retreat in the Laptev (*1*) and East Siberian (*2*) seas in zones of rapid thermal erosion.

3 – erosion rates averaged over two seas. Inset shows a typical coastal exposure of ice complex, Shirokostan Peninsula.

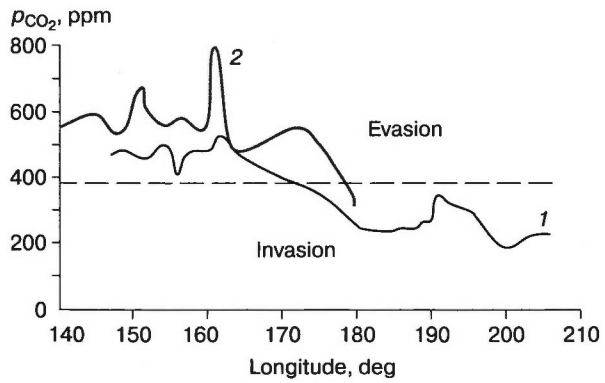

Fig. 3. CO_2 partial pressure in coastal-shelf waters of Arctic seas of East Siberia in the conditions of common ice-free season (curve *1*) and erosion of ice-rich coast (curve *2*).

Dashed line is present atmospheric CO_2.

EFFECT OF DESTABILIZED CARBONATE BALANCE ON REGIONAL CLIMATE

Warming in the Arctic decreases the magnitude of the partial CO_2 pressure gradient between water and air (Fig. 4) due to greater activity of processes destroying the permafrost coast. Organic carbon, which was formerly stored in permafrost, comes into the sea. This reduces the capacity of Arctic seas for taking up carbon dioxide, and the water-air gradient of CO_2 partial pressure becomes prone to reversal, i. e., the release becomes more probable than the uptake (Fig. 4). The release of CO_2, in turn, would decrease its partial pressure in water and increase the $CaCO_3$ percentage on dissociation of bicarbonates. Thereby the system may be expected to recover its equilibrium with atmospheric CO_2 and, possibly, return to invasion of carbon dioxide (Fig. 5).

However, this does not happen for the shortage of solid carbonates in the eastern Arctic seas. Their dissolution consumes a relatively small part of CO_2 which is released into the water on oxidation of organic carbon provided by coastal erosion. Its greater part becomes gaseous thus increasing the partial pressure. This destabilizes the carbonate balance in the coastal-shelf waters along the zones of rapid coastal retreat.

As the water temperature rises, the solubility of carbon dioxide decreases while its partial pressure grows and thus favors the evasion. In the eastern Arctic seas, this regularity works in water with a salinity over 20 ‰ but is less pronounced in the shelf where salinity is below 13 ‰ (Fig. 6). Therefore, the carbonate balance in coastal waters may shift to lower CO_2 partial pressures but higher $CaCO_3$ and pH (Fig. 5), possibly, because the aggressive part of free CO_2 is spent on dissolution of solid carbonates brought from the mainland. The system responds to this shift by CO_2 invasion despite the relatively high water temperature.

Thus, destabilization of the CO_2 – carbonate system of the Arctic seas is attendant with release of carbon dioxide and the ensuing accumulation of calcium carbonate. The uptake of atmospheric CO_2, and dissolution of carbonates as its consequence, reflect the stable state of the CO_2 – carbonate system of both seas. The climate, the dynamics of destructive processes in the permafrost coast, and the carbonate balance in the eastern Arctic seas are in reciprocal relationship. The loss of equilibrium in the CO_2 – carbonate system pushes up the otherwise caused climate change in the Arctic.

This may be explained as follows. The thermodynamic model of the annual ocean-air cycle [*Kagan et al., 1986*] predicts that doubling of atmospheric CO_2 (from 280 to 560 ppm) should cause a 1.4 °C warming of the mean annual air temperature north of 60° N

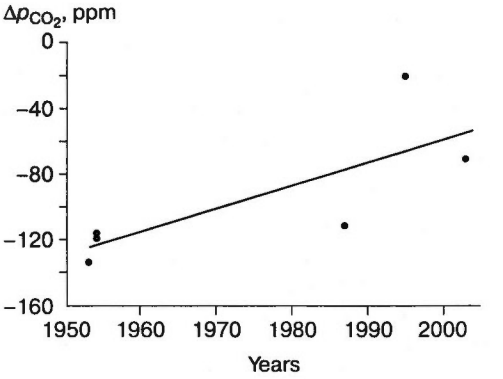

Fig. 4. CO_2 partial pressure gradient between water of eastern East Siberian Sea and air, according to [*Musina, 1960; Feely et al., 2001; Razumov, 2003; Pipko et al., 2005*].

Negative gradient corresponds to CO_2 uptake.

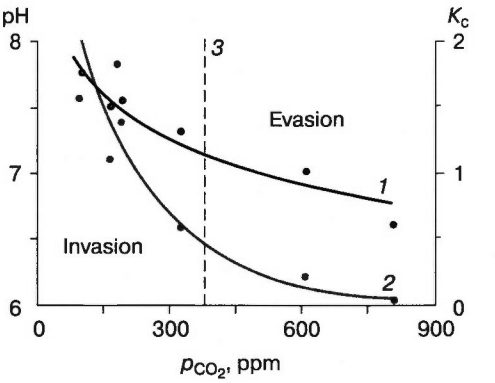

Fig. 5. CO_2 partial pressure (p_{CO_2}) in East Siberian Sea plotted against hydrogen ion activity pH (curve *1*) and against water saturation with carbonates K_c (curve *2*) at present CO_2 partial pressure in atmosphere (dashed line *3*).

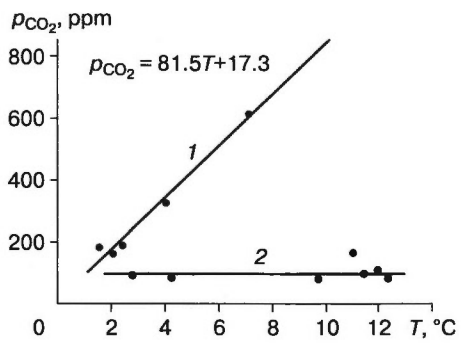

Fig. 6. CO_2 partial pressure (p_{CO_2}) in seawater plotted against its temperature (T), at water salinities of 20–30 ‰ (*1*) and 2–13 ‰ (*2*).

(0.75 °C for summer temperature and 1.7 °C for winter temperature). Over the period from the early 1960s to 2008, the CO_2 partial pressure in air in the Northern Hemisphere became 75 ppm higher, which, according to the thermodynamic modeling, can cause a 0.37 °C increase in the mean annual air temperature north of 60° N. Data from 14 weather stations from Vize Island to Dezhnev Cape show a mean annual air temperature rise of 1.0–2.7 °C in the same period (1.8 °C on average) [*Grigoriev et al., 2009*]. Thus, the contribution of atmospheric CO_2 increase into the observed warming is about 20 %.

Therefore, warming in the Northern Hemisphere more likely has other major controls than CO_2 increase. This may be 20- and 50-year cycles of the Earth's axis nutation driven by tidal forces [*Grigoriev et al., 2006*] and related changes in water circulation in the World ocean and global atmospheric transport.

CONCLUSIONS

Climate change to warming or cooling, which influences the coastal dynamics, may result from nutation cycles driven by tidal forces. Destabilization of the carbonate balance in seawater is not the cause of climate change but only can increase its magnitude.

In the contemporary climate conditions, the Arctic seas generally keep their potential for CO_2 uptake in spite of high organic carbon input to the water and summer warming. However, further warming and coastal erosion may aggravate the carbonate balance instability in the East Siberian Arctic seas and reduce considerably their CO_2 uptake capacity.

References

Are F.E., 1985. Thermal Erosion of Coast: Fundamentals of Prediction [in Russian]. Nauka, Novosibirsk, 172 pp.

Feely R.A., Sabine Ch.L., Takahashi T., et al., 2001. Uptake and storage of carbon dioxide in the ocean: The global CO_2 survey. Oceanography, 14 (4), 18–32.

Grigoriev M.N., Zhang R.V., 2008. Drastic change of coastal permafrost processes under recent warming within the East Siberian Arctic region, in: Drastic Change under the Global Warming. Proc., First Intern. Symp. on the Arctic Research (ISAR-1), Miraikan, Tokyo, Japan, pp. 191–194.

Grigoriev M.N., Razumov S.O., Kunitsky V.V., et al., 2006. Dynamics of the Russian East Arctic Sea coast: major factors, regularities and tendencies. Kriosfera Zemli, X (4), 74–94.

Grigoriev M.N., Kunitsky V.V., Zhang R.V., et al., 2009. Warming-related changes of cryological, landscape, and hydrological conditions in the East Siberian Arctic. Geografiya i Prirodnye Resursy, No. 2, 5–11.

Kagan B.A., Ryabchenko V.A., Safrai A.S., 1986. Response of the ocean-air system to atmospheric CO_2 doubling and its seasonal variations. Okeanologiya, XXVI (3), 365–375.

Musina A.A., 1960. Water chemistry in the Arctic seas. Voprosy Gidrokhimii Arkticheskogo Basseina (Problems of Water Chemistry in the Arctic Seas), 218, 5–65 (AARI Transactions, Leningrad).

Pipko I.I., Semiletov I.P., Pugach S.P., 2005. Carbonate system dynamics in the East-Siberian region: coastal zone. Rep. 5th Arctic Coastal Dynamics Intern. Workshop, Montreal, Canada, pp. 89–93.

Razumov S.O., 2000. Rate of coastal erosion as a function of climate and geomorphology of the coast. Geomorfologiya, No. 3, 88–94.

Razumov S.O., 2003. Coastal cryogenic processes and carbonate balance of the coastal waters of eastern Arctic seas in the light of a changing climate. Proc. 8th Intern. Conf. on Permafrost. Zurich, Switzerland, Book 2, pp. 935–939.

Received
21 February 2011

SCIENTIFIC JOURNAL
EARTH'S CRYOSPHERE

Kriosfera Zemli, 2011, vol. XV, No. 4, pp. 69–71 http://www.izdatgeo.ru

GAS HYDRATES

METASTABLE STATES OF GAS HYDRATES AT PRESSURES BELOW THE 'ICE–HYDRATE–GAS' EQUILIBRIUM

V.P. Melnikov, A.N. Nesterov, L.S. Podenko, A.M. Reshetnikov, V.V. Shalamov

Institute of Earth's Cryosphere, Siberian Branch of the Russian Academy of Sciences, PO box 1230, Tyumen, 625000, Russia; nesterov@ikz.ru

Reported are experimental results on the behavior of methane, propane, and carbon dioxide hydrates at temperatures below 273 K and pressures below the 'ice–hydrate–gas' equilibrium, when ice is the stable phase. The study has furnished evidence for the formation of intermediate supercooled (metastable) water during gas hydrate dissociation. The pressures of hydrate dissociation into supercooled water and gas were measured at the temperature ranges 253–273 K for methane hydrate, 263–273 K for propane hydrate, and 249–273 K for carbon dioxide hydrate. The gas hydrates have been recognized to keep metastable for a long time within the P–T area in the phase diagram bounded by the 'ice–hydrate–gas' and 'supercooled water–hydrate–gas' metastable equilibrium lines. Contrary to what has been assumed for self-preservation of gas hydrate, their metastability has no relation with ice coating on hydrate particles.

Gas hydrates are crystalline compounds forming from water and low-molecular gases. In nature they exist as hydrates of natural gases and are widespread in submarine environments below depths 350–400 m or below 200–250 m in the permafrost zone [*Istomin and Yakushev, 1992*]. Within the latter, gas hydrates can exist also outside their present-day geological stability zone even at 150–200 m depths due to self-preservation in the pore space of frozen rocks. These are the so-called relic gas hydrates [*Istomin and Yakushev, 1992*] which store large amounts of natural gas and thus have good economic prospects [*Yakushev et al., 2005*].

Self-preservation of gas hydrates has been commonly attributed to ice coating that forms upon hydrate particles at the onset of their dissociation and precludes free gas release [*Davidson et al., 1986; Istomin and Yakushev, 1992*]. Ice formation on dissociation of hydrates has been proven experimentally but its very mechanism remains poorly understood.

One self-preservation mechanism, which was theoretically grounded in terms of equilibrium thermodynamics, implies that hydrates dissociated at temperatures below 273 K can go through intermediate metastable phases of supercooled water and cubic ice [*Istomin et al., 2006*]. However, there was no reliable experimental evidence for the existence of these metastable phases before our studies.

Below we present main highlights of our study aimed at checking experimentally whether the metastable states of gas hydrates can exist during gas hydrate dissociation below the ice melting point.

The experiments were performed with methane, propane, and carbon dioxide hydrates. The gas hydrate dissociation was studied using visual microscopy technique combined with P–T measurements.

Details of the experimental setup and procedure used in this work are given elsewhere [*Reshetnikov, 2010*]. In brief, gas hydrates were formed in a high-pressure reactor placed inside a thermostatic cooler in order to maintain the required temperature. Optical observation was carried out through viewing windows on the reactor's lateral surface using a cathetometer with its telescope ocular fitted with a digital camera. The digital image was displayed on a monitor in real-time mode and saved on DVD.

The samples of gas hydrates were prepared in the following way. Distilled water (1.0–1.5 g) was sprayed over a Plexiglass plate set vertically inside the reactor between the viewing windows. Before that, both the reactor and the plate were cooled down to 253–258 K to let ice form on the plate surface as a spherical segment with the 0.15–2.5 mm base diameter and a height of 0.3 mm. After vacuuming and charging with the hydrate-forming gases, the reactor was heated slowly to above the ice melting point. The formation of hydrates was inferred from visual absence of liquid in the samples on the plate.

For gas hydrate dissociation, first the chosen temperature was set up in the reactor and then pressure was decreased slowly. In the course of dissociation, the gas hydrate samples changed their surface patterns as insular liquid appeared with gas releasing from it. The pressure at which the first change became visible was assigned the dissociation pressure P_d.

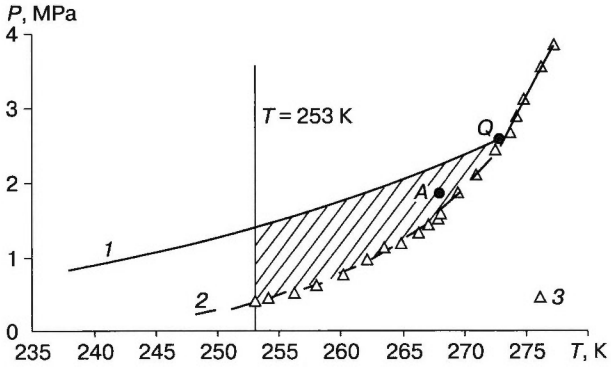

Fig. 1. State diagram of the 'water–methane' system (with excess gas), a fragment:

1 – equilibrium line 'ice (water at $T > 273$ K)–gas hydrate–gas' [*Istomin and Yakushev, 1992*]; *2* – predicted metastable extension of the 'water–gas hydrate–gas' equilibrium line at $T < 273$ K [*Istomin et al., 2006*]; *3* – gas hydrate dissociation pressure P_d, our data; $T = 253$ K is the temperature limit at which supercooled water formation on methane hydrate dissociation was observed; *Q* is the quadrupole point corresponding to coexistence of ice + water + gas hydrate + gas; *A* is the point on the phase diagram corresponding to *P–T* conditions of the experiment with metastable methane hydrate (see text for explanation).

Table 1. **Coefficients *A* and *B* in Equation (1)**

Hydrate-forming gas	*A*	*B*, K	Temperature range, K
Methane	24.763	6509.1	253–273
Propane	54.607	15 402.0	263–273
Carbon dioxide	28.61	7774.7	249–273

Figure 1 shows P_d for methane hydrate. At temperatures above those at the quadrupole equilibrium point (T_Q), the P_d values coincide with the equilibrium dissociation pressure of bulk hydrates. At temperatures below T_Q and up to $T = 253$ K, the P_d values fall on the predicted extension of the 'water–hydrate–gas' equilibrium line into the area where supercooled water can exist. Similar results were obtained for propane and CO_2 hydrates, with the only difference that P_d were measured till 263 K for the former and 249 K for the latter.

Least-square processing of the data has yielded the following temperature dependence of the dissociation pressure (with the regression coefficient 0.998):

$$\ln (P_d/P_0) = A - B/T, \qquad (1)$$

where $P_0 = 1$ MPa, *T* is the temperature in K, and *A*, *B* are the empirical coefficients (Table 1).

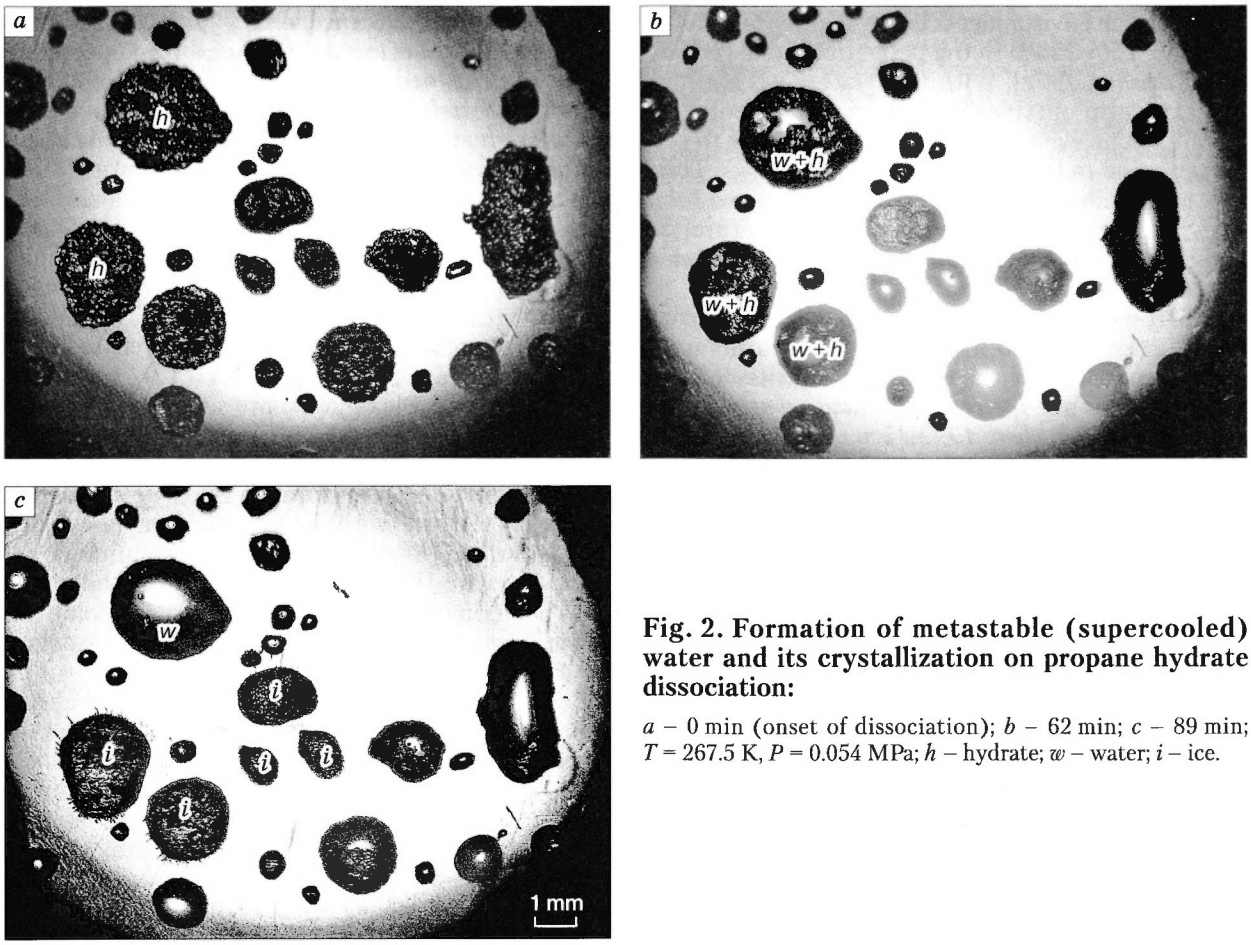

Fig. 2. Formation of metastable (supercooled) water and its crystallization on propane hydrate dissociation:

a – 0 min (onset of dissociation); *b* – 62 min; *c* – 89 min; $T = 267.5$ K, $P = 0.054$ MPa; *h* – hydrate; *w* – water; *i* – ice.

The dissociation enthalpy ΔH was calculated using the measured pressures P_d, with the Clausius–Clapeyron equation: ΔH = 51.7 kJ/mol for methane hydrate, ΔH = 129.4 kJ/mol for propane hydrate, and ΔH = 58.4 kJ/mol for carbon dioxide hydrate. The predicted enthalpy values agree well with the published ones for dissociation of the respective hydrates into water and gas.

Figure 2 shows an example of successive visible changes observed during dissociation of propane hydrate at 267.5 K. At this temperature, propane hydrate is known to dissociate into ice and gas at the equilibrium pressure 0.137 MPa [*Sloan and Koh, 2008*]. However, the first change in the samples was observed at a pressure as low as 0.054 MPa when propane hydrate dissociated into supercooled water and gas (Fig. 2, *a*, *b*). Some drops of supercooled water remained in the metastable state and did not crystallize even 1.5 hr after having appeared (Fig. 2, *c*).

The gas hydrate samples behaved in an unusual way within the *P–T* area bounded by the 'ice–hydrate–gas' equilibrium line and 'supercooled water–hydrate–gas' metastable equilibrium line (hatched area in the phase diagram of Fig. 1). When the methane hydrate samples showed no visible signature of dissociation for 14 days of continuous examination at 268 K and 1.9 MPa (point *A* in Fig. 1), we began to reduce pressure in the reactor while maintaining the same temperature. Water formed immediately following the intersection of 'supercooled water–hydrate–gas' metastable equilibrium line. The formation of supercooled water means that the hydrate samples were free from ice. Indeed, had there been ice in the samples, no supercooled water would have been observed: this water crystallizes rapidly as it can never coexist with ice. Therefore, the stability of the methane hydrate samples in the metastable state (point *A* in Fig. 1) has no relation with self-preservation through ice coating of hydrate particles. The long-term existence of metastable hydrates in the *P–T* area where ice is a stable phase and the appearance of supercooled (metastable) water as an intermediate phase is thermodynamically forbidden, is evidence that the dissociation of hydrates into ice and gas in the form of a direct solid-solid transition is kinetically impeded.

Similar behavior was observed also for other methane hydrate samples in the area bounded by the 'ice–hydrate–gas' equilibrium line and 'supercooled water–hydrate–gas' metastable equilibrium line and the 253 K isotherm, as well as for propane and CO_2 hydrates in the area bounded by the same lines and the 263 K and 249 K isotherms, respectively.

Thus, the laboratory tests have proven that the metastable states (gas hydrate, supercooled water) on dissociation of gas hydrates can really exist for a long time (on the experiment scale) at the temperature below 273 K. As inferred from the measured metastable equilibrium pressure for the systems 'water-methane hydrate', 'water-propane hydrate', and 'water-carbon dioxide hydrate', the gas hydrate stability within the *P–T* area bounded in the phase diagram by the 'ice–hydrate–gas' and 'supercooled water–hydrate–gas' lines has no relation with self-preservation but is rather due to kinetic impediment of dissociation into ice and gas.

The study was supported by grant 10-05-00270-a from the Russian Foundation for Basic Research; it was carried out as part of Integration Project 09-62 of the Siberian Branch of the Russian Academy of Sciences and Project 11-6 of a Basic Research Program of the RAS Earth Science Department.

References

Davidson D.W., Garg S.K., Gough S.R., et al., 1986. Laboratory analysis of naturally occurring gas hydrate from sediment of the Gulf of Mexico. Geochim. et Cosmochim. Acta, 50, 619–623.

Istomin V.A., Yakushev V.S., 1992. Natural Gas Hydrates [in Russian]. Nedra, Moscow, 236 pp.

Istomin V.A., Kvon V.G., Durov V.A., 2006. Metastable states of gas hydrates. Gas Hydrates, Spec. Issue of Gazovaya Promyshlennost, 32–35.

Reshetnikov A.M., 2010. Metastable States at Gas Hydrate Dissociation below 273 K: An Experimental Study [in Russian]. Candidate Thesis, Tyumen, 123 pp.

Sloan E.D., Koh C.A., 2008. Clathrate Hydrates of Natural Gases. Boca Raton, CRS Press Taylor and Francis Group, 721 pp.

Yakushev V.S., Perlova E.V., Makhonina N.A., 2005. Metastable (relic) gas hydrates: distribution, resources, and economic prospects. Kriosfera Zemli, IX (1), 68–72.

Received
6 February 2011

Kriosfera Zemli, 2011, vol. XV, No. 4, pp. 72–74 http://www.izdatgeo.ru

FORMATION OF SUPERCOOLED WATER ON DISSOCIATION OF GAS HYDRATES FROM NUCLEAR MAGNETIC RESONANCE DATA

V.A. Vlasov, A.G. Zavodovsky, M.Sh. Madygulov, A.M. Reshetnikov

Institute of Earth's Cryosphere, Siberian Branch of the Russian Academy of Sciences, PO box 1230, Tyumen, 625000, Russia; zag-2-57@yandex.ru

Dissociation of CFC-12 (Freon-12) hydrate into gas and supercooled water at low temperatures has been discovered in a pulsed nuclear magnetic resonance (NMR) study of disperse ice. Supercooled water was investigated experimentally in terms of its quantity dynamics during dissociation. The dissociation rates in two gas hydrate samples were measured under different experimental conditions. Supercooled water was found out to crystallize on the surfaces and inside gas hydrate particles at different P–T conditions of CFC-12 hydrate dissociation.

The present study continues earlier experimental research on the mechanism of gas hydrate dissociation into gas and supercooled water at subzero temperatures [*Melnikov et al., 2007, 2009, 2010*]. The objective of the first project stage was to expand the scope of gases forming hydrates that dissociate as 'gas hydrate → supercooled water + gas'. At the second stage, the dissociation process has been checked through direct experimental measurements using pulsed nuclear magnetic resonance (NMR) which is a reliable analytical tool applied lately to explore gas hydrate formation [*Aichele et al., 2009; Gao et al., 2009*]. There is reason to believe [*Watanabe and Wake, 2009*] that NMR can reveal the appearance of supercooled water in the beginning of gas hydrate dissociation and, moreover, can trace the dynamics of its content. This data has important implications for the dissociation mechanism, as well as for the role of supercooled water in the effect of gas hydrate self-preservation [*Istomin et al., 2006*].

The reported experiments were run with CFC-12 (CCl_2F_2 chlorofluorocarbon, or Freon-12) selected for its ability to form hydrates at low pressures. This facilitated the instrumental work performed on a Bruker *Minispec – mq* pulsed NMR relaxometer operating at the resonance frequency 19.65 MHz for hydrogen nuclei. Another advantage of CFC-12 is the lack of hydrogen nuclei which simplifies NMR analysis and allows recording signals from water molecules only (either free as liquid water or ice, or bound in hydrates).

The starting materials for preparing gas hydrate samples were distilled water and technological CFC-12. To promote hydrate formation, ice was used in ~400 μm grains and the samples were subjected to cyclic temperature changes [*Stern et al., 1996*] between −10 and +3 °C; the pressure of gaseous CFC-12 was maintained at 150 kPa. As a result, we obtained a system consisting of a great number of very small contiguous CFC-12 hydrate particles which enclosed cores of unreacted ice (or water, depending on the final temperature of the run). Note that as the number of runs increased from 1 to 8, the degree of ice-to-hydrate transformation P_h grew from 42 to 94 %, respectively.

The dynamics of liquid water content was studied by means of NMR relaxometry from free induction decay (FID) following a 90° pulse [*Chizhik, 1991*]. The technique was applied to estimate the T_2^* magnetic relaxation times separately for liquid water, ice, and gas hydrate in specially prepared CFC-12 hydrate samples, in order to isolate liquid water NMR signals. At temperatures between −10 and 0 °C, the characteristic FID times were T_{2l}^*, T_{2h}^* ~ 10 μs from ice and CFC-12 hydrate while liquid water relaxed at T_{2w}^* ~1.5 ms. With this knowledge, we estimated the FID amplitude A_m at the time t_s = 70 μs elapsed after the 90° pulse (Fig. 1). The signals from ice and gas hydrate being almost zero at that time, the measured FID amplitude corresponded uniquely to liquid water.

Before the NMR measurements in CFC-12 hydrate samples, the amplitude A_m was calibrated against the liquid water weight using standard samples with similar relaxation parameters ($CuSO_4$ aqueous solution). Furthermore, the experimental procedure was tested on CFC-12 hydrate dissociation at positive temperatures. In this temperature range, as we expected, the amount of liquid water released on decomposition of gas hydrate into water and gas obviously increased beyond the 'water–hydrate–gas' equilibrium line in all experiments. The dissociation process was also recognized from pressure increase in the box with the samples.

Additional water which may appear during gas hydrate dissociation at negative temperatures was revealed by NMR analysis using two samples with different initial degrees of ice-to-hydrate transformation: P_h = 68 % for sample 1 and P_h = 90 % for sample 2.

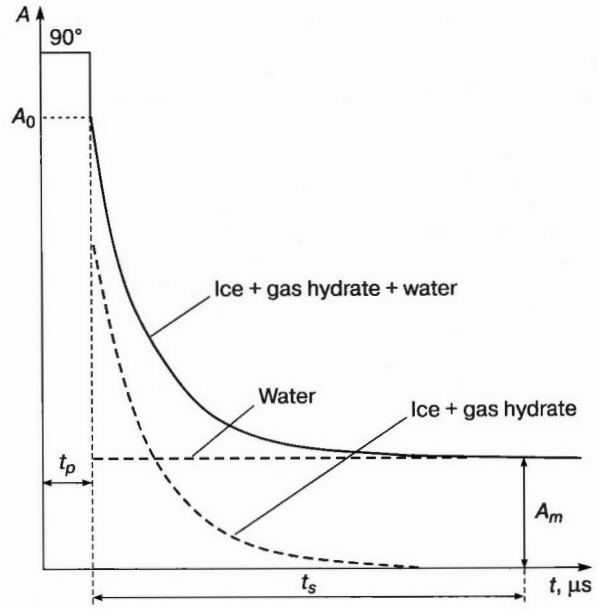

Fig. 1. Beginning of FID in the system ice + gas hydrate + water.

Dashed line is modeling results. A_0 is initial FID amplitude; A_m is FID amplitude at time t_s elapsed after 90° pulse; t_p is pulse duration.

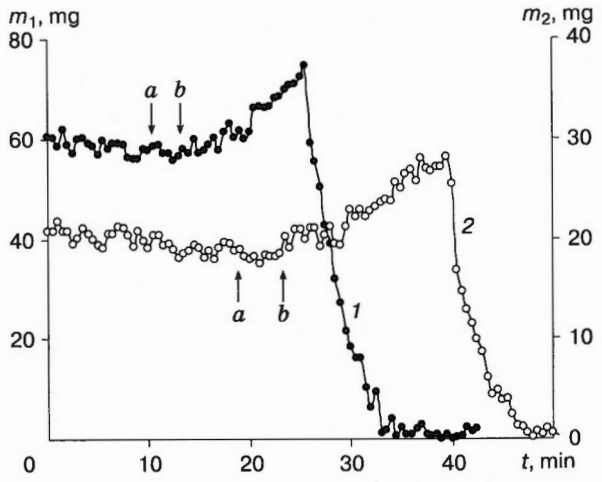

Fig. 2. Time-dependent variations in contents of supercooled water while pressure was reduced above the sample.

1: Sample 1, temperature −1 °C, stepwise lowered pressure (at 5 to 10 kPa); *2*: Sample 2, temperature −3 °C, pressure lowered at 3 kPa/min. Arrows point to contents across the equilibrium lines of ice–hydrate–gas (*a*) and supercooled water–hydrate–gas (*b*).

In the beginning of the experiment, the prepared samples stayed at the temperature +3 °C and the pressure of hydrate-forming gas 150 kPa for at least an hour, in order to ensure complete melting of unreacted ice in the cores of gas hydrate particles, which was confirmed by stable measured A_m. At the following step, samples 1 and 2 were cooled to −1 °C and −3 °C, respectively, at a rate of 0.5 K/min, at ~150 kPa pressure of CFC-12 over the samples. The subsequent transition to the domain of hydrate thermodynamic instability was at constant temperatures and the pressures lowered stepwise (stepsize varied from 5 to 10 kPa) for sample 1 or continuously at a mean rate of 3 kPa/min for sample 2.

The content of liquid water (Fig. 2) changed in the same way in the two samples irrespective of both their temperature and mode of pressure reduction. Note that additional supercooled water released on dissociation of CFC-12 hydrate in sample 2 appeared near the 'supercooled water–hydrate–gas' equilibrium line we obtained through extrapolation of experimental data from [*Byk, 1980*] onto the subzero temperature domain. In sample 1 of more supercooled water, however, it occured at 15 kPa below this line for the difficulty to precisely constrain the dissociation pressure reduced in the stepwise mode.

The dynamic growth of supercooled water recorded in Fig. 2 corresponds to a constant rate of CFC-12 hydrate dissociation, which we estimated at ~1 mg/min for the given samples and experimental conditions. Furthermore, we also calculated the maximum thicknesses of water films on the surfaces of gas hydrate particles, with regard to the total content of the formed liquid water, which were no larger than 4.2 and 3.6 μm for samples 1 and 2, respectively.

At some point after its peak, the content of liquid water began to decrease as a result of crystallization, at a rate more than an order of magnitude faster than the dissociation rate (Fig. 2). Note two pieces of the curves that record the crystallization of bulk water into ice at rates times different from each other. The early segment corresponds to crystallization of additional water released on dissociation on the surfaces of hydrate particles while the late one is crystallization of water that existed originally inside the particles. This is quite reasonable as, being an endothermic process, dissociation cools down the surface water and increases the probability for ice nucleation in it. On the other hand, crystallization beginning from the surface triggers the water-to-ice phase change in the liquid cores of gas hydrate particles.

Thus, the NMR analysis has provided solid evidence for dissociation of CFC-12 hydrate into gas and supercooled water at subzero temperatures, which may be a starting point for further estimating the magnetic-relaxation parameters of this water.

The study was partly supported by grant 10-05-00270-a from the Russian Foundation for Basic Research and was carried out as part of Project 13.7.4 of the Basic Research program of the RAS Presidium and Interdisciplinary Project 62 of the Siberian Branch of the Russian Academy of Sciences.

References

Aichele C.P., Chapman W.G., Rhyne L.D., 2009. Nuclear magnetic resonance analysis of methane hydrate formation in water-in-oil emulsions. Energy and Fuels, 23, 835–841.

Byk S.Sh., Makogon Yu.F., Fomina V.I., 1980. Gas Hydrates [in Russian]. Khimiya, Moscow, 296 pp.

Chizhik V.I., 1991. Nuclear Magnetic Relaxation. A Student's Manual [in Russian]. Leningrad University Press, Leningrad, 256 pp.

Gao S., Chapman W.G., House W., 2009. Application of low field NMR T_2 measurements to clathrate hydrates. J. Magnetic Resonance, 197, 208–212.

Istomin V.A., Yakushev V.S., Makhonina N.A., et al., 2006. Effect of self-preservation in gas hydrates. Gas Hydrates. Special Issue of Gazovaya Promyshlennost, 36–46.

Melnikov V.P., Nesterov A.N., Reshetnikov A.M., 2007. Formation of supercooled water on dissociation of propane hydrates at $T < 270$ K. Dokl. Phys. Chem., 417 (1), 304–307.

Melnikov V.P., Nesterov A.N., Reshetnikov A.M., et al., 2009. Evidence of liquid water formation during methane hydrates dissociation below ice point. Chem. Eng. Sci., 64, 1160–1166.

Melnikov V.P., Nesterov A.N., Reshetnikov A.M., et al., 2010. Stability and growth of gas hydrates below the ice–hydrate–gas equilibrium line on the P–T phase diagram. Chem. Eng. Sci., 65, 906–914.

Stern L.A., Kirby S.H., Durham W.B., 1996. Peculiarities of methane clathrate hydrate formation and solid-state deformation, including possible superheating of water ice. Science, 273, 1843–1848.

Watanabe K., Wake T., 2009. Measurement of unfrozen water content and relative permittivity of frozen unsaturated soil using NMR and TDR. Cold Regions Sci. and Technol., 59, 34–41.

Received
23 February 2011

SCIENTIFIC JOURNAL
EARTH'S CRYOSPHERE

Kriosfera Zemli, 2011, vol. XV, No. 4, pp. 75–78 http://www.izdatgeo.ru

PERMAFROST MICROBIOLOGY

DISTRIBUTION OF MICROORGANIZMS IN FROZEN GROUND

V.P. Melnikov[1], V.V. Rogov[2], A.N. Kurchatova[3], A.V. Brouchkov[4], G.I. Griva[1]

[1] *Tyumen Science Center, Siberian Branch of the Russian Academy of Sciences, 86, Malygina str., Tyumen, 625026, Russia; melnikov@ikz.ru, grivag@mail.ru*
[2] *Lomonosov Moscow State University, Department of Geography, 1, Leninskie Gory, Moscow, 119991, Russia; rogovvic@mail.ru*
[3] *State Oil and Gas University, 38, Volodarskogo str., Tyumen, 625000, Russia; kanni@mail.ru*
[4] *Lomonosov Moscow State University, Department of Geology, 1, Leninskie Gory, Moscow, 119991, Russia; brouchkov@hotmail.com*

Various microbial forms have been discovered *in situ* in ice lenses within frozen loam by means of optical and electron microscopy. Migration of bacteria on freezing of fine-grained soil has been investigated in experiments. The viability of bacteria may be maintained by processes associated with ice segregation. Ice lenses in cryotic soils appear to be the best habitat for sustainable microbial life.

INTRODUCTION

The cryosphere (sphere of cold and ice) controls biodiversity, as well as the lithosphere, the atmosphere, the hydrosphere, and the biosphere. Besides the inhabited Earth, cryosphere exists on other planets as well: the still colder planets of Mars, Jupiter, Saturn, and Uranus store great amounts of ice and have almost fully glaciated satellites. Increasingly growing recent attention has been given to the role of ice in the origin of planets, star systems, and in the space as a whole. Ice had existed before the Solar System formed and before water appeared on the Earth. Ice is and will be present in the Universe whichever change the latter may run. Owing to its physical properties, ice is an ideal place for life to emerge, as it provides an incubator with minimum temperature gradients, a shelter from killing radiation, and protection from dangerous chemicals.

The original hypothesis of biota dormancy in the Earth's cryosphere has been undermined with ample evidence for the existence of viable microbial life in natural ice and in frozen ground of various genetic types [*Zvyagintsev et al., 1985, 1990; Abyzov, 1993; Gilichinsky et al., 1993; Vorobieva et al., 1997; Brushkov et al., 2006*]. The possibility for microorganisms to remain alive and metabolically active in perennially cold environments has been widely reported [*Friedmann, 1994; Gilichinsky and Wagener, 1995; Rivkina, 1998; Vishnivetskaya et al., 2000; Christner et al., 2003*].

Most psychrophilic (cryophilic) organisms, i.e., those capable of growth and reproduction in cold temperatures from −10 to +20 °C, are stable against the freezing stress. This strength can be of biotic or abiotic origin. The biotic factors are, for instance, special forms of cysts or spores bacteria can develop to adapt to harsh conditions, or special compounds (sugars and proteins) they can secret to survive in frozen sediment and in ice sheets. Unfrozen water in permafrost is an abiotic stability factor, which acts as both a cryoprotector and an environment for transport of nutrients and metabolism. There are many things that remain unclear but ever more data has been appearing on the wonderful viability of microbial organisms discovered in frozen ground [*Brushkov et al., 2009*].

It is surprising how bacteria can remain viable in pre-Holocene permafrost despite the known vulnerability of proteins and DNA to macromolecular damage. Of special interest in this respect is investigating the spatial and ecological links of microorganisms with other permafrost components, such as mineral matrix particles, ice lenses, unfrozen water, and air. Some evidence of these patterns was obtained while studying the cryotic microstructure [*Rogov, 2009*], but no special research has been undertaken so far.

MATERIALS AND METHODS

The distribution of bacteria in frozen ground was studied in samples collected from the well-known section of Mamontova Gora (Russian for *Mammoth Hill*) in Central Yakutia, on the left bank of the Aldan River, 325 km upstream of its inflow into the Lena. An outcrop in terrace III of the Aldan exposes allu-

vium that, since the earliest Quaternary, has filled the Lower Aldan basin lying along the junction between the Verkhoyansk Foredeep and the Siberian craton.

The lower section consists of Middle Pleistocene sand and loamy sand thinly interbedded with wet ice-cemented flood-plain loamy sand. Up the section there follows an ice complex with thick Late Pleistocene and Holocene ice wedges.

According to geological data, cooling and related freezing of the sediments began in the late Pliocene. Paleoclimate reconstructions for the area predict that temperatures in the Pleistocene were from −12 to −32 °C in winter and from +12 to +16 °C in summer seasons [*Bakulina and Spektor, 2000*]. The presence of ice wedges indicates that the permafrost did not thaw during the Holocene climate optimum. Thus, the ice lenses in the lower section must be of the same age as the sediments.

The river has strongly eroded its bank at the locality (more than 1 m of land washed out every year), which prevents the sediments from repeated freezing. Sampling was from the lower part of the outcrop over the water surface, 0.9–1.0 inward from the vertical wall. The ground microstructure was examined in 4–5 kg monolith blocks, and the samples for microbiological studies were about 50 g. Sampling was performed with metal instruments sterilized in ethanol and flame. The samples were sterile packed and transported in thermostatic containers with coolants at −5 °C, i.e., close to the natural conditions.

The sampled ground is laminated silt consisting of alternated thinner light-color and thicker dark-color layers, with thicknesses 0.5–1.0 mm, respectively. The cryostructure is made up of thin (0.05–0.10 mm) broken layers that inherit the sedimentary bedding combined with vertical, sometimes discontinuous, 0.1 mm lenses (Fig. 1, *a*). The ice layers consist of isometric or slightly elongate polygonal crystals from 10 × 15 to 30 × 80 μm.

The soil samples contained a cultivable bacterium capable of both aerobic and anaerobic growth. It belongs to the *Bacillus* genus but is more likely a new species most closely related to *Bacillus simplex* and *B. macroides* which are 96–97 % homological with 16S rRNA [*Brushkov et al., 2009*].

The bacterium is psychrotolerant and can be metabolically active at −5 °C. It is relatively large (1.0–1.5 × 3–6 μm) and rod-shaped; it forms chains in the culture and can develop round spores. It is immobile, haemolytic, and gram-positive. The bacteria shows catalase and oxydase activity, reduces nitrates, and can grow within a broad temperature range.

In the laboratory, the bacillus grew slowly at −5 °C (growth signature became evident after two or three months) in both frozen and cooled environments. Although growth upon an artificial substrate is possible at subzero temperatures, no visible colonies were observed on the frozen samples.

The samples were examined by means of optical and electron microscopy in specimens preconditioned in different ways. Frozen fresh chips were studied after vacuum drying; the most detailed information was from replicas of frozen samples. The method was developed by one of us [*Rogov, 2009*] to investigate the soil microstructure. Preliminary optical microscopy of the replicas revealed microorganisms in ice lenses within frozen ground. At the following stage, the replicas were scanned by a LEO 1450 VP raster electron microscope, using an in-built spectrometer for identifying the bacteria and their environment.

EXPERIMENTS AND RESULTS

The largest bacteria existing as round or ovoid cells from 5 to 10 μm were discovered in the middle of an ice layer, in groups of 5 to 8 individuals (Fig. 1, *b*); some cells grew at the ice-rock boundary. Other bacteria found in small ice lenses were rod-shaped with rounded ends, similar in their morphology to plated *Bacillus* (Fig. 1, *c*). Almost no colonies were observed, which may be evidence of very slow or no reproduction in frozen rocks. However, some images attested to the very possibility for such slow growth, about the ice flow rate. No signature of symbiosis was seen either. The organic origin of the cells was validated by spectrometry which showed salts (especially $CaCl_2$) in the environment. The distribution of salts and colloids as a reticulate coat around the cells became evident in vacuum-dried specimens. The coat had a complex composition dominated by calcium, iron, and silicium compounds (Fig. 1, *e*).

The presence of microbial life in frozen ground poses challenges for both microbiological and geocryological sciences. The results of the reported study furnish evidence for obvious links between the freezing, moisture transport, and ice formation processes and the distribution of ice-dwelling bacteria.

This hypothesis was checked in an experiment with a ground system of sterile kaoline made in a plastic cylinder, 50 mm in diameter and 250 mm high. Kaoline saturated with distilled water to a content of 40 % lay over 0.5–1.0 mm thick coarse sand fully impregnated with a solution containing the culture of *Bacillus cereus*. The system was exposed to one-dimensional freezing in a special device at the surface temperature −4 °C. After freezing, the upper 3 cm of kaoline developed a stratified cryostructure, with 3–4 mm thick ice lenses; the following 7.5 cm of the sample was massive; the lowermost layer (2.5 cm) remained thawed. Then the redistribution of bacteria was investigated, by plating without cultivation, in 250 μl ground samples from the upper and lower layers. As a result, we obtained 71 plate colonies in the former (frozen kaoline with segregated ice) and 25 colonies in the latter (massive kaoline). The presence

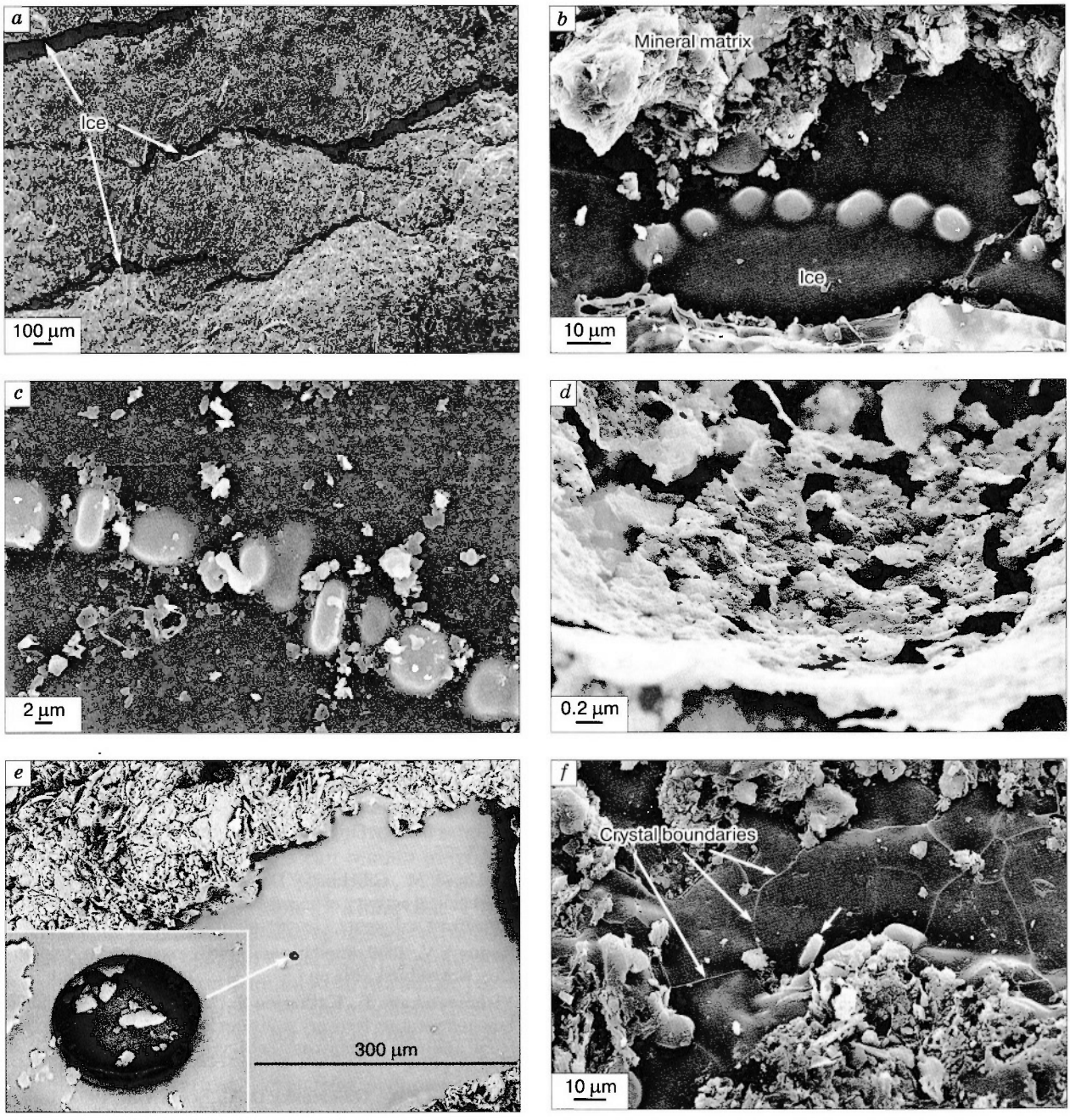

Fig. 1. Distribution of ice and bacteria in frozen ground.

a – segregated ice in loam; *b*, *c* – cells of various geometries in ice lenses; *d* – mineral coat around a cell; *e* – cells of *Bacillus cereus* in ice from kaoline (inset is magn. ×30); *f* – cells of *Bacillus* sp. in an ice lens.

of sporadic bacterial cells in segregated ice was confirmed microscopically (Fig. 1, *e*).

DISCUSSION

The experiment demonstrated the possibility for ice segregation and for migration of bacteria toward the freezing front in the course of moisture flow. The mechanism of this migration is not quite clear. Possibly, it occurs by cryogenic desiccation while moisture, together with growing ice crystals, moves along the cracks.

Another important issue concerns with the location of microbial cells relative to ice crystals. Microbial cells found in Taylor Glacier in Antarctica were

located in small veins of water between individual ice crystals [*Doyle et al., 2008*] where dissolved nutrients and gases necessary to maintain metabolism may provide suitable life conditions. However, the cells we observed in ice lenses from frozen loam did not show such localization.

Natural ice as a microbial habitat is remarkable by being a multicomponent system with mobile solid surfaces that border upon fluid and gas inclusions. As the ice crystal surfaces become warmer, the liquid films thicken up and develop a branched capillary system on further heating. The total length and diameter of the capillaries depend on the amount of free and bound water and on its salinity that controls the eutectic temperature. The crystal morphology and cryotextures in ground ice also depend on the grain size and mineralogy of sediments. The life conditions for bacteria in the water capillary system appear extreme because of their instability in space (osmotic gradient) and time (diurnal and seasonal temperature gradients). Thus, the ice crystal interior with multiple gas-fluid and organic-mineral inclusions may be a better environment to sustain microbial life.

On the other hand, the ice genesis being definitely an ecology control, the patterns of microbe cells in natural ice may result either from snow-to-ice transformation or from freezing and icing in wet fine-grained sediments. The experimentally observed bacterial patterns (Fig. 1, *f*) indicate that microorganisms can participate in migration and segregation of ice because the capillary size and the structure defects (vertical and horizontal desiccation cracks) in freezing sediments are large enough to let the cells through.

Another agent that can further maintain bacterial life in frozen sediment is the adsorption of salt ions from pore fluid and formation of a saline water coat which impedes icing in cells and in their surroundings. Note that spectrometry shows $CaCl_2$ to be the common salt deposited on the cell periphery, this being the most active agent among the ice-borne salts to reduce the water freezing temperature. There may be also other survival factors. Namely, some cells were found out to keep their relation with the mineral substrate, which is implicit evidence of their viability.

CONCLUSIONS

1. Microorganisms in frozen ground show a distribution indicating their ability to migrate while rock is freezing and to localize in segregated ice.

2. Ground ice is apparently the best permafrost habitat for sustainable and comfortable life of diverse microbial forms.

3. Salt-bearing gas-fluid inclusions inside and between ice crystals provide suitable life conditions as they prevent cells and their ambient material from freezing.

References

Abyzov S.S., 1993. Microorganisms in the Antarctic ice, in: E.I. Friedman (Ed.), Antarctic Microbiology, Willey-Liss Inc., N.Y., pp. 265–295.

Bakulina N.T., Spektor V.B., 2000. Paleoclimate reconstructions for the Neogene of Yakutia from spore-pollen data, in: G.N. Maksimov, A.N. Fedorov (Eds.), Climate and Permafrost [in Russian], Institute of Permafrost, Yakutsk, pp. 21–32.

Brushkov A.V., Katayama T., Fukuda M., et al., 2006. A late Quaternary ice wedge from the Fox Permafrost Tunnel in central Alaska is a time capsule for gas and bacteria. SIM News, Magazine Soc. Industr. Microbiol., 56 (1), 10–16.

Brushkov A.V., Griva G.I., Melnikov V.P., et al., 2009. Fossil microbial organisms in permafrost as possible objects for gerontology. Uspekhi Gerontologii, 22 (2), 253–258.

Christner V.C., Mosley-Thompson E., Thompson L.G., et al., 2003. Bacterial recovery from ancient glacial ice. Environ. Microbiol., 5 (5), 433–436.

Doyle S., Amato P., Christner B., 2008. Life in and under the Antarctic ice sheets. Microscopy Today, 16 (3), 6–10.

Friedman E.I., 1994. Permafrost as microbial habitat, in: Microorganisms in Permafrost, Rus. Acad. Sci., Puschino, pp. 21–26.

Gilichinsky D., Wagener S., 1995. Microbial life in permafrost: a historical review. Permafrost and Periglacial Processes, 6, 243–250.

Gilichinsky D.A., Soina V.S., Petrova M.A., 1993. Cryoprotective properties of water in the Earth cryolithsphere and its role in exobiology. Origin of Life and Evolution of the Biosphere, 23, 65–75.

Rivkina E.M., Gilichinsky D., Wagener S., et al., 1998. Biogeochemical activity of anaerobic microorganisms from buried permafrost sediments. Geomicrobiology, 15, 187–193.

Rogov V.V., 2009. Fundamentals of Cryogenesis [in Russian]. Geo, Novosibirsk, 203 pp.

Vishnivetskaya T., Kathariou S., McGrath J., et al., 2000. Low-temperature recovery strategies for the isolation of bacteria from ancient permafrost sediments. Extremophiles, 4, 165–173.

Vorobieva E.A., Gilichinsky D.A., Soina V.S., 1997. Life in the cryosphere: a view of the problem. Kriosfera Zemli, I (2), 60–66.

Zvyagintsev D.G., Gilichinsky D.A., Blagodatsky S.A., 1985. Longevity of microbial organisms in perennially frozen sediments and buried soils. Mikrobiologiya, 54, 155–161.

Zvyagintsev D.G., Gilichinsky D.A., Khlebnikova G.M., et al., 1990. Comparative characteristics of microbial cenoses from frozen ground of different ages and genesis. Mikrobiologiya, 59, 332–338.

Received
5 February 2011

Kriosfera Zemli, 2011, vol. XV, No. 4, pp. 79–87 http://www.izdatgeo.ru

BIOGEOCHEMISTRY OF PERMAFROST IN CENTRAL YAKUTIA

A.V. Brouchkov[1], V.P. Melnikov[1], M.V. Schelchkova[2], G.I. Griva[3], V.E. Repin[4], E.V. Brenner[4], M. Tanaka[5]

[1] *Tyumen State Oil and Gas University, 56, Volodarskogo str., Tyumen, 625000, Russia; brouchkov@hotmail.com*
[2] *Ammosov North-East Federal University, 58, Belinskogo str., Yakutsk, 677000, Russia; rector-svfu@ysu.ru*
[3] *Tyumen Science Center, Siberian Branch of the Russian Academy of Sciences, 86, Malygina str., Tyumen, 625000, Russia; brouchkov@hotmail.com*
[4] *Institute of Chemical Biology and Fundamental Medicine, Siberian Branch of the Russian Academy of Sciences, 8, Akad. Lavrentieva, Novosibirsk, 630090, Russia; niboch@niboch.nsc.ru*
[5] *Hokkaido University, Kita 8, Nishi 5, Kita-ku, Sapporo, 060-0808, Japan; kouryu@general.hokudai.ac.jp*

Permafrost is widespread in the Northern Hemisphere and is as old as hundreds of thousands to millions of years. Frozen ground stores living microorganisms which remain unfrozen in the relatively warm environment (–2...–8 °C) but are immobilized and may be about the age of the host permafrost. A strain of *Bacillus* sp. was isolated from ~3 Ma permafrost and its 16S rDNA sequence was identified. A large group of microorganisms including fungi was isolated from the wedge ice. Permafrost deposits contain invertase, urease, katalase and dehydrogenase.

INTRODUCTION

Biochemical activity of permafrost and existence of microorganisms in it were discovered quite long ago [*Lozina-Lozinsky, 1972; Friedmann, 1994*]. In the late 1970s, bacteria, fungi, diatoms, and other organisms were discovered at the Antarctic Vostok station [*Abyzov et al., 1979*]. There have been reports of bacterial metabolism in low-temperature environments [*Clein and Schimel, 1995*] and of microbial life that survived at subzero temperatures in ancient deposits [*Ashcroft, 2000; Nicholson et al., 2000; Katayama et al., 2007*]. Microorganisms are stable against freezing and can bear it easily [*Lozina-Lozinsky, 1972*]. On the other hand, it is known that a part of water (over 10 %) in various materials can remain unfrozen at temperatures below –20 °C [*Brushkov, 1995*].

Bacteria can keep viable for a long time. The survival time of *Anthrax bacillus* spores was estimated at about 105 years [*Repin et al., 2008*]. Colonies were cultured from bacteria found in 40 Ma amber [*Greenblatt et al., 1999*]. However, the evidence these sporadic finds can provide for exceptional tenacity of microbial life is less reliable than that from purposive studies of permafrost. Permafrost occupies an enormous area worldwide and reaches 65 % of the territory in Russia. Its temperatures range most often between –2 and –8 °C and the age is locally as old as millions of years [*Ershov, 1988*].

At present there has been no proof that microorganisms would be capable of growing in permafrost where the growth is impeded by cell immobility, shor nutrients, and poor conductance of water films. Aging cultures stop growing even in laboratory. Water crystallization and arrest of metabolism reduces the growing capacity [*Lozina-Lozinsky, 1972*]. Unfrozen water in –2 and –4 °C permafrost exists in very thin (0.01–0.1 μm) films, far below the size of microorganisms. These channels are virtually unfit for life support, and any significant migration of cells is hardly possible. That is why bacteria in permafrost must be relict forms, their age being constrained by their stratigraphic position, freezing history, and data on optic aminoacid isomers; further implicit constraints are from biodiversity.

The tenacity of microorganisms in permafrost remains puzzling. Fossil DNA of mummies, mammoths, amber-entrapped insects, and other organisms turn out to be destroyed. The theory predicts that even small DNA fragments (100–500 nucleotides) can preserve no longer than 10 kyr in a normal climate and 1 myr the longest in cold areas [*Willerslev and Cooper, 2005*]. There may exist some mechanisms that prevent bacterial DNA from accumulation of defects. We describe some biogeochemical features of permafrost in Yakutia, mostly with the example of Mamontova Gora (Russian for *Mammoth Hill*) outcrop in Aldan and report some preliminary data on the discovered organisms.

MATERIALS AND METHODS

Samples for biogeochemical studies of frozen ground were collected from outcrops and underground structures at several sites. One is the Mamontova Gora (*Mammoth Hill*) site located on the left bank of the Aldan River, 325 km upstream of its inflow into the Lena.

The river incision exposes Neogene-Pleistocene (from 16 Ma to a few kyr) alluvium deposited during Pleistocene glaciations. Neogene sand is frozen; permafrost is shallow or exposed at eroded surfaces.

Judging by the cryostructure, Neogene sediments froze up after their deposition and lithification. Middle Pleistocene sand shows signs of syngenetic (syndepositional) freezing: ice and soil veins at different levels. Therefore, permafrost may have existed continuously through the Pleistocene and, hence, the microorganisms found there must be very old. Neogene-Middle Pleistocene sand lies under up to 7–10 m thick Upper Pleistocene loam and silt which enclose wedge ice.

Sampling was from upright bluff walls, at depths 0.9–1.0 m below the active layer (which in the conditions of continuous erosion was no thicker than a few centimeters). Given that the outcrop is being rapidly eroded by the river (at least several meters annually), the sampled sediments appear to have been perennially frozen. Yearly spring floods take the slumped ground away, which prevents sediments from obstruction, deformation, and repeated freezing. The sediments, consisting of Middle Miocene (10–12 Ma) fine sand [*Baranova et al., 1976*], appear to have been cooled and frozen up in the latest Pliocene, about 3–3.5 Ma ago [*Bakulina and Spektor, 2000*] and never thawed later on because of the cold Yakutian climate. According to regional paleoclimate reconstructions, mean annual air temperatures through the Pleistocene were from −12 to −32 °C in winter and from +12 to +16 °C in summer [*Bakulina and Spektor, 2000*]. Thus, the age of permafrost at the Mammoth Hill site may reach 3.5 Ma. More samples were collected from younger wedge ice in Yakutia, from an underground gallery of the Institute of Permafrost (Yakutsk), as well as from frozen ground on the left bank of the Lena at the Neleger observatory site.

Permafrost sampling was with all precaution possible in the field. The microstructure of frozen ground was examined in 4–5 kg monolith blocks, and the samples for microbiological studies were about 50 g. Sampling was performed with metal instruments sterilized in ethanol and flame. The collected samples were sterile packed and transported in thermostatic containers with coolants at −5 °C, i.e., close to the natural conditions.

The physicochemical properties of the samples were determined by means of common procedures for soils: Turin wet combustion for total organic content (TOC) and humus; gasometry for carbonates; potentometry for pH; gravimetry for field water content; and Kachinsky procedure for grain-size composition. The activities of soil hydrolase enzymes (invertase, urease, and phosphatase) and oxidoreductases (dehydrogenase and katalase) were measured following the standard procedures [*Schelchkova, 2009*]. Aliquots for analyses were from samples that were powdered in the frozen state and mixed. Organic remnants were not removed. The analyses were run in triplicate. See Table 1 for the list of samples analyzed for enzymatic activity and Table 2 for the physicochemical properties of sediments of the 50-m high Mammoth Hill terrace.

Diluted samples of different percent concentrations were placed, under sterile conditions, to Petri dishes with YPD, MRS, and NA environments, as well as in meat-extract broth, in anaerobic and aerobic conditions.

For the sequence analysis, DNA was extracted using a Fast DNA kit for soil (BIO 101 Inc., Vista, CA). The 16S rRNA genes were amplified by a polymerase chain reaction (PCR) with primer sets specific to bacteria. The PCR process was run in 20 μl using a GeneAmp PCR System 2700 (Applied Biosystems, Foster City, CA); the amplicons were subject to electrophoresis and cleaning with a Wizard SV Gel and PCR Clean-Up System (Promega, Madison,

Table 1. **Description of samples. Dating according [*Markov, 1973*]**

Sample No.	Age	Description
2	Upper Pleistocene	Subaerial loam, 20 cm above ice wedge-bearing sediments. Dense loam with abundant plant roots and plant remnants, frozen, light brown, plastic on thawing. Wavy-bedded cryostructure; ice lenses 1–3 mm thick, exposed ice content about 50 %
3	Upper Pleistocene	Ice wedge-bearing sediments, ~1 m below loam base
5	Middle Pleistocene	About 8 m downslope from hill top, 10 m far from No. 6 sampling location. Exposed gray sand with light gray interbeds. Massive structure, with dark spots of organic matter. Approximate age 150 kyr BP
6	Middle Pleistocene	Left valley side where proximal outcrop is located, before proximal cirque; upper slope part, 10 m downslope from hill top. Gray loam, frozen, with necrons, including green stalks. Massive cryostructure, with ~ 1 cm thick ice lenses. A Middle Pleistocene ice vein, rather distinct on scraping, with a soil vein above it. Approximate age 150 kyr BP
7	Middle Pleistocene	Trench, middle terrace slope, below outcrop where Nos. 1–6 were sampled, about 25 m upslope from water table. Exposed gray medium-grained sand, with alternating plane and cross bedding, lying over a pebble bed. Age of sediments above pebbles 300 kyr BP
8	Miocene	Beginning of 50-m terrace, about 90 m far from the left-hand side of the Aan-Appa Brook mouth, downstream Aldan River. Exposed Neogene sand. Trenching about 25 m upslope from water table. Gray sand, interbedded dark gray and yellowish medium to coarse sand. Cross bedding mixed with plane bedding, abundant "unconformities". A pebble bed, up to 20 cm thick, with fossil wood material above it, wherefrom the sample was collected. Approximate age 12 Ma

Table 2. **Physicochemical properties of 50-m terrace deposits at Mammoth Hill site**

Sample	pH aqu.	TOC, %	Humus, %	$CaCO_3$, %	Field water content, %	Hygroscopic moisture, %	Specific weight	Number of particles of size (mm)					Total	
								1–0.25	0.25–0.05	0.05–0.01	0.01–0.005	0.005–0.001	<0.001 mm	<0.01 mm
2	8.02	1.66	2.86	4.76	60.26	0.24	2.58	0.7	13.5	42.9	12.2	13.5	17.2	42.9
3	8.14	1.47	2.53	2.20	72.83	2.38	2.48	0.6	7.5	44.5	15.5	13.5	18.4	47.4
5	7.83	0.69	1.19	0	24.97	0.22	2.62	54.7	22.8	8.5	1.7	1.6	10.7	14.0
6	8.10	1.27	2.19	0	75.12	1.81	2.50	7.8	9.7	33.0	12.3	14.7	22.5	49.5
7	7.63	0.04	0.07	0	29.79	0.11	2.70	71.0	26.1	1.0	0.4	0.6	0.9	1.9
8	4.84	1.25	2.16	0	32.60	0.08	2.63	69.3	21.0	3.5	1.2	2.3	2.7	6.2

USA). The purified amplicons were cloned into the pCR2.1 vector and *E. coli* culture with the TA cloning kit (Invitrogen) following the recommendations of the manufacturer. A 16S rDNA-bearing plasmid DNA was prepared from an overnight culture with the Mini prep spin kit (Quiagen, Crawley, UK). Purified plasmid DNA was sequenced on an ABI PRISM 3100 Genetic Analyzer with the Big Dye Terminator cycle-sequencing kit (Applied Biosystems). The sequence length reached 1488 bp. The sequence was compared with similar sequences of reference organisms by BLAST search. A phylogenetic tree was constructed with CLUSTAL W.

SPORE-POLLEN ANALYSIS

The frozen Pleistocene deposits of the 50-m terrace of Mammoth Hill contain abundant tree and shrub pollen assemblages (50.8 %) with almost equal proportions of conifer (26.0 %) and small-leaved (24.8 %) plants. Among gymnosperms, highest percentages are of *Larix* (15.6 %) while other species have progressively lesser percentages: 6.8 % *Pinus sylvestris*, 2.0 % *Pinus pumila* and 1.4 % *Picea* (*P. obovata* and *P.* cf. *ajanensis*). The small-leaved plants are mostly shrubs: 13.0 % *Alnaster*, 4.2 % *Betula exilis*, and 1.4 % *Salix*. Tree birch pollen is within 6.2 % (*Betula* sect. *Albae*, *B. platyphylla*). Grass-subshrub assemblages constitute 48.6 % of pollen, with highest abundances of *Artemisia* (41.1 %), a typical representative of dry steppe environments. Generally, comparison between fossil and extant spore-pollen spectra has been ambiguous. Some samples record deposition in a drier and, possibly, colder climate while others appear to be deposited in a warmer and wetter environment relative to the present one.

ENZYMATIC ACTIVITY

The enzymatic activity of ancient permafrost was investigated in comparison with that of present cryosols, for nine common soil types of the middle-taiga subzone of Central Yakutia [*Schelchkova, 2009*] including forest (lessive) and meadow (chernozem-like, sod-gley, and alas) cryosols.

The present soils possess the entire hydrolase and oxidoreductase range we studied (Table 3). The presence of hydrolyzing enzymes of carbohydrate, nitrogen, and phosphoric metabolism is evidence of digestion and enrichment in simple sugars and mineral compounds of phosphorus and nitrogen. The topsoil (A1) horizons of cryosols are rich in invertase. Urease activity being more variable, the frozen soils may be of low, medium, or high urease enrichment. Unlike the hydrolytic enzymes, dehydrogenase, is involved in redox reactions of biogenesis in humus, along with phenoloxidase enzymes, and in a way reflects the intensity of humification in soils. Dehydrogenase in the cryotic soils of Central Yakutia is of low or medium contents. Thus, the present soils show signs of all main reactions of organic compounds (breakdown and humification) typical of soil formation processes.

Catalase activity is an indicator of biological activity in soils. Soil catalase, as well as the intracellular one, is important as it decomposes hydrogen peroxide which is toxic for living organisms. Catalase activity in soils normally depends on the total organic content (TOC) and amount of microorganisms. Cryosols most often have low or medium catalase enrichment, and the enzymatic activity decreases downward proportionally to progressive decrease in TOC and biogenic components. Invertase, urease, and catalase are present throughout the soil profile while phosphatase and dehydrogenase activity is restricted to A1 topsoil (Table 3). As to dehydrogenase, the latter fact characterizes its function and indicates that humification reactions are especially active in the A1 horizon. The presence of phosphatase in A1 only is evidence of slow phosphoric metabolism. Cryosols are generally poor in mineral phosphorus, and in Central Yakutia they have low or medium enrichment in hydrolytic and redox enzymes, which are most active in topsoil.

The data we obtained were used to calculate enzymatic activity statistics for three horizons (A, B and BC (C)) in cryosols: arithmetic means, variance limits, and confidence intervals (Table 4). It is reasonable to use the statistics for comparing modern

Table 3. **Enzymatic activity of cryosols, Central Yakutia**

Horizon	Depth, cm	Invertase, mg glucose/(g·hr)	Urease, mg NH_4^+/(g·24 hr)	Phosphatase, mg FF/(g·hr)	Dehydro-genase, mg TFF/(10 g·24 hr)	Catalase, ml O_2/(g·min)
Lessive high-effervescent cryosol						
A	0–5(9)	0.57	1.36	0.576	3.860	1.3
B	28–38	0.25	0.30	0	1.244	1.1
BC_{ca}	50–70	0.27	0.01	0	0	0
Lessive solodic cryosol						
A	0–6	2.62	37.77	8.98	–	11.42
B	10–30	0.45	3.86	0.97	–	0.55
BC	50–100	0.03	1.58	0	–	0.14
Alas tussock-sapropel-gley soil						
A	0–22	0.55	10.81	14.91	–	5.04
LD_1	22–40	0.29	8.45	0	–	0.81
LD_2	40–68	0.26	7.66	0	–	1.09
Alas tussock-meadow soil						
LD_1	0–23	1.34	13.45	0.81	–	3.07
LD_2	23–40	0.09	9.19	0	–	0.79
B_{ca}	50–110	0.33	0	0	–	0.33
Alas steppe soil						
LD_1	0–19	0.81	2.06	0.88	–	4.95
B_{ca}	19–103	0.42	0.77	0	–	0.07
Chernozem cryosol						
A	0–19	2.95	5.00	5.25	4.15	1.60
B	47–72	0.74	0.40	0	0	0.69
C	72–102	0.49	0.20	0	0	0.54
Meadow-chernozem cryosol						
A	0–12(14)	4.23	2.86	3.37	3.00	2.54
B_{ca}	45–80	0.81	0.22	0	0	0.57
C	80–100	0.55	0.10	0	0	0.13
Tussock-gley cryosol						
A	3–18	3.03	1.16	1.27	2.75	1.58
B_g	58–70	0.21	0.36	0.49	0	0.40
C	70–90	0.23	0.25	0.43	0	0.20
Meadow-to-forest transitional cryosol						
A	2–21	3.29	1.31	5.58	1.70	2.27
B_{ca}	37–78	0.65	0.15	0	0	0.10
BC	80–100	0.35	0.12	0	0	0.03

frozen soil and ancient permafrost in terms of enzymatic activity. The 30 kyr to 12 Ma frozen sediments of the 50-m terrace bear signature of activity for some enzymes we studied (Table 5). Invertase activity shows up in all samples being the highest in Upper and Middle Pleistocene sediments. Its magnitude is commensurate with that in mineral horizons B of modern cryosols (Tables 4, 5). Urease activity has been found in three out of six samples (Nos. 2, 3, 5) from the Upper and Middle Pleistocene section, with its magnitude fitting the confidence interval of urease activity of B and BC horizons in modern cryosols of Central Yakutia (Table 6). Dehydrogenase activity appears in two of the six samples (Middle Pleistocene): it is quite low in No. 5 and rather high in No. 6 (3.225 mg TFF/(10 g·24 hr)) fitting the confidence interval of that in modern topsoil. Catalase activity is present in Upper Pleistocene samples and one of three Middle Pleistocene samples, and is as low as in mineral horizons BC and in soil-forming sediments of modern cryotic soils. As for phophotase activity, it has not been observed in the fossil permafrost samples from the Mammoth Hill site.

Thus, invertase is the most persistent enzyme surviving in permafrost. Its activity shows up in samples of all ages from Miocene to Late Pleistocene. Urease, dehydrogenase, and catalase are less preserved being restricted to Upper and Middle Pleistocene deposits of some samples, while phosphatase lacks from fossil permafrost.

Table 4. **Statistics of enzymatic activity of cryosols in Central Yakutia**

Enzyme	Horizon	n	$M \pm m$	Lim	$M \pm tm$ ($p = 0.05$)
Invertase	A	9	2.535 ± 0.454	0.55–4.24	1.65–3.42
	B	9	0.499 ± 0.084	0.09–0.81	0.34–0.66
	BC (C)	8	0.314 ± 0.057	0.03–0.55	0.20–0.42
Urease	A	9	8.421 ± 3.959	1.16–37.77	0.66–16.18
	B	9	2.633 ± 1.233	0.15–8.45	0.22–5.05
	BC (C)	8	1.240 ± 0.935	0–7.66	0–3.07
Phosphatase	A	9	4.625 ± 1.598	0.58–14.91	1.49–7.94
	B	9	0.054 ± 0.054	0–0.49	0–0.16
	BC (C)	9	0.048 ± 0.048	0–0.43	0–0.09
Dehydrogenase	A	5	3.092 ± 0.435	1.70–4.15	2.24–3.94
	B	5	0.249 ± 0.242	0–1.24	0–0.74
	BC (C)	5	0 ± 0	0–0	0–0
Catalase	A	9	3.686 ± 1.085	0.70–11.42	1.56–5.81
	B	9	0.564 ± 0.055	0.07–1.10	0.36–0.77
	BC (C)	8	0.308 ± 0.127	0–1.09	0.06–0.56

Note. n – number of samples; $M \pm m$ – arithmetic mean; Lim – variance limits; $M \pm tm$ (at probability $p = 0.05$) – confidence interval.

Table 5. **Enzymatic activity of 50-m terrace deposits**

Sample No.	Geologic period	Invertase, mg glucose/(g·hr)	Urease, mg NH_4^+/(g·24 hr)	Phosphatase, mg FF/(g·hr)	Dehydro-genase, mg TFF/(10 g·24 hr)	Catalase, ml O_2/(g·min)
2	Upper Pleistocene	0.644	0.164	0	0	0.2
3	Upper Pleistocene	0.690	0.043	0	0	0.2
5	Middle Pleistocene	0.362	0.042	0	0.361	0
6	Middle Pleistocene	0.684	0	0	3.225	0.1
7	Middle Pleistocene	0.399	0	0	0	0
8	Miocene	0.155	0	0	0	0

In the stratigraphic profile of the 50-m terrace, the activity of invertase, urease, and catalase shows a generally decreasing depthward trend. Samples of fine grain sizes (loam) and rich in organic matter have higher enzymatic activity than in coarser sandy loam and sand (Table 6). There is high positive correlation between invertase and catalase activity and clay-silt fraction percentage (correlation coefficient r = = 0.769–0.911), as well as between catalase activity and TOC and humus contents ($r = 0.752$). Other positively associated attributes are invertase activity vs. humus and organic contents ($r = 0.445$–0.447), urease activity vs. TOC and silt fraction percentages ($r = 0.422$–0.525), and dehydrogenase activity vs. percentage of clay-silt fraction. This proportionality is due to the fact that enzymes in soils are most often immobilized, i.e., are bound with the surfaces of fine organic and mineral particles. Sorptive activity is the highest in mineral particles smaller than 0.001 mm (silt fraction and colloids, after Kachinsky) due to high dispersion and abundance of clay minerals and humus. Enzymes coming into soils are stabilized on soil minerals and organic matter by means of ion, hydrogen, and covalent bonds. The bonds with organic-mineral colloids can be very strong which, in turn, makes protein molecules resistant against unfavorable environment agents (e.g., microbial proteolysis) and maintains their long tenacity. Low temperatures in permafrost likewise arrest microbial activity and sustain the immobilized enzymes. According to our earlier thermodynamic studies of active invertase in buried soils from Upper Pleistocene deposits, inver-

Table 6. **Correlation relationships (r) of enzyme activities with some physicochemical properties of permafrost**

Parameter	Invertase	Urease	Dehydrogenase	Catalase
Clay-silt	0.910789*	0.422323***	0.478089***	0.882493*
Silt	0.872943*	0.376933	0.579961***	0.768905**
Fine silt	0.892061*	0.435522***	0.460784***	0.899808*
Humus	0.445122***	0.524052***	0.137730	0.751701**
TOC	0.447233***	0.525079***	0.137399	0.753424**

Note. r reliable to probability $*p \le 0.01$; $**p \le 0.05$; $***p \le 0.2$.

tase is either free or bound there, while the immobilized invertase has a high activation energy and thermal stability [*Ashcroft, 2000*]. Being a membrane-bound enzyme, dehydrogenase – unlike invertase, urease, and catalase – is not secreted by bacteria like extracellular hydrolases. Therefore, its presence in permafrost may be evidence of living or dead bacterial cells.

RESULTS: ISOLATION AND IDENTIFICATION OF MICROORGANISMS

Frozen Miocene sediments at the Mammoth Hill site contained a cultivable bacterium capable of both aerobic and anaerobic growth, the optimal growth temperature being +37 °C. It is a relatively large (1.0–1.5 × 3–6 μm) rod-shaped bacillus which develops chains in the culture (Fig. 1) and can form spores. It is immobile and gram-positive. It belongs to the *Bacillus* genus but is more likely a new species.

The 16S rRNA gene sequence of the bacillus reported in this study was deposited in DDBJ/EMBL/GenBank under accession number AB178889 and entry ID 20040510203204.24251. It is most closely related with *Bacillus simplex* and *B. macroides* which are 96–97 % homological with 16S rRNA.

Growth of bacteria at low temperatures was reported earlier [*Ashcroft, 2000*]. *Bacillus anthracis* is known to easily survive freezing [*Repin et al., 2008*], though the optimal temperature for its growth is rather high. Spores of *Bacillus* are especially resistant [*Nicholson et al., 2000*]. For instance, *B. thuringiensis* and *B. macroides* were found in amber with a radiometric age of 120 Ma [*Greenblatt et al., 1999*]. Therefore, the discovery of a viable bacillus in Miocene-Pleistocene permafrost at the Mammoth Hill site is not surprising. The capability of developing spores was known in gram-positive *Bacillus, Clostridium, Streptomyces*, etc. [*Nicholson et al., 2000*] and has been recently discovered also in gram-negative microorganisms. Thus, spore formation is a widespread survival mechanism which may involve horizontal gene transfer.

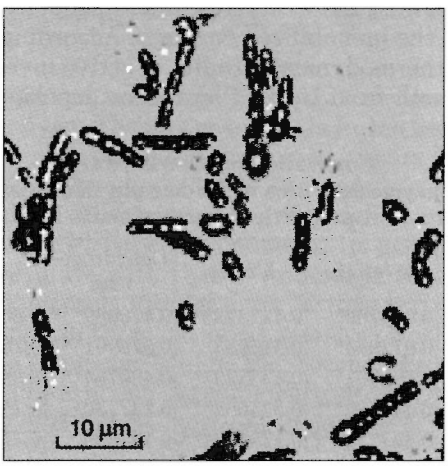

Fig. 1. Isolated strain *Bacillus* F (Gram coloration).

Furthermore, we cultured a number of other microorganisms from the Mammoth Hill permafrost (Fig. 2, 3) and extracted DNA from some cultures. The latter cultures were also exposed to the PCR process and 16S ribosomal DNA sequencing, whereby the following species were obtained: *Planococcus* sp. Tibet-IIVa1, *Arthrobacter sulfonivorans, Bacillus mojavensis, Jeotgalicoccus psychrophilus, Psychrobacter pulmonis*, etc. Some main biochemical properties of the isolates are listed in Table 7.

White mycelium has been found in an underground gallery of the Institute of Permafrost (Yakutsk) at a depth about 7 m below the ground surface. Similar mycelium was reported from the Fox Permafrost Tunnel in Alaska. The species (strain PF) was identified according to its morphology and 18S rRNA amplified gene sequence. It is closely related to *Penicillium echinulatum* and may be a new species. Samples of permafrost were pretreated, together with samples of strains *P. echinulatum* from the culture bank, and incubated at 25, 5, and –5 °C. The strains PF from permafrost and IFO 7760 and IFO 7753 *P. echinulatum* showed different patterns of spore formation and growth: PF was growing quite rapidly at –5 °C. Note that the isolates grew in Petri dishes at –5 °C, both in crystallized and supercooled (potato agar) media, more rapidly in the former. The strain *Penicillium echinulatum* isolated from permafrost beneath the Permafrost Institute in Yakutsk may be extant and brought from the surface, though being well adapted to the cold and feeding conditions of the underground gallery. Furthermore, this species can grow in aerobic conditions only, and its ability of growing in permafrost appears not very realistic.

Much younger (25–40 kyr) wedge ice samples from Yakutia and Alaska contained tens of microorganism species isolated with the same procedure [*Katayama et al., 2007*]. Most of those bacteria were gram-positive and closely related to *Arthrobacter* and *Micrococcus* spp. while mycelium was affiliated with *Geomyces* sp.

In this respect it is noteworthy that the life span of the most stable variola virus agrees with the estimates we obtained (several hundreds of years) [*Repin et al., 2008*]. Of special interest are obviously the microorganisms that long remain preserved in cold natural environments [*Friedmann, 1994; Katayama et al., 2007*]. Their longevity may be maintained by combinatorial transformations predicted before [*Repin et al., 2008*], possibly, somehow with participation of biocatalytic ribozymes which are stable and active at subzero temperatures. One may explain the great diversity of relict microorganisms isolated from the 25–40 kyr wedge ice [*Katayama et al., 2007*] in terms

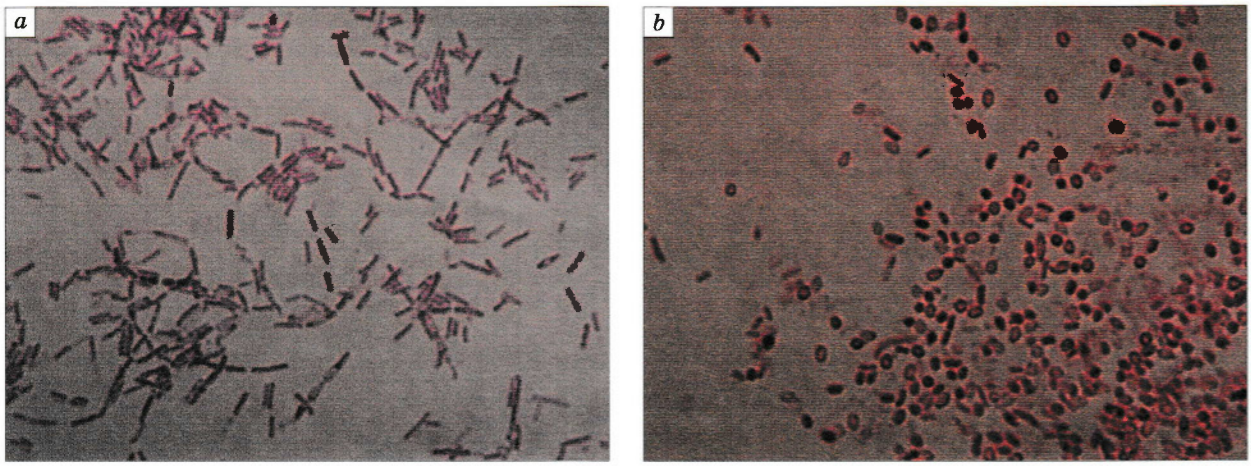

Fig. 2. Cell morphology of bacterial strains 17 (*a*) and 40 (*b*) isolated from frozen Neogene sand at Mammoth Hill (Gram coloration, magn. ×1500).

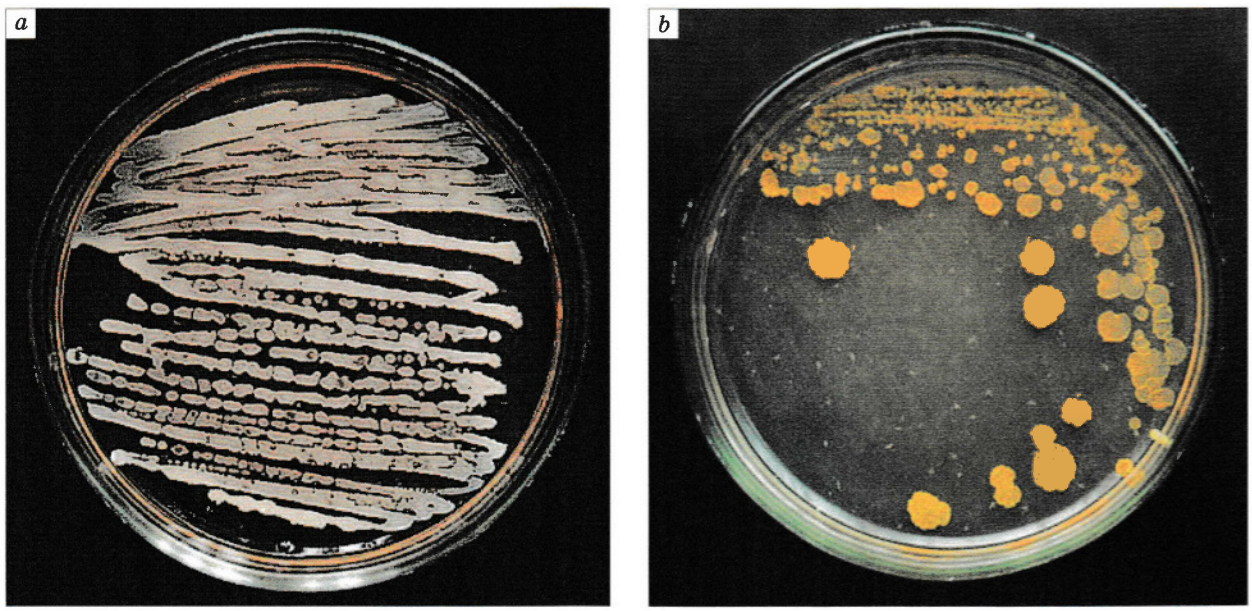

Fig. 3. Colonies of bacterial strains 6 (*a*) and 27 (*b*) isolated from frozen Neogene sand at Mammoth Hill.

of viability coding in plasmid-like mobile genetic structures.

Thus, the tenacity of microorganisms is hard to explain by retardation of life activity in anabiosis. If bacteria can form spores with almost arrested metabolism [*Nicholson, 2000*], the above calculations for denaturation, at least DNA, are especially relevant. The diversity of DNA damage mechanisms (metylation, desamination, apurinization, formation of thymine dimmers, cross-links, and breaks) implies, within the limits of the given hypothesis, revision to the assumed life time of biological macromolecules which must be ever shorter. The survival must be maintained by some special repair or conservation mechanisms.

CONCLUSIONS

1. A strain of *Bacillus* sp. was isolated from ~3 Ma permafrost at the Mammoth Hill site in Yakutia and its 16S rDNA sequence was identified; the same permafrost samples contained also other microorganisms. Younger permafrost (25–40 kyr) contained a large group of microorganisms including mycelium.

2. Low temperatures in permafrost arrest microbial activity and sustain immobilized enzymes. Permafrost deposits store invertase, urease, catalase, and dehydrogenase. The latter is a membrane-bound enzyme, is not secreted by bacteria into the environment, and its presence in permafrost may be evidence of living or dead bacterial cells.

Table 7. **Biochemical activity of strains isolated from fossil permafrost at Mammoth Hill site**

Parameters		Strains													
		6	13	15	17	20	27	29	30	32	33	34	37	40	F
Gram coloration		+	+	+	+	+	+	+	+	+	+	+	+	+	+
Pigmentation		yellow	–	–	–	–	–	–	–	yellow	–	yellow	–	–	–
Spore:	shape	–	S, E	S, E	E	E	E	E	E	–	–	–	–	E	E
	position	–	C, T	C, T	C	C	C	C	C	–	–	–	–	C	C
	inflated sporangium	–	+/–	+/–	–	–	–	–	–	–	–	–	–	–	–
Mobility		+	+	+	+	+	+	+	+	+	+	+	+	+	+
Anaerobic growth		+	–	–	–	+	+	–	–	+	–	+	+	+	+
Catalase activity		+	+	+	+	+	+	+	+	+	+	+	+	+	+
Oxidase activity		+	+	+	+	+wk	+wk	+wk	+	+	+wk	+wk	+wk	–	+wk
Foges–Proskauer test		–	+	+	+	–	–	+	+	–	+	–	–	–	–
Citrate use		–	+	+	+	+	–	+	+	–	+	–	–	+	–
Nitrate reduction		+	+gas	+gas	+gas	+	+	+gas	+gas	+gas	+gas	+gas	+gas	+	+gas
Hydrolisis	casein	–	–	–	–	–	–	–	–	–	–	–	–	–	–
	gelatine	–	+	+	+	+	+	+	+	+	+	–	–	+	+
	amylum	–	–	–	–	–	–	–	–	+	+	+	–	–	–
Acid formation from	glucose	–	–	–	–	–	–	–	–	–	–	–	–	–	–
	mannite	–	+	+	+	–	–	+	+	–	+	–	–	–	–
	arabinose	–	–	–	–	–	–	–	–	–	–	–	–	–	–
	xylose	–	–	–	–	–	–	–	–	–	–	–	–	–	–
	lactose	–	–	–	–	–	–	–	–	–	–	–	–	–	–
	mannose	–	+	+	+	+wk	+	+	+	–	–	+wk	–	+	+
	sorbitol	–	–	–	–	–	–	–	–	–	–	–	–	–	–
Growth at	2 °C	–	–	–	–	–	–	–	–	–	–	–	–	–	–
	8 °C	+	+	+	+	+	+	+	+	+	+	–	+	+	+
	43 °C	+	+	+	+	+	+	+	+	–	+	–	–	+	+
	6.5 % NaCl	+wk	+wk	+	+	–	–	+	+	–	+	–	–	+	+wk
	10 % NaCl	–	–	–	–	–	–	–	–	–	–	–	–	–	–
	15 % NaCl	–	–	–	–	–	–	–	–	–	–	–	–	–	–
	pH 4	–	–	–	–	–	–	–	–	–	–	–	–	–	–
	pH 5	–	+wk	+wk	+wk	–	–	+wk	–	+	–	–	–	+wk	+wk
	pH 5.5	+	+	+	+	+	+	+	+	+	+	+	–	+	+
	pH 8.5	+	+	+	+	+	+	+	+	–	+	+	+	+	+
	pH 9	+	+	+	+	+	+	+	+	–	+	+	+	+	+
	pH 10	–	+	+	+	+	+	+	+	–	+	–	–	+	+
	pH 10.5	–	+	+	+	+	+wk	+	+	–	+wk	–	–	+	+
	pH 11	–	+	+	+	+	+wk	+	+	–	+wk	–	–	+wk	+wk
BEA formation:	ammonia	–	–	–	–	–	–	–	–	–	–	–	–	–	–
	indole	–	–	–	–	–	–	–	–	–	–	–	–	–	–
	H_2S	+	–	+	+	+	–	+	+	+	+	+	+	–	+

Note. S – spherical spore; E – elliptic spore; C – centric position of spore; T – terminal position of spore; minus – negative reaction, plus – positive reaction, +wk – weakly positive reaction.

We wish to thank academician V.V. Vlasov (Institute of Chemical Biology and Fundamental Medicine, Novosibirsk) for overall scientific support and discussions. Thanks are extended to people from the Ministry of Environment of Sakha Republic (Yakutia) who helped us with the field work.

References

Abyzov S.S., Bobin N.E., Kudryashov B.B., 1979. Microbiological studies of a glacier in Central Antarctica. Izv. AN SSSR. Ser. Biol., No. 6, 828–836.

Ashcroft F., 2000. Life at the Extremes. University of California Press, Berkeley, 326 pp.

Bakulina N.T., Spektor V.B., 2000. Paleoclimate reconstructions for the Neogene of Yakutia from spore-pollen data, in: G.N. Maksimov, A.N. Fedorov (Eds.), Climate and Permafrost [in Russian], Institute of Permafrost, Yakutsk, pp. 21–32.

Baranova Yu.P., Ilyinskaya I.A., Nikitin V.P., et al., 1976. The Miocene in the Area of Mamontova Gora [in Russian]. Nauka, Moscow, 284 pp. (Transactions, GIN SO AN SSSR, Issue 233).

Brushkov A.V., Vlasov A.N., Merzlyakov V.P., et al., 1995. The effect of local phase transitions on deformability of plastic-frozen soils. Geoekologiya. Inzh. Geologiya, Gidrogeologiya, Geokriologiya, No. 5, 71–77.

Clein J.S., Schimel J.P., 1995. Microbial activity of tundra and taiga soils at subzero temperatures. Soil Biol. Biochem., 27, 1231–1234.

Ershov E.D. (Ed.), 1988. Geocryology of the USSR. European Part [in Russian]. Nedra, Moscow, 358 pp.

Friedmann E.I., 1994. Permafrost as microbial habitat, in: Viable Microorganisms in Permafrost, Rus. Acad. Sci., Pushchino, pp. 21–26.

Greenblatt C.L., Davis A., Clement B.G., et al., 1999. Diversity of microorganisms isolated from amber. Microbial Ecol., 38, 58–68.

Katayama T., Tanaka M., Moriizumi J., et al., 2007. Phylogenetic analysis of bacteria preserved in a permafrost ice wedge for 25,000 years. Appl. Environ. Microbiol., 4, 2360–2363.

Lozina-Lozinsky L.K., 1972. Essays on Cryobiology [in Russian]. Nauka, Leningrad, 288 pp.

Markov K.K. (Ed.), 1973. Section of Modern Deposits of Mammoth Mountain [in Russian]. Moscow University Press, Moscow, 190 pp.

Nicholson W.L., Munakata N., Horneck G., et al., 2000. Resistance of Bacillus endospores to extreme terrestrial and extraterrestrial environments. Microbiol. Mol. Biol. Rev., 64, 548–572.

Repin V.E., Pugachev V.G., Taranov O.S., et al., 2008. Potential hazard from microorganisms coming from the past, in: G.G. Boeskorov, A.N. Tikhonov, N. Suzuki (Eds.), The Yukagir Mammoth [in Russian]. St. Petersburg University, St. Petersburg, pp. 183–190.

Schelchkova M.V., 2009. Thermodynamic indicators of active invertase from buried Late Pleistocene soils in northern Yakutia. Sib. Ekol. Zhurn., No. 2, 195–201.

Willerslev E., Cooper A., 2005. Ancient DNA. Proc. Roy. Soc. B., 272, 3–16.

Received
10 February 2011

Kriosfera Zemli, 2011, vol. XV, No. 4, pp. 87–90 **http://www.izdatgeo.ru**

ORGANIC COMPONENTS IN BOTTOM SEDIMENTS FROM THE LOWER YENISEI, THE GYDA BAY, AND THE KARA SEA SHELF

L.Z. Granina, E.L. Goldberg, V.S. Panov*, N.N. Sushenzeva*, Yu.V. Sryvkina*, T.V. Khodzher

Limnological Institute, Siberian Branch of the Russian Academy of Sciences,
3, Ulan-Batorskaya str., Irkutsk, 664033, Russia; khodzher@lin.irk.ru
**Institute of Archaeology and Ethnography, Siberian Branch of the Russian Academy of Sciences,*
17, Akad. Lavrentieva, Novosibirsk, 630090, Russia; pvs7zeitlos@gmail.com

Samples of bottom sediments from the Yenisei lower reaches, the Gyda Bay, and the Kara Sea shelf have been analyzed for organic carbon and nitrogen. The contents of both organic carbon and organic nitrogen depend on the grain size of sediments and are controlled by deposition conditions (sedimentation rates, provenance, etc.). The carbon-to-nitrogen ratios (C/N), as well as the carbon isotope composition ($\delta^{13}C$), indicate the terrigenous component in organic matter to decrease off the shore. The vertical patterns of the same parameters have implications for the steadiness of sedimentation.

The contents and changes of organic components in bottom sediments of the Arctic seas can provide clues to many issues, such as features of the organic carbon cycle in a given area, high-latitude lithogeny, paleogeography and past climate change, the contribution of the Arctic seas into the current methane cycle, etc. [*Romankevich and Vetrov, 2001; Levitan et al., 2007; Shahova et al., 2009*]. Although many publications on the subject have been available, any new information from the hardly accessible Arctic terrains is of special interest.

Below we report data on bottom sediment samples collected in August through October 2009 from the lower reaches of the Yenisei, the Gyda Bay, and the Kara Sea shelf. See Fig. 1 for the location map of sampling sites and main results. Sixty samples, in-

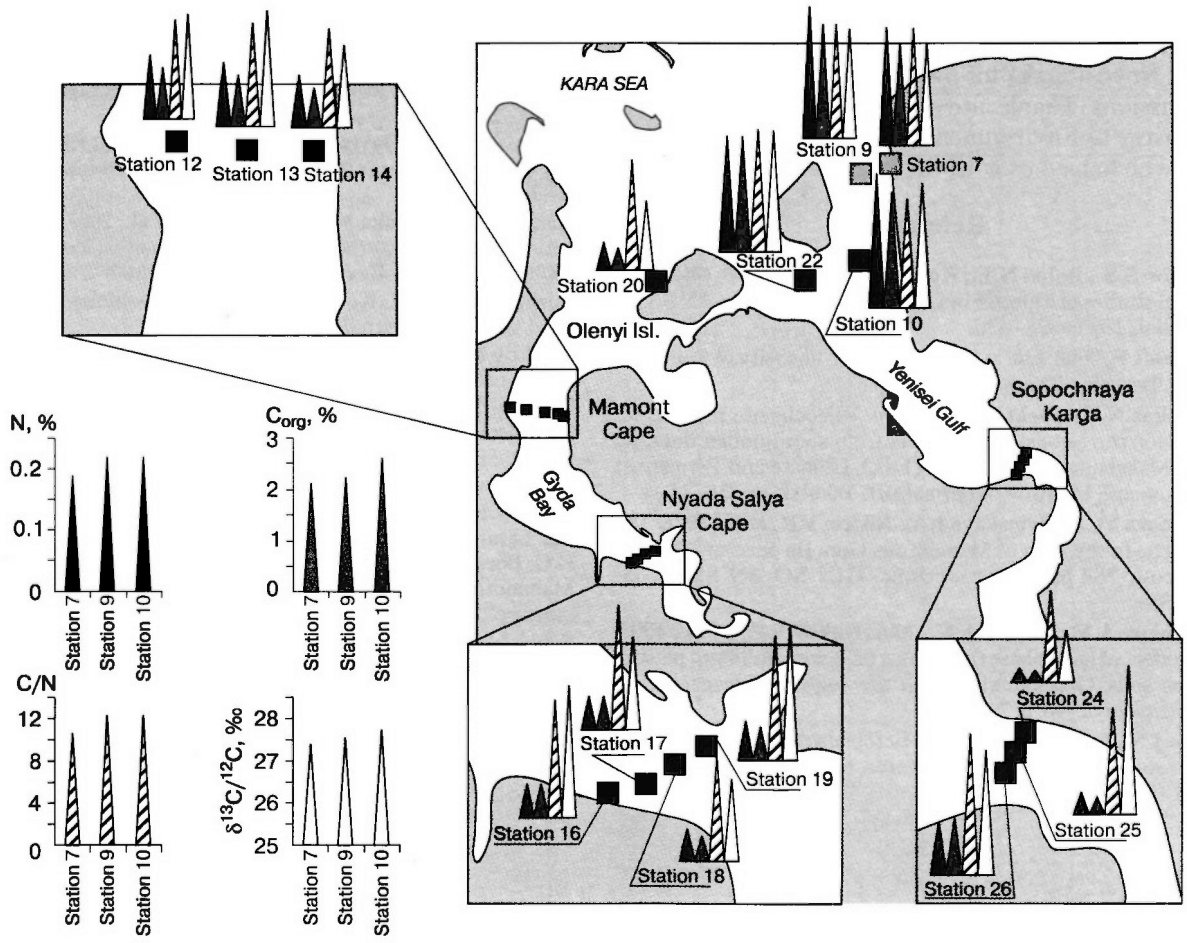

Fig. 1. Location map of sampling sites in lower Yenisei, Gyda Bay, and Kara shelf, with contents of organic nitrogen (N_{org}) and organic carbon (C_{org}), C_{org}/N_{org} ratios, and carbon isotope composition ($\delta^{13}C/^{12}C$) in surface bottom sediments.

cluding six cores from 18.5 to 75 cm long and ten samples from the bottom surface, were analyzed for the concentrations of organic carbon (C_{org}) and nitrogen (N_{org}) and for $\delta^{13}C/^{12}C$ ratios ($\delta^{13}C$) relative to the VPDB (Vienna Pee Dee Belemnite) standard. The carbon and nitrogen contents were determined using gas chromatography with a catarometer (elemental analysis, Euro Vector Acetanilide) to an accuracy at least 0.01 % and 0.02 % (standard deviations for N_{org} and C_{org}, respectively); $\delta^{13}C$ was measured by isotope-ratio mass spectrometry, to a precision no worse than 0.12 ‰ (measured on the Aldrich citric acid standard). The results are reported as means of two runs for each sample.

The nitrogen and carbon concentrations vary from 0.015 to 0.221 % (N_{org}) and 0.14 to 2.60 % (C_{org}), the range spanning more than an order of magnitude. The C_{org} range approaches that in marine sediments from the southwestern Kara Sea (0.13 to 2.10 %) [*Belyaev et al., 2010*]. The minimum concentrations are from the bottom surface at a freshwater station (site 24) and the maximum ones are from marine sediments at site 10 (Fig. 1). Bottom sediments at offshore sites (7, 9, 10, 22) consist of pelitic material and, correspondingly, are notably richer in both elements relative to freshwater sediment sites. For instance, N_{org} and C_{org} in the core of site 9 are more than twice that in the Gyda Bay cores (Fig. 2). The only offshore site with low N_{org} and C_{org} is station 20 near Sibiryakov Island in rather sandy sediments. The sediments at freshwater site 24 which contain the lowest amounts of N_{org} and C_{org} likewise differ in a high sand percentage. These results agree with published evidence of rather high C_{org} in pelitic sediments from the relatively deepwater part of the Yenisei Gulf (up to 1.85 % [*Lein et al., 1996*]) and from the depocenter of the tidal mixing front of river-borne and transformed marine waters (up to 2.5–3.0 % [*Kodina et al., 2009*]).

The ratio of organic carbon to organic nitrogen (C/N) has implications for the origin of organic matter (OM) in bottom sediments. The C/N ratios we

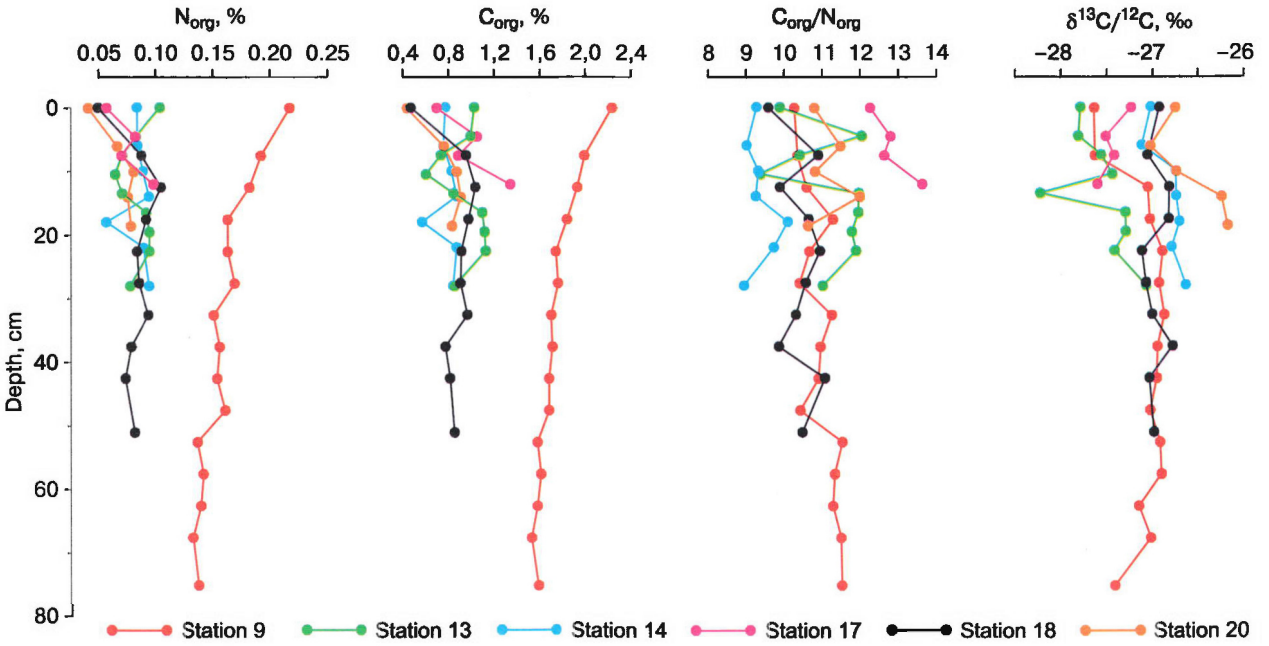

Fig. 2. Vertical patterns of organic carbon and nitrogen contents (C_{org} and N_{org}) and ratios (C_{org}/N_{org}), and carbon isotope composition ($\delta^{13}C/^{12}C$) in surface bottom sediments of lower Yenisei, Gyda Bay, and Kara shelf.

obtained vary from 8.9 at site 24 to 13.5 at site 26, both stations being located within the same Yenisei profile. The difference may be due to sediment provenance. Namely, sediments from site 26, which is located at the swampy Gyda Peninsula and, especially, on the shallower left bank of the Yenisei where most of river-borne particulate matter is deposited, contain a greater percentage of terrigenous OM. The high terrigenous input to sediments at station 26 is consistent also with the carbon isotope composition (see below). The C/N ratios at site 24 are low, possibly because both organic components (N_{org} and C_{org}) are very low there (see above). At the other stations, this ratio is markedly larger (10.0 to 11.5, see Figs. 1, 2) indicating quite a high percentage of terrigenous organic matter. High C/N ratios (12.3) were measured at site 13 where organic input is with the relatively large Gyda and Yuribei rivers and waters that drain the swampy land nearby.

The C/N ratio commonly increases with depth due to leading decomposition of nitrogen-bearing organic compounds. In the cores we analyzed, the downward increasing pattern is restricted to offshore site 9, where a steady sedimentation is supposed. C_{org} and N_{org} in the core from site 9 decrease with depth while the C/N ratio grows slowly (Fig. 2). The vertical patterns in all other cores are rather chaotic and record random changes in sedimentation conditions. In the Gyda Bay these changes may be associated with river-borne and paludal terrigenous fluxes, while at offshore station 20 the terrigenous input may be from neighbor Sibiryakov island.

The maximum and minimum $\delta^{13}C$ values were measured in bottom surface samples. They range from −28.5 ‰ in the lower Yenisei (site 26) to −26.2 ‰ in the Kara shelf (site 20) (Fig. 2) following the typical seaward $\delta^{13}C$ gradient. Low $\delta^{13}C$ are known to characterize terrestrial organic matter, but isotope data from high-latitude regions cannot provide unambiguous evidence of OM genesis [*Kodina et al., 2009*]. A similar $\delta^{13}C$ of −28.7 ‰ was reported from the Ob estuary (Kara Sea) [*Kodina et al., 2001*]. The seaward trend of progressively higher $\delta^{13}C$ in the zone of Yenisei influence (from −27.9 ‰ $\delta^{13}C$ in the estuary fresh water to −22.4 ‰ offshore [*Kodina et al., 2009*]) may result from metabolic activity of heterotrophic microorganisms in the stratified water column and from a notable input of secondary biological production. The vertical profile of $\delta^{13}C$ is quite uniform (Fig. 2).

Thus, the contents of organic nitrogen and carbon in the lower Yenisei, Gyda Bay, and Kara shelf sediments depend on the sediment provenance. The C/N ratios, as well as the carbon isotope composition, record a seaward decrease in the terrigenous input to organic matter. The vertical patterns of the same parameters indicate steady sedimentation to be restricted to a single offshore site in the Kara Sea. Deposition in the Gyda Bay occurred at changeable conditions, possibly, associated with riverine and paludal sediment input.

We wish to thank A.A. Fedotov and I.V. Tomberg from the Limnological Institute, Irkutsk for the sampling work. The study was carried out as part of Project 20.7 ("Integrate studies of the Arctic shelf. Permafrost and Arctic shelf in a changing climate; stability of ecosystems and gas hydrates; organic matter disposal") of Program 20 of the Presidium of the Russian Academy of Sciences.

References

Belyaev N.A., Peresypkin V.I., Ponyaev M.S., 2010. Organic carbon in water, particulate matter, and surface bottom sediments in the western Kara Sea. Okeanologiya, 50 (5), 748–757.

Kodina L.A., Lyutsarev S.V., Bogacheva M.P., 2001. The isotope composition of organic carbon in ice-rafted material as a provenance indicator for the Arctic drift ice, in: An Experience of Systematic Oceanographic Studies in the Arctic [in Russian]. Nauchnyi Mir, Moscow, pp. 244–255.

Kodina L.A., Stepanets O.V., Galimov E.M., 2009. Isotope geochemistry of organic matter and radioactivity in the Kara Sea, in: The System of the Laptev Sea and the Arctic Fringing Seas [in Russian]. Moscow University, Moscow, pp. 122–136.

Levitan M.A., Lavrushin Yu.A., Shtain R., 2007. The History of Deposition in the Arctic and in the Subarctic Seas for the Past 130 kyr [in Russian]. GEOS, Moscow, 404 pp.

Lein A.Yu., Rusanov I.I., Savvichev A.S., et al., 1996. Biogeochemical processes associated with sulfur and carbon cycles in the Kara Sea. Geokhimiya, No. 11, 1027–1044.

Romankevich E.A., Vetrov A.A., 2001. Organic fluxes into the Russian Arctic seas, in: An Experience of Systematic Oceanographic Studies in the Arctic [in Russian]. Nauchnyi Mir, Moscow, pp. 227–243.

Shakhova N.E., Sergienko V.I., Semiletov I.P., 2009. The contribution of the East Siberian shelf into the present methane cycle. Vestnik RAN, 79 (6), 507–518.

Received
13 February 2011

Kriosfera Zemli, 2011, vol. XV, No. 4, pp. 90–92 **http://www.izdatgeo.ru**

WATER CHEMISTRY AND PHYTOPLANKTON IN THE GYDA BAY (KARA SEA)

I.V. Tomberg, A.D. Firsova, L.M. Sorokovikova, N.P. Sezko, T.V. Pogodaeva, T.V. Khodzher

Limnological Institute, Siberian Branch of the Russian Academy of Sciences, 3, Ulan-Batorskaya str., Irkutsk, 664033, Russia; kaktus@lin.irk.ru

Presented are water chemistry and phytoplankton (abundance and biomass) data from the Gyda Bay, an underexplored area of the Kara Sea. Water chemistry varies over the bay being controlled by the tributary rivers in its southern and central parts and by the Kara Sea in the northern part. Correspondingly, the water has extremely low total dissolved solids (32 to 250 mg/l) in the former and a much higher salinity (up to 6600 mg/l) in the latter. Phytoplankton consists mostly of diatoms. Its distribution patterns correlate with the seawater salinity, the highest abundance and biomass of algae being found in the more freshwater part of the Gyda Bay.

The Gyda Bay located in the southern Kara Sea between the Ob Bay and the Yenisei Gulf is a ~200 km long and ~62 km wide gulf that cuts deep into the Gyda Peninsula. The sea in the Gyda Bay is rather shallow (5–8 m), with many banks. This is an area of harsh Arctic climate, with an open-water season shorter than 80 days. The bay receives water from the Gyda (Nyarmesalya) River and other smaller tributaries flowing into it from the south [*Treshnikov, 1985*].

Integrate offshore studies in the Gyda Bay were carried out in September 2009. Surface and bottom waters were sampled from the more freshwater southern part (sites 16–19) and the more saline northern part (sites 11–15) of the bay (Fig. 1).

Water chemistry was analyzed following the classical procedures [*Bordovsky and Ivanenkov, 1978; Wetzel and Likens, 1991; Baram et al., 1999*]. The phytoplankton samples were collected and studied with common hydrobiological methods [*Utermöhl, 1958; Guseva, 1959; Kozhov and Melnik, 1978*] and with scanning electron microscopy (on a *Phillips SEM 525* microscope).

Water chemistry in the Gyda Bay varies over the area. Water is of low salinity in the southern part, which is fed by the Gyda and Yuribei rivers as well as by numerous brooks flowing out of lakes. Total dissolved ions measured in samples from stations in the middle of the southern profile (17, 18) varied from 32 to 56 mg/l, and the ion composition was

mostly of hydrocarbonate and calcium. On the ends of the profile, the salinity was slightly higher (112 mg/l and 210 mg/l at sites 16 and 19, respectively); chloride and sodium ions predominated, possibly, due to the surface runoff input controlled by marine aerosols. The bottom water was 3–5 mg/l more saline than the surface water.

Water temperature varied along the profile from 9.6 °C (station 16) to 10.6 °C (station 19), and pH decreased from 7.65 to 7.55, respectively. The dissolved oxygen contents were similar in the surface and bottom waters being 10.88–11.30 mg/l.

The water samples from the southern bay contained low Si (0.10–0.15 mg/l) and P from analytical zero to 0.005 mg/l (higher values were measured at station 19). The nitrogen contents in nitrate and ammonium compounds were similar at all sites, in the ranges 0.10–0.14 and 0.06–0.10 mg/l, respectively; nitrate N was in trace amounts.

The northern part of the Gyda Bay is under the influence of the Kara Sea, which largely controls its water chemistry. The pH values measured in that bay part were higher (7.86–7.95) than in the south; total dissolved ions were one or two orders of magnitude higher, and the chemistry was rather chloride-sodic. In spite of quite a shallow water depth (~10 m) and a small temperature difference between the surface and bottom layers (no more than 0.3 °C), water showed density stratification. Note that steady southern wind blowing during the whole period of observations provided influx of fresher and lighter water from the bay center, which spread in the surface layer of the northern bay part. The salinity varied from 3100 mg/l (site 11) to 5970 mg/l (site 15) in the surface water but was higher (4700–6600 mg/l) near the bottom.

Dissolved oxygen at sites of the northern profile was more or less uniform in lateral and vertical dimensions (10.7–11.15 mg/l). Biogenic elements in the north were higher than in the south. The measured Si contents were the highest in samples from the middle of the profile (1.75 mg/l) and did not exceed 0.92 mg/l near the shore. As for mineral P, its concentrations likewise increased from 0.014 mg/l at coastal sites to 0.024 mg/l farther offshore. Note that the depth distribution of silica and phosphates did not change within a site. Nitrogen occurred in the nitrate and nitrite forms (up to 0.08 mg/l NO_3^- and 0.003 mg/l NO_2^-); ammonium N was found in trace concentrations in surface water only.

Phytoplankton in the analyzed water samples from the Gyda Bay contained marine and freshwater algae species (Fig. 2), and there were some species we failed to identify. Most of the identified seventy seven species were diatoms (49 %) and green (21 %) or blue-green (10 %) algae. Fewer species found at that period belonged to cryptophytes (6 %) and dynophytes (3 %).

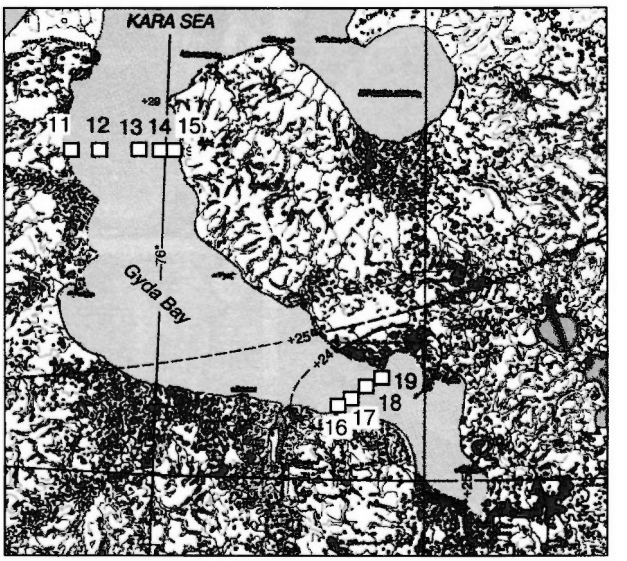

Fig. 1. Location map of sampling sites in the Gyda Bay.

The freshwater part of the bay (sites 16–19) abounded in phytoplankton. The highest abundances (43 to 36 % of total diatom count) were in freshwater species of *Aulacoseira* – *A. islandica, A. subarctica, A. ambigue* (Grun.) Sim, while the percentages of marine taxa (*Thalassiosira baltica, T. bramaputrae, T. nodenskiöldii*, and *Cyclotella choctawhatcheeana*) and spores of *Chaetoceros* Ehr were low (2.0–6.5 % in abundance and 3.5–17.0 % in biomass). Green algae abundances were likewise relatively high (15 to 24 % of total diatom count), especially the genera *Scenedesmus* Meyen, *Monoraphydium* Kom.-Leg., and *Pediastrum* Meyen. The total abundance of phytoplankton in that bay part varied from $0.495 \cdot 10^6$ to $1.153 \cdot 10^6$ and the biomass was 380 to 871 mg/m^3.

More saline water (stations 11–15) showed more depleted phytoplankton compositions, with the abundances from $0.009 \cdot 10^6$ to $0.015 \cdot 10^6$, and the biomass from 7 to 12 mg/m^3. Diatoms were the dominant phytoplankton group (55–80 % of total abundance and 90–96 % of total biomass). The diatom species were *Thalassiosira baltica* (Grun.) Ostf, *T. bramaputrae* (Ehr.) Håk. et Locker, *Cyclotella choctawhatcheeana* Prasad, *Chaetoceros decipiens* Cleve. There were also minor amounts of marine pelagic and neritic arctoboreal species *T. nodenskiöldii* Cl., and spores of *Chaetoceros*. The freshwater taxa made up 33–70 % and 10–38 % of total diatom count and biomass, respectively. They were *Aulacoseira islandica* (O. Müll.), *A. subarctica* (O. Müll.) Haworth and *Fragilaria crotonensis* Kitton species, small representatives of the *Stephanodiscus* Ehr. genus and the species *Monoraphydium*.

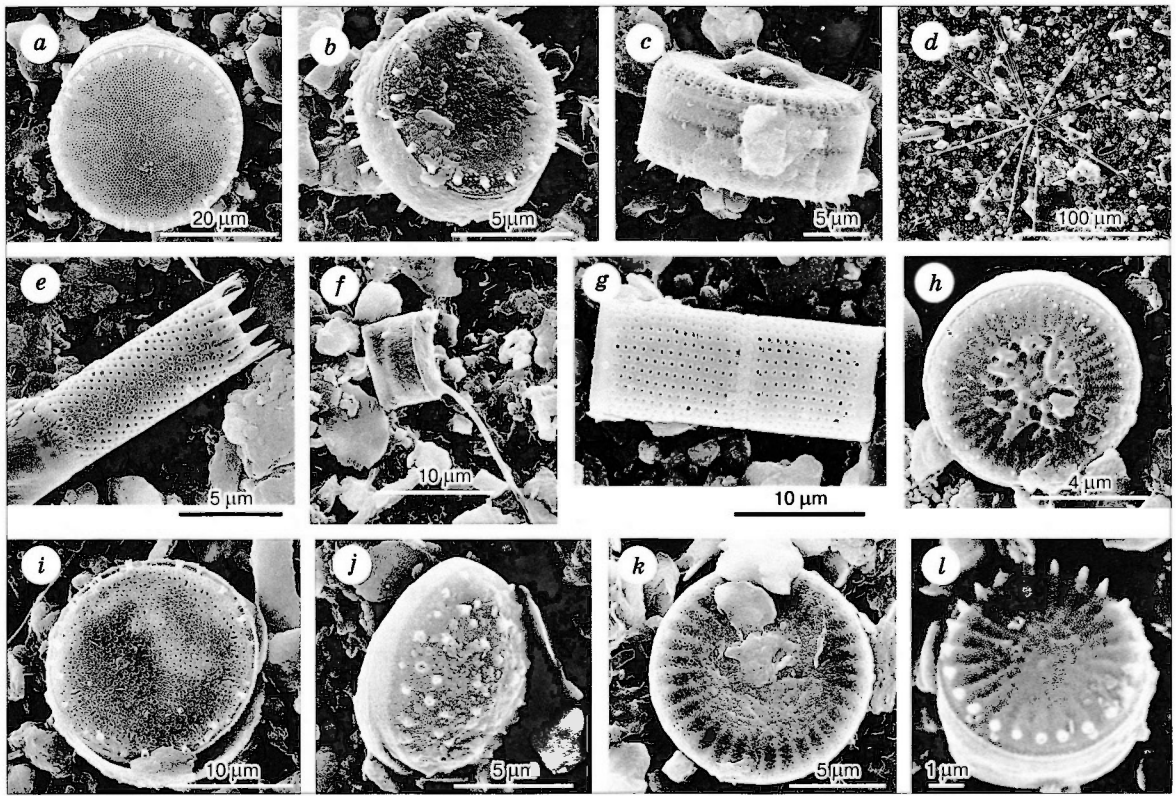

Fig. 2. Dominant phytoplankton species identified in the Gyda Bay in September 2009.

a – Thalassiosira baltica; b – Thalassiosira guillardii; c – Cyclotella meneghiniana; d – Asterionella formosa; e – Aulacoseira subarctica; f – Chaetoceros decipiens; g – Aulacoseira islandica; h – Cyclotella tripartita; i – Thalassiosira sp.; *j* – spore of *Chaetoceros; k – Cyclotella choctawhatcheeana; l – Stephanodiscus minutulus.*

Thus, the water salinity in the Gyda Bay increases in the northern direction, being fresher in the southern part of the bay at the account of inflowing hydrocarbonate-calcium riverine water. The coastal water is enriched in Cl, Na, and Mg ions. The northern bay part influenced by the Kara Sea has more saline water, with chloride-sodic chemistry.

Out of seventy seven identified phytoplankton species of marine and freshwater algae, 49 % are diatoms. The fresher southern part of the bay has a greater phytoplankton biomass but lower concentrations of biogenic elements than the more saline northern part. The water of the bay is well aerated in the ice-free seasons.

The study was carried out as part of Project 20.7 ("Integrate studies of the Arctic shelf. Permafrost and Arctic shelf in a changing climate; stability of ecosystems and gas hydrates; organic matter disposal") of Program 20 of the Presidium of the Russian Academy of Sciences.

References

Baram G.I., Vereschagin A.L., Golobokova L.P., 1999. The use of microcolumn liquid chromatography wit UV detection for determining anions in environment objects. Analiticheskaya Khimiya, 54 (9), 962–965.

Bordovsky O.K., Ivanenkov V.N. (Eds.), 1978. Methods of Chemical Studies of the Ocean [in Russian]. Nauka, Moscow, 270 pp.

Guseva K.A., 1959. Methods of phytoplankton count. Transactions, Institute of Biology of Water Reservoirs [in Russian], Issue 5, 44–51.

Kozhova O.M., Melnik N.G., 1978. Guide for Plankton Count [in Russian]. Irkutsk University, Irkutsk, 51 pp.

Treshnikov A.F. (Ed.), 1985. The Arctic. An Atlas [in Russian]. GUGK, Moscow, 204 pp.

Utermöhl H., 1958. Vervollkommnung der quantitativen Phytoplankton Methodik. Mitt. Intern. Verh. Intern. Verein. Limnol., 9, 1–39.

Wetzel R.G., Likens G.E., 1991. Limnological Analyses. Springer-Verlag, N.Y. etc., 391 pp.

Received
25 February 2011

Kriosfera Zemli, 2011, vol. XV, No. 4, pp. 93–95 http://www.izdatgeo.ru

A CULTIVABLE MICROBIAL COMMUNITY IN THE LOWER YENISEI AND THE KARA SEA SHELF: DIVERSITY AND DISTRIBUTION

M.Yu. Suslova, V.V. Parfenova, O.N. Pavlova, T.Ya. Kostornova, A.P. Fedotov

Limnological Institute, Siberian Branch of the Russian Academy of Sciences, 3, Ulan-Batorskaya str., Irkutsk, 664033, Russia; suslova@lin.irk.ru

Microbial biota was studied in samples of water and bottom sediments from the Kara Sea and the Yenisei estuary collected in August through October 2009. The study included estimating the abundances of organotrophic, psychrophilic, and hydrocarbon-oxidizing bacteria, as well as spore-forming *Bacillus* genus. *Bacillus* made up 41.3 % of the total Kara Sea organotrophic community in the water and surface sediments and 54 % in the Yenisei. Hydrocarbon oxidizers isolated by filtering were the least abundant in the Yenisei estuary and the most abundant along the Dikson Village – Sibiryakov Island profile. The abundances of microorganisms in bottom sediment samples were two orders of magnitude higher than in the water, psychrophiles being the dominant group.

The necessity for studying the biogeochemical activity of microbial communities in the Kara Sea permafrost ecosystems has been increasingly evident with the progress of petroleum exploration in the Arctic shelf.

The earliest microbiological research in the Kara Sea was undertaken in 1935 by B.L. Isachenko and V.S. Butkevich [*Isachenko, 1951; Butkevich, 1958*] who revealed microorganisms in the seawater and assessed their biomass, having noted low abundances of saprophytes (10^3 to 10^4 cells/ml). Later estimates gave similar abundance values [*Kriss, 1959, 1976*]; higher numbers of bacterial cells were found in the southwestern Kara Sea in 1981 [*Teplinskaya, 1989*]. The total bacterial abundance in the Kara Sea was measured to be n10^3 to n10^4 cells per milliliter, which is an order of magnitude lower than in other Arctic seas [*Saliot et al., 1996*]. In 1993, a team from the Institute of Microbiology (Moscow) investigated the Kara Sea and the Yenisei and Ob estuaries [*Mitskevich and Namsaraev, 1994*] in terms of bacterial abundances (which was from $(2–3)\cdot10^3$ to $(250–280)\cdot10^3$ cells in a ml of seawater) and carbon and sulfur cycles. More data on bacterial abundances and production in the Kara Sea and the Yenisei and Ob estuaries collected in 2001 was reported in [*Meon and Amon, 2004*]. Hydrocarbon-oxidizing bacteria in the Central Arctic were first studied by V.V. Ilyinsky and his colleagues and were detected in very low abundances (no more than 1000 cells per liter) [*Ilyinsky, 1995*].

The objective of this study was to assess the abundances of different bacterial groups (organotrophs, psychrophiles, hydrocarbon oxidizers, and spore-forming *Bacillus* genus) in the water and surface bottom sediments of the Kara Sea shelf and the Gyda and Yenisei gulfs.

Microorganisms were studied in water and sediment samples collected during a cruise on R/V *Sovetskaya Arktika* in August through October 2009, at 13 stations on the Kara Sea shelf (Fig. 1, *a*) and 11 stations in the estuary and lower reaches of the Yenisei (Fig. 1, *b*).

The cultivable microbial community on the Kara Sea shelf (Fig. 1, *a*) sampled at stations along the profile from the Cape Kuznetsovsky to Dikson Village (W1–6) consisted mostly of psychrophiles which were four times more abundant than organotrophs. There were two distribution patterns at the six sampled stations. Psychrophiles had greater abundances in the bottom water than near the surface at stations W1–3: 113 against 17 colony-forming units (cfu) per milliliter, in spite of a small water temperature difference. At stations W4–6 located closer to Dikson they, on the contrary, decreased depthward from 191 to 34 cfu/ml as the water temperature fell to 1.5 °C and the salinity increased to 26.3 ‰ near the bottom. The abundance of organotrophic bacteria was within 45 cfu/ml. Hydrocarbon oxidizers and *Bacillus* in water samples along the Cape Kuznetsovsky – Dikson profile were, respectively, 23–600 cfu/100 ml and 3–33 cfu/ml (the greater numbers near the bottom in both groups).

A different structure of the microbial community was observed at stations W7–9, 20–22 (Kara Sea shelf) and W23 (northern end of Yenisei Gulf) (Fig. 1, *a*). Specifically, organotrophs (up to 2132 cfu/ml) were more abundant than the other microbial groups. The total bacterial abundance was the highest at W20, with dominant organotrophs, psychrophiles, and *Bacillus* (2132, 2304, and 686 cfu/ml, respectively) (Fig. 1, *a*). Hydrocarbon-oxidizing bacteria were detected in large numbers in the Kara Sea shelf seawater from stations W5, 7–9, the highest being 1200 cfu/100 ml in bottom water at W7 (Fig. 1, *a*).

Water in the lower Yenisei River contained abundant psychrophilic bacteria (Fig. 1, *b*) at all stations except W28, 29 on the Karepovsky – Cape Doro-

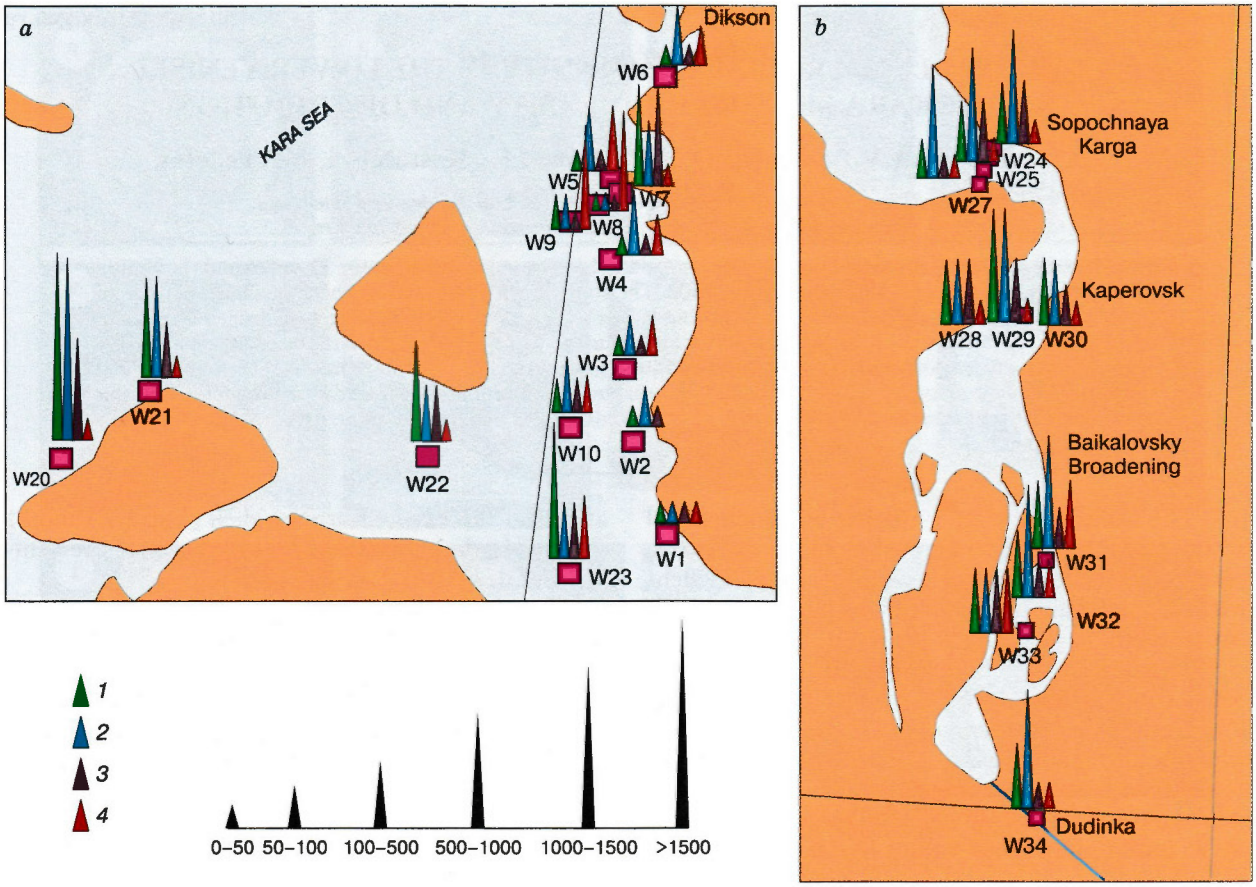

Fig. 1. Distribution of microbial groups in Kara Sea shelf (*a*) and Yenisei Gulf (*b*), in surface water.

Microorganisms: *1* – organotrophs, *2* – psychrophiles, *3* – *Bacillus* genus (cfu/ml); *4* – hydrocarbon oxidizers (cfu/100 ml). W1–W34 are station numbers.

feevsky profile where mesophile organisms had slightly greater abundances. The average abundances of organotrophs and psychrophiles were, respectively 408 cfu/ml and 550 cfu/ml. *Bacillus* genus constituted 54 % of the organotrophic community (Fig. 1, *b*). Hydrocarbon oxidizers were present in all samples of surface water in the profile across the Baikalovsky broadening (100, 200, 300 cfu/100 ml), while did not exceed 30 cfu/100 ml in all other samples (Fig. 1, *b*).

The bacterial abundances in bottom sediments were estimated in samples from five stations of the Kara Sea shelf (W7, 9, 10, 20, 22) and the Sopochnaya Karga – Cape Narzoi profile (W24–26), and were found to be two orders of magnitude higher than in the water: from $17 \cdot 10^3$ to $220 \cdot 10^3$ cfu/g. Psychrophiles were rather abundant both in the Kara shelf ($(54.5–220) \cdot 10^3$ cfu/g) and in the Yenisei ($(54–73) \cdot 10^3$ cfu/g). Hydrocarbon-oxidizing bacteria had greater abundances in the shelf than in the river sediments ($3.7 \cdot 10^3$ cfu/g against $0.45 \cdot 10^3$ cfu/g).

Generally, the microbial community was the poorest in water samples from the Yenisei Gulf – Dikson profile (W1–7), with organotrophs, psychrophiles, and *Bacillus* no greater than 45, 191, and 33 cfu/ml, respectively. The highest abundances of these groups were measured in the Kara Sea between Olenii and Sibiryakov islands. The percentages of spore-forming *Bacillus* relative to the total abundance of organotrophs were, respectively, 54 % and 45.5 % in the water and bottom sediments of the Yenisei and 41.3 and 41.1 % in the Kara Sea. The spores were 8 % in the water but as high as 74 % in the sediment, i.e. bottom sediments act as a spore-storing substrate. The highest abundances of hydrocarbon oxidizers were measured in seawater from the Kara shelf at stations of the Dikson – Sibiryakov Island profile (up to 1200 cfu/100 ml) and decreased progressively away from the open sea to no more than 30 cfu/100 ml in the Yenisei water. All analyzed microbial groups had greater bottom sediment abundances in the shelf than in the river.

Thus, an active microbial community lives in the Arctic area of the Kara Sea shelf and the Yensiei estuary. Microbes of all groups we studied have been found in all samples, the psychrophiles which grow at 4–6 °C being the most abundant. The growth of psychrophilic bacteria, both in water and in bottom sediment, is maintained by low-temperature conditions, as well as by large organic fluxes carried by the river. The shelf-estuary transition where fresh and saline water are intensely mixing is favorable for growth of microorganisms being a zone of rapid accumulation and recycling of organic carbon. This inference follows from the estimated abundances of microorganisms that can recycle both digestible (organotrophs and psychrophiles) and non-digestible (spore-forming and hydrocarbon oxidizing bacteria) organic matter. The presence of hydrocarbon oxidizers provides evidence for hydrocarbon input into the waters of the area and for self-cleaning in the ecosystem, which is also consistent with the predominance of *Bacillus* genus which participate in bacterial destruction of non-digestible organic compounds, including hydrocarbons. The abundances of hydrocarbon oxidizers are the highest especially in the water near Cape Kuznetsovsky.

The reported study has been the first step in discovering the microbial diversity in the Arctic to bridge the gap still existing in the knowledge of microbial life in the cryosphere.

The study was carried out as part of Project 20.7 of the Russian Academy of Sciences.

References

Butkevich V.S., 1958. Bacterial population of Arctic seas and its distribution in water and soil [in Russian]. Selected Transactions, AN SSSR, Moscow, Vol. II, pp. 77–134.

Ilyinsky V.V., 1995. Bacterial plankton of surface waters in the Central Arctic during calendar spring seasons. Mikrobiologiya, 64 (5), 696–704.

Isachenko B.L., 1951. Microbial characteristics of bottom sediment and water in the Kara Sea [in Russian]. Selected Transactions, AN SSSR, Moscow, Leningrad, pp. 334–363.

Kriss A.E., 1959. Marine (Deepwater) Microbiology [in Russian]. Izd. AN SSSR, Moscow, 455 pp.

Kriss A.E., 1976. Microbiological Oceanography [in Russian]. Nauka, Moscow, 78 pp.

Meon B., Amon R.M.W., 2004. Heterotrophic bacterial activity and fluxes of dissolved free amino acids and glucose in the Arctic rivers Ob, Yenisei and the adjacent Kara Sea. Aquat. Microb. Ecol., 37, 121–135.

Mitskevich I.N., Namsaraev B.B., 1994. Abundances and distribution of bacterial plankton in the Kara Sea in September 1993. Okeanologiya, 34 (5), 704–708.

Saliot A., Cauwet G., Cahet G., et al., 1996. Microbial activities in the Lena River delta and Laptev Sea. Mar. Chem., 53, 247–254.

Teplinskaya N.G., 1989. Bacterial plankton and benthos in the Kara Sea, in: Ecology and Biological Resources of the Kara Sea [in Russian]. Kola Science Center, AN SSSR, Apatity, pp. 29–37.

Received
27 February 2011

SCIENTIFIC JOURNAL
EARTH'S CRYOSPHERE

Kriosfera Zemli, 2011, vol. XV, No. 4, pp. 96–98 http://www.izdatgeo.ru

METHODS OF PERMAFROST STUDIES

SEISMIC STUDIES IN FROZEN GROUND

A.G. Skvortsov, A.M. Tsarev, M.R. Sadurtdinov

Institute of Earth's Cryosphere, Siberian Branch of the Russian Academy of Sciences, PO box 1230, Tyumen, 625000, Russia; agskvortsov@mail.ru

The specificity of seismic soundings in frozen ground is defined by the features of the permafrost-related wavefield. According to years-long experience of the authors, shear-wave surveys with the use of the *SH* phase are an efficient tool to study unfrozen layers (taliks) above permafrost and the subsurface structure. Joint use of compressional and shear velocity data is workable in estimating the state and properties of frozen ground.

INTRODUCTION

The permafrost-related seismic wavefield, especially that of soft sediments, has a number of specific features. They result from the seismic and lithological heterogeneity of the section and its variations in space and time associated with seasonal temperature change and other factors. The wave patterns may bear prominent reflection contrasts and velocity reversals. Many sections comprise a shallow-lying thin layer with high seismic velocities. Such layers may be seasonally frozen ground, frozen coarse soil, or pavement (concrete or asphalt) within urban or industrial areas. These layers produce velocity reversals in the seismic section [*Skvortsov, 2005*] and cause the respective dramatic changes to the *SH* (horizontally polarized) shear-wave field. The geocryological seismic sections of this kind [*Skvortsov, 1997*] require special acquisition methods. The awareness of the permafrost specificity can make basis for the appropriate choice of techniques and is a prerequisite of their efficiency.

Seismic surveys in permafrost have many objectives [*Melnikov et al., 2010*] that belong to three main groups: (i) estimating the depth to the permafrost table, (ii) imaging the section structure, and (iii) studying the state and properties of frozen ground.

ESTIMATING THE DEPTH TO THE PERMAFROST TABLE

The depth to the permafrost table is estimated in the course of contouring natural and man-caused layers of unfrozen ground (taliks) and measuring their thickness, which may be tens of meters.

The problem is successfully resolved with refraction surveys commonly used in shallow seismic exploration in land conditions of a normal seismic section [*Skvortsov, 1997*]. However, *P*-wave refraction shooting is poorly applicable to permafrost sections because some layers may remain unresolved [*Tsarev et al., 2010*]. The missed layers, often a zone of full hydraulic saturation, introduce large errors (up to 40 % or more) to the estimates of talik thickness (Fig. 1, *a*). Higher resolution in this case can be achieved with *SH* refractions [*Ponomareva and Skvortsov, 2006*].

A still better alternative is to use a special technique of high-resolution shear-wave reflection (SWR) profiling with *SH* phases designed at the Institute of Earth's Cryosphere (Tyumen). The phenomenological background of the new method consists in dramatic changes of the *SH* wavefield in cases of velocity reversal [*Skvortsov, 2005*]. Thus the respective reflections from shallow (few meters) interfaces become recordable at certain favorable conditions [*Snegirev et al., 2003*].

See Fig. 1 for some examples of refraction and SWR data used to predict the geometry and thickness of man-caused onshore taliks.

Studying inner-shelf taliks (shallow water, tidal zone) has gained ever more importance lately with the development of the Arctic shelf, but there were no appropriate acquisition methods till recently.

Research in this line has been run at the Institute of Earth's Cryosphere since 2006 [*Skvortsov et al., 2007a, b; Sadurtdinov et al., 2009*]. The shelf section was found out to bear a thick undersaturated layer below the ground surface in which water saturation of rocks is impeded by entrapped air. The layer thickness is highly variable and can reach 2 m or more. *P*-wave surveys are often inapplicable in this case as they can provide acceptable resolution only outside the tidal zone. As the available experience shows, the *P*-wave method has the same limitations also in lakes and rivers within or outside the permafrost zone.

On the other hand, *SH* surveys are workable in estimating the depth to the permafrost table under

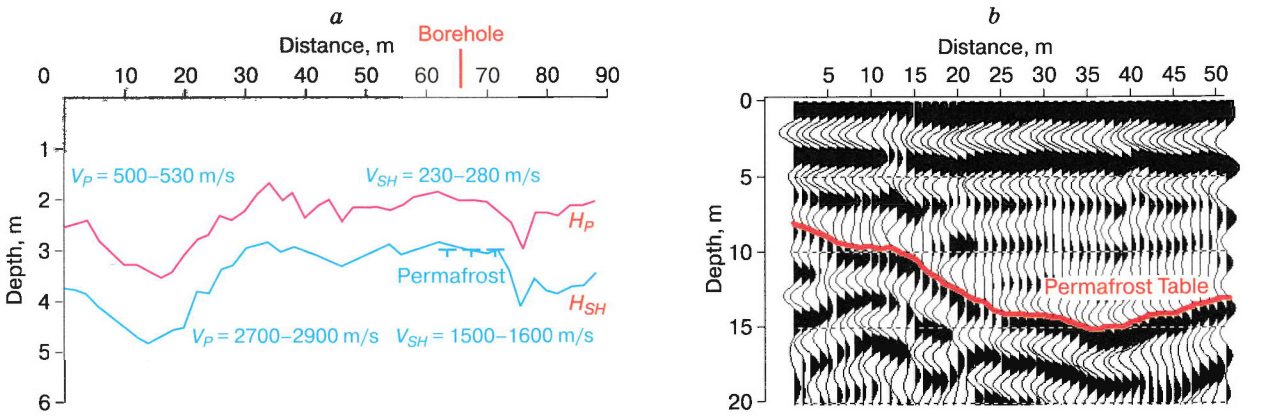

Fig. 1. Examples of contouring man-caused unfrozen layers with the use of refracted (*a*) and reflected (*b*) *SH* waves.

a: Mirnyi; *b*: Norilsk; H_P and H_{SH} are depths to permafrost surface estimated with compressional (*P*) and shear (*S*) waves, respectively; V_P and V_{SH} are compressional and shear (*SH*) wave velocities, respectively.

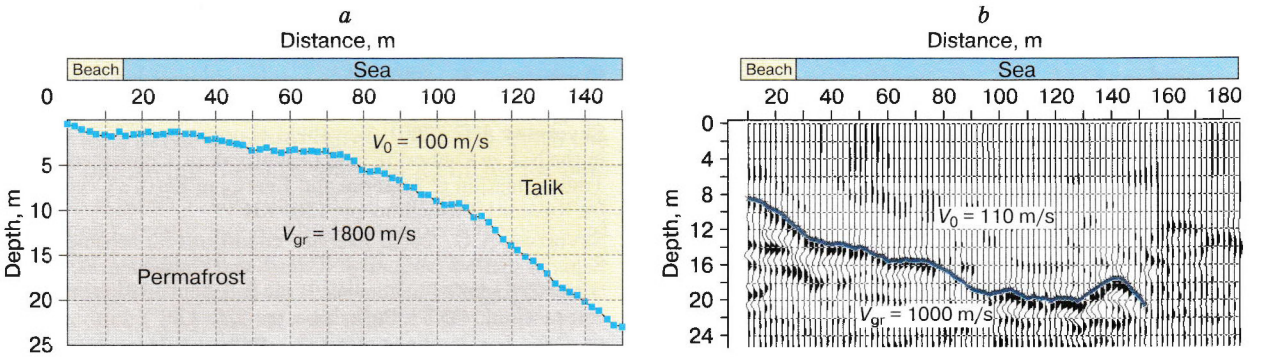

Fig. 2. Examples of contouring unfrozen layers in inner shelf with the use of refracted (*a*) and reflected (*b*) *SH* waves.

a: Yamal, Cape Kamennyi; *b*: Pechora mouth, Bolvansky site; V_0 is *SH* velocity in unfrozen layer; V_{gr} is interface *SH* velocity at permafrost surface.

shallow water. Shallow interfaces are resolvable with refracted waves (Fig. 2, *a*), but deeper taliks are better resolved with *SH* reflections (Fig. 2, *b*).

Special methods and technology of bottom surveys have been developed additionally for offshore survey.

IMAGING THE PERMAFROST SECTION

When sounding frozen ground, one has to bear in mind the specificity of its seismic section, namely, the presence of many prominent interfaces and velocity reversals, including those near the permafrost surface. In these conditions, refraction shooting is often difficult or impossible, and reflection surveys become a better choice [*Malkova et al., 2008; Skvortsov et al., 1992, 2009*], especially, *SH* reflections. The absense of converted waves make the *SH* wavefield simpler to provide more reliable seismic data [*Skvortsov, 2001*].

Summer acquisition in frozen ground faces difficulties associated with the active layer, especially if the thaw depth is multiple of the wavelength. In the

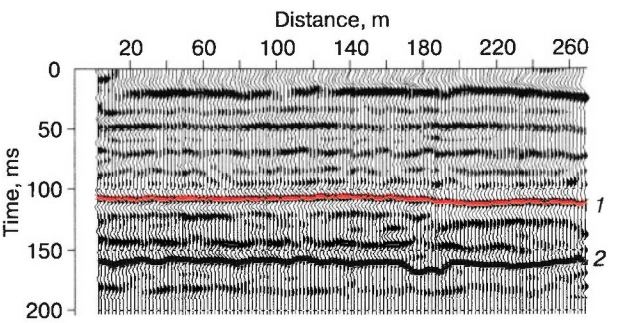

Fig. 3. A high-resolution SWR cross section near a kimberlite pipe in Yakutia.

1 – a reflection from Jurassic clay surface at depth about 55 m; *2* – Ordovician limestone surface at a depth of 80–90 m with a local low which may be a trap for placer diamond.

latter case, the wavefield bears intense reverberation multi-cycle waves [*Skvortsov, 2002*], and reflections from seismic interfaces within permafrost become ill resolvable. At shallow thaw depths, reflections are recordable if the source is placed on the permafrost surface [*Skvortsov et al., 1992*]. For this reason, it is preferable to image the structure of frozen ground in winter seasons to avoid thaw effects. Better results are obtained if land measurements with the SWR method are checked against downhole vertical seismic profiling (VSP) where possible.

Figure 3 presents an example permafrost section to a depth of 100 m collected with SWR profiling and checked against VSP data [*Skvortsov, 2005*].

STUDYING THE STATE AND PROPERTIES OF FROZEN GROUND

Compressional- and shear-wave velocity data have implications for elastic properties, strength, and strain of rocks, including frozen ground.

In the latter case, there is a separate problem of estimating the degree of permafrost "sluggishness", for which an approach based on Poisson's ratio patterns was suggested in [*Melnikov et al., 2010*].

Poisson's ratios in frozen sand-clay sediments at a low salinity of pore fluid are known to range between 0.25 and 0.40 depending on the grain-size composition but can reach 0.47–0.50 in water-saturated unfrozen sediments. Thus, Poisson's ratio can be a proxy of sluggishness associated with the amount of unfrozen water.

According to our results, joint analysis of velocity patterns and velocity ratios can provide reliable estimates of permafrost sluggishness. Therefore, the suggested approach is applicable to detect cryopegs (brine lenses) and zones of high-salinity pore fluid.

CONCLUSIONS

The choice of seismic acquisition methods and techniques should stem from knowledge of wavefield specificity within the study area.

Supra-permafrost unfrozen ground, including that under shallow water, is resolvable by *SH* refraction seismic surveys in the case of a normal velocity profile but *SH* reflections are more efficient in the presence of velocity reversals.

High-resolution shear-wave reflection (SWR) profiling with the use of *SH* phases is an advantageous tool for studying the structure of frozen ground.

Joint analysis of velocity patterns and velocity ratios (Poisson's ratio) is useful to estimate the elastic constants and the state of permafrost.

The study was supported by grants 08-05-00421a and 06-05-79071-k from the Russian Foundation for Basic Research and grants from the Tyumen Province Academy. It was carried out as part of Program 20 of the Russian Academy of Sciences, Program 11 of the Earth's Science Department of RAS, and Program 122 of the Siberian Branch of the RAS.

References

Malkova G.V., Skvorstov A.G., Sadurtdinov M.R., et al., 2008. Seismic surveys applied to study unfrozen ground in onshore Pechora bay, in: Resources of Arctic and Highland Terrains. State and Prospects of Engineering-Geological Permafrost Studies. Proc. Intern. Conf. Tyumen, 21–24 April 2008 [in Russian]. Express, Tyumen, pp. 311–313.

Melnikov V.P., Skvortsov A.G., Malkova G.V., et al., 2010. Seismic studies of frozen ground in Arctic areas. Russian Geology and Geophysics (Geologiya i Geofizika), 51 (1), 134–142 (169–177).

Ponomareva O.E., Skvorstov A.G., 2006. Studies of surface geologic processes in Nadym district, West Siberia: Methods and results, in: Theory and Practice of Earth's Permafrost Appraisal. Proc. Intern. Conf. [in Russian]. Book 1. TGNU, Tyumen, pp. 272–274.

Sadurtdinov M.R., Skvortsov A.G., Tsarev A.M., 2009. Shallow-water submarine seismic surveys of shallow subsurface, in: Geophysics for Engineering and Mineral Exploration. Proc. 5th Intern. Workshop, Gelendzhik (On-line version).

Skvorstov A.G., 1997. Wave patterns in unconsolidated permafrost. Kriosfera Zemli, I (3), 66–72.

Skvorstov A.G., 2001. Wavefield of upper permafrost section in the Nakyn kimberlite field (Yakutiya), in: Conservation and Transformation of Material and Energy in Earth's Cryosphere [in Russian]. Pushchino, pp. 130–131.

Skvortsov A.G., 2002. Extreme conditions for seismic wavefields in shallow permafrost: Causes and consequences, in: Extreme Cryogenic Phenomena: Basic and Applied Aspects. Proc. Intern. Conf., ONTI, Pushchino, pp. 170–171.

Skvortsov A.G., 2005. High-resolution shallow shear-wave seismic surveys, in: Engineering Geophysics, Proc. Intern. Conf., Moscow University Press, Moscow, pp. 16–18.

Skvortsov A.G., Hunter J.A., Goriainov N.N., et al., 1992. High-resolution shear-wave reflection technique for permafrost engineering applications. New results from Siberia, in: Proc. 62nd Annual Intern. SEG Meeting, New Orlean, USA, pp. 382–383.

Skvortsov A.G., Malkova G.V., Drozdov D.S., et al., 2007a. Seismic-cryological conditions in the Arctic inner shelf, in: Geophysics for Engineering and Mineral Exploration. Proc. 3rd Intern. Workshop, Gelendzhik, pp. 196–198.

Skvortsov A.G., Malkova G.V., Sadurtdinov M.R., et al., 2007b. Cryological conditions of the inner shelf in the Pechora Bay (Bolvanskii site), from seismic data, in: Cryogenic Resources of Arctic Region. Proc. Intern. Conf., TyumGNGU, Salekhard, Book 1, pp. 170–173.

Skvortsov A.G., Drozdov D.S., Malkova G.V., et al., 2009. Seismic-cryological conditions of petroleum provinces in northern Russia. Abstracts, Workshop Tyumen-2009 (On-line version).

Snegirev A.M., Velikin S.A., Istratov V.A., et al., 2003. Geophysical monitoring in permafrost areas, in: Permafrost, Proc. 8th Intern. Conf., ICOP, Zurich, pp. 1079–1084.

Tsarev A.M., Skvortsov A.G., Sadurtdinov M.R., 2010. An experience of permafrost engineering applications of seismic methods, in: Geophysics for Engineering and Mineral Exploration. Proc. 5th Intern. Workshop, Gelendzhik (On-line version).

Received
8 February 2011

Kriosfera Zemli, 2011, vol. XV, No. 4, pp. 99–103 http://www.izdatgeo.ru

ADVANCED THERMOLUMINESCENCE DATING OF PERMAFROST: A NEW APPROACH

V.S. Sheinkman, V.P. Melnikov

Institute of Earth's Cryosphere, Siberian Branch of the Russian Academy of Sciences, PO box 1230, Tyumen, 625000, Russia; vlad.sheinkman@mail.ru

Precise age determination is an important tool to study frozen ground as it can be used, through extrapolation, to reconstruct the history of permafrost and to predict its future evolution. However, precise dating is difficult because the classical age methods designed for a narrow time span and a limited number of rock types are inapplicable to permafrost. Having compared several recent techniques, we selected advanced thermoluminescence dating as a procedure best appropriate for frozen ground. The present paper concerns with the dating technology, advantages of the new approach, and testing results.

The formation of permafrost was associated with climate change reflected in the sequence of Quaternary events. Deciphering the rhythms of the process is a key research objective which requires good chronological ties. The age ties provide indispensable reference for reconstructing milestone events as an outline for the past history and possible future of permafrost. Yet, getting this data is not so easy for technological limitations in the standard dating methods. With the aim of improving the instrumental facilities for permafrost studies at the Institute of Earth's Cryosphere (Tyumen), recent age methods have been inventoried in order to extend the scope of rocks and related events fit for dating. As a result, advanced thermoluminescence (TL) dating was selected as the best appropriate procedure for frozen ground, which was tested on different objects in Russia and abroad [*Sheinkman et al., 2001, 2011; Sheinkman, 2002a, b; Shlukov and Sheinkman, 2002, 2007*].

The advantages of the new approach become clearer when compared with other methods of permafrost dating analyzed in their specificity. This specificity is often poorly understood, which brings about errors in the inferred chronology and makes interpretations ever more problematic, the available dates of many permafrost complexes being few and controversial. There are several reasons for this situation. Dating implies identifying a physical process the rocks have undergone and, thus, selecting the respective proxy to be plotted in time series. However, people who study the physics of the process may be unaware of permafrost formation details while those who use the age data rarely look into geochronological technologies far enough to update them.

Rocks are commonly dated proceeding from radioactivity, which is employed in different ways in two large groups of age methods based on radiometry or dosimetry. The two differ in the dating principles and in sampling procedures. The *radiometric* techniques stem from radioactive decay of a radionuclide timer in a certain closed system when the concentration of the progeny indicates how long the timer has stayed in the system. For instance, the decay of ^{14}C accumulated in organic matter allows quite exact timing of organic-bearing rocks, but within a limited span of 40–50 kyr by the common procedure or up to 70–75 kyr by accelerator mass spectrometry (AMS) which appeared not long ago. The AMS technique is applicable to other radioactive elements as well but these can provide only implicit evidence for the age of permafrost. Accumulation of ^{10}Be and ^{26}Al on the surface (a few mm layer) of quartz-bearing bedrock, for example, can measure the time when the rock was exposed on the surface and thus record the respective events. Note that these time spans are already as long as hundreds of thousand or millions of years. Yet, the radiometric dating instruments are expensive and sophisticated. That is why, although being highly precise and easy in the required sampling, radiometry is of a limited use for frozen ground where timer radioactive elements are scarce.

The methods of *dosimetry*, among which is the one we describe, make an alternative to radiometry as they employ radioactivity in a reverse way. Instead of the decay products left in rocks, dating is against the amount of radiation dose the minerals have absorbed, i.e., measured is the gain of radioactive energy rather than its loss. Most techniques are based on stimulated luminescence (thermally stimulated luminescence in our case) of ubiquitous timer minerals, commonly silicates, for the age spans of hundreds of kyr. In the case of frozen ground, however, there is a pitfall of climate noise the silicate timers being highly sensitive to environment changes.

After a number of experiments, we have found out how to avoid the negative effects in dating permafrost without loosing the advantages of the thermoluminscence technique. In the TL method, luminescence is stimulated in minerals which can be both dosimeters and luminophors and, when heated, can re-emit as light the previously absorbed energy from external radiation fields. Bearing in mind that the

earlier obtained ages of many dosimeter minerals may be wrong, our primary objective was to select the most reliable timer mineral. It was quartz, which stands out against other minerals in its well-defined lattice, chemical stability, high strength, and ubiquitous occurrence in almost any rock. Its pronounced and explicitly documented properties can provide a realistic time reference for most of the objects of our interest.

Quartz shows low luminescence at temperatures about 150–400 °C. The process is as follows. Quartz absorbs radiation at the account of free electrons released upon its bombardment with radiation products, especially gamma quanta. Having gained additional energy from the γ quanta, electrons in the valence shells become excited and some escape from their places leaving a positive hole charge. The escaping electrons wander over the molecule for some time (and this time characterizes the metastable state of the molecule), but there are positively charged sites other than the hole carriers: the capture sites or electron traps. The free electrons tend to recombine according to the tendency of the electron ensemble to return to its stationary state: some move back to the valence shell when they meet holes but others fall into traps to be taken up.

Traps with high capture energy (deep traps) in the timer mineral become at some point emptied and then recharged from the ambient radiation in a newly formed rock. This process can be diagnostic of the time the timer mineral stays in the rock, i.e., can be used in dating the latter. The traps, which are controlled by the lattice structure, may be hard to recognize. Quartz is a good timer mineral as it has been well studied, and traps are easily spotted in its regular lattice. According to our experience [*Sheinkman, 2002a; Shlukov and Sheinkman, 2002, 2007*], electron traps in quartz are stable and appear to arise at vacancies left by oxygen anions. For various reasons, quartz originates with a certain number of oxygen vacancies and, if oxygen anions are absent, positive charges form in their place with a capture energy about that of the hole charges in the valence shells. This is the main type of electron traps in quartz.

On heating to high temperatures, electrons leave the traps with emission of photons (light quanta), and this luminescence shows up clearly as a peak at about 300 °C. (There are also smaller traps in quartz, but they are less important). In other words, the energy the mineral can store in electron traps can release upon heating while the equivalent light sum can be measured and assigned to traps of a certain type.

The following objective consisted in choosing the procedure for estimating the energy stored by the dosimeter mineral. However, before we had to solve the sampling problem because its previous rules could not provide reliable dating.

In our case, the sampling rules were determined empirically and subjected to statistical checks to avoid random signatures. That required dramatic methodological changes, namely, using mass sampling instead of collecting few single samples and developing special techniques for treating large quantities of sampled material.

Note that frozen ground is a particular object, and TL analysis should be applied with regard to all minute details of sedimentation. The exposure time of the timer mineral is commonly estimated from TL peaks corresponding to the amount of energy (radiation dose) the mineral has received and the activity of the radiation field in the analyzed rock. This seeming straightforwardness and the tendency of simplifying the sampling procedure led to controversy, because the rules of TL sampling actually should be very strict. That is what we have found out.

First, sampling and measurements of radioactivity should be performed *in situ*, in a monolith block of rock, at least 1.2–1.5 m below the surface (length of gamma-ray tracks), with regard to possible migration of mobile radionuclides along cracks. The simplified procedure accepted earlier, with sampling near the ground surface, without *in situ* measurements, and calculation from the element abundances in a sample [*Aitken, 1985*] will not do. A sample receives ambient radiation from a piece of rock as a whole (up to several tons), in which radioactive elements are randomly scattered, but the rock block is too big and heavy to be collected as a sample; otherwise, taking into account the scatter of radionuclides in it is unrealistic. Yet, that standard procedure has been still in use, and we held a special experiment to estimate the error it may run. Samples were collected from different depths and the earlier simplified sampling procedure turned out to give tens of percent greater scatter of ages than the one we suggest.

Second, one has to bear in mind that only carefully bleached (quasi-zeroed) sediments containing a timer mineral are fit for dating. It means that the electron traps should be as empty as possible before the timer mineral becomes buried; only since that time on, the absorption of a new radiation dose in the sedimenting material will be the age criterion, and only then the dosimeter mineral can become a timer. There are two main ways of bleaching. One is by heating the timer mineral to above 300 °C, which allows dating to be applied to objects stored in permafrost, such as baked pottery, deposits affected by forest fires or hot lavas before burial, etc. The other way to empty electron traps in quartz is uniform UV radiation, which means a possibility of TL dating on aeolian sand previously exposed to the sunlight or on fine-grained deposits washed in the alluvium of river spits and deltas.

Third, TL dating is applicable to rocks in which the radiation field is stable. This field is produced

mostly by U- and Th-series isotopes, as well as by ^{40}K, with their half-lives far longer than the age of the dated rocks (of the order of many hundreds of kyr). Nevertheless, the stability of the radiation source does not necessarily mean the stability of radiation the timer mineral has been exposed to, because some filters may arise from time to time between the mineral and the source. A part of radiation may be intercepted by water films that coat mineral grains and, being either present or absent, can change the dose. On the other hand, one may be positive only about the radioactivity measured at present, i.e., one has to be sure the values may be extrapolated safely to the greatest part of the dated period. Therefore, only the rocks that have not experienced significant changes in ice and water contents are suitable for TL dating, namely, monolith permafrost outside the active layer.

Fourth, no correction can allow for all wrong estimates of radiation received by the timer mineral. Spike dates always occur and can be leveled out only through mass sampling and statistical checks, which, being too cumbersome [*Frechen and Dodonov, 1998*], have been rarely applied in the standard dating procedure [*Aitken, 1985*]. Furthermore, shortcomings have been found also in the basic principles of the latter [*Shlukov et al., 1993*].

Dating implies comparing signals from a sample which has absorbed most of radiation energy with those from test bleached samples. Bleaching (conventional datum) is quite simple: one has to expose a sample to UV light. However, recharging has been commonly done with laboratory high-energy radiation for the sake of rapidity. Our experiments showed that the intense radiation as short as a few days and the slow natural radiation in low fields for thousands of years are quite different in their effect on dosimeter minerals. The reason is that the natural TL kinetics turns out to be second-order, as it was revealed experimentally [*Shlukov and Sheinkman, 2002, 2007*], instead of the theoretically predicted first-order kinetics which was assumed *a priori* in the traditional TL dating technology and biased strongly (up to several times) the dates.

The kinetics of luminescence concerns with laws of its buildup and decay in luminophor minerals. Luminescence is defined by the probability of uptake and release of photons [*Fok, 1964; Antonov-Romanovsky, 1966; Prokhorov, 1990*]. In the simplest case when the duration of the process is neglected, it is an exponential function:

$$I = I_0 \exp(-t/\tau).$$

The decay kinetics of recombination luminescence (as in our case) in a wide time range is approximated by the Becquerel hyperbola:

$$I = I_0/(1 + pt)^{\alpha},$$

where I_0, I are, respectively, the luminescence intensities at the times t_0 and t; τ is the Einstein coefficient corresponding to the mean time while the electron ensemble stays excited; p is the constant responsible for the lattice structure; α is the order of kinetics (1 and 2 for the first and second order, respectively).

In the first-order kinetics, the excitation time is relatively short: luminescence builds up quickly and decays instantaneously, i.e., electrons rapidly leave the traps and return to the valence shells. The TL curve in the first-order model has a sharp peak (Fig. 1, *b*), and most of its rising part is virtually in mirror symmetry with the falling segment. Theoretically this pattern corresponds to the case when repeated capture of electrons is impossible. However, in the second-order kinetics, the electron ensemble remains in the metastable state for a relatively long

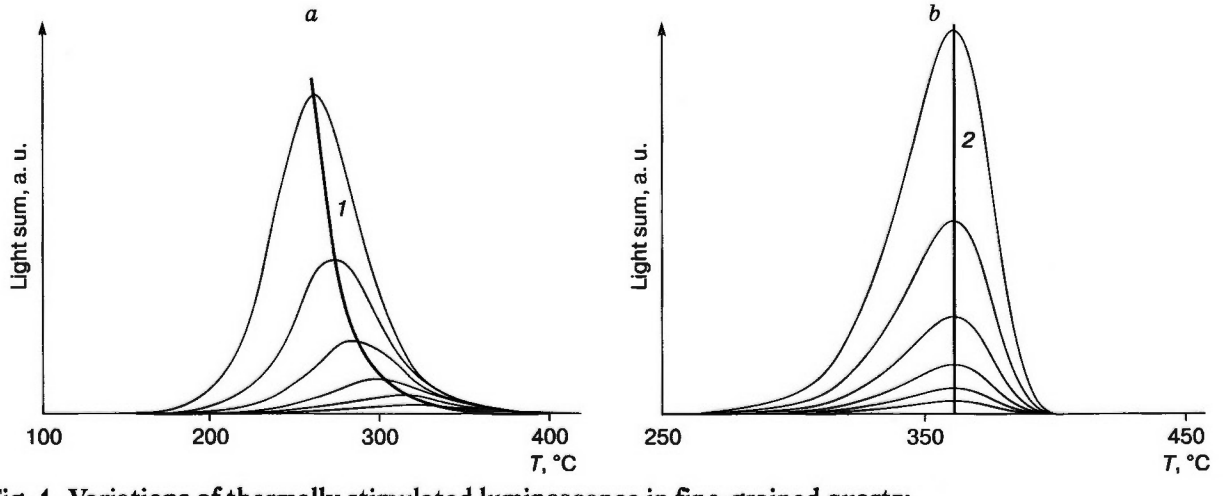

Fig. 1. Variations of thermally stimulated luminescence in fine-grained quartz:

a – second-order TL kinetics: experiment; *b* – first-order TL kinetics: theory; curves *1* and *2* show position of TL peak lines. See text for explanation.

time, and luminescence decays slowly (even though it builds up rapidly) because the once released electrons can be captured again at neighbor traps and escape again. In this case, the TL curve has a low slope in the region of high temperatures (Fig. 1, *a*).

Luminescence in the two cases is estimated in different ways. Namely, luminescence is proportional to electron metastability time (with some factor) at first-order kinetics ($\alpha = 1$) but their relationship is exponential in the second-order case ($\alpha = 2$). Yet, the previous TL dating method has been based on the first-order kinetics model, which became "canonical". The light sum in that model was just fixed instead of being calculated with regard to its slow decay, and that was the cause of dating errors.

The order of kinetics can be identified mainly in a graphic way and required a careful experimental work with the quartz samples in our case. Repeated tests with quartz particles from different sites [*Shlukov and Sheinkman, 2002, 2007*] showed that, when viewed in detail, the TL process is clearly delayed at high temperatures (Fig. 1, *a*). Therefore, the treatment of samples and the data processing had to be different and to proceed from the second-order kinetics, i.e., the basic principle of TL dating needed a major revision.

In the standard procedure, the tested sample is divided into equal aliquots, and each aliquot is irradiated in laboratory at a high intensity increasing progressively for each following aliquot. Then the time dependence of the received dose (dose curve) is extrapolated according to the logarithmic saturation law, and the age of the sample is calculated from its position on the dose curve (Fig. 2, *a*) assuming that the stimulated luminescence reflects a simple TL signal with the first-order kinetics (Fig. 2, *c*).

However, this extrapolation turns out to be wrong [*Shlukov and Sheinkman, 2002, 2007*]. Irradiation in high-energy fields, which are orders of magnitude more intense than those in natural rocks, gives rise to reversals in the state of electron ensemble and reactivates small traps that are dormant in natural conditions. As a result, the TL signal bears peaks associated with those additional traps (dashed line in Fig. 2, *d*), and the dose curve departs strongly from the theoretical one (Fig. 2, *b*). Inasmuch as laboratory irradiation is rather expensive, the aliquots are commonly few, and may bias the ages if correspond to the

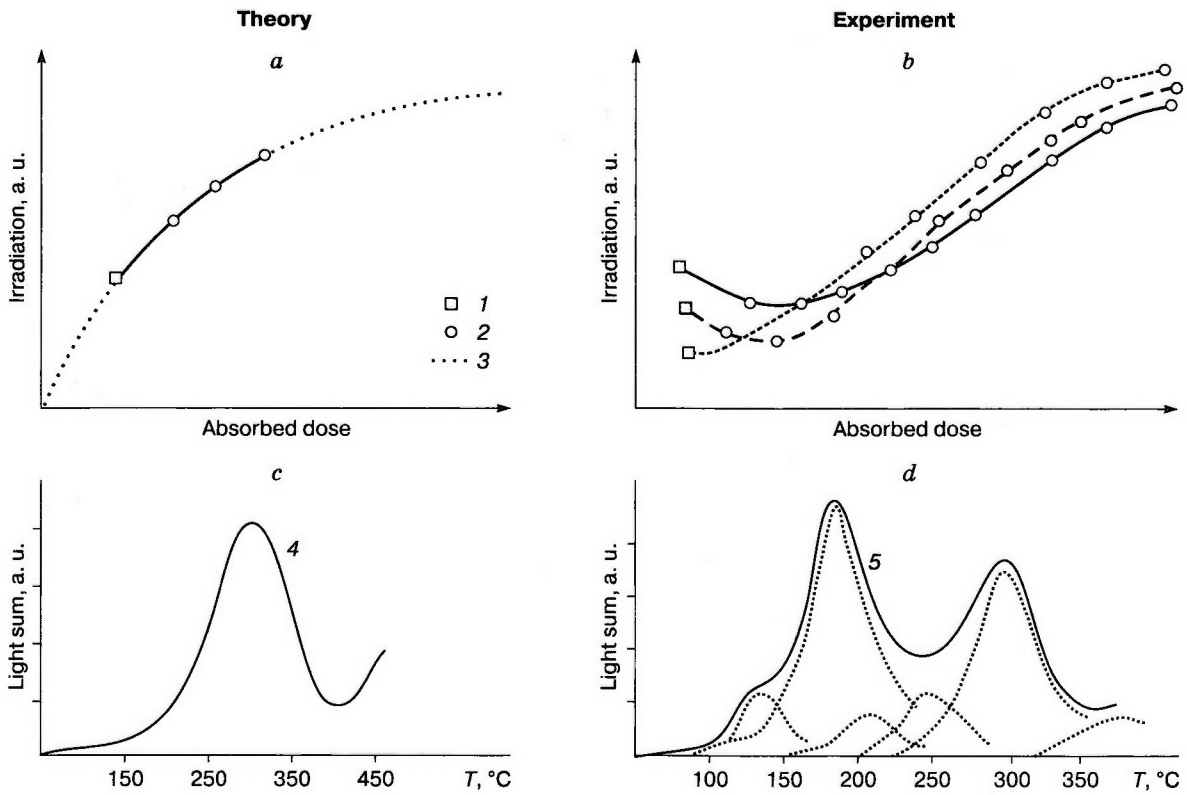

Fig. 2. Theoretical interpretation of data in the standard TL dating approach (*a*, *c*) and its real application (*b*, *d*) in experiment:

1 – radiation dose received by the tested sample *in situ*; *2* – radiation dose received by aliquots of the tested samples after their rapid laboratory irradiation in a high-energy field; *3* – extrapolated time dependence of radiation dose; *4* – TL curve of the tested sample; *5* – TL curve of the laboratory irradiated sample.

distorted segments of the dose curve. Furthermore, the classical procedure estimates the total TL signal while the peaks and troughs are averaged and elevated to the level of a virtual plateau. The main focus being on the averaged luminescence peak, the optical properties of quartz have been neglected but they differ in different quartz varieties, as it was shown in experiments, and likewise influence the output luminescence. Nevertheless, even after our data had been published [*Shlukov and Sheinkman, 2002, 2007*], the followers of the standard procedure took the way of making the dating instruments more sophisticated (and thus more expensive) and applying corrections rather than changing the principles.

With the aim of obtaining a reliable and, if possible, straightforward method which would allow treating a large number of samples, we refused the previous unreliable dating criteria and cumbersome procedures. In the new approach, they are the coordinates of TL peaks in the dose curve, instead of the peak intensity, that make a more reliable age criterion based on second-order TL kinetics. This criterion, which stems from the more stable thermal rather than optical properties of quartz, was missed in the first-order kinetic TL model as its recognition would require a different problem formulation and instrumental background. The validity of the suggested approach has been confirmed in repeated tests: the younger the sample (Fig. 1, *a*) the lower and the higher-temperature its TL peak. The range of these shifts toward high temperatures (over 100 °C) is quite enough to obtain precise dates.

Thus, the new criterion cancels the drawbacks of the standard methods and changes the very approach to TL dating. The suggested technique is an order of magnitude cheaper and much easier to perform than the classical procedures, which makes it a high-quality and accessible tool for investigating permafrost. Its reliability has been validated additionally by checking the new TL dates against radiometric dating [*Shlukov and Sheinkman, 2002, 2007; Sheinkman et al., 2011*].

In conclusion, we note that the background for geoscience applications of TL dating was first developed in the 1960s by G.V. Morozov in the Ukraine and A.I. Shlukov in Russia [*Morozov, 1968; Shlukov et al., 1993*]. The Russian science has laid a solid foundation in this field of research and long remained the leader, but the leadership has been lost lately and alarming tendencies are currently appearing. Some geoscientists (see the review in [*Sheinkman, 2008*]) suggest to refuse TL dating at all referring to its ambiguous results without proper understanding the idea of the method while others praise foreign technologies which try to repair the drawbacks through updating the instruments. Yet, both ways are deadlock.

The suggested approach based on studies in Russia does not claim to be panacea but it allows making good progress in solving the urgent dating problem and, moreover, creates prerequisites for advance in geochronology of permafrost. This is especially important as the chronological constraints of events in geosciences are crucial for synthesis of the existing experience and gaining new knowledge. In this respect the new approach can be used for systematizing all available data with reference to the time scale.

References

Aitken M.J., 1985. Thermoluminescence Dating. Acad. Press, N.Y., 359 pp.

Antonov-Romanovsky V.V., 1966. Kinetics of Photoluminescence in Crystalline Phosphors [in Russian]. Nauka, Moscow, 324 pp.

Fok M.V., 1964. Introduction into Kinetics of Luminescence in Crystalline Phosphors [in Russian]. Nauka, Moscow, 283 pp.

Frechen M., Dodonov A.E., 1998. Loess chronology of the Middle and Upper Pleistocene in Tadjikistan. Geol. Rundschau, 87, 2–20.

Morozov G.V., 1968. Application of the TL Method for Studying Loess Deposits. Authors's Abstract, Candidate Thesis [in Russian]. Kiev, 23 pp.

Prokhorov A.M. (Ed.), 1990. Physical Encyclopedia [in Russian]. Book 2, Sov. Entsikl., Moscow, 703 pp.

Sheinkman V.S., 2002a. Timing glacial deposits of Gorny Altai and checking dating results from Dead Sea sections, with paleoglaciological implications. Materialy Glatsiologicheskikh Issledovanii, 93, 17–25.

Sheinkman V.S., 2002b. Late Pleistocene invasion of Palaeo-Dead Sea into the lower Zin Valley, the Negev Highlands, Israel. Europ. Geosci. Union Stephan Mueller Spec. Publ. Ser., Vol. 2, 113–122.

Sheinkman V.S., 2008. Quaternary glaciation in Siberian mountains: general laws and analysis of data. Materialy Glatsiologicheskikh Issledovanii, 105, 51–72.

Sheinkman V.S., Plakht J., Mazor E., 2001. Makhtesh Hazera, the Zin valley and the Dead Sea basin: evolutionary links, in: B. Krasnov and E. Mazor (Eds.), The Makhteshim Country: a Laboratory of Nature. Geological and Ecological Studies in the Desert Region of Israel, Pensoft, Sofia-Moscow, pp. 97–121.

Sheinkman V.S., Melnikov V.P., Panyukov D.A., 2011. A new approach to TL dating and its realization in Siberia, in: Proc. XVIII INQUA Congress, Bern, Elsevier (in press).

Shlukov A.I., Sheinkman V.S., 2002. Saturation of 300 °C peak of quartz: a working hypothesis, in: LED 2002, 10th Intern. Conf. on Luminescence and Electron Spin Resonance Dating, Reno, Nevada, USA, p. 161.

Shlukov A.I., Sheinkman V.S., 2007. Dating the highest sediments of the Dead Sea Late Pleistocene. Precursor by new TT-technique. Quatern. Intern., 382, 167–168.

Shlukov A.I., Shakhovets S.A., Voskovskaya L.T., et al., 1993. A criticism of standard TL dating technology. Nucl. Instruments and Methods in Phys. Res., 73, 373–381.

Received
19 February 2011

SCIENTIFIC JOURNAL
EARTH'S CRYOSPHERE

Kriosfera Zemli, 2011, vol. XV, No. 4, pp. 104–106 http://www.izdatgeo.ru

PERMAFROST ENGINEERING: STABILITY OF STRUCTURES AND FOUNDATIONS

A NOVEL HEAT-INSULATING MATERIAL FOR THERMAL STABILIZATION OF SOILS

K.S. Ivanov

Institute of Earth's Cryosphere, Siberian Branch of the Russian Academy of Sciences, PO box 1230, Tyumen, 625000, Russia; 4terminator@mail.ru

The study has proven the feasibility of obtaining a novel heat-insulating material with an apparent density of 290–580 kg/m^3, a compressive strength of 1.7–7.8 MPa, and a water absorption of 4 %. Heat treatment of a mixture of diatomite and alkali at 95 °C increases the leaching rate of amorphous SiO_2 while the resultant soluble sodium silicates promote foaming of the charge during sintering at 775 °C and decrease its apparent density. The new heat insulator is similar to the traditional foam glass in its structure and properties and thus can be used to protect the foundations of engineering structures.

The damaging frost action on the foundations of engineering structures built and operated in permafrost zones, such as thermokarst, thaw settlement and frost heaving of soils, require special preventive measures while constructing. The measures mitigating this frost action include, primarily, thermal stabilization of foundations which allows construction upon any soil, with only regard to its load-bearing capacity [*Tsitovich, 1973*]. In addition to making ventilated cellars, withdrawal of heat released by the building, and the use of special cooling (or heating) devices, etc., thermal stabilization of soils is achieved with heat-insulating materials. For instance, creating a sod layer reduces the freezing depth by a factor of 1.5 relative to open ground [*Kiselev, 1985*]. That is why any heat insulator laid on the ground surface will preclude heat flux and provide thermal stabilization of foundations.

Until recently the applicability of most heat-insulating materials to soil protection was limited by their ability of accumulating moisture (wetting). This is known, specifically, for expanded clay (keramzit) used as footing pads beneath paving, which looses its insulating capacity on saturation [*Kiselev, 1985*]. Therefore, a material with the minimum thermal conductivity and water uptake will be the best choice for heat insulation.

In the current practice, frost heaving effects and the thaw depth in permafrost are reduced using extrusion foam polystyrene plates. There is encouraging experience of employing this material as footing for buildings, highways, and railways [*Alekseev and Bek-Bulatov, 2007*]. However, foam polystyrene can loose its heat-proof properties and fail by natural destruction of the polymer, this making its endurance debatable.

Foam glass is an efficient insulator free from the above drawbacks. This is hardened glass foam with closed pores (its porosity reaches 97 %), which resists water uptake and loss of thermophysical properties. With its 140 kg/m^3 density, foam glass has a thermal conductivity of 0.045 W/(m·K) and an ultimate load of 50 t/m^2 (0.5 MPa) [*Goryainov and Goryainova, 1982*]. Its incombustibility, high chemical resistance, and unlimited lifetime make foam glass an exceptional material, but it is too expensive because of expensive starting materials and a complicated energy-consuming production technology.

Therefore, it is urgent to obtain heat-insulating materials similar to foam glass in their properties but based on cheap minerals. The author of this study has investigated the feasibility of obtaining foam silicate, an analog of foam glass, using widespread silicic rocks and alkali additions, within the limits of the project "Sintered Heat-Insulating Material on the basis of Mineral Resources of the Tyumen Region" supported by the Tyumen Region Governor.

The idea of obtaining foam silicate consists in alkalic leaching of amorphous silica from siliceous rocks. This well known method of making liquid glass has been of moderate use so far because of a refractory insoluble sludge which, in our case, is a useful component of the mixture with a significant amount of clay. Soluble alkaline silicates form low-melting eutectics and thus facilitate the transition of the batch into a melting state at temperatures below 700 °C [*Iler, 1979*] while crystallization water released from clay minerals in the insoluble precipitate acts as a foaming agent in the charge.

The study was performed using diatomite from the Kamyshlov deposit in the Sverdlovsk region, with 42.5 amorphous SiO_2, 8.9 Al_2O_3, and 3.3 Fe_2O_3

(in wt.%). The charge with diatomite/40 % NaOH at a solution ratio 2.3:1.0 was mixed and filled with water until it became homogeneous, and then placed in a thermostat at 20 and 95 °C. The solution ratio was chosen proceeding from the fact that diatomite contains 40 % amorphous silica which yields a soluble silicate solution (SSS) with the mole ratio SiO_2/Na_2O $m = 3$. The SiO_2 yield (in percent of diatomite dry weight) and the m ratio in the charge after leaching were estimated following the technique reported in [*Sokolovich, 1963*].

After the leaching was over, cylindrical pellets, 3.4 cm in diameter and 1.6 cm thick, were fabricated from the charge by pressing at 2 MPa, as well as granules 5–8 mm in diameter made by rolling on a plate granulator. The pellets and granules dried at 100 °C to constant weight were then sintered and foamed in stainless steel moulds in air, with the treatment schedule of heating at 25 °C/min, 20 min exposure to 775 °C, and slow cooling together with the furnace at ~1 °C/min) to room temperature. During heating, the granules became foamed and welded together into solid massive porous silicate, from which samples were cut in the form of 30 × 30 × 30 mm cubes.

Inasmuch as foaming of the diatomite-alkali charge largely depends on the SiO_2 yield (YS), the first step consisted in investigating the kinetics of SiO_2 extraction at different temperatures (Fig. 1). As a result, heating to 95 °C was found out to notably accelerate the process: already in 30 min of exposure at 95 °C, YS was 3.3 times that at 20 °C, for the same exposure time (42.5 % against 12.9 %), and almost did not grow further.

The YS dependence of the foaming process in the batch after its leaching for different time spans was explored on cylindrical pellets (see Fig. 2 for their photographs after heating). The images show the volume and the apparent density of the foam silicate pellets to be proportional to YS. Growth of m along with YS likely causes an increase in the amount of liquid in the charge while sintering and/or its earlier appearance, which promotes better foaming. Thus, it is SSS rather than alkali that is responsible for the temperature of liquid formation. This inference is supported by the fact that pellets molded immediately after mixing crack and do not foam on heating, but foaming resumes as dry crystalline sodium silicate ($Na_2O{\cdot}SiO_2{\cdot}9H_2O$) is used instead of alkali, with an equivalent amount of water added.

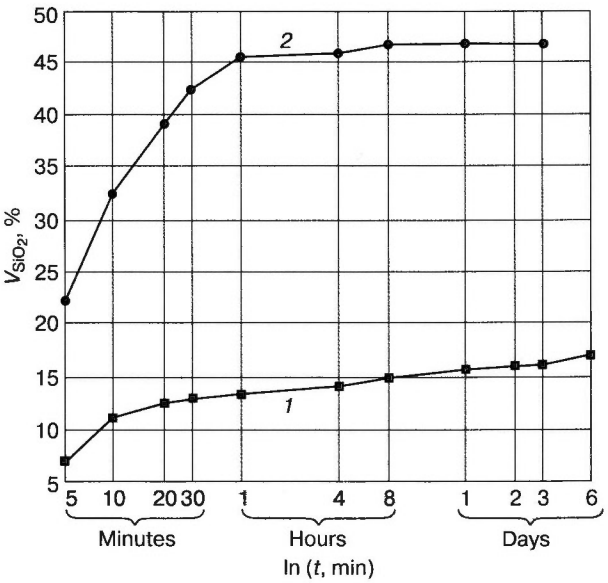

Fig. 1. Kinetics of SiO_2 yield (YS) at different temperatures:

1 – 20 °C; *2* – 95 °C.

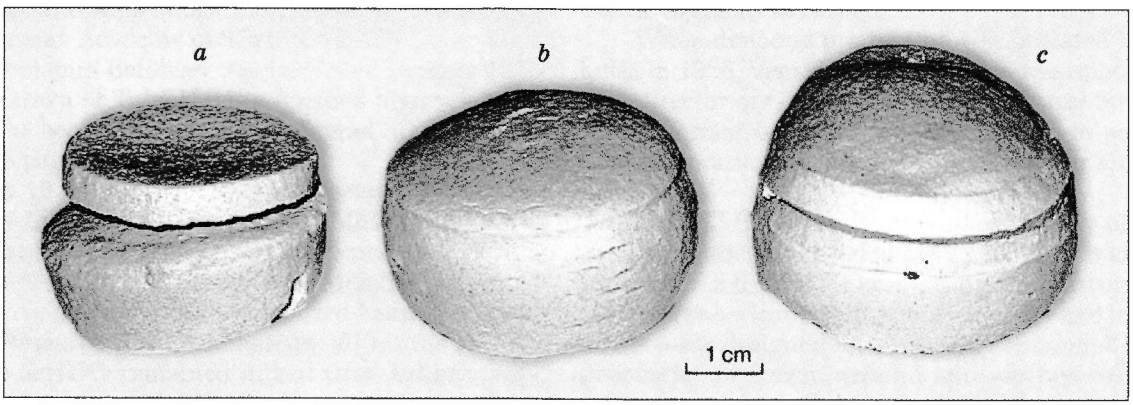

Fig. 2. SiO_2 yield (V_{SiO_2}) plotted versus apparent density (ρ) of diatomite-alkali charge after heating (T) for different time spans (t):

a – V_{SiO_2} = 13.3 %, ρ = 550 kg/m^3, T = 20 °C, t = 60 min; *b* – V_{SiO_2} = 32.5 %, ρ = 350 kg/m^3, T = 95 °C, t = 10 min; *c* – V_{SiO_2} = 42.5 %, ρ = 280 kg/m^3, T = 95 °C, t = 30 min.

Rising the heat-treatment temperature to 800 °C causes an about 10–15 % density increase of the pellets, possibly, as the liquid phase becomes progressively less viscous while the release of crystallization water ceases after 740 °C [*Lazutkina et al., 2006*]. The samples develop sizeable open pores, up to 1 cm in diameter, by coalescence of smaller pores.

Further experiments were run with grains made from charges with different amounts of extracted SiO_2. As YS increased from 13.3 to 42.5 %, the apparent density and the compressive strength of the grains changed from 580 to 290 kg/m^3 and from 7.8 to 1.7 MPa, respectively. Water uptake in all samples was within 2 vol.%. The thermal conductivities of the samples with the densities 290 and 580 kg/m^3 were 0.08 and 0.14 W/(m·K). The samples had a uniform structure consisting of closed cells with an average diameter of 1.5 mm. The cell surfaces had glassy luster and varied in color from stone to green-gray.

The suggested method can be used to obtain foam silicate which will allow minimizing destructive cryogenic effects being both a heat and water insulator as it can prevent moisture from migration into vulnerable zones of foundations.

References

Alekseev A.G., Bek-Bulatov A.I., 2007. The use of foam polystyrene insulator ("PENOPLEKS") for reducing frost heaving of soil beneath shut walls. Stroit. Materialy, No. 6, 38–40.

Goryainov K.E., Goryainova S.K., 1982. Technology of Heat-Insulating Materials and Products [in Russian]. Stroiizdat, Moscow, 296 pp.

Iler R.K., 1979. The Chemistry of Silica. Willey, N.Y., 866 pp.

Kiselev M.F., 1985. Preventing Soils from Frost Heave Deformation [in Russian]. Stroiizdat, Leningrad, 132 pp.

Lazutkina O.R., Kazak A.K., Temereva A.A., et al., 2006. Prospects of using diatomite material from the Sverdlovsk Region in enameling production. Glass and Ceramics, 63 (3–4), 97–98.

Sokolovich V.E., 1963. Rapid method of determining the modulus of sodium silicate solution. Glass and Ceramics, 20 (9), 471–472.

Tsitovich N.A., 1973. Mechanics of Frozen Soils [in Russian]. Vysshaya Shkola, Moscow, 448 pp.

Received
24 February 2011

SCIENTIFIC JOURNAL
EARTH'S CRYOSPHERE

Kriosfera Zemli, 2011, vol. XV, No. 4, pp. 107–108 http://www.izdatgeo.ru

CHRONICLE

Balobaev Veniamin Tikhonovich
(02.01.1930–04.09.2011)

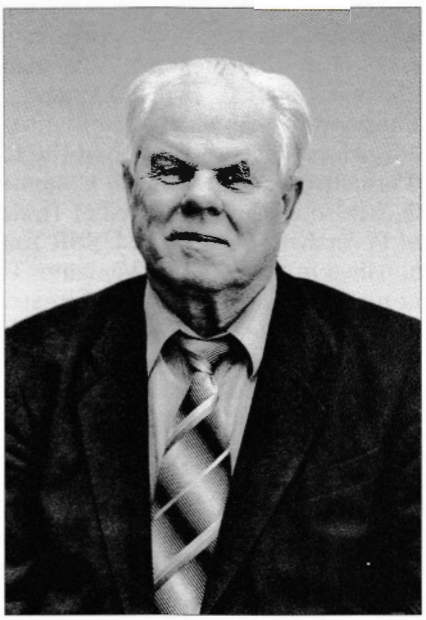

Veniamin Tikhonovich Balobaev passed away suddenly on 4 September 2011, at an age of 81. He was research advisor of the Russian Academy of Sciences at Melnikov Permafrost Institute (Yakutsk), veteran of work, honored worker of the national economy of Yakutia (Sakha Republic), Doctor of Geology and Mineralogy, Correspondent Member of the Russian Academy of Sciences (RAS).

Veniamin Balobaev was born on 2 January 1930 in the town of Tula. Having finished high school in 1948, he became student at Leningrad State University, Department of Physics.

In 1953 he was placed on research job at Obruchev Institute of Permafrost in Moscow but a few months later in October of the same year, Pyotr F. Shvetsov, RAS Correspondent Member, suggested to recruit him for a newly organized Yakutsk Permafrost Research Station. Thereon, all his life and research activity remained linked with Yakutia, permafrost science, and Permafrost Institute which stemmed later from the Yakutsk Research Station. While working for the Institute, V.T. Balobaev had achieved a great success in science having become a brilliant expert in permafrost issues, renown in Russia and abroad, and a holder of many titles, positions, and awards.

The working carrier of Veniamin Balobaev began in southern Yakutia where he participated in geophysical exploration of permafrost with a survey group at the Council for Productive Forces of the USSR Academy of Science.

When diamond production was initiated in Yakutia in 1956, Veniamin Tikhonovich was appointed vice-director of Geological and Geophysical Surveys at the Permafrost Institute which aimed at permafrost exploration for development of the Mir kimberlite pipe.

In 1962 Balobaev founded a laboratory of geothermal studies and headed it till 1994. It was at that time when a device for calibrating thermistors was built under his leadership, new techniques and instruments were designed for measuring thermophysical properties of frozen ground and various existing methods were brought to a single standard, and when investigation of terrestrial heat flow began in permafrost and subpermafrost zones. Theoretical and field studies with his participation yielded a geothermal model and a heat flow map of North Eurasia.

From 1994 to 2001 Veniamin Balobaev was associate director of the Institute responsible for research management. In that hard time when funding for science from the government was severely cut down all over the country for problems in national economy, great credit must go to Balobaev who had preserved all principal lines of research the Institute was running, as well as all its human and logistic resources.

V. Balobaev's 58-years work in science was overwhelmingly fruitful. He has developed a new field of geothermics for frozen ground and created exceptional models for paleoreconstructions and predictions of permafrost behavior. He is the author of more than 150 publications, including such fundamental books as "General Permafrost Science", "Thermophysical Studies of Permafrost in Siberia", "Subsurface Thermal Field of Siberia", "Temperature, Permafrost, and Radiogenic Heat in the Crust of North Asia", etc. The fundamental treatise "Geothermics of Permafrost in the Lithosphere of North Asia" he published in 1991 contained an important inference that negative temperatures in the upper crust resulted uniquely from heat exchange conditions on the surface whereas deep heat flux was the only control of permafrost thickness in places where it is large. In that study Balobaev proved, theoretically and experimentally, the broad extent of transient frozen ground in North Eurasia and modeled the lithospheric paleothermal field. The book has become a reference one for everybody engaged in permafrost research: for experienced scientists as well as for undergraduate or postgraduate students.

V. Balobaev has contributed a lot to education: he has brought up many skilled researchers and was scientific advisor of numerous candidate and doctor theses in geosciences. He was member of international and Russian associations in permafrost and geothermics, member of Cryology Scientific Council of the Russian Academy of Sciences, vice chairman of the Dissertation Council at the Permafrost Institute in Yakutsk, editor in scientific journals.

In recognition of his accomplishments in science and elsewhere, Veniamin Balobaev was awarded several medals, orders, and prizes, namely Order of People's Friendship; four medals, among which Medal for Great Service to the Country, Second Class; two bronze prize medals of VDNKh (Exhibition of Economic Achievements); award badge of Golden Sigma with Diamond; numerous certificates of merit from different institutions (Russian Government, Siberian Branch of the Russian Academy of Sciences, CPSU Central Committee, USSR Supreme Soviet, Central Council of Trade Unions, and from Central Committee of USSR Young Communist League).

Veniamin Tikhonovich was a charming personality, full of creative spirit, passionate for the nature of severe North, a keen scientist, and patriot of the institute he worked for. He possessed worldly wisdom and exceptional encyclopedic knowledge, being always ready to share it with everybody around. He was distinctive and enthusiastic in everything he was doing in his everyday life: motoring, hunting, fishing, gardening, or mushrooming. People knew him as a wonderful family man, a head of a large united family.

The life of Veniamin Balobaev is a glowing example of excellent expertise, dedication, diligence, and creativity. Anybody who met him will keep memory of the prominent scientist and remarkable personality.

Friends and colleagues